Revision of the central carbon metabolism in a photoautotrophic organism

Dissertation

In fulfilment of the requirements for the degree "Dr. rer. nat."

of the Faculty of Mathematics and Natural Science

at Kiel University

submitted by

Sarah Hildebrandt

Kiel

December 2020

This dissertation was accomplished as part of the Young Research Group

"Bioenergetics in Photoautotrophs" headed by Dr. Kirstin Gutekunst.

First referee: Prof. Dr. Rüdiger Schulz

Second referee: Prof. Dr. Frank Kempken

Date of oral examination: 01.03.2021

"Exactly!" said Deep Thought.

So once you do know what the question actually is,

you'll know what the answer means.

- Douglas Adams, The Hitchhiker's Guide to the Galaxy

"Absence of evidence is not evidence of absence".

- Martin Rees

Publications

Parts of this work were/will be published in the following articles:

Theune, M.L., **Hildebrandt, S.**, Steffen-Heins, A., Bilger, W., Gutekunst, K., Appel, J. (2020): *In-vivo* quantification of electron flow through photosystem I-cyclic electron transport makes up about 35% in a cyanobacterium. *Biochimica et Biophysica Acta - Bioenergetics* (accepted)

Makowka, A., **Hildebrandt, S.**, Boehm, M., Gutekunst, K.: The Entner-Doudoroff pathway branches off the oxidative pentose phosphate pathway in the cyanobacterium *Synechocystis sp.* PCC 6803 (under preparation)

Abbreviations

Abbreviation	Definition
°C	Degree Celsius
ACN	Aconitase
ACS	Acetyl-CoA synthetase
ADP	Adenosine diphosphate
AK	Acetate kinase
Amp^R	Ampicillin Resistance cassette
AOTF	Acousto-optic tunable filter
AP	Alkaline phosphatase
ATP	Adenosine triphosphate
BG11	Blue-Green 11
$CaCl_2$	Calcium chloride
CBB	Calvin-Benson-Bassham
Cm^R	Chloramphenicol resistance cassette
$Co(NO_3)_2$	Cobalt nitrate
CO_2	Carbon dioxide
CP12	Chloroplast protein 12
CS	Citrate synthase
CsoSCA	Carboxysome shell carbonic anhydrase
CSPD	Dinatrium-3-(4-methoxyspiro[1,2-dioxetan-3,2´(5´-chloro)tricyclodecan]-4-yl) phenylphosphate
$CuSO_4$	Copper-2-sulfate
DAHP	Dihydroxyacetone phosphate
DDH	Lactate dehydrogenase
DIG	Digoxigenin
DIRK	Dark-interval relaxation kinetics
DNA	Deoxyribonucleic acid
ED	Entner-Doudoroff
EDA	2-keto-3-deoxygluconate-6-phosphate (KDPG) aldolase
EDD	Phosphogluconate dehydratase
EDTA	Ethylenediaminetetraacetic acid
EMP	Embden-Meyerhof-Parnas
Em^R	Erythromycin Resistance cassette

ENO	Enolase
FBA	Fructose bisphosphate aldolase
FBP	Fructose 1,6-bisphosphate
Fdx	Ferredoxin
$FeNH_4$	Ammonium iron-3-sulfate
FUM	Fumarase
GABA	ϒ-aminobutyric acid
GABA-AT	ϒ-aminobutyrate aminotransferase
GAP	Glyceraldehyde 3-phosphate
GAPDH/GAP2	Glyceraldehyde 3-phosphate dehydrogenase
GDC	Glutamate decarboxylase
GDH	Glucose dehydrogenase
GFP	Green fluorescence protein
GK	Gluconate kinase
GLG	Glycogen synthase
Gm^R	Gentamycin Resistance cassette
GND	6-phosphogluconate dehydrogenase
GOGAT	Glutamine oxoglutarate aminotransferase
GOI	Gene of interest
GP	Glycogen phosphorylase
GS	Glutamine synthase
H_3BO_3	Boric acid
His	Histidine
HK	Hexokinase
HV	High voltage
ICL	Isocitrate lyase
IDH	Isocitrate dehydrogenase
K_2HPO_4	Dipotassium phosphate
KDPG	2-keto-3-deoxygluconate-6-phosphate
Km^R	Kanamycin resistance cassette
LB	Lysogeny broth
MDH	Malat dehydrogenase
ME	Malic enzyme
$MgSO_4$	Magnesium sulfate
$MnCl_2$	Magnesium chloride

MS/MSY	Malat synthase
Na_2CO_3	Sodium carbonate
Na_2EDTA	Ethylenediaminetetraacetic acid disodium salt
Na_2MoO_4	Sodium molybdate
$Na_2S_2O_3$	Sodium thiosulfate
NaCl	Potassium chloride
NAD	Nicotinamide adenine dinucleotide
NADPH	Nicotinamide adenine dinucleotide phosphate
$NaNo_3$	Sodium nitrate
NaOH	Potassium hydroxide
NH^{4+}	Ammonium
Nm	Nanometer
ODH	α-ketoglutarate dehydrogenase
OGDC	2-oxoglutarat decarboxylase
OPP	Oxidative pentose phosphate
PAT	Phosphate acetyltransferase
PCC	Pasteur culture collection
PCR	Polymerase chain reaction
PDH	Pyruvate dehydrogenase
PEP	Phosphoenolpyruvate
PEPC	Phosphoenolpyruvate carboxylase
PFK	6-phosphofructokinase
PFOR	Pyruvate ferredoxin oxidoreductase
PGAM	Phosphoglycerate mutase
PGI	Phosphoglucose isomerase
PGK	Phosphoglycerate kinase
PGL	6-phosphogluconolactonase
PGM	Phosphoglucomutase
PMT	Photomultiplier
PPS	Phosphoenolpyruvate synthetase
PRK	Phosphoribulokinase
PYK	Pyruvate kinase
RbCl	Rubidium chloride
RPE	Ribulose-5-phosphate epimerase
RPI	Ribulose-5-phosphate isomerase

rpm	Rounds per minute
Rubisco	Ribulose-1,5-bisphosphate carboxylase/oxygenase
SCS	Succinyl-CoA synthase
SDS	Sodium dodecyl sulfate
Sp.	Species
$Spec^R$	Spectinomycin resistance cassette
SSADH	Succinic semialdehyde dehydrogenase
SSC	Saline-sodium citrate
STED	Stimulated emission depletion
TAL	Transaldolase
TBE	Tetrabromoethane
TCA	Tricarboxylic acid
TES	N-Tris(hydroxymethyl)methyl-2-amonethane sulfonic acid
TKT	Transketolase
TPI	Triosephosphate isomerase
TPP	Thiamine pyrophosphate
TRIS	Tris(hydroxymethyl)aminomethane
WT	Wildtype
XFP	Xylulose-5- phosphate/fructose-6-phosphate phosphoketolase
YFP	Yellow fluorescence protein
$ZnSO_4$	Zinc sulfate
ZWF	Glucose-6-phosphate dehydrogenase

Summary

The central carbon metabolism of cyanobacteria and other photoautotrophic organisms can be divided generally into assimilation/anabolism (photosynthesis and CO_2-fixation) and dissimilation/catabolism (carbohydrate oxidation and respiration). While in photosynthesis CO_2 is reduced to carbohydrates, cell respiration describes the opposing reaction in which carbohydrates are oxidized to CO_2. When glucose and light are present as sources of energy, photomixotrophic conditions exist. This leads to catabolic (glycolytic pathways) and anabolic (Calvin-Benson-Bassam cycle) reactions taking place at the same time, which can be catalyzed by the same enzymes but in opposing directions in large parts. In contrast to plants (eukaryotes), cyanobacteria (prokaryotes) possess no intracellular compartments to spatially separate opposing processes. How cyanobacteria's metabolism is organized and how futile cycles or competition for intermediates are avoided is still mostly unclear.

Particularly interesting is in *Synechocystis sp.* PCC6803 the glycolytic Entner-Doudoroff (ED) pathway which proceeds exclusively in the catabolic direction and does not overlap with the Calvin-Benson-Bassham (CBB) cycle enzymatically. So far, it has been postulated that the ED pathway plays an essential role in the regeneration and replenishment of the CBB cycle (Makowka et al. 2020), however, its function as a catabolic pathway, in *Synechocystis*, is not yet fully understood and how exactly 6P-gluconate for the ED pathway is formed enzymatically is also still ambiguous.
Within this work, it could finally be determined that the Enter-Doudoroff (ED) pathway exclusively branches off the oxidative pentose phosphate (OPP) pathway and does not additionally result from a flux via a glucose dehydrogenase /gluconate kinase (GDH/GK) pathway in *Synechocystis*.

It has been hypothesized that if 3P-glycerate originated from the CBB cycle feeds the gluconeogenesis or is involved in the regeneration of the CBB cycle; no pyruvate can be generated via the lower glycolysis. Via growth experiments, it could be shown that, in *Synechocystis,* the Entner-Doudoroff (ED) pathway is essential when the lower glycolysis is interrupted. *Synechocystis* mutants were created in which an enzyme of lower glycolysis was deleted and examined physiologically under photoautotrophic, photomixotrophic and heterotrophic conditions. Mutants without active lower glycolysis were not viable, which indicated that the ED pathway could not fully compensate for the lower glycolysis. However, the growth of incompletely segregated mutants deteriorated significantly under photomixotrophic and heterotrophic conditions if the ED pathway was unfunctional too. This indicated that the ED pathway might represent an alternative pyruvate source to the lower glycolysis.

Pyruvate is mainly oxidized to acetyl-CoA, which can be described as the central intermediate in carbon metabolism. Therefore, we hypothesized that the ED pathway´s pyruvate might also represent an alternative route to provide acetyl-CoA. It is assumed that in *Synechocystis*, in addition to lower glycolysis, acetyl-CoA can also be produced via the phosphoketolase (PK) pathway. Physiologically and enzymatically, however, the PK pathway has not yet been characterized in *Synechocystis* in detail.
Within this work *Synechocystis* deletion mutants, in which the putative key enzymes of the PK pathway were deleted, were produced and physiologically examined. *Synechocystis* cells without a functional ED and PK pathway grew reduced under photoautotrophic, photomixotrophic and heterotrophic conditions in comparison to cells in which the PK pathway was impaired only. We, therefore, hypothesize that the ED pathway might represent an alternative pathway to yield acetyl-CoA during these metabolic conditions.

Due to continually changing environmental conditions, cyanobacteria are dependent on regulating the central carbon metabolism quickly and efficiently. It was postulated that the formation of metabolons and enzyme clusters compensates for the lack of cellular compartmentalization and that the formation of metabolons is a way to regulate metabolism, efficiently and rapidly. It is assumed that metabolons and enzyme clusters belong to the "basic equipment" of metabolic regulation in prokaryotes and eukaryotes. However, to prove the existence of a protein-protein interaction unequivocally, *in vivo* methods are required that enable a "look into the cell". Fluorescence microscopy is best suited for this. Various *in vitro* studies postulated that in *Synechocystis*, the enzymes phosphoribulokinase (PRK) and glyceraldehyde-3-phosphate dehydrogenase (GAP2) of the anabolic CBB cycle are regulated in a light-dependent manner. The protein CP12 mediates this regulation by forming a light-dependent trinary complex with PRK and GAP2. In darkness, the PRK-CP12-GAP2 complex is formed stopping the CBB cycle. In light, the complex dissolves and the CBB cycle is reactivated.
Within this work, the light- depended organization and dynamics of the PRK-CP12-GAP2 complex formation were demonstrated, for the first time, *in vivo*. Also, cluster signals of GAP2 under photomixotrophic condition indicated that the assembly of the PRK-CP12-GAP2 complex might also be regulated glucose-dependent.
This approach served to reiterate fluorescence microscopy as a suitable method to investigate the organization and dynamics of enzyme complexes *in vivo* as well as to establish a positive control for further experiments investigating the organization and dynamics of anabolic and catabolic enzymes of the central carbon metabolism.

Zusammenfassung

Der zentrale Kohlenstoffmetabolismus von Cyanobakterien und anderen photoautotrophen Organismen kann allgemein in Assimilation/Anabolismus (Photosynthese und CO_2-Fixierung) und Dissimilation/Katabolismus (Oxidation von Kohlenhydraten und Zellatmung) unterteilt werden. Während in der Photosynthese CO_2 zu Kohlenhydraten reduziert wird beschreibt die Zellatmung, die entgegengesetzte Reaktion indem Kohlenhydrate zu CO_2 oxidiert werden. Wenn Glukose und Licht als Energiequellen vorhanden sind, liegen photomixotrophe Bedingungen vor. Dies führt dazu, dass gleichzeitig katabole (glykolytische Wege) und anabole (CBB-Zyklus) Reaktionen stattfinden, die unteranderem durch dieselben Enzyme aber in entgegengesetzte Richtung katalysiert werden. Im Gegensatz zu Pflanzen (Eukaryoten) besitzen Cyanobakterien (Prokaryoten) keine intrazellulären Kompartimente, um gegenläufige Prozesse räumlich zu trennen. Wie der zentrale Kohlenstoffmetabolismus von Cyanobakterien organisiert ist und Leerlaufzyklen sowie Konkurrenz um Zwischenprodukte vermieden wird, ist größtenteils noch unklar.

In Bezug auf die metabolische Organisation von *Synechocystis sp*. PCC6803, ist der Entner-Doudoroff (ED) Weg besonders interessant, da er ausschließlich katabol verläuft und enzymatisch keine Überschneidungen mit dem Calvin-Benson-Bassham (CBB) Zyklus besitzt. Bisher wurde postuliert, dass der ED-Weg eine wesentliche Rolle bei der Regeneration und Wiederauffüllung des CBB-Zyklus spielt (Makowka et al. 2020), seine Funktion als kataboler Weg in *Synechocystis* ist jedoch noch nicht vollständig geklärt. Wie genau 6P-Gluconat für den ED-Weg enzymatisch gebildet wird, war ebenfalls noch unklar. Im Rahmen dieser Arbeit konnte festgestellt werden, dass der ED-Weg in *Synechocystis* ausschließlich vom oxidativen Pentosephosphatweg (OPP-Weg) abzweigt und nicht zusätzlich aus einem Fluss über den Glucose-Dehydrogenase/Gluconat-Kinase (GDH/GK) Weg resultiert.

Es wurde angenommen, dass wenn 3P-Glycerat aus dem CBB-Zyklus die Glukoneogenese speist oder für die Regeneration des CBB-Zyklus benötigt wird, kein Pyruvat durch die untere Glykolyse erzeugt werden kann. Durch Wachstumsexperimente konnte gezeigt werden, dass der ED-Weg wichtig ist, wenn der Fluss durch die untere Glykolyse unterbrochen ist. Es wurden *Synechocystis* Mutanten erzeugt, in denen ein Enzym der unteren Glykolyse deletiert war und physiologisch unter photoautotrophen, photomixotrophen und heterotrophen Bedingungen untersucht. Mutanten ohne funktionelle untere Glykolyse waren nicht lebensfähig, was darauf hinweist, dass der ED-Weg die untere Glykolyse nicht vollständig kompensieren kann. Das Wachstum von unvollständig segregierten Mutanten verschlechterte sich jedoch unter photomixotrophen und heterotrophen Bedingungen signifikant, wenn zusätzlich der ED-Weg blockiert war. Dies deutete darauf hin, dass der ED-Weg eine alternative Pyruvatquelle zur unteren Glykolyse darstellen könnte.

Pyruvat wird hauptsächlich zu Acetyl-CoA oxidiert, das als zentrales Zwischenprodukt im Kohlenstoffmetabolismus bezeichnet werden kann. Daher stellten wir die Hypothese auf, dass das Pyruvat des ED-Weges eine alternative Acetyl-CoA-Quelle darstellen könnten. Es wird angenommen, dass in *Synechocystis* neben der unteren Glykolyse, Acetyl-CoA zusätzlich über den Phosphoketolaseweg (PK-Weg) hergestellt wird. Physiologisch und enzymatisch wurde der PK-Weg von *Synechocystis* jedoch noch nicht im Detail charakterisiert. Im Rahmen dieser Arbeit wurden *Synechocystis*-Deletionsmutanten hergestellt und physiologisch untersucht, in denen die mutmaßlichen Schlüsselenzyme des PK-Weges deletiert wurden. *Synechocystis* Zellen ohne funktionalen ED- und PK-Weg wuchsen schlechter unter photoautotrophen, photomixotrophen und heterotrophen Bedingungen im Vergleich zu Zellen, bei denen nur der PK-Weg beeinträchtigt war. Wir nehmen daher an, dass der ED-Weg eine alternative Acetyl-CoA-Quelle darstellen könnte.

Aufgrund sich ständig ändernder Umweltbedingungen sind Cyanobakterien darauf angewiesen, den zentralen Kohlenstoffmetabolismus schnell anpassen zu können. Es wurde postuliert, dass die Bildung von Metabolonen und Enzymclustern den Mangel an zellulärer Kompartimentierung kompensieren kann und einen Mechanismus darstellt, den Metabolismus schnell und effizient zu regulieren. Es wird angenommen, dass Metabolone und Enzymcluster zur "Grundausstattung" der Stoffwechselregulation in Prokaryoten und Eukaryoten gehören. Um jedoch das Vorhandensein einer Protein-Protein-Wechselwirkung eindeutig nachzuweisen, sind *in vivo* Methoden erforderlich, die einen „Blick in die Zelle“ ermöglichen. Hierfür eignet sich am besten die Fluoreszenzmikroskopie.
Verschiedene *in vitro* Studien zeigten, dass in *Synechocystis* die Enzyme Phosphoribulokinase (PRK) und Glycerinaldehyd-3-Phosphat-Degydrogenase (GAP2) des anabolen CBB-Zyklus, lichtabhängig reguliert werden. Das Protein CP12 vermittelt diese Regulation durch Bildung eines lichtabhängigen ternären Komplexes mit PRK und GAP2. In Dunkelheit wird ein PRK-CP12-GAP2-Komplex gebildet, der den CBB-Zyklus stoppt. Im Licht löst sich der Komplex auf und der CBB-Zyklus wird reaktiviert.
In dieser Arbeit wurde erstmals *in vivo* die lichtabhängige Organisation und Dynamik der PRK-CP12-GAP2-Komplexbildung demonstriert. Zusätzlich weisen Clustersignale von GAP2 unter photomixotrophen Bedingungen darauf hin, dass die Assemblierung des PRK-CP12-GAP2-Komplexes glukoseabhängig reguliert sein könnte.
Die Experimente dienten außerdem dazu, die Fluoreszenzmikroskopie als geeignete Methode zur Untersuchung der Organisation und Dynamik von Enzymkomplexen *in vivo* zu bestätigen und eine Positivkontrolle für weitere Experimente zur Untersuchung der Organisation und Dynamik von anabolen und katabolen Enzymen des zentralen Kohlenstoffmetabolismus zu etablieren.

Table of contents

1. Introduction

1.1. A cell in a cell: The great evolutionary leap from compartment to compartmentalization

Two fundamental characteristics that define life are, (i) that there is a compartment in which energy can be converted effectively and directed, and (ii) that this "compartment" can propagate (Purves et al. 2007). The smallest and oldest unit that is capable of doing this is the cell. Exactly when life began is unknown, but little evidence suggests that the first cells, which can also be referred to as membrane-encased reaction spaces, emerged around 3.5 billion years ago and gave the starting signal for terrestrial evolution (Noffke et al. 2013; Soo et al. 2017). Whether the first cells were heterotrophic and required inorganic substances from the environment (Bada and Lazcano 2002; Orgel 2008; Sutherland 2017; Muchowska et al. 2017), or lived autotrophically and fixed CO_2 (Martin et al. 2003; Lane and Martin 2012; Weiss et al. 2016; Schönheit et al. 2016) is controversial. Both hypotheses are postulated, even the third option that there was a parallel development is discussed (Gutekunst 2018). Regardless of which trophy was lived first, an estimated 3.2 to 2.5 billion years ago, the first cells were metabolically developed to the point that they performed oxygenic photosynthesis (Buick 2008; Planavsky et al. 2014; Soo et al. 2017). It is assumed that these first oxygenic photoautotrophic prokaryotes were cyanobacteria (Hohmann-Marriott and Blankenship 2011; Blankenship 2017; Soo et al. 2017). Through oxygenic photosynthesis, such amounts of oxygen had been produced and at the same time enormous quantities of CO_2 had been bound, that about half a billion years later, the great oxidative event took place. "Our" atmosphere was created (Soo et al. 2017). Based on geological data (Fischer et al. 2016), it is assumed that the oxygenic photosynthesis was carried out far more successfully and evolved more advanced than the anoxygenic photosynthesis, since the inorganic compounds Fe^{2+}, H_2S and H_2 were only available as potential electron donors to a limited extent. The oxidation of H_2O, however, represented a much larger source of electrons (Hohmann-Marriott and Blankenship 2011).

Around 900 million years ago, this enabled the next major ecological event, the emergence of eukaryotes through endosymbiosis (Shih and Matzke 2013). The endosymbiotic theory describes the process in which a unicellular symbiont is phagocytosed into the host's intracellular compartment. In the case of photosynthetic multicellular organisms, the host will probably have been a phagotrophic bikont living in freshwater and the endosymbiont a cyanobacterium, closely related to the now known *Nostocales* and *Stigonematales* (Deusch et al. 2008; Dagan et al. 2013).

During evolution, the cyanobacteria went through three necessary steps to become a fully integrated organelle, a chloroplast: (i) The development of membrane-bound transporters were necessary, which regulate the molecular exchange between endosymbiont and the host. (ii) The endosymbiont had to be metabolically fully integrated into the host and (iii) the reproductive cycles had to be adapted to one

another (Ligrone 2019), resulting in the transformation of increasingly more parts of the genome to the host's cell nucleus, some genes were lost entirely. Only a small part of the original genome, also known as the plastome or chloroplast genome, remained in the now fully integrated organelle (Barbrook et al. 2010). Based on analyses of the nucleus sequence of eukaryotes, it is assumed that the endosymbiosis was not a single event and that the chloroplast developed several times in eukaryotes (Howe et al. 2008). The chloroplast enabled eukaryotic cells to become photoautotrophic. This host eukaryotic cell was the ancestor of the *Archaeplastida*, which merely means "ancient chloroplasts". Being a photoautotrophic eukaryote, turned out to be such a tremendous evolutionary advantage, that they soon occupied extensive aquatic and terrestrial niches. The flora was born.

1.2. Today's cyanobacteria: A brief fact check

Due to their external appearance and color, cyanobacteria are often referred to as blue-green algae, a misleading denotation since cyanobacteria are prokaryotic organisms, while algae belong to the eukaryotic clade (Leliaert et al. 2012). They can cope with a wide variety of environmental conditions and occur in freshwater, sea, soil, microbial mats and on stones (Sukenik et al. 2012; Paerl and Paul 2012; Stal 2012). They are also viable in extreme environments such as deserts (Belnap 2003), hot springs (Strunecký et al. 2019) and even on the surface of the International Space Station (ISS) (Baqué et al. 2017). Cyanobacteria can form filaments, live in groups but also individually and are characterized by their high adaptability and rapid growth (Whitton and Potts 2012). About 6300 different species are currently known (Nabout et al. 2013). Cyanobacteria are affecting our everyday life on various levels. Many of them are used industrially, e.g. to produce biofuels (Farrokh et al. 2019), food supplements (Marsan et al. 2018), biofertilizer (Mishra and Pabbi 2004; Saadatnia and Riahi 2009), biodegradable plastic (Philip et al. 2007) and pharmaceutically usable secondary metabolites (Mayer et al. 2007; Gademann and Portmann 2008; Wase and Wright 2008). Furthermore, they can also be used for bioremediation of, e.g. heavy metals, pesticides, naphthalene and crude oil (Kesaano and Sims 2014; Hamouda et al. 2016; Kumar et al. 2016). Hitherto, 85 cyanobacteria have been genomically fully sequenced (Fujisawa et al. 2017). It all started in 1996 with the complete sequencing of *Synechocystis sp.* PCC 6803 (hereafter *Synechocystis*) (Kaneko et al. 1996). It is a unicellular, non-diazotrophic, freshwater cyanobacterium that was discovered and isolated in a Californian freshwater lake, in 1968 (Stanier et al. 1971; Ikeuchi and Tabata 2001). Today it is one of the most investigated cyanobacterium (Pelroy et al. 1972) since it is naturally competent to take up DNA from its environment (Barten and Lill 1995) and therefore very easy to manipulate genetically (Grigorieva and Shestakov 1982). *Synechocystis* is metabolically extraordinarily flexible and is able to grow photoautotrophically, photomixotrophically and heterotrophically (Anderson and McIntosh 1991; Zavřel et al. 2017).

1.3. *Synechocystis*: A journey into the central carbon metabolism

The central carbon metabolism of cyanobacteria and other photoautotrophic organisms can be divided generally into assimilation/anabolism (photosynthesis and CO_2-fixation) and dissimilation/catabolism (carbohydrate oxidation and respiration; Hoch et al. 1963). During photosynthesis, CO_2 is reduced to carbohydrates. During cell respiration, which describes the opposing reaction of the photosynthesis, carbohydrates are oxidized to CO_2 (Figure 1:1).

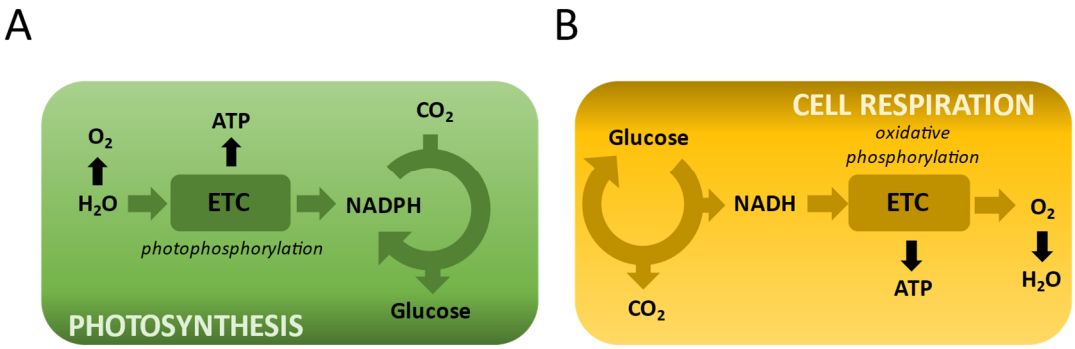

Figure 1:1: Schematic comparison of photosynthesis and cell respiration. ETC: electron transport chain. (Cornell 2016, from the original, slightly modified graphically)

Photosynthesis can be divided into two processes: (i) The light reaction, in which electrons from photocatalytic water splitting are fed into the electron transport chain and reducing equivalents in the form of ferredoxin, NAD(P)H and ATP are generated (Arnon 1971). (ii) The Calvin-Benson-Bassam (CBB) cycle (Calvin 1962), which uses the reducing equivalents of the light reaction to fix CO_2 and to generate carbohydrates (glycogen, starch) to maintain metabolism in darkness (Saha et al. 2016) and to produce intermediates.

However, cell respiration can be described by three processes: (i) The glycolytic pathways, that catalyze the oxidation of glucose to pyruvate, providing the cell with resulting intermediates (substrates for e.g. amino acids), reducing equivalents and energy (ATP) in darkness and light. Exclusively during light, the intermediates and reducing equivalents also serve to replenish and regenerate the CBB cycle (Makowka et al. 2020). For *Synechocystis*, four different glycolytic pathways have been described so far. The Embden-Meyerhof-Parnas (EMP) pathway (Kresge et al. 2005), which can be divided into upper and lower glycolysis, the oxidative pentose phosphate (OPP) pathway (Jansén et al. 2010), the Entner-Doudoroff (ED) pathway (Chen et al. 2016) and the phosphoketolase (PK) pathway (Alagesan et al. 2013; Xiong et al. 2015). (ii) The tricarboxylic acid (TCA), cycle in which acetyl-CoA is completely oxidized to CO_2 and intermediates are formed as precursors for amino acids (Ito et al. 2019), nucleotides and fatty acids synthesis. (iii) The respiration, in which electrons are transferred from NADH back to oxygen via an electron transport chain to generate energy in the form of ATP (Shimakawa et al. 2014).

Roughly summarized, the photosynthesis and cell respiration can also be referred to as a molecular supply-demand system (Hofmeyr and Cornish-Bowden 2000; Rohwer and Hofmeyr 2008; Christensen et al. 2015; Matuszyńska et al. 2019). *Synechocystis,* as well as other aquatic living photoautotrophs, are necessarily able to adapt rapidly in metabolism to changing environmental conditions.

Due to streams, waves, etc., they are regularly exposed to varying light intensities and glucose concentrations. Glucose is mainly present as dissolved organic carbon from dead organic material (Alonso and Pernthaler 2006; Klingner et al. 2015). During the blooming of phytoplankton, e.g., the glucose concentration within waters can vary greatly (Teeling et al. 2012). If glucose and light are present as energy sources, photomixotrophic conditions exist. This results in catabolic (glycolytic pathways) and anabolic (CBB cycle) reactions are taking place simultaneously. This was confirmed by flux analyses mapping simultaneous flux through the OPP pathway and the CBB cycle (Yang et al. 2002; Nakajima et al. 2014).

It was assumed that the pathways bidirectionality play a minor role and only exist under photomixotrophic conditions since several enzymes are shared by both opposing reactions risking inhibition. However, Makowka et al. 2020 found that the catabolic pathways are also crucial under photoautotrophic conditions. The mapping of the carbon metabolism (Figure 1:2) conveys the picture of catabolic pathways existing exclusively for the generation of pyruvate, intermediates, ATP and reducing equivalents, and that they always process the pathway completely. Two aspects contradict this assumption: (i) Under photoautotrophic conditions none of these products is required since photosynthesis is carried out and (ii) the simultaneous processing of the CBB cycle (which is the reversed OPP- and upper EMP pathway) would lead to futile cycles. It has been hypothesized that so-called shunts are formed, branching off the "classic" catabolic pathway in order to replenish the CBB cycle in anaplerotic reactions. According to current knowledge, shunts branch off from the upper EMP pathway (PGI shunt), and OPP pathway (OPP shunt). In addition, it is postulated that the entire ED pathway can function as a shunt, especially since the catabolic ED pathway does not overlap with opposing reactions of the anabolic CBB cycle. It has not long been known that the ED pathway plays a role in the carbon metabolism of *Synechocystis* (Chen et al. 2016).

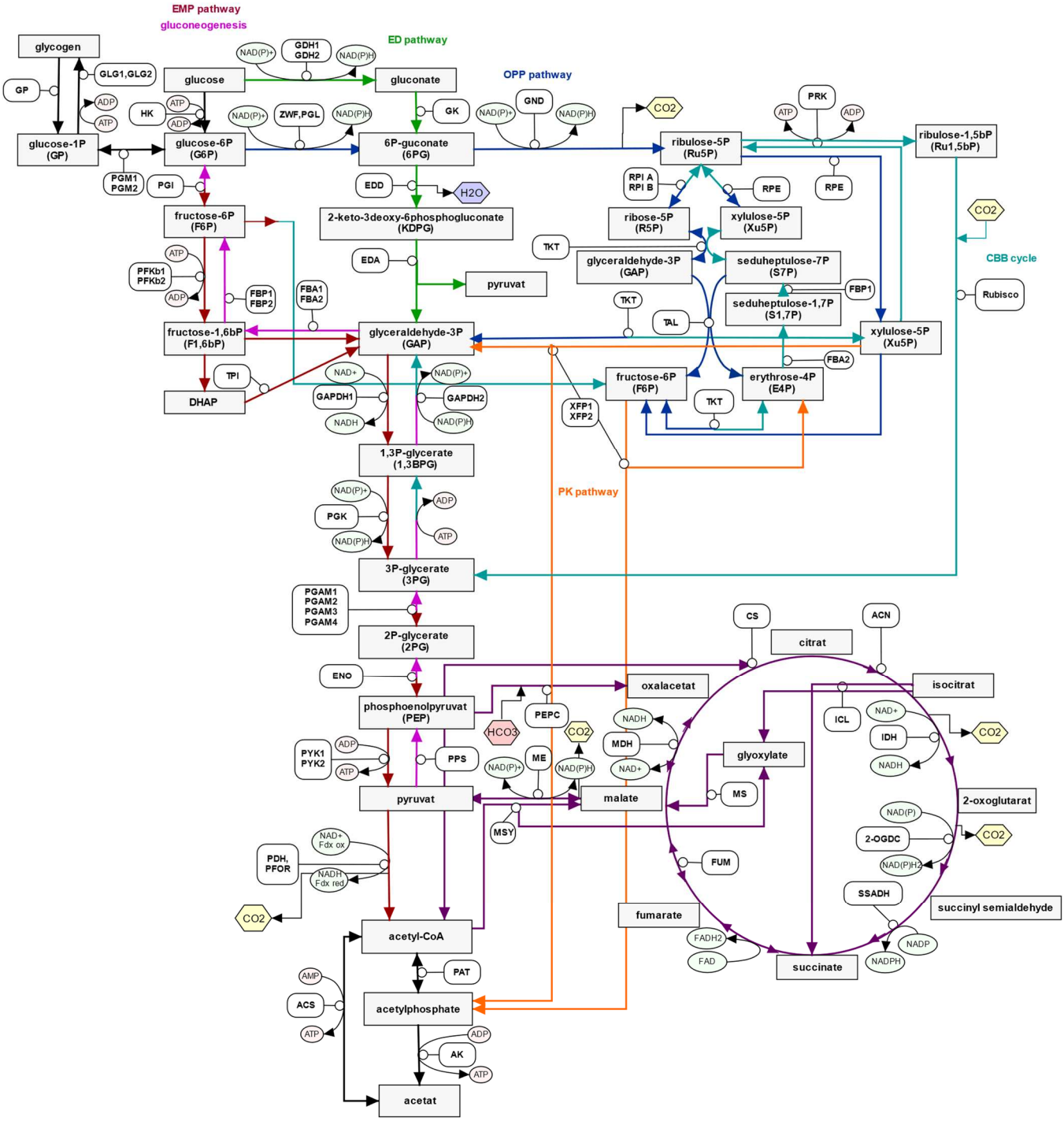

Figure 1:2: Overview of glycolytic routes in Cyanobacteria. Green: Entner-Doudoroff (ED) pathway. Red: Emden-Meyerhof-Parnas (EMP) pathway. Pink: gluconeogenesis. Blue: Oxidative pentose phosphate (OPP) pathway. Cyan: Calvin-Benson-Bassam (CBB) cycle. Orange: Phosphoketolase (PK) pathway. Purple: TCA cycle. GP: glycogen phosphorylase; GLG: glycogen synthase; HK: hexokinase; PGM: phosphoglucomutase; PGI:phosphoglucose isomerase, GDH: glucose dehydrogenase, ZWF: glucose-6-phosphate dehydrogenase; PGL: 6-phosphogluconolactonase; PFK:6-phosphofructokinase; FBP: fructose 1,6-bisphosphate; TPI: triosephosphateisomerase; GK: gluconate kinase; EDD: phosphogluconate dehydratase; EDA: KDPG-aldolase; GAPDH: glyceraldehyde phosphate dehydrogenase; PGK: phosphoglycerate kinase; PYK: pyruvate kinase; ENO: enolase; PGAM: phosphoglycerate mutase; PPS: phosphoenolpyruvate synthetase; PDH: pyruvate dehydrogenase; PFOR: pyruvate ferredoxin oxidoreductase; ACS: acteyl CoA synthetase; PAT: phosphate acetyltransferase; AK: acteate kinase; ME: malic enzyne ;PEPC: phosphoenolpyruvate carboxylase; MDH: malat dehydrogenase; FUM: fumarase; MS/MSY: malat synthase; CS: citrate synthase; ACN: aconitase; ICL: isocitrate lyase; IDH: isocitrate dehydrogenase; 2-OGDC: 2-oxoglutarat decarboxylase; SSDAH: succinic semialdehyde dehydrogenase; GND: 6-phophogluconate dehydrogenase; PRK: phosphoribulokinase; XFP: xylulose-5- phosphate/fructose-6-phosphate phosphoketolase; RPI: ribulose-5-phosphate isomerase; RPE: ribulose-5-phosphate epimerase; TKT: transketolase; TAL: transaldolase.

1.3.1. The Entner-Doudoroff pathway

Evolution studies assume that the Entner-Doudoroff (ED) pathway preceded the Emden-Meyerhof-Parnas (EMP) pathway (Romano and Conway 1996), resulting in the ED pathway and the EMP pathway being very similar. Both pathways represent the most common glycolytic routes of prokaryotes (Romano and Conway 1996; Meléndez-Hevia et al. 1997; Kim and Gadd 2008). It was postulated that 57% of the annotated prokaryotes oxidize glucose via an EMP pathway, 27% via an ED pathway and that 14% are capable of using both pathways (Flamholz et al. 2013).

Considering only sequenced cyanobacteria, blast analyses showed that 92% have a KDPG aldolase (EDA, the key enzyme of the ED pathway) and that 57% of the cyanobacteria code for a PFK (the key enzyme of the upper EMP pathway). Noticeable, the 8% who do not possess a KDPG aldolase, are native to nutrient-rich freshwater (Chen et al. 2016). In the natural aquatic habitat, cyanobacteria are seldom primarily limited by ATP, since there is enough light over open water to process photosynthesis. It is more likely nutrients being the limiting factor.

The first impression is that the EMP pathway is energetically more advantageous, as more than double the amount of ATP per glucose molecule is generated than via the ED pathway. However, the ED pathway functions as a short track to generate pyruvate and as a possibility to supply the Calvin-Benson-Bassham (CBB) cycle, the gluconeogenesis or the lower glycolysis with glyceraldehyde-3P (GAP), according to requirements of the cell. Fewer enzymatic proteins are required for the conversion of glucose to pyruvate, which leads to a higher metabolic driving force of intermediate reactions (Bar-Even et al. 2012). Flamholz et al. postulated 2013 that the choice between ED and EMP pathways is a compromise between glycolytic ATP yield and protein cost. For fermentative anaerobic prokaryotes, the EMP pathway is the only source of ATP. In aerobic organisms, however, only a fraction of the ATP requirement is generated within the glycolytic routes (Fuhrer et al. 2005; Kim and Gadd 2008).

Several variants of the ED pathway have been described so far. Classically, catalyzed by phosphogluconate dehydratase (EDD), 6P-gluconate is converted to 2-keto-3-deoxy-phosphogluconate (KDPG), which is formed exclusively in the ED pathway. Subsequently, the KDPG is finally split into pyruvate and glyceraldehyde-3P (GAP) via the KDPG aldolase (EDA; Figure 1:2). In contrast, archaea predominantly employ a non-phosphorylating ED pathway in which non-phosphorylated gluconate is converted into 2-keto-3-deoxygluconate (KDG; Selig et al. 1997; Sutter et al. 2016)

As distinct as the actual ED pathway can be organized, the origin of glucose to 6P-gluconate varies between different organisms too. Classically, the glucose is phosphorylated to glucose-6P via a hexokinase and then oxidized to 6P-gluconate via glucose-6P-dehydrogenase (ZWF; Conway 1992; Kopp et al. 2020). However, *E. coli,* e.g. can bypass this section completely by oxidizing glucose to gluconate via a glucose dehydrogenase (GDH), and further phosphorylating the gluconate to 6P-gluconate via a gluconate kinase (GK). Since *E.coli* enables glucose and gluconate transporters, both can be metabolized

directly (Peekhaus and Conway 1998). Regarding *Synechocystis*` ED pathway, physiology studies indicated that the entrance might involve a GDH/GK pathway (Chen et al. 2016). Enzyme studies, on the other hand, could not demonstrate any enzyme activity of the potential GDHs in *Synechocystis* (Makowka 2019).

1.3.2. The Phosphoketolase pathway

Another and also respectively newly discovered *Synechocystis'* glycolytic pathway (Figure 1:2) is the phosphoketolase (PK) pathway (Xiong et al. 2015). The PK pathway has been extensively investigated for many prokaryotes, e.g. *Bifidobacteria* (Fandi et al. 2001; Meile et al. 2001; Fushinobu 2010), *Clostridia* (Liu et al. 2012), *Lactobacillus* (Posthuma et al. 2002), *Lactococcus* (Scheidig et al. 2019) and *Pseudomonas* (Petrareanu et al. 2014). Only recently a phosphoketolase pathway was also found or described in the cyanobacteria *Anabaena* (Sánchez et al. 2010; Moriyama et al. 2015), *Cyanothece* (Alagesan et al. 2013), *Synechococcus sp., Gloeobacter violaceus* (Sánchez et al. 2010) and *Synechocystis* (Knoop et al. 2013; Xiong et al. 2015). However, little is known about the physiological significance for photoautotrophic organisms, since a phosphoketolase (XFP) hasn't been found in higher plants. XFPs are thiamine pyrophosphate (TPP) dependent enzymes that also require divalent cations (Yevenes and Frey 2008). To date, two subfamilies of XFPs have been described, according to their substrate specificity (Sánchez et al. 2010), one specific for xylulose-5P and one that is comparable specific for xylulose-5P and fructose-6P. Fructose-6P is converted into erythrose-4P and acetyl phosphate (Schramm et al. 1958), whereas xylulose-5P is converted to acetyl phosphate and glyceraldehyde-3P (GAP) (Heath et al. 1958). To date, the dual fructose-6P/xylulose-5P-phosphoketolase has only been detected in *Bifidobacteria*, employed as a key enzyme of the fermentative pathway "bifid-shunt" which is characteristic to this species. (Grill et al. 1995; Meile et al. 2001; Fushinobu 2010).

In addition, a study in which an artificial phosphoketolase pathway was investigated in *E.coli* indicates that XFP is capable of converting sedoheptulose-7P to ribose-5P and acetyl phosphate. However, the metabolic importance of this reaction is still unclear (Krüsemann et al. 2018).

The conversion of xylulose-5P or fructose-6P to glyceraldehyde phosphate dehydrogenase (GAP) or erythrose-4P, runs parallel to the oxidative pentose phosphate (OPP) pathway and opposing to the Calvin-Benson-Bassham (CBB) cycle. The oxidation of xylulose-5P or fructose-6P to acetyl phosphate, however, short cuts the CBB cycle, bypasses the lower glycolysis, is catabolic only and does not overlap with any anabolic reactions. It is a short track to produce acetyl phosphate which subsequently can either be oxidized to acetate or reduced to acetyl-CoA. A reaction in which no CO_2 is released, and reduction equivalents are produced (Bogorad et al. 2013; Lin et al. 2018). Based on flux analyses, Xiong et al. 2015 hypothesized that the PK pathway is an important route to generate acetyl-CoA. Organic acid production assays and H-NMR analysis revealed under heterotrophic conditions, the

deletion of the enzyme phosphoketolase (XFP1, slr0453) led to a substantial reduction of acetate (Xiong et al. 2015), which can be used as a building block for the biosynthesis of needed metabolites (Thiel et al. 2017; Miao et al. 2020). In addition, it has been hypothesized that the degradation of hexoses or pentoses is energetically more advantageous to the OPP pathway since ATP can be obtained during the dephosphorylation of acetyl phosphate to acetate (Wolfe 2005; Sánchez et al. 2010). The phosphoketolase has, therefore, already been postulated as an essential regulator of the carbon economy (Bogorad et al. 2013; Kocharin et al. 2013).

1.3.3. The lower glycolysis

The phosphoketolase (PK) pathway might play an essential role in providing acetyl-CoA, the most important route for acetyl-CoA production is, however, the lower glycolysis. Another reason why the PK pathway and its metabolic significance in *Synechocystis* has remained undiscovered for such a long time is that acetyl-CoA can also be generated from the oxidation of pyruvate, catalyzed by the pyruvate dehydrogenase (PDH) complex and a pyruvate/ferredoxin oxidoreductase (PFOR; Figure 1:2). In this context, pyruvate is mainly referred to as the product of the Emden-Meyerhof-Parnas (EMP) pathway. However, the production of pyruvate in the lower glycolysis cannot only be attributed to the EMP pathway, as the Entner-Doudoroff (ED) and oxidative pentose phosphate (OPP) pathway also supply the lower glycolysis with glyceraldehyde 3P (GAP; Young et al. 2011). By bioinformatical simulation mapping, it was shown that in addition to the "classic" lower glycolysis, many stoichiometrically possible pathways theoretically exist to convert glyceraldehyde-3P (GAP) to pyruvate. However, the combination of thermodynamics and biophysical aspects limits any biochemical alternatives to the lower glycolysis, which was therefore postulated to be the most optimal pathway with the highest “flux than any biochemically possible alternative" (Court et al. 2015).

Glyceraldehyde-3P (GAP) represents the substrate of the lower glycolysis and is oxidized to 1,3P-glycerate via glyceraldehyde-3P-dehydrogenase (GAPDH1, in *Synechocystis,* annotated as GAP1). 1,3P-glycerate is then oxidized to 3P-glycerate via phosphoglycerate kinase (PGK). 3P-glycerate can also be fed into the lower glycolysis as a product of the CO_2 fixation via the CBB cycle and then dephosphorylated to 2P-glycerate via phosphoglycerate mutases (PGAM) and converted to phosphoenolpyruvate (PEP) via enolase (ENO) subsequently. PEP is generated exclusively in the lower glycolysis and not only serves as a substrate for the generation of pyruvate but also supplies essential metabolism, such as the shikimate or chorismate pathway to synthesize amino acids (Appendix Figure 1). In addition, PEP with bicarbonate (HCO_3^-) can be converted into oxaloacetate via the phosphoenolpyruvate carboxylase (PEPC). PEPC is found in most cyanobacteria and is accountable for 25% of CO_2 fixation in *Synechocystis* (Takeya et al. 2017; Veaudor et al. 2020).

Studies also showed that *Synechocystis sp.* PCC 6803 (Angermayr et al. 2014) and *Synechococcus* PC 7942 (Luinenburg and Coleman 1990) were not able to grow photoautotrophically without a functional PEPC. The conversion of PEP to pyruvate is catalyzed by pyruvate kinase (PYK). It is particularly noticeable that several annotated potential isoenzymes of PGAM and PYK, as well as of the phosphoketolase are present in *Synechocystis* and other prokaryotes. In eukaryotic cells, the isoenzymes of PGAM and PYK are located in various compartments and perform different tasks (Carreras et al. 1982; Ambasht and Kayastha 2002; Jablonsky et al. 2013). Since prokaryotes are evolutionary older, the question arises whether isoenzymes in unicellular cells also fulfil different functions or whether they are not isoenzymes at all? The exact functions have not yet been investigated (Jablonsky et al. 2013).

1.4. Metabolic channelling: An all-in-one solution for metabolic regulation

For a long time, the image was conveyed that, enzymes, substrates, products, intermediates, etc. exist "free" and unorganized, in uncompartmentalized organisms; a contradiction in terms of how complex the metabolism of prokaryotes can be. Metabolic complexity always requires an efficient organization. Due to continually changing environmental conditions, prokaryotes require an organizational system that can quickly regulate the metabolic flux. Eukaryotes organize their metabolism primarily by compartmentalizing the cell, preventing undesired crosstalk between the metabolic processes. Among others, communication and maintenance between the pathways take place via enzymes for signal transduction, transcription regulation and via specific transporters. The compartmentalization of a cell enabled the development of a highly specialized secondary metabolism and thus the possibility of giving a chemical response to environmental stimuli (e.g. phytohormones, secondary metabolites). Plants are able to sense their environment and adapt their metabolism accordingly (Engineer et al. 2016). Various studies have shown that so-called "guard cells" contain signaling pathways and components sensing the environment (Weyers et al. 1983; Edwards and Bowling 1985; Webb et al. 1996; Brearley et al. 1997; Hu et al. 2010). Guard cells can thus directly influence stomatal movement in the event of changes in the CO_2 ratio. For cyanobacteria, it has been postulated that the regulation of metabolism is primarily triggered by sensing the internal metabolic status and less by sensing external influences (Galperin 2005; Orthwein et al. 2020). Studies on rice plants have shown that the expression level of glycolytic enzymes is adjusted depending on the CO_2 concentration (Fukayama et al. 2009). For *Synechocystis*, however, changing CO_2 ratios had little or no effect on the expression level of glycolytic enzymes (Wang et al. 2004; Eisenhut et al. 2007). Therefore, it was assumed that the regulation of the metabolism could take place post-translationally. Regarding recurring environmental influences, such as day/night cycles, shading and temperature changes, this would be a time- and an energy-saving possibility to quickly adapt primary and secondary metabolism (Obata 2019).

In 1985, Srere described a "supramolecular complex of sequential metabolic enzymes and cellular structural elements" which he called "metabolon" (Figure 1:3).

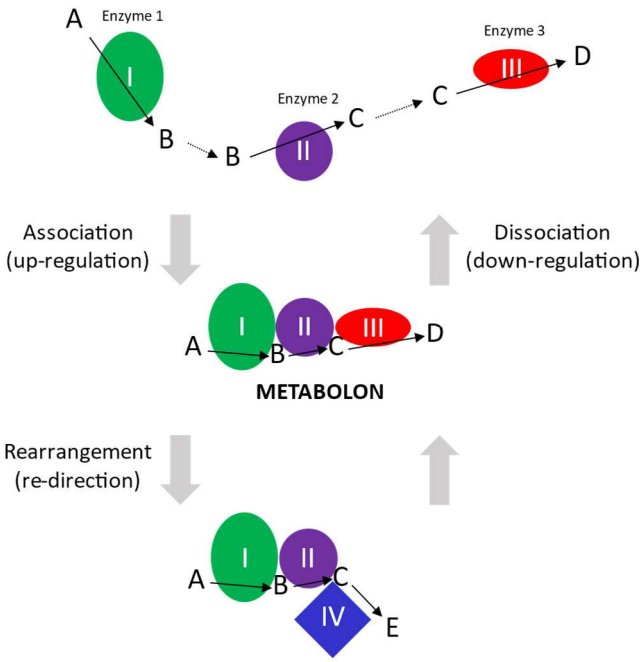

Figure 1:3: "Metabolic regulation by a dynamic metabolon. A schematic diagram showing the regulation of metabolic pathways by a dynamic metabolon. A pathway in which product D is synthesized from substrate A via the reactions catalyzed by enzyme I, II, and III (arrows) is assumed. B and C are the pathway intermediates. Association of the metabolon will enhance the pathway reactions and is expected to up-regulate the pathway. On the other hand, the dissociation of metabolon will down-regulate the pathway. When the enzyme III is replaced with enzyme IV which catalyze the conversion of C to E, the metabolic flux is re-directed to the production of E". (Obata 2019, from the original, slightly modified graphically)

He postulated that these supramolecular assemblies are based on five features: (i) The substrate is channelled. (ii) The metabolic flux is regulated through association/dissociation of enzymatic units. (iii) The complex interacts with structural cell elements. (iv) Possible enzyme localization is limited, and (v) the gene expression of the enzyme units is based on similar characteristics.

In summary, a post-translational enzymatic organization system that can compensate for the lack of a compartment was described. Today more than 30 years later, metabolons have been described in all kinds of organisms, eukaryotic and prokaryotic. Whether named as metabolon, substrate channel or metabolic channel, the crucial feature is that the intermediate is kept within an enzyme complex (microenvironment) and is catalyzed by the enzymes of the complex without diffusing into the bulk phase (Obata 2019). This process can be catalyzed by static channelling (protein-surface structure-dependent) as well as dynamic channelling (transient). As assumed, there are several advantages of organizing and regulating enzymes through the formation of a metabolon (Spivey and Merz 1989; Jørgensen et al. 2005; Obata 2019): (i) The reactions can run faster. The active sides of the flanking enzymes are closer to each other, and channelled intermediates can be passed on catalytically more efficiently. (ii) The metabolic flux can be adapted more quickly to changing environmental conditions. (iii) Metabolic branching points can be defined, and thus the ratio of the metabolic flux of different pathways can be regulated (iv) The local concentration of the intermediates can be increased.

(v) Since the intermediate does not pass into the bulk phase, the kinetic conditions are better. (vi) The cell is protected from its own cytotoxic substances. (vii) Intermediates having a regulating effect on enzymes do not interact. (viii) Metabolic crosstalk between enzymes of different synthesis pathways is controlled and coordinated, and (ix) intermediates that are used by several metabolic pathways are coordinated as well.

The description of such a "supra" enzyme complex fundamentally changed the understanding of the metabolic organization and put the term "compartmentalized" under a new evaluation. Even if Srere (1985) has set high requirements for the definition of "metabolons", there are many metabolic systems that are referred to as such, since the priorities are set differently depending on the research focus. Many substrate channels have been detected, and it was postulated that metabolons are ubiquitous in the entire metabolic network of plants. Today, researchers define a wide variety of systems as metabolons: (i) Heteromeric enzyme complexes, like pyruvate dehydrogenase complex and 2-oxoglutarate dehydrogenase (Sheu and Blass 1999), (ii) partially channelled metabolic pathways, e.g. the bitter acid biosynthesis in hop (Li et al. 2015), (iii) channelling of successive enzymes only, as for the isoflavonoid pathway of several leguminous (Du et al. 2010) and (iv) entirely channelled metabolic pathways that are associated with structural elements of the cell, like the TCA cycle (D'Souza et al. 1983; Sumegi et al. 1984, 1993; Kispal et al. 1986; Fernie et al. 2018; Sweetlove et al. 2018).

1.4.1. CP12: A redox-responsive protein

The prime example of how efficiently the metabolism can be regulated and organized via a heteromeric enzyme complex is the ternary PRK-CP12-GAPDH (phosphoribulokinase-chloroplast protein-12-glyceraldehyde 3-P dehydrogenase) enzyme complex, which regulates the CO_2 fixation via the Calvin-Benson-Bassham (CBB) cycle in a light-dependent manner (McFarlane et al. 2019; Figure 1:4).

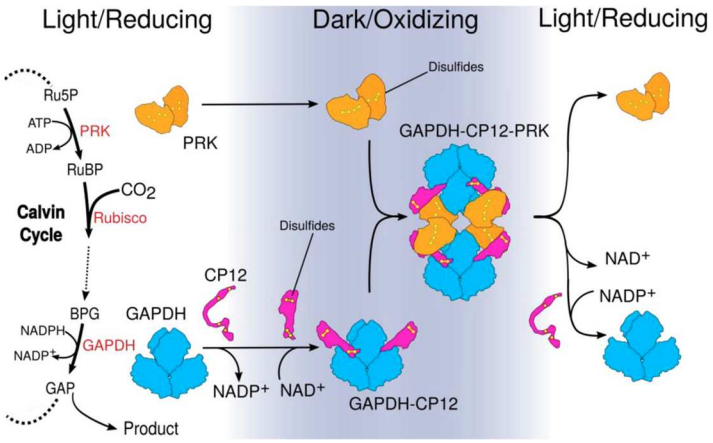

Figure 1:4: Regulation of carbon fixation by forming a redox depending enzyme complex. "GAPDH (blue) activity is at the branch point between regeneration of RuBP or central metabolism. In the dark, the oxidizing environment causes intramolecular disulfide bridges to form within CP12 (pink) and PRK (orange). In parallel $NADP^+$ bound to GAPDH is exchanged for NAD^+. CP12 binds to GAPDH, reducing its activity. Pre-ordered CP12s subsequently recruit PRK, blocking PRK active sites to the substrate and GAPDH active sites to NADP(H). When returning to the light, disulfide reduction by thioredoxin dissociates the complex, releasing GAPDH and PRK" (McFarlane et al. 2019).

The CO_2 fixation by the CBB cycle depends on the redox state of the chloroplast stroma in plants (Buchanan 1980; Scheibe 1991; Geiger and Servaites 1994) and of the thylakoid membrane in cyanobacteria or other photoautotrophic prokaryotes (Wedel and Soll 1998; Peña et al. 2010; Burnap et al. 2015).

PRK catalysis ATP dependent the conversion of ribulose-5P to ribulose-1,5bP. Ribulose-1,5bP is the substrate of Rubisco, which uses ribulose-1,5bP to fix CO_2 and to generate two molecules of 3P-glycerate. 3P-glycerate can in following steps either be further converted to pyruvate via the lower glycolysis or reduced to create glycogen via the gluconeogenesis. Cyanobacteria employ two different glyceraldehyde-3P-dehydrogenases (GAPDHs), GAP1 and GAP2. GAP1 operates exclusively catabolic and is essential for the glycolytic glucose breakdown (Koksharova et al. 1998). However, GAP2 is an essential enzyme of the anabolic CBB cycle, part of the ternary PRK-CP12-GAP2 complex and catalyses the reductive reaction of glycerate-1,3bP to glyceraldehyde 3-phosphate (GAP) generating NADPH.

The basic principle of the PRK-CP12-GAPDH complex is as follows: In the dark, CP12 forms a complex with PRK and GAPDH, which inactivates the CBB cycle. In the light, the enzyme complex dissolves, which leads to an immediate reactivation of the CBB cycle.

In detail, no formation of the PRK-CP12-GAPDH complex will occur with thioredoxins (Maeda et al. 1986; Kamo et al. 1989; Ruelland and Miginiac-Maslow 1999; Collin et al. 2003; López-Calcagno et al. 2014) being reduced by a ferredoxin thioredoxin reductase system (Buchanan 1991; Dai et al. 2004) during light. The reduction leads to an activation of the CBB cycles key enzymes, phosphoribulokinase (PRK) and glyceraldehyde-3-phosphate dehydrogenase (GAPDH, in *Synechocystis,* annotated as GAP2; Ruelland and Miginia-Maslow 1999; Schürmann and Jacquot 2000; Buchanan and Balmer 2005; Schürmann and Buchanan 2008; Michelet et al. 2013). PRK is activated directly by its two disulfides reduced (Thieulin-Pardo et al. 2015). GAPDH, however, does not have any disulfides itself, the redox regulation takes place via the two disulfide bonds of the CP12 protein (Pohlmeyer et al. 1996; Wedel et al. 1997). During oxidized conditions, disulfides bonds between PRK and CP12 are formed. Next, CP12 binds GAPDH, which leads to the inactivation of GAPDH and PRK and stops the CBB cycle and thus also the CO_2 fixation (Howard et al. 2008). Since this enzyme assembly is light/dark dependent and therefore highly dynamic, in light, the disulfide bonds come loose, and PRK and GAPDH reactivate, consequently CO_2 can be fixed again. Studies on *Pea* leaves illustrated the dynamic nature of this process, via a combination of Blue Native PAGE and SDS PAGE. Depending on the incubation in high light or darkness, a shift in band size could be observed. The enzyme complex dissociated or associated within 1min (Howard et al. 2008; López-Calcagno et al. 2014).

1.4.2. The importance of metabolons in the regulation of the primary carbon metabolism

The best example and the first supramolecular complex to be named "metabolon" is the tricarboxylic acid (TCA) cycle (Srere 1985). For mammals, the composition, the catalytic conditions and the tertiary structure of the TCA metabolon were examined in numerous studies (D'Souza et al. 1983; Moore et al. 1984; Vélot et al. 1997; Shatalin et al. 1999). However, in plants, the interactome of the TCA cycle was only recently annotated (Obata 2019). The difficulty in investigating a dynamic metabolon is it being unstable; additionally, results based on one method often produce false-negative results. It became necessary to merge the results of several methods and to reinterpret them. By examining *Arabidopsis* cells via yeast-to-hybrid assays (Y2H), split-luciferase assays (split-LUC), affinity purification mass spectrometry (AP-MS) and green fluorescence protein-(GFP)-tag-based affinity assays; a reliable plant mitochondrial TCA-cycle protein-protein interaction could be mapped (Zhang et al. 2017). The data indicated a metabolic channelling from fumarate to 2-oxoglutarate. ^{13}C-isotopic dilution experiments on isolated potato mitochondria support this result (Zhang et al. 2017).

It is postulated that the TCA cycle of eukaryotes and prokaryotes is based on a malate dehydrogenase (MDH) / citrate synthase (CS) / aconitase (CAN) enzyme interaction. Whether mammals (Srere 2000), bacteria (Meyer et al. 2011) or plants (Fernie et al. 2018) the enzymatic channelling of the TCA cycle is very similar. Substrate channelling is an essential tool for regulating metabolism. Whether primary or secondary metabolism. Therefore, it was unsurprising that Giegé et al. hypothesized in 2003 the glycolysis (hexokinase, aldolase, triosephosphate isomerase, glyceraldehyde 3P-dehydrogenase, phosphoglycerate mutase, enolase, pyruvate kinase) in *Arabidopsis* being organized as a metabolon as well. Further research followed, in which the glycolytic metabolon was also proven in mammal cells, other plants, yeasts and heterotrophic and photoautotrophic bacteria (Taylor et al. 2003; Giegé et al. 2003; Brandina et al. 2006; Graham et al. 2007). Performing protease protection assays and 2D-protein separations, it was possible to detect that glyceraldehyde-3-phosphate dehydrogenase (GAPDH 1), aldolase, phosphoglycerate mutase (PGM) and enolase (ENO) are also localized on the outer and not, as previously discussed, only on the inner mitochondrial membrane. This *in vitro* result was complemented with fluorescence images which also confirmed the localization *in vivo* for the first time (Giegé et al. 2003). Via additional ^{13}C isotopic dilution experiments, it was then confirmed that these enzymes are organized as metabolons (Graham et al. 2007). The binding to the outer mitochondrial membrane was found to be dynamic depending on the respiratory level. It is postulated that the presence of the glycolytic metabolons on the outer membrane made the availability of the substrates (pyruvate) for the TCA cycle more efficient. Metabolons mostly consist of "soluble" enzymes that are bound to a membrane or proteins (Jørgensen et al. 2005). It is known that lipids, depending on their biochemical status, can form "micro-domains" so-called "rafts" which serve as places for the assembly of metabolons (Zajchowski and Robbins 2002).

Such a domain is also provided by the endoplasmic reticulum (ER) membrane. Rafts are used to organize the localization of metabolons. In plants, it has been shown that pathogens have an influence on these rafts resulting in changes of the metabolites localization, controlled and guided by the actin skeleton (Chuong et al. 2004). It has long been assumed that a cytoskeleton only exists in eukaryotes (Alberts et al. 2002). Parallel to the understanding that prokaryotes are not only "sacculi with freely diffusing proteins" (Celler et al. 2013) the assumption that they also have a cytoskeleton was developed. In the meantime, homologous structures have been described for tubulin (Bi and Lutkenhaus 1991), actin (Jones et al. 2001), and intermediate filament proteins (Ausmees et al. 2003) as well as, exclusively prokaryotic structures (Koonin and Aravind 2002; Kühn et al. 2010). The cytoskeleton is discussed being a speedy means of travel, to bring metabolons to the scene of "action". It is highly discussed that carboxysomes play a role in the regulation of enzyme efficiency and substrate channelling (Bobik 2006). They have been identified as the first bacterial polyhedral organelles (Gantt and Conti 1969; Shively et al. 1970) and represent so-called microcompartment (Yeates et al. 2008). The carboxysome is separated from the cytoplasm by a membrane and consists exclusively of proteins (Cannon et al. 2010), which could potentially be a suitable surface for the assembly of enzymes respectively, enzyme complexes or even metabolons. A form of carboxysome mediated enzyme organization has already been demonstrated in *Halothiobacillus neapolitanus*, in which the carboxysome shell carbonic anhydrase (CsoSCA) is attached to the inner protein shell, while the Rubisco is located inside the carboxysomes lumen (Yeates et al. 2008; Cannon et al. 2010; Kerfeld et al. 2010; Agapakis et al. 2012). Recent studies, in the organism *Microcystis aeruginosa* PCC7806 (Barchewitz et al. 2019) also postulate that the carboxysome itself has the potential to assemble and dissemble. *In vivo* fluorescence microscopy studies revealed a migration of Rubisco from the carboxysome to the cytoplasm or thylakoid membrane. The authors speculated that among other factors, the formation of the PRK-CP12-GAPDH complex, the Rubisco delocalization, as well as the oligomerization of the shell proteins, are closely related (Barchewitz et al. 2019)

2. The working hypothesis of this dissertation

2.1. The Entner-Doudoroff pathway plays an essential role in supplying *Synechocystis sp.* PCC 6803 with pyruvate and acetyl-CoA

Chen et al. described the Entner-Doudoroff (ED) pathway in *Synechocystis sp.* PCC 6803, firstly in 2016. So far, it has been postulated that the ED pathway plays an essential role in the regeneration and replenishment of the CBB cycle (Makowka et al. 2020). However, how exactly 6P gluconate for the ED pathway is formed enzymatically and its function as a catabolic pathway, in *Synechocystis*, are not yet fully understood. Initial physiology studies indicated that the ED pathways' entry is catalyzed by a glucose dehydrogenase /gluconate kinase (GDH/GK) pathway (Figure 2:1; Chen et al. 2016). Newest enzyme studies, however, could not detect any enzyme activity for putative GDHs and hypothesized that the entrance of the ED pathway is catalyzed by hexokinase (HK) parallel to the oxidative pentose phosphate (OPP) pathway (Makowka 2019). We hypothesize that *Synechocystis* does not occupy a GDH/GK pathway. To finally clarify the question of how the entry of the ED pathway is organized, hexokinase deletion mutants (*Δhk)* were generated and together with potential glucose dehydrogenase deletion mutants (*Δgdh1Δgdh2)*, physiologically examined. If a functional GDH/GK pathway exists in *Synechocystis*, the deletion of the hexokinase would have to be compensated.

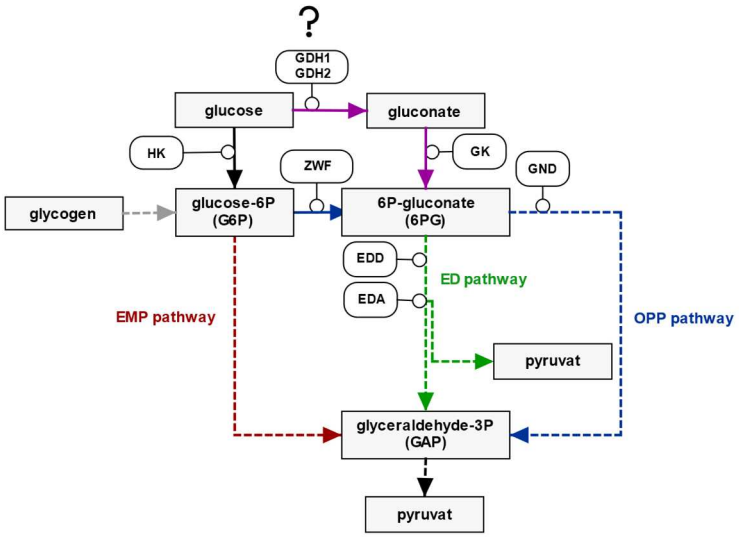

Figure 2:1: Two possible entries of the Entner-Doudoroff (ED) pathway. Simplified scheme of the central carbon metabolism in *Synechocystis*. Purple: Potential (?) entry via the glucose dehydrogenase/gluconate kinase (GDH/GK) pathway. Black: Entrance shared with the oxidative pentose phosphate (OPP) pathway via the hexokinase (HK).

Additionally, it is still unclear whether the ED pathway represents an alternative route that provides pyruvate, when there is no flux through the lower glycolysis (e.g. during gluconeogenesis or Calvin-Benson-Bassham (CBB) cycle replenishing; Figure 2:2 B), and whether or to what extent the pyruvate produced in the ED pathway is required as a precursor for the production of acetyl-CoA (Figure 2:2 A).

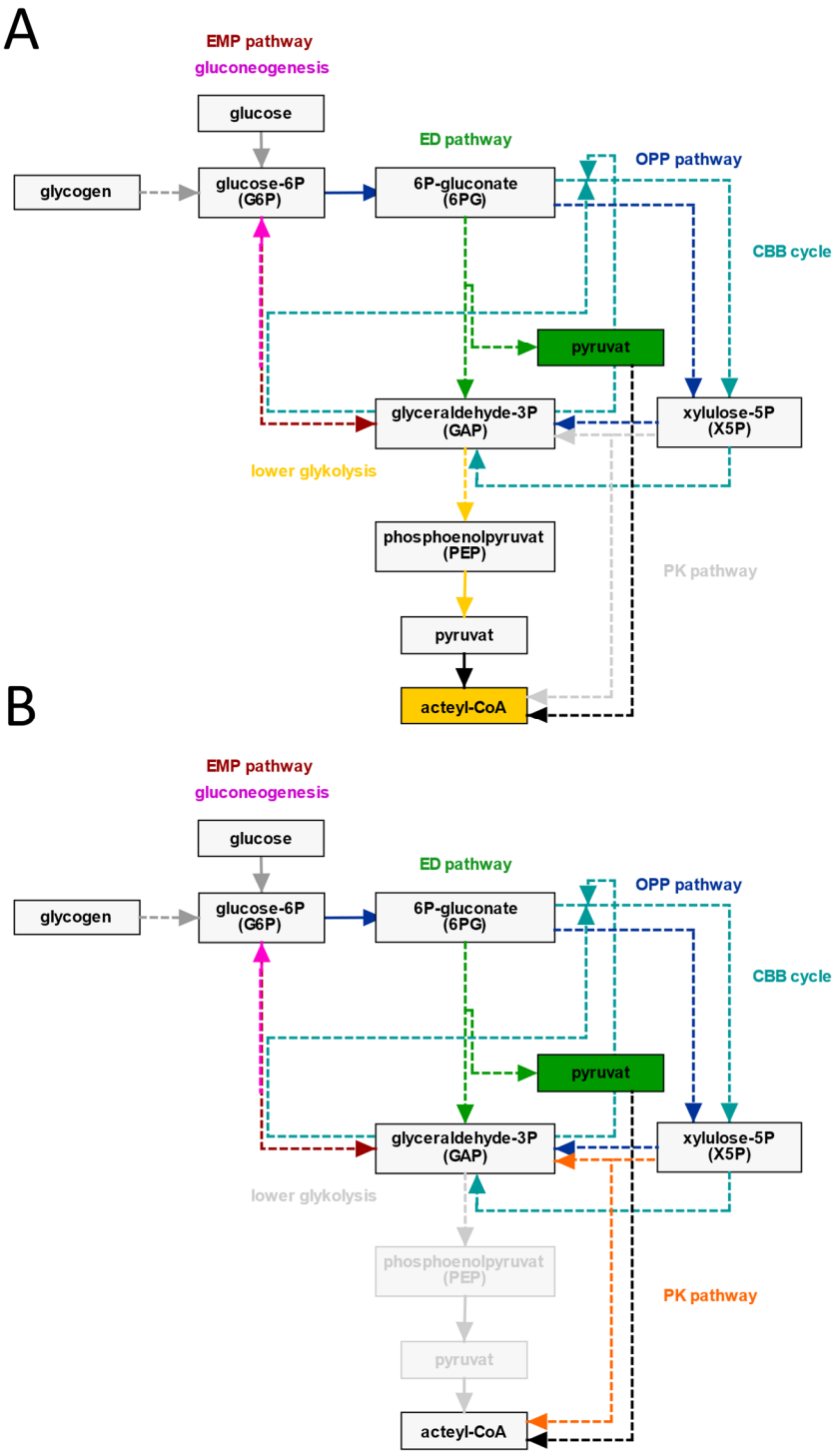

Figure 2:2: Entner-Doudoroff (ED) pathway as an alternative route to provide pyruvate and acetyl-CoA. Simplified scheme of the central carbon metabolism in *Synechocystis*. (A) ED pathway compensates for the phosphoketolase (PK) pathway. (B) ED pathway compensates for the lower glycolysis. OPP: oxidative pentose phosphate, CBB: Calvin-Benson-Bassham, EMP: Emden-Meyerhof-Parnas.

It might be that via the phosphoketolase (PK) pathway, the majority of acetyl-CoA is generated (Alagesan et al. 2013; Anfelt et al. 2015). In *Synechocystis*, the PK- and the ED pathway were only recently detected. Therefore, they are not yet characterized physiologically or enzymatically fully. Regarding the lower glycolysis, the enzymatic process has been well researched, but little is known about the metabolic

relevance of individual enzymes. To clarify the importance of the ED pathway within the catabolic carbon metabolism and to further characterize the PK pathway and lower glycolysis, deletion mutants (*eno/Δeno*, *Δpyk1pyk2/Δpyk2)* of the lower glycolysis and the phosphoketolase (PK) pathway (*Δxfp1Δxfp2*) were generated and physiologically characterized.

2.2. Fluorescence microscopy is a suitable method for *in vivo* imaging dynamics of enzyme assemblies

Especially in photoautotrophic prokaryotes, metabolons, substrate channels, and enzyme clusters might be crucial features to regulate the metabolic flux and to compensate for lacking cellular compartmentalization. The prime example of how efficiently the metabolism can be regulated via such enzyme complex is the ternary PRK-CP12-GAPDH enzyme complex, which regulates the CO_2 fixation light-dependent. Numerous *in vitro* studies in which the enzymes were characterized, purified and structurally modelled (Pohlmeyer et al. 1996; Wedel et al. 1997; McFarlane et al. 2019), as well as in which flux analyses (Howard et al. 2008) were carried out, and the localization was examined via immunoelectron microscopy (Agarwal et al. 2009), assume a light-dependent dynamic of the PRK-CP12-GAPDH enzyme complex. However, *in vivo*, the assembly and disassembly of the light-dependent enzyme complex have not yet been demonstrated.

We hypothesize that the PRK-CP12-GAP2 complex assembly and disassembly can be detected by fluorescence microscopy. This approach should serve as a "proof of principle" of fluorescence microscopy as a suitable method to investigate *in vivo*, the organization and dynamics of enzyme complexes as well as a positive control for further experiments investigating the organization and dynamics of anabolic and catabolic enzymes of the central carbon metabolism.

Since it has been discovered that glycolytic pathways as the Entner-Doudoroff (ED), oxidative pentose phosphate (OPP) and Emden-Meyerhof-Parnas (EMP) pathway do not only exist for breaking down glucose to pyruvate and acetyl-CoA, and also function as so-called glycolytic shunts under photoautotrophic conditions replenishing the Calvin-Benson-Cycle CBB cycle (Makowka et al. 2020), the question arises how this process is organized enzymatically. Photomixotrophically, the cell has a high supply on bioavailable carbon, bound in the form of CO_2 by the Rubisco of the CBB cycle and by the breakdown of glucose via the glycolytic pathways. Therefore, we hypothesize that the key enzymes of the CBB cycle and the glycolytic enzymes of the ED, OPP, and EMP pathway could also be organized in light and glucose-dependent manner via enzyme complex assemblies.

3. Aim of this dissertation

(i) Experimental confirmation that the Enter-Doudoroff (ED) pathway exclusively branches off the oxidative pentose phosphate (OPP) pathway and does not additionally result from a flux via the glucose dehydrogenase/gluconate kinase (GDH/GK) pathway in the cyanobacterium *Synechocystis sp.* PCC 6803.

(ii) Characterization of the physiological role of the phosphoketolase (PK) pathway in the cyanobacterium *Synechocystis sp.* PCC 6803.

(iii) Characterization of the physiological role of the lower glycolysis in the cyanobacterium *Synechocystis sp.* PCC 6803.

(iv) Establishing fluorescence microscopy as a suitable method to investigate the organization and dynamics of enzyme complexes *in vivo.*

(v) Experimental analysis concerning dynamic processes in the organization of anabolic and katabolic key enzymes in *Synechocystis sp.* PCC 6803.

4. Material and Methods

4.1. Material

4.1.1. Chemicals, medium and buffers

Used chemicals were purchased from Roth (Karlsruhe, Germany), Merck (Darmstadt, Germany), Sigma Aldrich (Steinheim, Germany) and Macherey-Nagel (Düren, Germany). The Kniese tubes were obtained from Erich Eydam KG (Kiel, Germany). Water for preparation of buffers and solutions was ultra-purified by a lab water purification system (Purelab Chorus 1, Elga Labwater, Celle, Germany).

4.1.2. Cultivation media

BG11 medium was used to cultivate *Synechocystis*. LB medium was used to cultivate *E. coli*. Both media were used autoclaved (120°C for at least 20 min).

4.1.2.1. BG11 and LB medium

Six stock solutions were used to produce the BG11 medium. BG11, $MgSO_4$, K_2HPO_4, TES, $FeNH_4$ citrate and sodium sulfate (Table 4.1). The substances were dissolved in autoclaved H_2O. Thereafter, the BG11, nathiosulfate, $MgSO_4$ and K_2HPO_4 stock solutions were autoclaved. The TES and $FeNH_4$ citrate stock solutions were sterile filtered. TES was stored at 4°C. The remaining solutions were stored at room temperature. All solutions were always opened sterile.

To produce the final BG11 liquid medium, the BG11, $MgSO_4$, K_2HPO_4 and TES stock solutions were brought to the desired final concentration with the appropriate amount of autoclaved H_2O and were autoclaved. $FeNH_4$ citrate was added after autoclaving. To produce BG11 agar, $FeNH_4$ citrate was added to the medium before autoclaving. In addition, the medium was mixed with nathiosulfate and the appropriate amount of Bacto-Agar (Table 4.2).

To produce LB medium, all ingredients (Table 4.3) were dissolved in autoclaved H_2O and autoclaved. To produce LB agar plates, the appropriate amount of Bacto-Agar (Table 4.4) was added to the medium before autoclaving.

The freshly autoclaved agar media were immediately poured into sterile Petri dishes. Optional for all media, was the addition of sterile-filtered antibiotics and glucose (Table 4.2; Table 4.4).

Table 4.1: BG11-medium: Ingredients and their concentration.

solutions	ingredient	end conc.
BG11	$CaCl_2$	0.245 mM
	Citric acid	31.2 µM
	$Co(NO_3)_2$	0.17 µM
	$CuSO_4$	0.32 µM
	H_3BO_3	46.3 µM
	$MnCl_2$	9.1 µM
	Na_2CO_3	0.189 mM
	Na_2EDTA	2.79µM
	Na_2MoO_4	1.61 µM
	$NaNo_3$	17.6 mM
	$ZnSO_4$	0.77 mM
$MgSO_4$		0.304 mM
K_2HPO_4		0.175 mM
TES	N-Tris(hydroxymethyl)methyl-2-amoniethane sulfonic acid	5 mM
$FeNH_4$ citrate		22.8 µM
nathiosulfate		1mM

Table 4.2: BG11-medium: Supplements used in medium and agar are listed with relevant concentrations.

supplement		concentration
Bacto-Agar (for agar plates)		15 g/L
$Na_2S_2O_3$ (for agar plates)		1 mM
Glucose		10 mM (for medium)
Kanamycin	Km^R	50 mg/L
Spectinomycin	$Spec^R$	20 mg/L
Chloramphenicol	Cm^R	20 mg/L
Erythromycin	Em^R	25 mg/L
Gentamycin	Gm^R	5 mg/L (for agar plates) 2.5 mg/L (for medium)

Table 4.3: LB-medium: Ingredients and their concentration.

ingredient	concentration
Yeast extract	5 g/L
Tryptone	10 g/L
NaCl	10 g/L

Table 4.4: LB-medium: Supplements used in medium and agar are listed with relevant concentrations.

supplement		concentration
Bacto-Agar (for agar plates)		15 g/L
Ampicillin	Amp^R	100 mg/L
Kanamycin	Km^R	50 mg/L
Spectinomycin	$Spec^R$	20 mg/L
Chloramphenicol	Cm^R	20 mg/L
Erythromycin	Em^R	25 mg/L
Gentamycin	Gm^R	10 mg/L

4.1.3. Enzymes

Table 4.5: Polymerases used in this work.

enzymes	activity	supplier
Phusion DNA polymerase	2,5 U/µl	Thermo Fisher Scientific (Waltham, USA)
Dream Taq DNA polymerase	5 U/µl	

Table 4.6: Fast Digest restriction enzymes used in this work. Specific recognition sites were marked with a caret in sequence.

enzymes		activity	supplier
EcoR Ⅰ	G'AATTC	10 U/µl	Thermo Fisher Scientific (Waltham, USA)
EcoR Ⅴ	GAT'ATC	10 U/µl	
Hind Ⅲ	A'AGCTT	10 U/µl	
Xho Ⅰ	C'TCGAG	10 U/µl	
Pvu Ⅱ	CAG'CTG	10 U/µl	
Nde Ⅰ	CA'TATG	10 U/µl	
Sma Ⅰ	CCC'GGG	10 U/µl	
Nhe Ⅰ	G'CTAGC	10 U/µl	
BamH Ⅰ	G'GATCC	10 U/µl	

4.1.4. Oligonucleotides

Oligonucleotides, also called primers, are short DNA fragments that bind specifically to single-stranded DNA. Within the polymerase chain reaction (PCR), the primer pair thus defines the DNA section to be amplified. All oligonucleotides were manually designed and ordered from Sigma Aldrich (Steinheim, Germany). All Primers were diluted in sterile H_2O to a final concentration of 5µM. Sequencing primers were labelled "seq" or listed separately under sequencing primers. The other primers were used to produce the desired PCR product, like upstream and downstream regions of selected genes to knock-out or to amplify the antibiotic cassettes.

4.1.4.1. Knock-out mutants

Table 4.7: Primers designed and used in this work for generating knock-out mutant strains. The term "seq" defines primer used for checking the segregation level.

strain	primer	primer sequence (5' to 3')	$T_{Annealing}$
Δhk (sll0593)	GLK sll0593 FWD (1)	CTATAGGGCGAATTGGGTACCATTGGCCAAAAATAGCGCAAA	56°C
	GLK sll0593 REV (1)	CACCGGATCCCCGGGAATTCGGCCCCAAAGCCATTGAAAA	56°C
	GLK sll0593 FWD (3)	CACCGGATCCCCGGGAATTCGAAGTGGACATTTTTAGTTGTTAACTTTGC	56°C
	GLK sll0593 REV (3)	AGGGAACAAAAGCTGGAGCTCCAACACCCCTGGTCTTTGG	57°C
	Spec-cassette FWD_glk	TTTTCAATGGCTTTGGGGCCGAATTCCCGGGGATCCGGTG	59°C
	Spec-cassette REV_glk	CAACTAAAAATGTCCACTTCGAATTCCCGGGGATCCGGTG	59°C
Δpyk1 (sll0587)	PYK1_FOR_seq	GTCACCTGTGGGGGCATTACC	59°C
	PYK1_REV_seq	TATCTGCGCTGTTAGCTTGGCTAAC	59°C
	Cm-FOR	CTGCAGGAATTCGATATTATTGAAGCATTTATCAGGGTTATTGTCTCAT	64°C
	Cm-REV	AAGCTTGATGGCGGCACCTCGCTAA	65°C
pyk2/ Δpyk2 (sll1275)	PYK2_FOR_seq	TCCTTTAACAACGTCAACTGAGCGG	60°C
	PYK2_REV_seq	AGGAAAGCCAGCCCAATAGTCCG	60°C
	EmR_FOR	TCTAGATTACTTATTAAATAATTTATAGCTATTGAAAAGAGATAAGAATTGTTCA	58°C
	EmR_REV	GTCGACGAAAAAAGAAATTAGATAAATCTCTCATATCTTT	58°C
Δxfp1 (slr0453)	XFP slr0453 FWD (1)	CTATAGGGCGAATTGGGTACAACTCAACATCAGTGAAGAG	49°C
	XFP slr0453 REV (1)	CACCGGATCCCCGGGAATTCAAGTTATTTTGGCGTTAACC	49°C
	XFP slr0453 FWD (2)	CACCGGATCCCCGGGAATTCCCTTAACTAAAATCCCTGACAT	50°C
	XFP slr0453 REV (2)	AGGGAACAAAAGCTGGAGCTGAGTGGGGAAGAAACCCAAG	54°C
	xfp1	AACTCAACATCAGTGAAGAGGAATTGG	57°C
	xfp2	GAGTGGGGAAGAAACCCAAGAATTAG	57°C

Δxfp2 (sll0529)	XFP2_FOR_seq_2	TTTAAAGTCCCCCAAACTTGCCGGAGCTTTAGTGAGGAGATTT	68°C
	XFP2_REV_seq_2	GCAGTTCGGAACAATGGATGGCGGAATATTGGAAAAAGTTACAGAGTT	68°
	Kan-seq_FOR	AAGCCACGTTGTGTCTCAAAATCTCTGATGTTACATTGC	65°C
	Kan-seq_REV	CTGAGGTCTGCCTCGTGAAGAAGGTGTTGC	66°C
eno/Δeno (slr0752)	ENO-seq_FOR	GTCAAGATTTGTTGTTTTCTGCCCAGGCCTATCTCAA	65°C
	ENO-seq_FOR	CAAGTTAAGGTCATTGCTTCCTTGGCTTAGAACGG	64°C
	Cm-FOR	CTGCAGGAATTCGATATTATTGAAGCATTTATCAGGGTTATTGTCTCAT	64°C
	Cm-REV	AAGCTTGATGGCGGCACCTCGCTAA	65°C
putative Δgap1^{KmR} (slr0884)	GAP1 slr0884 FWD (1)	CTATAGGGCGAATTGGGTACATCTGGACATATCACAACCCACA	55°C
	GAP1 slr0884 REV (1)	CCCCCCCCCCCCTGCAGGTCACCAGGACATCCGACTTGCC	58°C
	GAP1 slr0884 FWD (2)	CCCCCCCCCCCCTGCAGGTCGTTTGGTATTTGTTAAGTTATCAAGCCC	55°C
	GAP1 slr0884 REV (2)	AGGGAACAAAAGCTGGAGCTCCGATCAACTGTTGATGTTAGTTGT	56°C
	KM-cassette FWD	GGCAAGTCGGATGTCCTGGTGACCTGCAGGGGGGGGGGGG	67°C
	KM-casette REV	AACTTAACAAATACCAAACGACCTGCAGGGGGGGGGGGG	67°C
putative Δpgam1 (slr1945)	PGAM1-seq_FOR	ATAGTAGTTTTAAACCATATCTAACGGATAGCGTGGTGCAACA	64°C
	PGAM1-seq_REV	TTGAGGGTTTTCTCTGCACTTTTGGCACTGG	64°C
	EmR_FOR	TCTAGATTACTTATTAAATAATTTATAGCTATTGAAAAGAGATAAGAATTGTTCA	58°C
	EmR_REV	GTCGACGAAAAAAGAAATTAGATAAATCTCTCATATCTTT	58°C
putative Δpgam2 (sll0395)	PGAM2-seq_FOR	CAAAACAATCAAATTTGAGAATATTTTGCCTGGG	59°C
	PGAM2-seq_REV	ACTCATGGCAAACTAGGCGATCGCATAGC	64°C
	Kan-seq_FOR	AAGCCACGTTGTGTCTCAAAATCTCTGATGTTACATTGC	65°C
	Kan-seq_REV	CTGAGGTCTGCCTCGTGAAGAAGGTGTTGC	66°C

4.1.4.2. *Fluorescence mutants*

Table 4.8: Primers designed and used in this work for checking the segregation level.

tagged protein	primer	primer sequence (5' to 3')	$T_{Annealing}$
EDA (sll0107)	EDA-seq_FOR_6	AAGGTCCCCTCGGCCAAATTCCCCTTATTCCCA	68°C
	EDA-seq_REV_6	TTGAATACTCTAATGGTTTGATGTCCGAAAAAGTCTAGTTTCTTCTATTCTTCGACCA	66°C
EDD (slr0452)	EDD_seq_FOR_3	CCTTGGTGCAAGAGGGGGATCAAATCACCATCGATGCT	69°C
	EDD_seq_REV_3	GAACAAGTCTATATCAGTCACTGCACCAAGGCTGCTGGAGGAAACT	69°C
GAP1 (slr0884)	GAP1-seq_FOR	GAATTTTGGGCTACACAGCAGATGATGT	60°C
	GAP1-seq_REV	GTTGTCCTCCTTGTCCCTGGTATTTTG	60°C

GAP2 (sll1342)	GAP2-seq_FOR_3	TTAAAGGAGTGTTGGAATACACCGATTTGG	59°C
	GAP2-seq_REV_3	ATGGGGAAAGTTTCGCCGGG	59°C
GND (sll0329)	GND-seq_FOR	GGCGAGAAGTGTTGATGCTGGC	59°C
	GND-seq_REV	CCTCGCAAACTTTCCCTCCAAACTT	60°C
PRK (sll1525)	PRK-seq_FOR	TAGAGGAAATGGTTTATGTGGAAAACCACC	59°C
	PRK-seq_REV	GGCATCATTATCCTCCCCAGAAATAAGC	59°C
ZWF (slr1843)	ZWF-seq_FOR	TAGATTGTATGTTGGGAGACCAAACCCTG	60°C
	ZWF-seq_REV	GTTGTCTAGCGCCTCGAATACGGA	61°C

4.1.4.3. Sequencing primer

Table 4.9: Sequencing primer designed and used in this work.

primer	primer sequence (5' to 3')	$T_{Annealing}$
M13_FOR	GTAAAACGACGGCCAGT	52°C
M13_REV	AGGAAACAGCTATGACCA	50°C
EmR-seq_REV	AATTAGATAAATCTCTCATATCTTTTATTCAATAATCGCATCCGATT	60°C
GmR-seq_REV	TTAGGTGGCGGTACTTGGGTCG	60°C

4.1.5. Bacteria and plasmids

Synechocystis is a unicellular bacterium which was examined in this work under autotrophic (light), mixotrophic (light, glucose) and heterotrophic (dark, glucose) conditions. Once the desired PCR product was amplified, it was introduced into a suitable cloning vector. In this work, mutants were generated using the pBluescript (pBs) or pUC57-Simple (pUC57) (Table 4.11; Table 4.13) vector.

The vectors were cloned via two methods. Some knock-out mutants were generated by Gibson assembly. For this procedure, the pBluescript cloning vector was used. The other part of the knock-out vector was generated by classic restriction and ligation into a customized pUC57-Simple vector, already including the gene-specific up- and downstream sequence.

Table 4.10: Cloning vectors used in this work.

plasmid	target organism	supplier
pBluescript	*E.coli*	Genscript Biotech (New Jersey, USA)
	Synechocystis	
pUC57-Simple	*E.coli*	
	Synechocystis	

4.1.6. Cyanobacteria strains

Synechocystis sp. PCC 6803 (glucose tolerant)

4.1.6.1. Mutants with single deletion

Table 4.11: Single knock-out mutant strains listed with their gene deletion, antibiotic resistance cassette and receiver plasmid.

strain	deleted genes	gene	AB	plasmid	reference
Δeda	KDPG-Aldolase	sll0107	Gm^R	pBs	Chen et al. 2016
eno/Δeno	Enolase	slr0752	Cm^R	pUC57	this thesis
Δgap1	Glyceraldehyde-3-phosphate dehydrogenase	slr0884	Cm^R	pBs	Spengler 2019 (unpublished)
putative gap1^{KmR}	Glyceraldehyde-3-phosphate dehydrogenase	slr0884	Km^R	pBs	this thesis
Δgdh1	Glucose-dehydrogenase 1	sll1709	Gm^R	pBs	Chen et al. 2016
Δgdh2	Glucose-dehydrogenase 2	slr1608	Km^R	pBs	Schreiber 2016
Δgnd	6-Phosphoglucinate dehydrogenase	sll0329	Em^R	pBs	Chen et al. 2016
Δhk	Hexokinase	sll0593	$Spec^R$	pBs	this thesis
putative pgam1	Phosphoglycerate mutase 1	slr1945	Em^R	pUC57	this thesis
putative pgam2	Phosphoglycerate mutase 2	sll0395	Km^R	pUC57	this thesis
Δpyk1	Pyruvate kinase 1	sll0587	Cm^R	pUC57	this thesis
pyk2/Δpyk2	Pyruvate kinase 2	sll1275	Em^R	pUC57	this thesis
Δxfp1	Phosphoketolase 1	slr0453	$Spec^R$	pBs	this thesis
Δxfp2	Phosphoketolase 2	sll0529	Km^R	pUC57	this thesis
Δzwf	Glucose-6-phosphate dehydrogenase	slr1843	Cm^R	TOPO	Chen et al. 2016

4.1.6.2. Mutants with multiple deletions

Table 4.12: Multiple knock-out mutant strains listed with their gene deletion.

strain	reference
ΔedaΔgnd	Makowka et al. 2020
ΔedaΔzwf	Makowka et al. 2020
eno/ΔenoΔeda	this thesis
eno/ΔenoΔedaΔxfp1	this thesis
eno/ΔenoΔedaΔxfp1Δgap1	this thesis
ΔgndΔzwf	this thesis
ΔgndΔzwfΔeda	this thesis
ΔhkΔgdh1	this thesis
ΔhkΔgdh1Δgdh2	this thesis

Δhk Δgdh2	this thesis
putative Δpgam1 Δpgam2	this thesis
Δpyk1 pyk2/Δpyk2	this thesis
Δpyk1pyk2/Δpyk2Δeda	this thesis
Δpyk1pyk2/Δpyk2Δedagap1 ^{KmR}	this thesis
Δpyk1pyk2/Δpyk2gap1 ^{KmR}	this thesis
Δxfp1Δxfp2	this thesis
Δxfp1Δxfp2Δeda	this thesis
Δxfp1Δxfp2ΔedaΔgap1	this thesis
Δxfp1Δxfp2Δgap1	this thesis
Δxfp1Δxfp2Δgap1	this thesis
Δxfp1Δxfp2Δpyk1Δpyk2	this thesis

4.1.6.3. Fluorescence mutants

Table 4.13: Fluorescence mutant strains listed with their gene number, type of fluorophore, antibiotic resistance cassette and receiver plasmid.

strain	gene number	fluorophore	tag	vector	AB	reference
EDA GFP-His	sll0107	eGFP	His	pUC57-Simple	Em^R	this thesis
EDA YFP-His		YFP			Gm^R	
EDD GFP-His	slr0452	eGFP			Em^R	
EDD YFP-His		YFP			Gm^R	
GAP1 GFP-His	slr0884	eGFP			Em^R	
GAP1 YFP-His		YFP			Gm^R	
GAP2 GFP-His	sll1342	eGFP			Em^R	
GAP2 YFP-His		YFP			Gm^R	
PRK GFP-His	sll1525	eGFP			Em^R	
PRK YFP-His		YFP			Gm^R	
GND GFP-His	sll0329	eGFP			Em^R	
GND YFP-His		YFP			Gm^R	
ZWF GFP-His	slr1843	eGFP			Em^R	
ZWF YFP-His		YFP			Gm^R	

4.1.6.4. Escherichia coli

Table 4.14: Competent cell strains used in this work.

Strain	Reference
KRX	Promega (Madison, Wisconsin, USA)
dH5α	

4.2. Molecular biological methods

4.2.1. Polymerase Chain Reaction (PCR)

The Polymerase chain reaction (PCR) is a method to amplify DNA fragments (Table 4.15). The PCR can be sectioned into denaturation, annealing and ligation. The annealing temperature ($T_{Annealing}$) depends on the GC percentage share and the length of the individual primer. The primer pair were thus designed, that the $T_{Annealing}$ is approximately identically to each other. $T_{Annealing}$ was calculated using the online software benchling (Benchling Inc; San Francisco, California) according to the Sanatalucia1999 algorithm (Bommarito et al. 2000). If non-optimal PCR products were amplified with the calculated $T_{Annealing}$, gradient PCRs were carried out to determine the optimal $T_{Annealing}$.

Table 4.15: Pipetting and temperature schemata for PCRs with the DreamTaq polymerase and the Phusion polymerase used in this work.

standard PCR (DreamTaq)						fusion PCR (Phusion)			
	5min	95°C	3.0µl	DNA	5µl	95°C	30sec		
	30sec	95°C	11.5µl	H_2O	28,5µl	98°C	30sec		
34x	30sec	$T_{Annealing}$	1.0µl	dNTPs	1.0µl	$T_{Annealing}$	1min	x 34	
	30sec	68°C	0.5µl	Polymerase	0.5µl	72°C	1min		
	5min	68°C	2.0µl	Buffer	10.0µl	72°C	10min		
	∞	12°C	1.0µl	Forward Primer	2.5µl	12°C	∞		
			1.0µl	Reverse Primer	2.5µl				
			∑20µl		∑50µl				

4.2.2. Gibson assembly

Gibson assembly is a method of generating and replicating DNA and enables the assembly of multiple overlapping DNA fragments in a single isothermal reaction (Gibson et al. 2009). The NEBuilder Hifi DNA Assembly Cloning Kit was used (New England Biolabs, Frankfurt am Main, Germany). This "Gibson mixture" is composed of a 5' exonuclease, a DNA polymerase and a DNA ligase. The exonuclease digests DNA fragments, creating single-stranded DNA overhangs. The fragments to be ligated to one another require complementary overhangs of at least 25bp. The DNA polymerase then fills the gaps in the annealed fragments. In the last step, the DNA ligase closes the gaps between the annealed

DNA fragments. This tool enables fragments to be inserted directly into a vector. For this, the vector was linearized and purified. The fragments for annealing were amplified via PCR (4.2.1). To achieve a higher rate of Gibson assembly, the fragments could also be gel purified. Fragments (1µl with a concentration of ~100ng per fragment) and the linearized vector were mixed in a 1:1 ratio. The total volume was determined to be 5µl by adding sterile H_2O. 15µl of the Gibson mixture (Table 4.16) were pipetted for each reaction. The reaction was initiated incubating at 50°C for 1-4h.

Table 4.16: Reagents of a Gibson assembly.

buffers	composition
5xisothermal reaction buffer (stored at-20°C	3ml 1M Tris/HCl pH 7.5, 150µl 2M $MgCl_2$, 60µl 100mM dGTP, 60µl 100mM dATP, 60µl 100mM dTTP, 60µl 100mM dCTP, 300µl 1M DTT, 1,5g PEG8000, 300µl NAD 100mM in 6ml H_2O
Gibson mixture	320µl 5xisothermal reaction buffer, 0.64µl T5 Exonuclease (10U/µl), 20µl Phusion DNA Polymerase (2U/µl), 160µl Taq DNA Ligase (40U/µl) and 699.4µl H_2O

4.2.3. *Synechocystis* C-terminal protein tagging toolkit: Generation of fluorescence mutants

To generate *Synechocystis* sp. PCC 6803 mutants in which a protein of interest is C-terminally tagged with fluorescence tag, a mutagenesis vector (Figure 4:1) was generated that harbored the following elements: About 250bp upstream of the site of insertion, typically the gene of interest (GOI) (Table 4.13), without the STOP codon (end of GOI), the sequence to be inserted into the genome (including a STOP codon) (Table 4.13, tagging cassette) and at least 250bp downstream of the site of insertion (Table 4.13, downstream). While the end of the GOI and the downstream sequence were always specific for the protein of interest, to allow for homologous recombination into the cyanobacterial genome to occur, the sequence to be inserted was independent of the protein of interest and among other elements contains the tag and a selection marker (Table 4.13).

The *Synechocystis* protein tagging toolkit was developed and designed by Dr. Marko Böhm and serves as a donor vector for the multiple fluorescence tags and an antibiotic resistance cassette. Additional features are a linker region with a TEV cleavage site that allows for the tag to be enzymatically cleaved from the target protein. Tagging cassettes can be excised with BamHI and EcoRI restriction enzymes (Table 4.6) and after gel extraction be used for a ligation reaction into the recipient vector.

The outlined strategy employs classic molecular biology techniques where unique restriction enzyme sites are used to excise a tagging cassette and insert them into a similarly prepared recipient or target vector. Since gene synthesis has become increasingly affordable, the recipient vector (pUC57-Simple, Table 4.10) containing the flanking elements and desired restriction sites in between, have been synthesized from Genscript (New Jersey, USA).

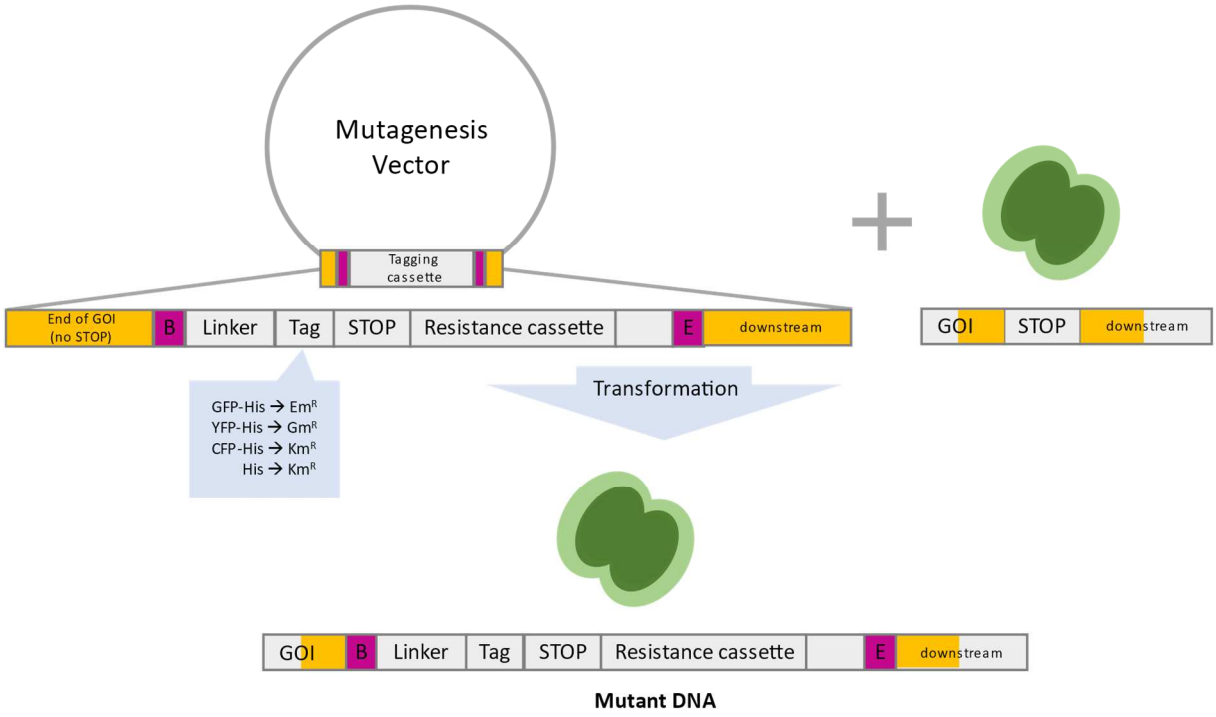

Figure 4:1: Scheme for the generation of a mutagenesis vector. The tagging cassette is enzymatically excised from a toolkit vector using BamHI and EcoRI restriction enzymes. The target or recipient vector contains the flanking sequences and BamHI and EcoRI restriction in between so that after ligation a mutagenesis vector that is specific for a protein of interest and harbours a specific tag / antibiotic resistance cassette combination is obtained. The mutagenesis vector is incorporated into the cyanobacterial genome by homologous recombination. The yellow boxes represent the DNA sequences that are matching, (gene of interest (GOI) and downstream sequence of GOI) and where homologous recombination occurs.

4.2.4. Restriction digestion

Restriction enzymes were used to cut plasmid DNA at specific base motifs, so-called recognition sites. This allowed DNA fragments to be introduced into the vector either via Gibson cloning or classic ligation. All the enzymes used were Thermo Scientific™ FastDigest Restriction enzymes obtained from Fermentas (Thermo Scientific™, Life Technologies GmbH, Germany). The digestion was always checked using gel electrophoresis (4.2.7).

4.2.5. High-copy plasmid DNA preparation from *E.coli*

To carry out a high-copy plasmid DNA preparation (Miniprep) from *E. coli*, a single colony was inoculated in 5ml LB medium (Table 4.3). With the addition of the appropriate antibiotic(s) (Table 4.4), the cells were incubated overnight at 37°C, 180rpm shaking. After a maximum of 12 hours of incubation, the cells were harvested, and the plasmids were isolated. High-copy plasmid DNA preparations from *E. coli* were performed using the NucleoSpin Plasmid Kit (Macherey-Nagel, Düren, Germany) according to the manufacturer's instructions (see Plasmid DNA purification User manual 2017, Rev. 10, p.15).

4.2.6. DNA sequencing

The sequencing (Sanger et al. 1977) of DNA and plasmids was carried out by the Institute for clinical molecular biology (IKMB) (Kiel, Germany) and the Genewiz (Leipzig, Germany).

4.2.7. Agarose-gel electrophoresis

Agarose gel electrophoresis is a method to separate DNA fragments according to their size. In this work, 0.8% agarose gels were used. A large gel chamber held a volume of approx. 150µl. 1.2µl of purified agarose was boiled in 150µl TBE buffer (Table 4.17) and then mixed with 1µl/ml ethidium bromide. Then the still hot and liquid agar-TBE-ethidium bromide mix was poured into the gel chamber. It was important to avoid air bubbles. The gel took about 20min to cool down and set. It is generally recommended to use freshly made gels. The gels could be stored for a maximum of 2 days in TBE buffer mixed with ethidium bromide at room temperature. Samples were loaded in the wells after the addition of 0.2 volumes (v/v) of 5 x loading buffer (Table 4.17). GeneRuler™ 1kb DNA Ladder (Thermo Scientific™, Life Technologies GmbH, Germany) was used to calibrate the size, and 1ng/µl λ-DNA/HindIII marker (Thermo Scientific™, Life Technologies GmbH, Germany) was utilized to determine the DNA concentration of the sample. Electrophoresis was performed with power supply at 5V/cm (High Voltage Power Pack P30, Biometra, Goettingen, Germany) for 50min. DNA could be visualized by using a UV light (TF 20 M Vilber Lourmat, Torcy, France) and photographs were taken by a PC connected live camera (EOS 2000D, Canon, Japan).

Table 4.17: Buffers and its composition used for agarose gel electrophoresis.

buffers	composition
TBE	890mM Tris (pH 8.3), 890mM H_3BO_3, 25mM Na_2EDTA, dissolved in H_2O
5x DNA loading buffer	50% (v/v) glycerol, 50% (v/v) 10x buffer TBE, 0.2 mg/ml bromophenol blue

4.2.8. Gel purification

DNA fragments from agarose gels were purified using the high pure PCR product purification kit (Roche, Mannheim, Germany) according to the manufacturer's instructions. The eluted DNA was then stored at -20°C.

4.2.9. Preparation of competent cells

The production of competent cells using rubidium chloride was carried out using the protocol of (Green and Rogers 2013). All buffers were sterile filtered beforehand. Particular attention had to be paid to a sterile working method. First, a single colony was inoculated from an LB agar plate in 2.5ml LB medium and incubated overnight at 37°C in a shaker at 180rpm. The next day the whole culture was used to inoculate 250ml LB medium containing 20mM $MgSO_4$. The cells were incubated in a 1l baffle flask until the OD A_{600} reached 0.4-0.6 (after approximately 2-3h). The cells were then centrifuged at 4,500g for 5min at 4°C (Sorvall GSA, Beckman JA-14). The supernatant was discarded. The cell pellets were then carefully resuspended in 0.4 volumes of ice-cold TFB1 (Table 4.18) of the total volume. 100ml TFB1 were used for 250ml cell culture. For the following steps, the cells were kept on ice and work was carried out in the cooling chamber at 4°C. The cells were incubated on ice for 5min. Then centrifuged again at 4,500g for 5min at 4°C. The supernatant was discarded. The cells were carefully resuspended in 1/25 of the original cell culture volume in ice-cooled TFB2 (Table 4.18). Accordingly, 10 ml TFB2 were used for 250ml culture. The cells were then incubated on ice for 15-60min and aliquoted in 50µl portions in Eppendorf tubes. To be able to store the aliquots for a long time, the tubes were then frost-frozen in liquid nitrogen and stored at -80°C.

Table 4.18: Buffers for preparation of competent cells.

buffers	composition
TFB1	30mM potassium acetate, 10mM $CaCl_2$, 50mM $MnCl_2$, 100mM RbCl, 15% glycerol, dissolved in H_2O, pH 5.8 (careful titration required)
TFB2	10mM MOPS, 75mM $CaCl_2$, 10mM RbCl, 15% glycerol, dissolved in H_2O pH 6.5

4.2.10. Transformation of *E.coli*

The transformation is a non-viral transfer of DNA into competent bacterial cells (4.2.9, Table 4.14). For this purpose, 1µl (~1µl) of the gel-purified plasmid was pipetted into 50µl competent cells and incubated on ice for 20 min. To make the bacterial membrane porous and thus more permeable to the DNA, the cells were subjected to a heat shock at 47°C for 45sec. Next, the cells were incubated on ice for 2min. After adding 600µl LB-medium (Table 4.3), the cells were incubated for at least 45min at 37°C in a preheated shaker at 180rpm. The cells were then plated out on the corresponding selection plates.

4.2.11. Transformation of *Synechocystis* and segregation of mutants

Synechocystis sp. PCC 6803 is a naturally competent cyanobacterium. This means that external homologous, as well as heterologous DNA, can be taken from the environment (Barten and Lill 1995). This ability is used to insert DNA into *Synechocystis* and to integrate it into the genomic DNA via homologous recombination and thus to produce mutants.

Synechocystis cells were grown in Kniese tubes (Eydam, Kiel, Germany) to an optical density of at least OD_{750} 1.0 in 250ml BG-11 medium (Table 4.1). The cultivation conditions corresponded to the normal autotrophic conditions (4.4.2). 250ml of the culture was used for a maximum of three transformations and was no older than four days. In the next step, the cells were pelleted by centrifuging at 8000g for 5min at room temperature and resuspended in 1.0ml of BG-11 medium (Centrifuge 5804R, Eppendorf). 200-300µl cell culture was mixed with 20µl (6-18µg) concentrated plasmid DNA and incubated on a shaker at 28°C, 180rpm for at least 6h. The cells were kept dark during this 6 h. After incubation, 80-100µl of cells were spread on sterile mixed cellulose ester membrane filters (pore size 0.2µm, Fischer scientific, Hampton, USA), which were laid on BG-11 agarose plates without any antibiotics. Triplicates were made and incubated in continuous light of 28µE/m^2/s at 28°C for 1-2 days. Then the filters were transferred to new plates supplemented with the corresponding antibiotic (Table 4.4) for selection of mutants. After about two weeks, single colonies could be picked and streaked onto fresh agar plates containing suitable antibiotic(s). Transformants were restreaked at least five times until PCR analyses (4.2.1) or Southern blotting (4.2.15) were performed to test for segregation. Copies of the new segregated mutant were stored at -80°C (4.2.12).

4.2.12. Preparation of cryo-cell stocks

Cryo-cell stocks were set up to store and secure the segregated mutant lines. 1.5ml of the cell culture (*Synechocystis sp*. PCC6803 or *E.coli*) was mixed with 500µl of 80% glycerol and stored at -80°C.

4.2.13. Genomic DNA isolation of *Synechocystis*

4.2.13.1. Small scale isolation

To check the segregation of the *Synechocystis* mutants via PCR, a small scale gDNA extraction was performed. First, cells (amount of one inoculation loop) were resuspended in 200µl TE buffer (Table 4.19). Second, 200µl ROTI^R phenol was added and vortexed for 1min (VortexGenie Pulse, Scientific Industries). After centrifugation for 5min at 10,000rpm (Centrifuge 5424, Eppendorf), the upper phase was transferred to a new reaction tube. 150µl chloroform was added. The vortex and centrifugation step were then repeated. The upper phase was transferred again into a new reaction tube. After adding 16µl of 3M sodium acetate and 400µl 95% EtOH the sample was gently inverted and incubated at -20°C overnight.

The sample was centrifuged at 4°C for 15min at 10,000rpm (Centrifuge 5424, Eppendorf). The supernatant was discarded, and the pellet washed with 500µl 70% EtOH and centrifuged for 2min (Centrifuge 5424, Eppendorf). The supernatant was discarded again. In order to dry the pellet, the opened reaction tube was incubated in the heating block for 15min. The pellet was resuspended in 20µl TE buffer. To use the DNA for a PCR, it was additionally diluted 1:100 in H_2O.

4.2.13.2. Big scale isolation

To check the segregation of *Synechocystis* mutants via Southern Blot, a big scale gDNA extraction was performed. First, cells from a half plate were resuspended in 100µl TE buffer (Table 4.19). Second, 100µl phenol-chloroform-isoamylalcohol (25:24:1) and 2µl SDS (10%) were added. Next, an equivalent volume of glass beads (0.16-0.17mm) was added and vortexed for 3min (VortexGenie Pulse, Scientific Industries). After centrifugation for 5min at 10,000rpm (Centrifuge 5424, Eppendorf), the upper phase was transferred to a new reaction tube. 100µl chloroform-isoamylalcohol (24:1) was added. The vortex and centrifugation step were then repeated. The upper phase was transferred again into a new reaction tube. After adding 5µl 3M sodium acetate and 500µl 95% EtOH, the sample was gently inverted and incubated at -20°C overnight. The sample was centrifuged at 4°C for 15min at 10,000rpm (Centrifuge 5424, Eppendorf). The supernatant was discarded, and the pellet washed with 1ml 70% EtOH and centrifuged for 2min (Centrifuge 5424, Eppendorf). The supernatant was discarded again. To dry the pellet, the opened reaction tube was incubated in the heating block for 15min. The pellet was resuspended in 20µl TE buffer overnight at 4°C.

Table 4.19: Chemicals used for genomic DNA isolation of *Synechocsytis.*

chemicals
chloroform
chloroform-isoamylalcohol (24:1)
ethanol (95%, 70%)
ROTI^R Phenol
phenol-chloroform-isoamylalcohol (25:24:1)
SDS (10%)
sodium acetate (3M, pH 5.3)
TE buffer (pH 7.4)

4.2.14. Estimation of DNA concentration and quality

The DNA concentration and quality were estimated using two different methods. For one, the DNA concentration was determined by performing gel electrophoresis and comparing the signal strength of the DNA with the defined signal strength/concentration of the quantity marker Lambda DNA/HindIII marker (Thermo Scientific™, Life Technologies GmbH, Germany). On the other hand, the concentration and purity of the DNA were determined using a Nanodrop (NanoDrop ND-1000 Spectrophotometer, Thermo Scientific™, USA). For this, 1µl of the extracted or eluted DNA was applied to the measuring device.

4.2.15. Southern Blot (DIG-system)

Southern blot is a hybridization method that enables specific gene sequences to be detected in a complex DNA mixture. In this work, this method is used to check the segregation of *Synechocystis* mutants.

4.2.15.1. DNA labelling

In the first step, so-called DIG-labelled DNA probes were produced using the PCR method. The polymerase Dream-Taq (Table 4.5) was used with the standard PCR protocol (Table 4.15). The only change was the usage of 5.0µl of the PCR-DIG labelling mix (Roche, Basel, Swiss) instead of 1.0µl.

4.2.15.2. Genomic DNA restriction digestion

About 100-200ng genomic DNA of wild type and mutants was digested with die specific chosen Fast Digest enzymes (Table 4.6). Digested DNA was loaded on a long 0.8% (w/v) agarose gel and run for about 1.5-2.0h at 180V. To check the size of the bands, a 2.0µl of DIG-marked lambda-DNA/HindIII-MarkerII (Roche, Basel, Swiss) was mixed with 15µl of a lambda-DNA/HindIII-Marker (Roche, Basel, Swiss), heated at 65°C for 4min and loaded on the gel.

4.2.15.3. Southern blotting

After the electrophoresis of the digested DNA, the gel was soaked in denaturation buffer (Table 4.20) twice for 15min and then submerged in neutralization buffer (Table 4.20) twice for 15min at room temperature. The DNA was blotted by capillary transfer to a nylon membrane (pore size 0.20µm, Macherey-Nagel, Düren, Germany) using 20x SSC buffer (Table 4.20) overnight. Whatman paper socked with 2x SSC (Table 4.22) was used to help to transfer the DNA (Figure 4:2). The DNA was bound to the nylon membrane by a UV-crosslinker (UV-Stratalinker 2400; Stratagene, San Diego, USA). The membrane with DNA could then be used immediately, or it could be stored dry at room temperature for further use.

Table 4.20: Buffers for southern blotting.

buffers	1l	1,5l	2,5l
Denaturation buffer	20g NaOH	30g NaOH	50g NaOH
	88g NaCl	132g NaCl	220g NaCl
	ad 1000ml H_2O	ad 1500ml H_2O	ad 2500ml H_2O
Neutralization	60.6g Tris/HCL	90.9g Tris/HCL	151.5g Tris/HCL
buffer	176g NaCl	264g NaCl	440g NaCl
pH 7.4	ad 1000ml H_2O	ad 1500ml H_2O	ad 2500ml H_2O
20x SSC	175.32g NaCl	263g NaCl	438.3g NaCl
pH 7.0	88.2g Na_3Citrat x $2H_2O$	132.3g Na_3Citrat x $2H_2O$	220.5g Na_3Citrat x $2H_2O$
	ad 1000ml H_2O	ad 1500ml H_2O	ad 2500ml H_2O

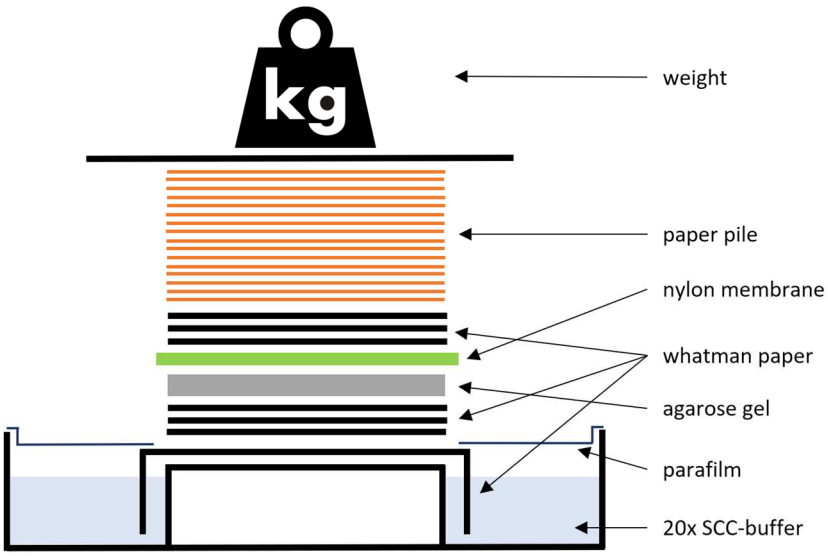

Figure 4:2: Scheme of a capillary southern blot setup. Blotting membrane: nylon membrane; weight: approx. 1.0kg.

4.2.15.4. Pre-hybridization and hybridization

The membrane was incubated with 30ml prehybridization buffer (Table 4.21) for 1h at 68°C in a hybridization tube in a hybridization oven (Biometra, Göttingen, Germany). Then the prehybridization buffer was poured off and frozen for reuse. Next, the hybridization buffer (Table 4.21) with 25ng/ml DIG-labelled probe, which had been previously denatured by heating up to 100°C for 10min and chilled directly on ice, was added. The hybridization was incubated overnight in the hybridization oven as well.

Table 4.21: Buffers for prehybridization and hybridization.

buffers	1l	2l	2.5l
Buffer 1 (Southern)	11.61g maleic acid	23.22g maleic acid	29.03g maleic acid
pH 7.5	8.77g NaCl	17.54g NaCl	21.93g NaCl
	8g NaOH	16g NaOH	20g NaOH
	ad 1000ml H_2O	ad 2000ml H_2O	ad 2500ml H_2O
Blocking solution (-20°C)	10g blocking solution + 100 ml Buffer 1 (Southern) briefly heat up lukewarm in the microwave. Don't let it boil!		
Pre-hybridization buffer	5x SSC buffer	25ml 20xSCC	
	0.1% sodium lauroylsarcosine	1ml 10% sodium lauroylsarcosine	
	0.02% SDS	200µl 10% SDS	
	1% blocking solution stock	10ml 10% blocking solution stock	
		ad 100ml H_2O	
Hybridization buffer	prehybridization buffer + 50µl DNA-labelled probe.		

4.2.15.5. Washing of the nylon membrane

On the next day, the membrane was washed twice for 5min with 2x SSC buffer (Table 4.22) at room temperature and then was washed twice for 15min with 0.1x SSC buffer (Table 4.22) at 68°C. All these four washing steps were performed in the hybridization tube.

After hybridization, the membrane was taken out in a clean box and was equilibrated in buffer 1 (Table 4.21) for 1min at room temperature. Then the membrane was incubated in buffer 2 (Table 4.22) without antibody for at least 1h at room temperature. After that, the buffer was exchanged with buffer 2 supplemented with 1/10000 dilution of 750units/ml Anti-DIG-AP Fab fragments (Roche, Basel, Swiss) and the membrane was incubated for exactly 30min (Figure 4:3).

The membrane was washed gently in washing buffer (Table 4.22) twice for 15min at room temperature and then shortly equilibrated in detection buffer 3 (Table 4.22) for 1min.

Table 4.22: Buffers for washing the nylon membrane.

buffers	1l	2l	2.5l
2xSSC	100ml 20x SSC	200ml 20x SSC	250ml 20x SSC
	10ml 10% SDS	20ml 10% SDS	25ml 10% SDS
	ad 1000ml H_2O	ad 2000ml H_2O	ad 2500ml H_2O
0.1xSSC	5ml 20x SSC	10ml 20x SSC	15ml 20x SSC
	10ml 10% SDS	20ml 10% SDS	25ml 10% SDS
	ad 1000ml H_2O	ad 2000ml H_2O	ad 2500ml H_2O
Buffer 2 (-20°C)	90ml buffer 1		
	10ml 10% blocking solution		
Buffer 2 + antibody	90ml buffer 1		
(-20°C)	10ml 10% blocking solution		
	antibody (reused 1:10000; new 1:20000)		
Washing buffer	3g Tween	6g Tween	7.5g Tween
	ad 1000ml buffer 1	ad 2000ml buffer 1	ad 2500ml buffer 1
Buffer 3 (detection)	12.11g Tris	24.22g Tris	30.29g Tris
pH 9.5	5.84g NaCl	11.68g NaCl	14.61g NaCl
	ad 1000ml H_2O	ad 2000ml H_2O	ad 2500ml H_2O

4.2.15.6. Detection

The membrane was then incubated with 2ml buffer 3, supplemented with 20µl 0.25mM “ready to use” CSDP-Star (Roche, Basel, Swiss) for 5min. The membrane was then placed between two plastic films and sealed airtight with a vacuum sealer. The foiled membrane was then placed in the X-ray cassette. The X-ray film (Thermo Scientific™ CL-XPosure™ Film, Life Technologies GmbH, Germany) was marked by a cut edge. First, a 1h exposure and optional an exposure overnight was carried out with a new X-ray film. A fully automatic developer (XR 24 NDT, Dürr NDT) was used to develop the X-ray film.

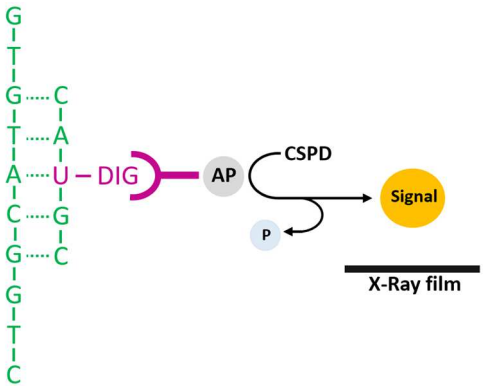

Figure 4:3: Detection principle of digoxigenin labelled DNA-fragments. The DIG-labelled probe hybridizes with blotted DNA. Alkaline phosphate is conjugated to the added anti-digoxigenin-antibody. The alkaline phosphatase dephosphorylates the added CSPD substrate, which results in chemiluminescence. The luminescence signal is detected with the X-ray film.

4.3. Protein biochemical methods

4.3.1. Protein isolation from *Synechocystis*

To isolate proteins from whole cell extracts from *Synechocystis*, the cells first had to be broken up on a small scale. For this purpose, 250ml of *Synechocystis* cells were transferred from a Kniese tube into a 50ml reaction tube (Sarstedt AG & Co.KG, Nümbrecht, Germany) and centrifuged at 3000rpm for 10min at 4°C (Centrifuge 5804R, Eppendorf). This step was repeated until the entire volume of the Kniese tube culture was pelleted in a single reaction tube (Sarstedt AG & Co.KG, Nümbrecht, Germany). With the help of a 50ml syringe filled with glass beads, approx. 200µl of glass beads were placed in 2ml Eppendorf tubes. The pellet was then resuspended in 500µl ACA buffer and transferred to one of the prepared 2ml reaction tubes (Eppendorf). The cell-glass beads mixture (0.16-0.17mm) (Table 4.23) was then vortexed three times for 2min in the cold room at 4°C (VortexGenie Pulse, Scientific Industries). The cell-glass beads mixture was then centrifuged at maximum rpm for 1min at 4°C (Centrifuge 5424, Eppendorf). The supernatant was transferred to a new reaction tube (Eppendorf AG, Hamburg, Germany). It was ensured that no glass beads were taken over.
In order to normalize the samples, the chlorophyll content was determined as described in 4.4.4.

Table 4.23: Buffers used for protein isolation from *Synechocystis*.

buffers	composition
ACA	750mM ε-amino caproic acid, 50mM Bis-Tris/HCL (pH 7.0), 0.5mM EDTA
Glass beads	0.17-0.18mm
2x SB (sample buffer)	125mM Tris pH 6.8, 4% (w/v) SDS, 40% (v/v) glycerol, 0.2% (w/v) bromophenol blue, 10mM dithiothreitol (DTT)
Overlay buffer	isopropanol

4.3.2. Urea polyacrylamide gel electrophoresis (Urea-PAGE)

Urea-PAGE is a method to separate complex protein mixtures according to their molecular weight using a polyacrylamide matrix (Laemmli 1970; Summer et al. 2009). The migration of the sample depends on the chosen acrylamide concentration. The denaturing effect of the urea enables bands to be separated and displayed more finely and clearly. In this work, 10% urea polyacrylamide gels were used.

4.3.2.1. Sample preparation

Protein samples for PAGE analyses were prepared by mixing with 120µl 2x sample buffer (SB) (Table 4.23). The amount of the individual protein sample was based on the respective chlorophyll concentration. Each protein sample contained 0.15µg chlorophyll. The mixture was incubated for 10min at 95°C, followed by transfer to ice and incubation for 1min. Insolubilized material was pelleted by centrifuge for 10sec at 14000rpm (Centrifuge 5424, Eppendorf).

Samples were either stored at –20°C or directly loaded into the stacking gel wells at maximum volumes of 15µl for 15-well gels. 5µl of the PageRulerTM Plus Prestained Protein Ladder (Thermo Scientific™, Life Technologies GmbH, Germany) was loaded as protein molecular weight markers for PAGE in this work.

4.3.2.2. PAGE preparation

The gels were self-cast, 1mm thick and routinely run in the Bio-Rad Mini-PROTEAN III vertical gel system (Bio-Rad Laboratories GmbH, München, Germany). The Urea PAGE was cast like classic PAGE. They consisted of a separation gel on the bottom and a spacer gel on top (Table 4.24). The individual buffers were mixed to produce the two gel layers. APS and TEMED (Table 4.24) were only added shortly before pouring, as they trigger the polymerization. The separation gel was poured approximately 3/4 into the vertical gel chamber and covered with 100% isopropanol. This prevented air bubbles and levelled the top edge of the gel. After about 20min the separation gel was polymerized entirely. The isopropanol was then poured off, and residues were sucked out with a piece of Whatman paper. Then the remaining 1/4 were filled up with the spacer gel. Combs with a thickness of 1mm and 15 wells were inserted into the still liquid spacer gel. It was essential to avoid air bubbles. When gels were polymerized, they could be used directly or covered with moist paper and kept at 4°C. It is important to note that the Urea gels should be used the next day at the latest.

Table 4.24: Buffers for Urea-PAGE preparation.

separation gel			
buffers	stock	10%	
acrylamide	30% (w/v); 37,5:1	8.33ml	16.67ml
375mM Tris	3M; pH 8.9	3.13ml	6.25ml
6M urea	powder	9g	18g
0.1% (w/v) SDS	10% (w/v)	0.25ml	0.50ml
0.1% (w/v) APS	10% (w/v)	0.25ml	0.50ml
0.01% (v/v) TEMED	100% solution	0.025ml	0.050ml
top up with water to		∑ 25ml	∑ 50ml
spacer gel			
buffers	stock	5%	
acrylamide	30% (w/v); 37,5:1	2.50ml	3.33ml
125mM Tris	3M; pH 6.8	1.88ml	2.50ml
0.1% (w/v) SDS	10% (w/v)	0.15ml	0.20ml
0.1% (w/v) APS	10% (w/v)	0.15ml	0.20ml
0.01% (v/v) TEMED	100% solution	0.015ml	0.20ml
top up with water to		∑ 15ml	∑ 20ml

4.3.2.3. Gel electrophoresis

A Bio-Rad PowerPac Basic (Bio-Rad Laboratories GmbH, München, Germany) was used as the running chamber for gel electrophoresis. Depending on the number of gels, the Leammli running buffer (Laemmli 1970) (Table 4.25) was filled up to the corresponding mark on the chamber. The gels were pre-run at 70 Volts for 10min until samples formed a distinct band and continued with a constant voltage of 120V for a period of 1.5h to 2h. The obtained gels were either stained with Coomassie (4.3.3) or used for immunoblotting analyses (4.3.4).

4.3.3. Coomassie-brilliant-blue staining of polyacrylamide gel

To assess the protein separation and the running behavior, in addition to the polyacrylamide gels for the Western Blot, polyacrylamide gels were stained with Coomassie. For this, the Urea-PAGE gels were incubated for 30min in the coomassie staining solution (Table 4.25) shaking at 30-50rpm (GFL 3016 shaker, Eydam, Kiel, Germany). The destaining solution-1 (Table 4.25) was then incubated for 5min. The second decolorization with destaining solution 2 (Table 4.25) was carried out overnight. Depending on the degree of discoloration, the washing process was repeated until the band pattern was visible with as little background as possible.

Table 4.25: Buffers used to run the gel electrophoresis and to stain and destain polyacrylamide gels.

buffers	composition
Coomassie (staining solution)	40% (v/v) ethanol, 10% acetic acid, 0.2%(w/v) Coomassie-brilliant blue-R-250
Distaining solution 1	40% (v/v) ethanol, 10% (v/v) acetic acid
Distaining solution 2	10% (v/v) acetic acid
Laemmli buffer	25mM Tris, 190mM glycine, 0.1% (w/v) SDS , pH 8.3

4.3.4. Immunoblotting analysis (Western Blot)

The immunoblot was constructed as described in Figure 4:4. All required buffers are listed in Table 4.26. It was important that the Whatman paper, as well as the nitrocellulose membrane, were moistened in the transfer buffer and that air bubbles were avoided when stacking. After assembly of the blot, the chamber was filled to the mark with transfer buffer. The protein transfer was carried out for 1h at 400mA or 55V (Bio-Rad PowerPac Basic, Bio-Rad Laboratories GmbH, München, Germany).

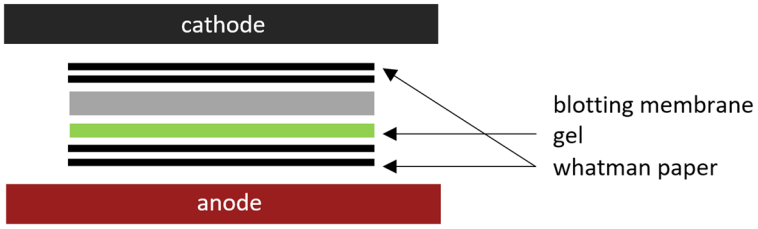

Figure 4:4: Scheme of an immunoblot setup (Western blot). The direction of transfer takes place from the cathode to the anode. Gel: Urea-PAGE gel; blotting membrane: nitrocellulose membrane.

After blotting or protein transfer, the gel and Whatman paper were disposed. The procedure for the nitrocellulose was as follows. First, the membrane was blocked with the blocking solution (Table 4.26) for 1h. It should be noted that the membrane was moved on a shaker (GFL 3016 shaker, Eydam, Kiel, Germany) during all incubation and washing steps. The blocking solution was then discarded, and the membrane was washed twice with PBS-T (Table 4.26). 20ml of the primary antibody (Table 4.27) was then added and incubated at 4°C overnight. Since the His-antibody is conjugated to horseradish peroxidase (HRP) (Table 4.27), no secondary antibody was necessary. However, with the blots incubated with the GFP-antibody (Table 4.27) was continued in a classic manner. For this, washing was carried out three times for 20min with PBS-T (Table 4.26) and then incubated for 60min with 20ml of the secondary antibody (Table 4.27). The following washing steps were then carried out for antiHis and antiGFP membranes, namely three times for 10min with PBS-T and then twice for 10min with PBS (Table 4.26).

Meanwhile, the ECL solutions 1 and 2 were prepared (Table 4.26), and the developer machine (XR 24 NDT, Dürr NDT) switched on to heat up. Further work steps were carried out in the darkroom with a red light. 10ml of both ECL solutions were added to the membrane, and these were placed between a transparent film. Next, the foiled membrane was placed in the X-ray cassette. The X-ray film (Thermo Scientific™ CL-XPosure™ Film, Life Technologies GmbH, Germany) was marked by a cut edge. First, a 1min exposure and then a 10min and optional a 1h exposure was carried out with new X-ray films. A fully automatic developer (XR 24 NDT, Dürr NDT) was used to develop the X-ray film.

Table 4.26: Buffers and solutions for immunoblotting analysis (Western Blot).

buffers and solutions	composition
10x PBS	150mM NaCl, 7.5mM Na_2HPO_4, 2.5mM NaH_2PO_4
1x PBS	150mM NaCl, 7.5mM Na_2HPO_4, 2.5mM NaH_2PO_4,
1x PBS-T	150mM NaCl, 7.5mM Na_2HPO_4, 2.5mM NaH_2PO_4, 0.1% (v/v) Tween 20
transfer buffer	3mM Na_2CO_3, 10mM $NaHCO_3$, 20% (v/v) methanol
blocking solution	1xPBS, 5% (w/v) milk powder
p-coumaric stock solution	90mM p-coumaric in DMSO
Luminol stock solution	250mM luminol in DMSO
ECL1	100mM Tris/HCL pH 8.5, 0.4mM p-coumaric acid, 2.5µM luminol
ECL2	100mM Tris/HCL pH 8.5, 100mM H_2O_2

Table 4.27: Antibody's used in this work.

antibody name	type	company	dilution
anti6xHis (monoclonal)	Mouse anti Penta Histidine Tag: HRP	Bio-Rad Laboratories, Inc. (California, USA)	1:1000
antiGFP (monoclonal)	Mouse anti Green Fluorescent Protein	Bio-Rad Laboratories, Inc. (California, USA)	1:5000
antiMouse (polyclonal)	Peroxidase AffiniPure Rabbit Anti-Mouse IgG + IgM (H+L)	Jackson ImmunoResearch Europe Ltd (Ely, UK)	1:10000

4.4. Physiological methods

4.4.1. Cultivation of *E.coli*

Transformed *E. coli* cells (4.2.10, Table 4.14) were grown for 1h in LB medium on a shaker at 37°C and 180rpm (4400 Innova Incubator Shaker, New Brunswick Scientific, Nürtingen, Germany). Transformed cells of *E. coli* were plated on LB agar plates supplemented with the respective antibiotic (Table 4.4). They were incubated at 37°C overnight in an incubator (T5050E, Heraeus, Hanau, Germany). For short-term storage, the plates were sealed with parafilm (Carl Roth GmbH, Karlsruhe, Germany) and kept in a refrigerator at 4°C. For long-term storage, freezing cultures were prepared as described (4.2.12) for *Synechocystis* and stored at -80 °C.

4.4.2. Cultivation of *Synechocystis sp*. PCC 6803

On BG-11 agar plates (Table 4.1, Table 4.2), *Synechocystis sp.* PCC 6803 was cultured autotrophically at 28°C and 50µE/m^2/s light intensity.

The phenotyping of cultures in which limited growth was found on the plate but not in liquid culture was complimented by growth tests on the plate. For this, a liquid culture from shaking flasks was brought to OD_{750} 1 and a dilution series of 10^0, 10^1, 10^2, 10^3, 10^4 was prepared. Thereafter, 4µl of the diluted cell samples were pipetted in series on a square BG-11 plate. The samples were scanned daily for nine days.

4.4.2.1. Cultivation in shaking flasks

In shaking flasks, *Synechocystis sp.* PCC 6803 was cultured autotrophically (without the addition of glucose), mixotrophically and heterotrophically (with the addition of 10mM glucose) in 50ml BG-11 medium on a shaker (Kreisschuettler 3020, GFL, Burgwedel, Germany) at 28°C and 50µE/m^2/s light intensity. Cultures that should be cultivated heterotrophically were completely covered with aluminium foil. Every 24h the heterotrophic cultures were incubated with light (50µE/m^2/s) for 10min. Cells from the BG-11 agar plates (see above) were used to inoculate shaking flasks.

4.4.2.2. Cultivation in Kniese tubes

In Kniese tubes (Eydam, Kiel, Germany), *Synechocystis sp.* PCC 6803 was cultured autotrophically (without the addition of glucose), mixotrophically and heterotrophically (supplemented with 10mM glucose) in 200ml BG-11 medium in a Kniese apparatus at 28°C, 50µE/m^2/s light intensity and a constant gassing with atmospheric air. Cultures that should be cultivated heterotrophically were cultivated entirely in the dark, except for 10min light incubation, daily.

If the cells showed reduced growth on the plate or could not be grown in shaking flasks at all, the cells were inoculated directly from BG-11 plates into the Kniese tubes. Otherwise, the cells were pre-cultivated in shaking flasks and then inoculated into Kniese tubes.

4.4.3. Optical density determination

The optical density of liquid *Synechocystis* cultures was determined photometrically (UV2501PC Photometer, Shimadzu, Kyoto) at OD_{750}. The BG-11 medium (Table 4.1) used to inoculate the cells was used as a blank reference. Samples with an OD_{750} >0.5 were diluted with BG11 medium before measurement.

4.4.4. Chlorophyll content determination

10µl of the WCE sample was resolved into 990µl methanol and pelleted for 1min at 14,000rpm (Centrifuge 5804R, Eppendorf). The absorbance of the supernatant was measured photometrically at OD_{666} and OD_{750}. Methanol was used as a blank reference.

Chlorophyll content was calculated according to the following formula.

$$chlorophyll\ content\ (\mu g/ml) = (OD_{666} - OD_{750}) \times 12.61 \times dilution\ factor$$

4.4.5. Growth rate analysis

The growth rate was determined using the protocol developed by Makowka 2019. To determine the growth rate, the slope ratio of the respective OD_{750} values was calculated for three consecutive cultivation days (day1-3, day2-4, day3-5 etc.) A mean value was calculated from these slope ratios, which represented the average slope of culture over the corresponding cultivation time. This value was determined for all biological replicas. Since the growth rates of photomixotrophic and heterotrophic cultures show larger fluctuations, the data were presented in boxplot diagrams instead of bar diagrams for better interpretation.

4.4.6. Glucose quantification

To determine the glucose concentration of photomixotrophic and heterotrophic cultures, the quantification of the glucose content was carried out according to Gründel et al. 2012 and Makowka 2019. The principle of the test is based on the enzymatic conversion of glucose to 6-phosphogluconate, which is proportional to the turnover of $NADP^+$ to NADPH, which in turn can be determined by a specific absorption point at 340nm.

First, 1ml of the culture (OD_{750} ~5) was centrifuged for 5min at 8000rpm (Centrifuge 5804R, Eppendorf). 50µl of the supernatant was transferred to a new Eppendorf cup and diluted 1:10 or 1:20.

For the glucose standard 50µl glucose solution with the concentrations 0mM, 0.625mM, 1.25mM, 2.5mM and 5mM glucose were prepared. Next, 940µl of the NADP buffer (Table 4.28) was added to all glucose samples and standards. The absorption was measured at 340nm. An acrylic cuvette was used for this. Thereafter, 10µl of the enzyme mixture (Table 4.28) was added to all samples and standards and incubated for 1h at 37°C. Finally, the absorption of the samples and the standard was measured again at 340nm. The initial values before the enzymatic reaction were then subtracted from the final values. The standard values were used to create a glucose calibration line. The glucose concentration was determined by inserting the sample values into the equation of the calibration line.

Table 4.28: Reagents, buffers and enzyme mixture for glucose determination. HK: hexokinase; G6PDH: glucose-6-phosphate dehydrogenase.

reagent	stock conc.	end conc.	dil.factor	end vol.	NADP buffer	enzyme mixture
Sample/Standard	< 5mM	<0.25mM	20	50µl	-	-
$NADP^+$	150mM	2mM	75	13.33µl	13.33µl	-
ATP	150mM	2mM	75	13.33µl	13.33µl	-
$MgCl_2$	300mM	3mM	100	10µl	10µl	-
HK/ G6PDH	340U/ml 170U/ml	0.17U 0.085U	2000	0.5µl	-	0.5µl
Tris-HCL (pH 7.4)	100mM	91.3mM	1.1	912.83µl	903.33µl	9.5µl
∑				1000µl	940µl	10µl

4.4.7. Fluorescence Microscopy and preparation of samples

In this work, the expression and localization of fluorophore tagged enzymes (Table 4.13; Capture 4.2.3) was investigated using fluorescence microscopy.

4.4.7.1. Preparation of samples

A strong dynamic of the tagged enzymes was observed in various microscopy test runs. This led to the development of a repeatable uniform process for sample preparation. First, the cells were precultivated in shaking flasks as described in 4.4.2.

For long time experiments, after 6 days, the preculture was used to inoculate new autotrophic, mixotrophic and heterotrophic cultures with an OD_{750} of 0.2 shaking flasks (4.4.2). After a further three days of growth, the cells were ready for microscopy. The heterotrophic culture samples were prepared in a dark room. For short time experiments, the precultures were used directly. The photomixotrophic cultures were incubated with 10mM glucose for 1min or 1h. Cultures that were to be incubated in the dark were covered with a light-proof cloth for 1min. To avoid environmentally related enzymatic changes or reorganizations, the cells were fixed in the climate chamber under cultivation condition.

For this, 276µl of cell culture was pipetted to 24µl of glutaraldehyde (25% glutaraldehyde solution, specially purified for use as an electron microscopy fixative, Sigma-Aldrich, St.Louise, USA) in a reaction tube (Eppendorf, Hamburg Germany). Glutaraldehyde is a fixative which is preferred for use in microscopy. It is an excellent cross-linking agent and enables a relatively stable and unadulterated fixation of cellular structures without blocking the enzymatic activity (Habeeb and Hiramoto 1968).

After fixation of the cells, the samples were gently centrifuged down at 4000rpm for 1min (Centrifuge 5424, Eppendorf). Then 4µl of the denser cell fraction were pipetted onto an agar plate and left to dry. Next, a small BG-11 agar cube (~1cm^3) with the cell sample was cut out with a scalpel and placed in reverse on a coverslip. This was placed in reverse on a purpose-built stainless-steel slide (Figure 4:5). The coverslip was fixed with standard petroleum jelly on the stainless-steel slide.

The stainless-steel slide was engineered by the research group of Prof. Dr. Conrad Mullineaux (Queen Mary University of London, UK). The slide was modified manufactured in the in-house university workshop (Christian-Albrechts-University of Kiel, Germany).

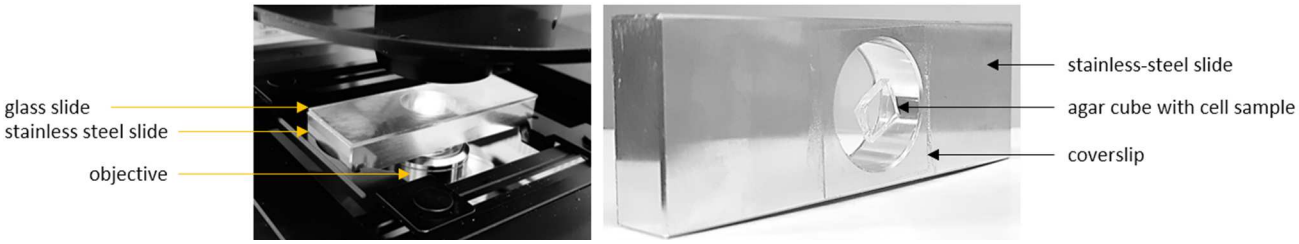

Figure 4:1: Stainless steel slide for microscopy of the *Synechocystis* fluorescence mutants. The stainless-steel slide offers the possibility of microscope the cells directly on agar cubes. The top of the stainless-steel slide is glued to a normal glass slide. The agar cube is placed on a coverslip. The coverslip is attached to the slide with a thin coating of petroleum jelly. Since it is an inverse CLSM, the object is placed upside down on the lens.

4.4.7.2. CLSM microscopy

All pictures were taken with the same CLSM microscope, type Leica TCS SP5. A HCX PL APO CS 63.0x1.40 OIL objective with a numerical aperture of 1.4 and a refraction index of 1.52 was used. Settings listed in Table 4.29.

Table 4.29: CLSM microscopy: Scanner and hardware settings.

Scanner and hardware settings	
Pinhole (m)	95.6µm
StepSize	0.05µm
Zoom	5
Line Average	6
Frame Average	1
Resolution	12 bits
Channels	3
Format-Width	1024 pixel
Format-Height	1024 pixel
AOTF (488)	13%
PMT (HV) YFP	920
PMT (HV) GFP	920
PMT (HV) CFP	920
PMT (HV) Chlorophyll	920
PMT Trans	235
Laser Argon visible	28%
Scan Speed	400Hz
Emission bandwidth PMT YFP: begin - end	520nm-540nm
Emission bandwidth PMT GFP: begin - end	503nm-515nm
Emission bandwidth PMT CFP: begin - end	470nm-500nm
Emission bandwidth PMT Chlorophyll: begin - end	670nm-695nm

4.4.7.3. Image analyses

The images were analyzed with ImageJ Fiji (Schindelin et al. 2012; Rueden et al. 2017). For each open image, the following commands in an ImageJ-macro (Marius Theune, unpublished) were used to analyze the cells and potential clusters inside of them. First, the "Split Channels" command was used to separate the image into the channels (1) brightfield, (2) Chlorophyll-Fluorescence, and (3) YFP- Fluorescence. A Median-Filter with a kennel size of 2px was used on the Chlorophyll-Fluorescence image to reduce noise. This image was converted into a binary-mask based on the threshold set before starting the analysis. These masks should represent all living cells based on their Chlorophyll-Fluorescence. The "Fill Holes" command was used on these masks to cover holes inside cells that might appear due to irregular chlorophyll distributions. The "Adjustable Watershed" with a setting of tolerance=1 was used to separate the masks into individual cells. After that, the “Analyze Particles” command with the setting of size500px circularity=0.3 was able to generate one region of interest (ROI) per cell based on the generated mask. For each ROI, the parameter area, mean YFP-Fluorescence, and YFP standard-deviation were analyzed. To analyze if clustered signals appeared in cells, the YFP-Fluorescence images were analyzed further. First, the YFP-Image was duplicated, and a Median-Filer was applied to reduce noise. After that, a threshold as high as two times the average YFP-Fluorescence of all cells per condition per replica was used to create a mask of all clustered signals. With the ROIs created before, each cell was selected. In this cell-ROI, the "Analyze Particles” command was used with the settings of size=5px circularity=0.25 to create a second set of ROIs representing clusters. With the Custer-ROIs, the number of clusters, the average intensity, and the average area of clusters for each cell was determent. Finally, the measurements: area, mean YFP fluorescence intensity, YFP standard deviation, number of clusters, the average cluster intensity, and the average area of clusters for each cell were stored in a .csv file and further analyzed with Microsoft Excel (Office 365; Microsoft, Washington USA), xlstat (Addinsoft; New York USA) and R (R Core Team 2020).

4.5. Experimental hierarchy and statistical data analysis

4.5.1. Growth analysis

All figures showing growth curves and growth rates are based on cultures that were grown at the same time in triplicate in three Kniese tubes. The OD_{750} of each Kniese tube was measured in triplicate. The mean and the standard deviation of these nine measuring values are shown in the figures. All growth curves were repeated in at least three independent experiments. A typical growth curve from those three replicates is shown in this work. The growth rate represents the data of all three independent experiments.

4.5.2. Fluorescence data analysis

All box plots, violin plots and bar charts show cell data based on data from three independent cell cultures. The mean values and standard deviations refer to the total sample size of the three independent tests. At least triplicates per culture were examined by fluorescence microscopy per experiment. Since GAP2 YFP-His mutants could not be completely segregated, it should be excluded that non-segregated cells are measured. Therefore, only GAP2 YFP cells were analyzed, which had a greater absolute fluorescence than twice the value of the absolute fluorescence of the corresponding WT (Table 4.30).

The signal to noise ratio (SNR) to represent the homogeneity of the fluorescence signal within the cell was calculated using the following formula.

$$SNR = \frac{fluorescence\ intensity\ (\mu_{sig})}{standard\ deviation\ (\sigma_{sig})}$$

The absolute fluorescence intensity showed the total measured fluorescence of a cell and was calculated using the following formula.

$$absolute\ fluorescence\ intensity = fluorescence\ intensity * area$$

Table 4.30: Thresholds for the selection of GAP2 YFP-His cells.

experiment	WT culture	threshold (double mean fluorescence intensity)
Short time	auto	415.63
	mixo 1min	404.19
	mixo 1h	698.99
	dark 1min	551.08
	mixo 1min dark 1min	353.90
	mixo 1h dark 1min	619.93
Long time	auto 3d	387.18
	mixo 3d	345.59
	hetero 3d	290.17

5. Results

5.1. Testing the existence of a glucose dehydrogenase/gluconate kinase pathway

The first question of this work was to find out how the entrance of the Entner-Doudoroff (ED) pathway in *Synechocystis sp.* PCC 6803 is organized. We had two hypotheses in this regard. The first hypothesis implies that glucose is converted into gluconate via the so-called glucose dehydrogenase/gluconate kinase (GDH/GK) pathway: Via gluconate kinase into 6P-gluconate (Figure 5:1 A). The second hypothesis suggests that the ED pathway shares its entrance with the oxidative pentose phosphate (OPP) pathway and that a GDH/GK pathway in *Synechocystis* does not exist. In this case, glucose would be converted into glucose-6P via the hexokinase (HK) and then into 6P-gluconate via the glucose-6-phosphate dehydrogenase (ZWF; Figure 5:1 B). The putative glucose dehydrogenase is annotated with two different enzymes, GDH1 (sll1709) and GDH2 (slr1608). However, enzyme tests could not demonstrate any enzyme activity for either of the two glucose dehydrogenases (Makowka 2019). It is therefore assumed that the two enzymes are not glucose dehydrogenases. If a functional GDH/GK pathway exists in *Synechocystis*, the deletion of the hexokinase would have to be compensated.

Therefore, to finally test which of the two pathways or possible both represent the entrance of the ED pathway, hexokinase (*hk*) and the putative glucose dehydrogenase (*gdh1, gdh2*) mutants were examined. The deletion mutants *Δgdh1, Δgdh2, Δgdh1Δgdh2* and *Δgnd*, have been made in a previous dissertation (Table 4.11). The hexokinase (*Δhk*) construct was made within this thesis (Table 4.11).

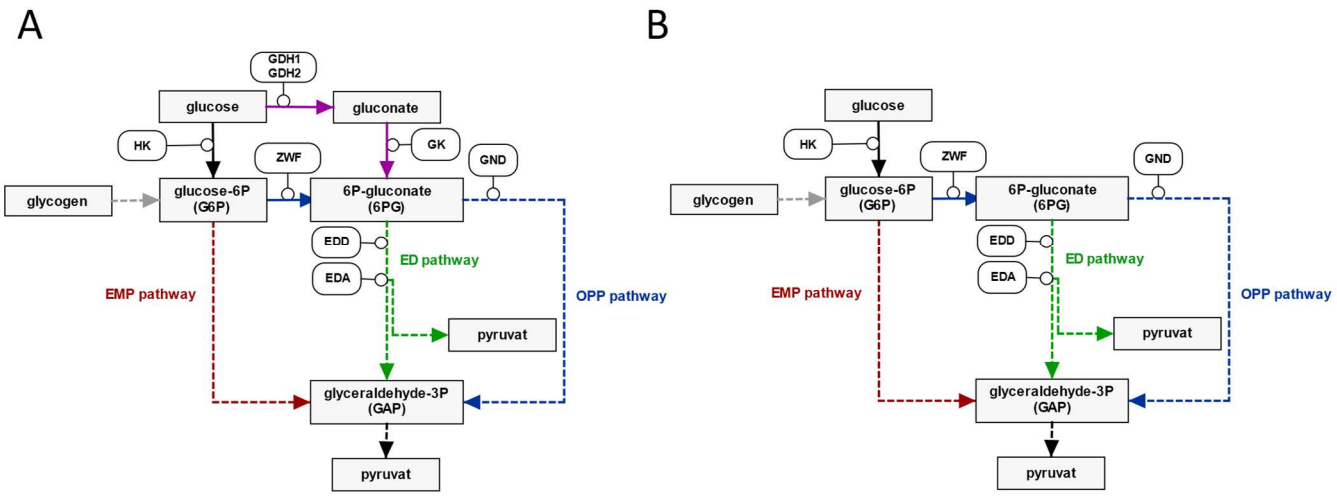

Figure 5:1: Two possible entrances of the Enter-Doudoroff (ED) pathway. Simplified scheme of the central carbon metabolism in *Synechocystis*. (A) Entrance via the glucose dehydrogenase/gluconate kinase (GDH/GK) pathway. (B) Entrance shared with the oxidative pentose phosphate (OPP) pathway via the hexokinase (HK). ZWF: glucose-6-phosphate dehydrogenase; GND: 6-phosphogluconate dehydrogenase; EDD: phosphogluconate dehydratase, EDA: 2-keto-3-deoxygluconate-6-phosphate (KDPG) aldolase; EMP pathway: Embden-Meyerhof-Parnas pathway.

5.1.1. Construction of the hexokinase (Δ*hk*) deletion mutants

The hexokinase (*hk*, sll0593) gene of the WT was replaced by a spectinomycin resistance cassette using homologous recombination. For this purpose, 200-300bp long DNA fragments, up- and downstream of the *hk* gene, were amplified by PCR (4.2.1). The Gibson primers for this are listed in (Table 4.7). Also, the spectinomycin resistance cassette was amplified via PCR. All PCR products were gel-purified (4.2.8). The Bluescript vector (Table 4.10) was opened with EcoRV (Table 4.6) and acted as the recipient vector. The two fragments, the spectinomycin resistance cassette and the opened vector were then cloned together via Gibson Assembly (4.2.2). For propagation, *E.coli* was transformed with the finished vector (4.2.9; 4.2.10) and segregated on LB plates containing spectinomycin (Table 4.3; Table 4.4). Then the vector was isolated via MiniPrep (4.2.5). The correctness of the sequence was checked by Sanger sequencing (4.2.6), using M13 primers (Table 4.9). After the sequence was found to be correct, *Synechocystis* WT and the deletion mutants *Δgdh1, Δgdh2, Δgdh1Δgdh2* and *gnd* were transformed with the vector (4.2.11) to produce double and triple mutants. For segregation, the transformed cultures were grown on BG-11 plates containing spectinomycin. The segregation was checked by a PCR and subsequently by gel electrophoresis (4.2.7). Primers (Table 4.7) upstream and downstream of *hk* were used for this. A PCR product of 1068bp was expected in the WT. A PCR product of 2702bp was expected in the mutants due to the incorporation of a spectinomycin resistance cassette. Since *Synechocystis* has many genome copies, it is also possible that *hk* was only deleted from a few genome copies. In this case, a double band would be expected in mutants that are not fully segregated. No *hk* gene could be amplified from genomic DNA (4.2.13) of the various *hk* mutants (Table 4.11, Table 4.12). Complete segregation of *Δhk, ΔhkΔgdh1, ΔhkΔgdh2, ΔhkΔgdh1Δgdh2* and *ΔhkΔgnd* could thus be confirmed (Figure 5:2). *ΔhkΔgdh1, ΔhkΔgdh2* and *ΔhkΔgnd* were not characterized further in this work.

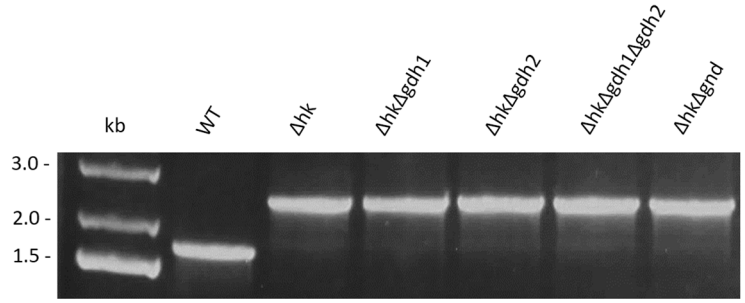

Figure 5:2: PCR with genomic DNA of *Synechocystis* WT and different *Δhk* mutants. It is showing that Δ*hk, ΔhkΔgdh1, ΔhkΔgdh2, ΔhkΔgdh1Δgdh2* and *ΔhkΔgnd* are completely segregated. GeneRuler™ 1kb Plus DNA ladder (lane 1). Expected size for WT: 1068bp and Δhk: 2702bp.

5.1.2. Growth analysis of the hexokinase (Δ*hk*) and glucose dehydrogenase (Δ*gdh*) deletion mutants

As a reminder, to find out whether the entry of the Entner-Doudoroff (ED) pathway is mediated via a glucose dehydrogenase/gluconate kinase (GDH/GK) pathway, a hexokinase (*Δhk*) mutant was constructed. We expected that if in *Synechocystis*, a functional GDH/GK pathway exists, the *Δhk* mutant would show no phenotype in growth. In this case, the putative GDH isoenzymes or only one of the two enzymes (GDH1 or GDH2) should be able to compensate for the deletion of *hk*. Conversely, if there is no functional GDH/GK pathway, the *Δhk* mutant cannot metabolize glucose and would not show any increase in growth under photomixotrophic or heterotrophic conditions, or should not be able to grow at all (Figure 5:3 G). For a physiological characterization, the growth of the *Δhk* and *Δgnd* mutants was examined under photoautotrophic, photomixotrophic and heterotrophic conditions. As a control, the cells were first cultivated photoautotrophically without glucose. As expected, no physiological difference could be measured for the Δ*hk* single mutant and the *ΔhkΔgdh1Δgdh2* triple mutant compared to the WT (Figure 5:3 A, D).

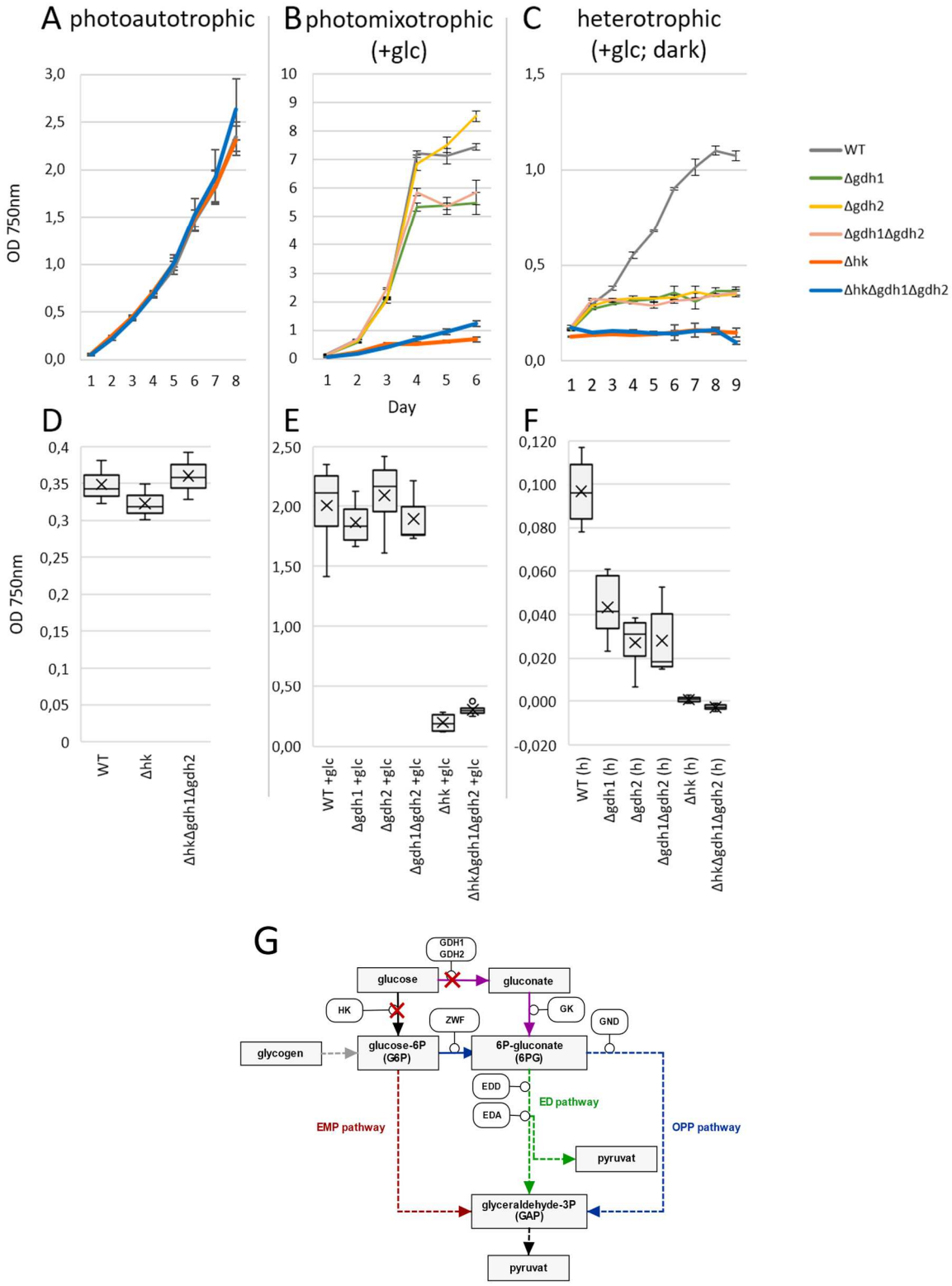

Figure 5:3: Growth of *Synechocystis* WT and different *Δgdh* and *Δhk* mutants. Cultures error bars represent the standard deviation from at least three independent cultures, each measured in triplicate. Each growth experiment was repeated at least three times independently to ensure reproducibility. In the graph, the data of one growth experiment is shown. (A) Cultures were grown under photoautotrophic conditions in continuous light. (B) Cultures were grown under photomixotrophic (+10mM glucose) conditions in continuous light. (C) Cultures were grown under heterotrophic (+10mM glucose, dark) conditions in the dark. (D) Cultures growth rate grown under photoautotrophic conditions in continuous light. WT n=9, *Δhk* n=9, *ΔhkΔgdh1Δgdh2* n=9. (E) Cultures growth rate grown under photomixotrophic (+10mM glucose) conditions in continuous light. WT+glc n=21, *Δhk*+glc n=15, *Δgdh1*+glc n=12, *Δgdh2*+glc n=12, *Δgdh1Δgdh2*+glc n=12, *ΔhkΔgdh1Δgdh2*+glc n=12. (F) Cultures growth rate grown under heterotrophic (+10mM glucose, dark) conditions in darkness. WT(h) n=12, *Δhk*(h) n=6, *Δgdh1*(h) n=15, *Δgdh2*(h) n=18, *Δgdh1Δgdh2*(h) n=18, *ΔhkΔgdh1Δgdh2*(h) n=6. (G) Simplified scheme illustrating the potential glucose dehydrogenase/ gluconate kinase (GDH/GK) pathway.

Then the single mutants *Δgdh1, Δgdh2, Δhk* the double mutant *Δgdh1Δgdh2* and the triple mutant *ΔhkΔgdh1Δgdh2* were cultured photomixotrophically with glucose. *Δgdh2* showed a normal phenotype and grew like the WT. *Δgdh1* and *Δgdh1Δgdh2* showed a similar slightly reduced growth in contrast to the WT. This may indicate that putative GDH1 is more relevant than putative GDH2. However, *Δhk* and *ΔhkΔgdh1Δgdh2* were not able to enhance their growth on glucose and showed autotrophic growth behavior (Figure 5:3 B, Figure 5:3 E). In the dark under heterotrophic conditions, a similar reduced growth to the WT could be measured for *Δgdh1, Δgdh2*, and the double mutant *Δgdh1Δgdh2*. A difference between the potential enzymes GDH1 and GDH2 could no longer be determined. *Δhk* and *ΔhkΔgdh1Δgdh2*, however, could not enhance their growth (Figure 5:3 C, F). For these mutants, the heterotrophic condition was lethal. To ensure that glucose cannot be metabolized by *Δhk* and *ΔhkΔgdh1Δgdh2*, additional enzyme tests were carried out (Figure 5:4).

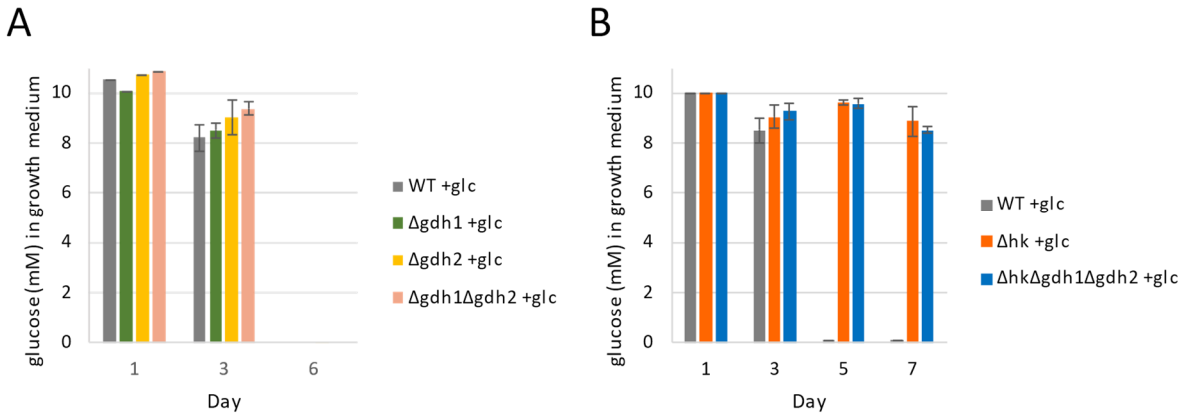

Figure 5:4: Glucose concentration in the growth medium of *Synechocystis* WT and different *Δgnd* and *Δhk* mutants in the course of the growth experiments (Figure 5:3). Cultures error bars represent the standard deviation from three independent measured technical replicates.

These confirmed the results of the growth experiments. As well as the WT, *Δgdh1, Δgdh2*, *Δgdh1Δgdh2* were able to completely metabolize glucose, within 6 days (Figure 5:4 A). In contrast, in the medium of *Δhk* and *ΔhkΔgdh1Δgdh2* cell cultures, the glucose concentration hardly decreased in the medium (Figure 5:4 B).

In summary, if the hexokinase is deleted, *Synechocystis* cannot consume glucose. Compensation through a GDH/GK pathway could not be observed. The second hypothesis that the Entner-Doudoroff (ED) pathway shares its entrance with the oxidative pentose phosphate (OPP) pathway could thus be confirmed.

These results lead to the conclusion that *Synechocystis* has no GDH/GK pathway. BLAST analyzes support this result (Mai 2020, unpublished; Figure 5:5).

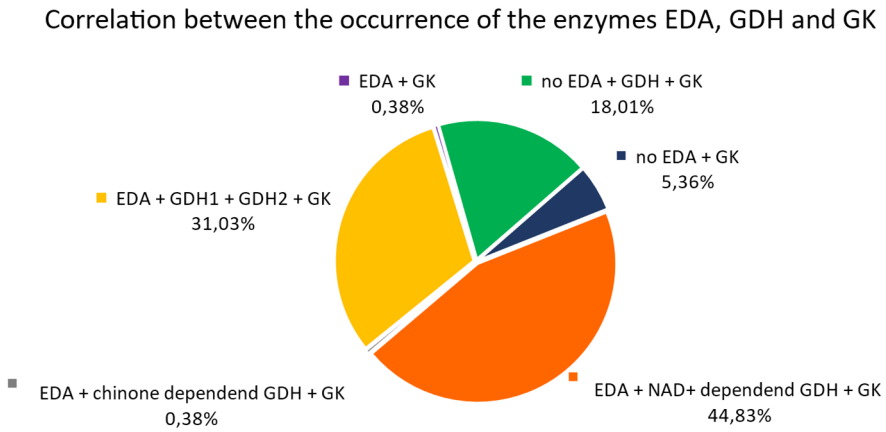

Figure 5:5: Occurrence of the KDPG aldolase (EDA) depending on the occurrence of the enzymes of the glucose dehydrogenase/ gluconate kinase (GDH/GK) pathway (GDH1, GDH2, GK). n=261 cyanobacteria were examined via BLAST-Analyses to have following homologous proteins sequences: Dark blue: cyanobacteria that have GK and no EDA; orange: cyanobacteria that have an NAD^+ dependent GDH; grey: cyanobacteria that have a quinone-dependent GDH; yellow: cyanobacteria that have GDH1, GDH2, GK and EDA, purple: cyanobacteria that have a GK and EDA; green: cyanobacteria that have no EDA, but a GK and at least one of the two GDH (Mai 2020, unpublished).

In *Synechocystis sp.* PCC 6803, for GDH and GK, no homologous protein sequences or only a slight match of the sequence in the genome could be detected. However, the analysis of 261 different cyanobacteria showed that the majority encode gluconate kinase and at least one glucose dehydrogenase if EDA is also present. *Synechocystis sp.* PCC 6803, therefore, presumably occupies a special position within the family of cyanobacteria with the absence of a GDH/GK pathway.

5.2. Physiological characterization of the lower glycolysis

The Calvin-Benson-Bassham (CBB) cycle provides the intermediate 3P-glycerate, which can be metabolized in three different ways. First, among others, the intermediate pyruvate can be metabolized via the lower glycolysis. Second, it can be converted to glyceraldehyde-3P (GAP) and be utilized for the regeneration of ribulose 5-P for another round of CO_2-fixation and third, it is used for gluconeogenesis. In conclusion, if 3P-glycerate feeds gluconeogenesis or is involved in the regeneration of the CBB cycle, no pyruvate would be provided from the CBB cycle via the lower glycolysis.

This leads to the second question in this thesis, whether the Entner-Doudoroff (ED) pathway represents an alternative route to provide pyruvate during these metabolic conditions. In other words, is EDA of importance for the provision of pyruvate under photoautotrophic, photomixotrophic and heterotrophic conditions when there is no flux through the lower glycolysis (Figure 5:6)?

To get a mutant, in which the lower glycolysis is interrupted, an enolase (*eno/Δeno*) deletion mutant was constructed. In addition, a *Δpgam1* and a *Δpgam2* deletion mutant were created for the cooperation partner AG Prof. Dr. Martin Hagemann of the University of Rostock. In this work, however, only the *eno/Δeno* mutant was characterized further.

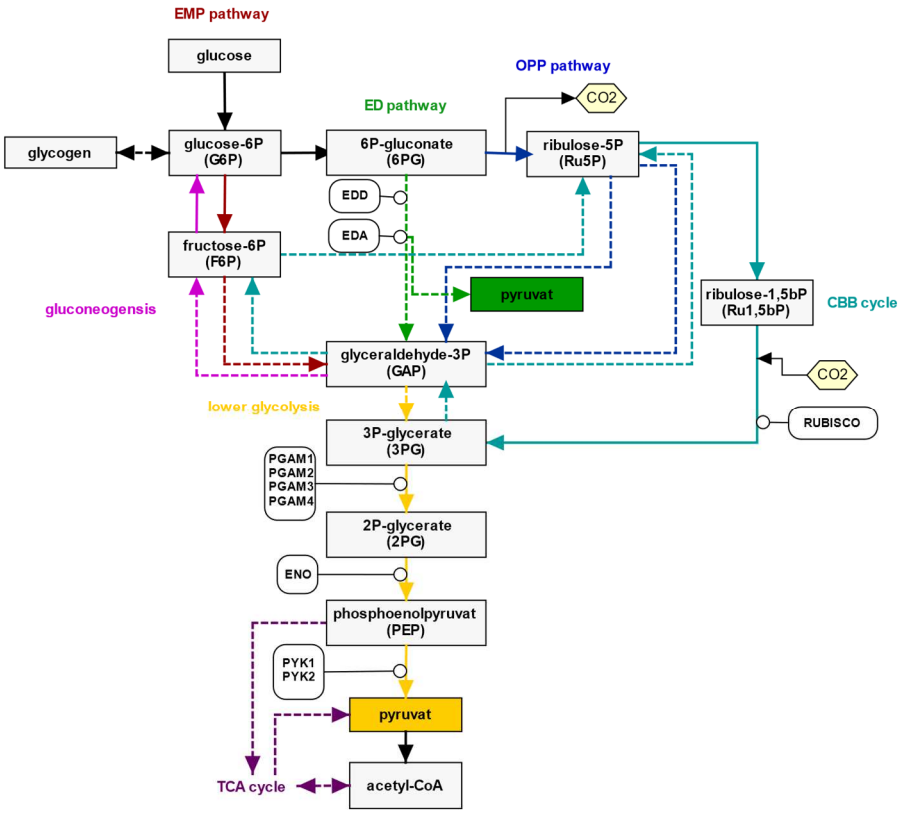

Figure 5:6: The lower glycolysis and Entner-Doudoroff (ED)-pathway as an alternative route to provide pyruvate. Simplified scheme of the central carbon metabolism in *Synechocystis*. 3P-glycerate of the Calvin-Benson-Bassham (CBB) cycle can alternatively be fed into lower glycolysis, gluconeogenesis or contribute to the regeneration of ribulose-1,5bP for CO_2 fixation. OPP: oxidative pentose phosphate, EMP: Emden-Meyerhof-Parnas.

5.2.1. Construction of the enolase (*enoΔeno*) and phosphoglycerate mutase (*Δpgam1, Δpgam2*) deletion mutants

The deletion mutants *Δpgam1* (slr1945), *Δpgam2* (sll0395), *eno/Δeno* (slr0752), *Δpyk1* (sll0587) and *pyk2/Δpyk2* (sll1275) were constructed (Table 4.11). Via homologue recombination, the *pgam1*-WT gene was replaced by an erythromycin resistance cassette. The *pgam2*-WT gene was replaced by a kanamycin resistance cassette. The *eno*-WT gene was replaced by a chloramphenicol resistance cassette. The flanking regions of putative *Δpgam1,* putative *Δpgam2* and *eno/Δeno*, were synthesized externally in a pUC57-Simple vector (Table 4.10). The vectors were opened through an EcoRV cutting side between the flanking regions. The antibiotic resistance cassettes for putative *Δpgam1,* putative *Δpgam2* and *eno/Δeno,* were produced by PCR and subsequently gel purified. After that, they were classically ligated into the vectors. As described in 4.2.5 and 4.2.6 the vectors were propagated, segregated and checked. After the sequences were found to be correct, *Synechocystis* WT cells were transformed with the putative *Δpgam1,* putative *Δpgam2* vectors (4.2.11). The segregation level of putative *Δpgam1* and putative *Δpgam2* was not tested in this work. The *Synechocystis* WT and the deletion mutant *Δeda, Δxfp1* and *ΔedaΔxfp1* were transformed with the *eno/Δeno* vector.

For segregation, the transformed cultures were grown on BG-11 plates containing the corresponding antibiotics. The transformation was attempted three times. However, it was not possible to delete all WT gene copies of *eno/Δeno* and to fully segregate the mutants (Figure 5:7).

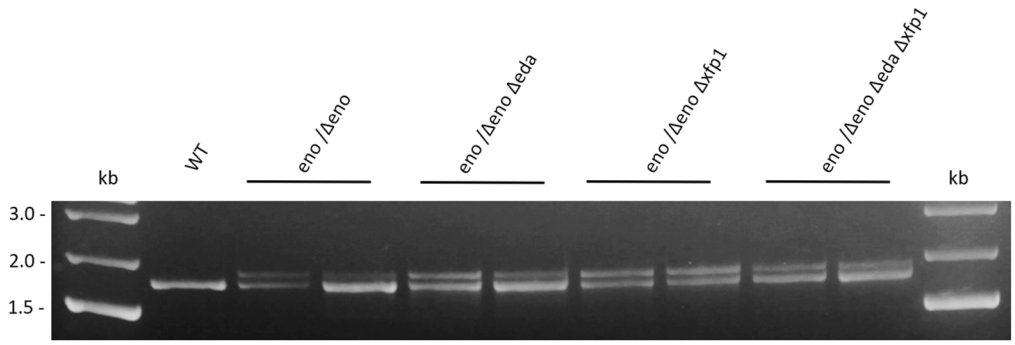

Figure 5:7: PCR with genomic DNA of *Synechocystis* WT and different *eno/Δeno* mutants. It is showing that *eno*, could not be deleted from all genomic copies in the respective mutants. GeneRuler™ 1kb Plus DNA ladder (lane 1, 11). Expected size for WT: 1749bp and *Δeno/Δeno*: 1847bp.

The function of the enolase in *Synechocystis* seems to be essential as it is the only enzyme that catalyzes the synthesis of phosphoenolpyruvate (*PEP*). PEP is not only the precursor of pyruvate but also of oxaloacetate. Oxaloacetate serves to replenish the TCA cycle. The TCA cycle produces reducing equivalents for respiration and intermediates for amino acid synthesis. Both are vital metabolic processes. According to that, the question of the extent to which the ED pathway can satisfy the pyruvate requirement if it is not generated by the lower glycolysis cannot be answered with an enolase mutant. Therefore, pyruvate kinase (*Δpyk1* and *pyk2/Δpyk2*) deletion mutant downstream of PEP was created.

5.2.2. Construction of the pyruvate kinase (*Δpyk1, pyk2/Δpyk2*) deletion mutants

There are two isoenzymes of pyruvate kinase in *Synechocystis*. PYK1 (sll0587) and PYK2 (sll1275). Via homologue recombination, the *pyk1*-WT gene was replaced by a chloramphenicol resistance cassette. The *pyk2*-WT gene was replaced by an erythromycin resistance cassette. The flanking regions of *Δpyk1* and *pyk2/Δpyk2*, were synthesized externally in a pUC57-Simple vector (Table 4.10). The vectors were opened through an EcoRV cutting side between the flanking regions. A chloramphenicol resistance cassette for *Δpyk1,* and an erythromycin resistance cassette for *Δpyk2,* were produced by PCR and subsequently gel purified. After that, they were classically ligated into the vectors. As described in 4.2.5 and 4.2.6, the vectors were propagated, segregated and checked. After the sequences were found to be correct, the *Synechocystis* WT and the deletion mutant *Δeda* and *Δxfp1Δxfp2* (4.2.11) were transformed with the *Δpyk2* vector. After the *Δpyk1* construct had also been completed, *Δeda* and the newly generated mutants *pyk2/Δpyk2*, *pyk2/Δpyk2Δeda*, *pyk2/Δpyk2Δxfp1Δxfp2* and the WT (4.2.11) were transformed with it. To produce the deletion mutants *Δpyk1pyk2Δpyk2Δgap1* ^{KmR} and *Δpyk1pyk2/Δpyk2-ΔedaΔgap1*^{KmR}, a new putative *Δgap1* ^{KmR} (sll0884) construct was additionally constructed with a kanamycin resistance cassette instead of a chloramphenicol resistance cassette.

Putative *Δgap1*^{KmR} was cloned via Gibson Assembly (4.2.2) and also propagated, segregated and checked. Thereafter, *Δpyk1pyk2/Δpyk2* and *pyk2/Δpyk2Δeda* were transformed with the putative *Δgap1*^{KmR} vector. The segregation level of, putative *Δgap1*^{KmR} was not checked, as the putative *Δgap1*^{KmR} mutants were not further analyzed in this work. For segregation, the transformed cultures were grown on BG-11 plates containing the corresponding antibiotics. The transformation was attempted at least three times, of not surviving mutants. However, transformation and segregation of *Δpyk1pyk2/Δpyk2Δeda* and *Δpyk1pyk2/Δpyk2ΔedaΔgap1*^{KmR} were not possible due to the inability to survive, missing both pyruvate kinase isoenzymes and *Δeda*. In other words, if the flow through the ED pathway and the lower glycolysis is closed, *Synechocystis* is no longer viable probably due to the inability to produce pyruvate.

The segregation level of the surviving mutants was checked by Southern Blot (4.2.15). Therefore, the genomic DNA of WT and all *Δpyk1* mutants was isolated (4.2.13) and digested with NcoI (Table 4.6). The genomic DNA of WT and all *pyk2/Δpyk2* mutants was isolated (4.2.13) and digested with HindIII (Table 4.6). As shown as in Figure 5:8, NcoI or HindIII cut in the WT of *pyk1* and *pyk2*, at different locations than in the respective antibiotic resistance cassettes of the deletion mutants (Figure 5:8).

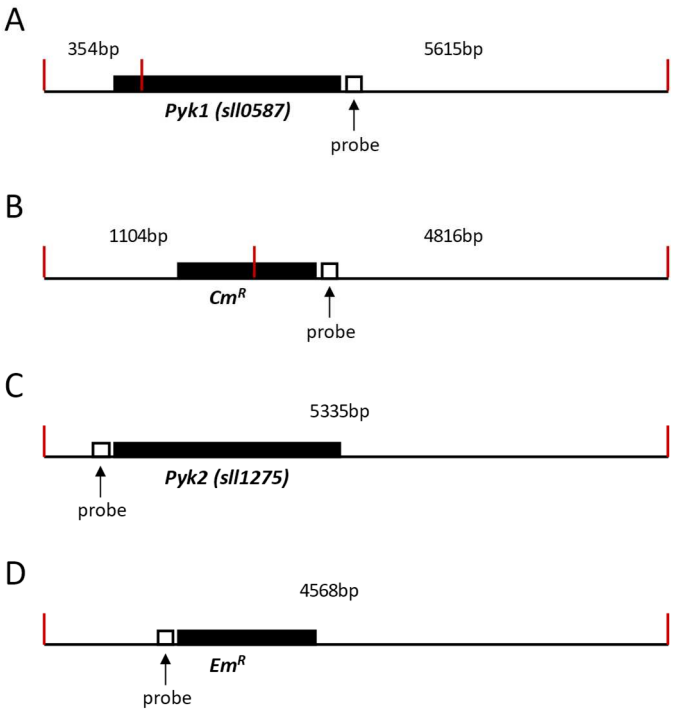

Figure 5:8: Position of restriction sites (shown in red) and hybridization site of PCR-probe. (A+B) *pyk1* WT and *Δpyk1* mutant DNA were digested with NcoI. (C+D) *pyk2* WT and *pyk2/Δpyk2* mutant DNA were digested with HindIII. (A) *pyk1* WT gene, (B) *Δpyk1*, (C) *pyk2* WT gene, (D) *pyk2/Δpyk2*.

It enables a distinction between WT copies and mutated copies. Complete segregation of *pyk1,* within the single mutant *Δpyk1,* the double mutant *Δpyk1pyk2/Δpyk2, Δpyk1Δeda* and the triple mutants *Δpyk1pyk2/Δpyk2Δgap1* could thus be confirmed (Figure 5:9 A).

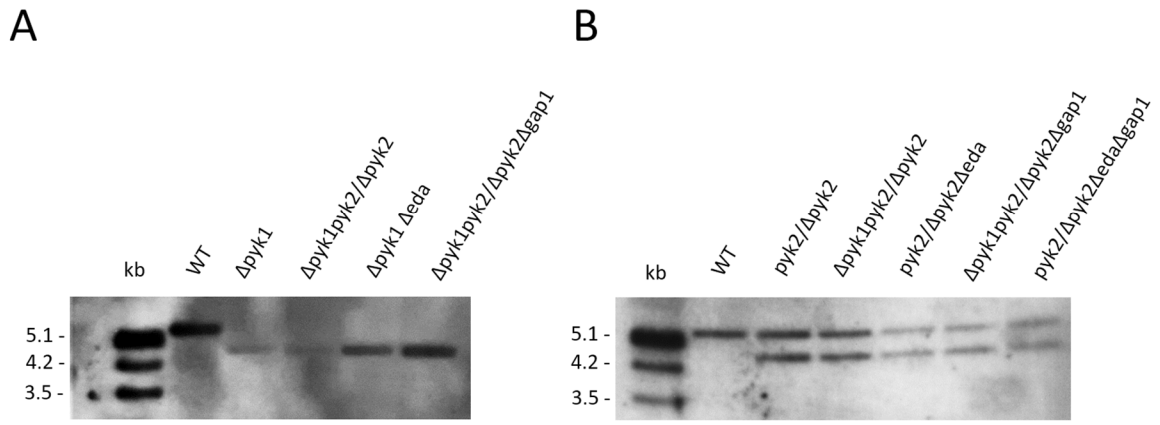

Figure 5:9: Southern blot with genomic DNA of *Synechocystis* WT and different *Δpyk* mutants. (A) It is showing that *Δpyk1, Δpyk1pyk2Δpyk2, Δpyk1Δeda* and *Δpyk1pyk2Δpyk2Δgap1*^{KmR} are completely segregated. DIG-labelled ʎ-HindIII ladder (lane 1). The blot was hybridized with a probe against *pyk1*. Expected size for WT: 5615bp and *Δpyk1*: 4816bp. (B) It is showing that *pyk2*, could not be deleted from all genomic copies in the respective mutants. DIG-labelled ʎ-HindIII ladder (lane 1). The blot was hybridized with a probe against *pyk2*. Expected size for WT:5335bp and *pyk2Δpyk2*: 4568bp.

However, complete segregation of *pyk2,* within the single mutant, *pyk2Δpyk2,* the double mutants, *Δpyk1pyk2/Δpyk2, pyk2/Δpyk2Δeda* and the triple mutants *Δpyk1pyk2/Δpyk2Δgap1*^{KmR} and *pyk2/Δpyk2ΔedaΔgap1*^{KmR} could thus be not confirmed. The level of segregation of *pyk2* in the mutant *pyk2/Δpyk2Δxfp1Δxfp2* was not tested. No matter in which of the tested mutants' lines, *Δpyk2* could not be segregated and seems to be essential for the survival of *Synechocystis* (Figure 5:9 B). This means that the lower glycolysis might be an indispensable source of pyruvate and cannot be completely compensated by the ED pathway.

5.2.3. Growth analysis of the pyruvate kinase (*Δpyk1, pyk2/Δpyk2*) deletion mutants

Since the simultaneous blocking of the Entner-Doudoroff (ED) pathway and lower glycolysis is lethal, we know that the ED pathway still plays a certain compensatory role in supplying the cells with pyruvate. Under which conditions and what extent, should be differentiated by growth experiments under photoautotrophic, photomixotrophic and heterotrophic conditions (4.4.2). To assess possible phenotypes of the mutants, growth was shown once through the optical density over time (4.4.3) and the growth values of the replicated growth curves (4.4.5).

Already during the generation of the deletion mutants, *pyk2/Δpyk2, Δpyk1pyk2/Δpyk2* and *pyk2/Δpyk2Δeda* showed a reduced growth behavior compared to the WT and *Δpyk1* on BG-11 plates. *pyk2eda* showed particularly reduced growth behavior. Cultivation of the cells on BG-11 plates wrapped in parafilm was even lethal. All *Δpyk* plates were therefore incubated in boxes without parafilm. At the beginning of the growth experiments, precultivation of *pyk2/Δpyk2Δeda* in shaking flasks and in Kniese tubes turned out to be lethal as well. We concluded that this was the first indications of the ED pathway being an important route to provide pyruvate even under autotrophic conditions. Surprisingly, under autotrophic conditions in Kniese tubes, *Δpyk1, pyk2/Δpyk2,* and *Δpyk1pyk2/Δpyk2* only showed minimally reduced growth in comparison to the WT (Figure 5:10 A,D).

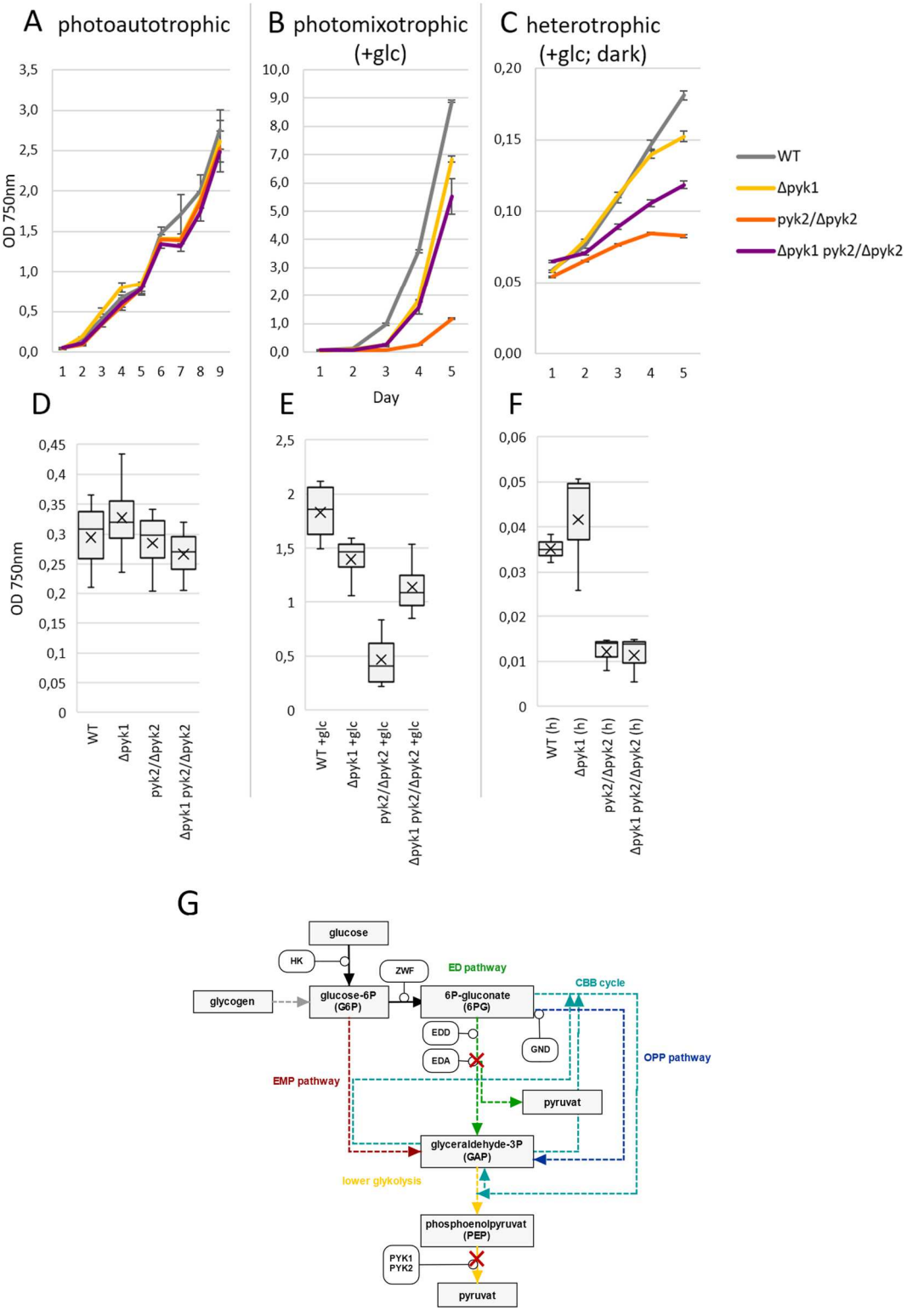

Figure 5:10: Growth of *Synechocystis* WT and different *Δpyk* mutants. Cultures error bars represent the standard deviation from at least three independent cultures, each measured in triplicate. Each growth experiment was repeated at least three times independently to ensure reproducibility. In the graph, the data of one growth experiment is shown. (A) Cultures were grown under photoautotrophic conditions in continuous light. (B) Cultures were grown under photomixotrophic (+10mM glucose) conditions in continuous light. (C) Cultures were grown under heterotrophic (+10mM glucose, dark) conditions in the dark. (D) Cultures growth rate grown under photoautotrophic conditions in continuous light. WT n=9, *Δpyk1* n=12, *pyk2/Δpyk2* n=12, *Δpyk1pyk2/Δpyk2* n=12. (E) Cultures growth rate grown under photomixotrophic (+10mM glucose) conditions in continuous light. WT+glc n=12, *Δpyk1*+glc n=12, *pyk2/Δpyk2*+glc n=12, *Δpyk1pyk2/Δpyk2*+glc n=12. (F) Cultures growth rate grown under heterotrophic (+10mM glucose, dark) conditions in darkness. WT(h) n=9, *Δpyk1*(h) n=9, *pyk2/Δpyk2*(h) n=9, *Δpyk1pyk2/Δpyk2*(h) n=9. (G) Simplified scheme illustrating the ED pathway and the lower glycolysis as possible routes to provide pyruvate.

Since *pyk2/Δpyk2Δeda* could not be cultivated in liquid cultures, the growth behavior under autotrophic conditions for the mutants *Δpyk1, pyk2/Δpyk2, Δpyk1pyk2/Δpyk2, Δpyk1Δeda, pyk2/Δpyk2Δeda* and *Δeda* were examined directly on plates. Spot assays were carried out for this (Figure 5:11).

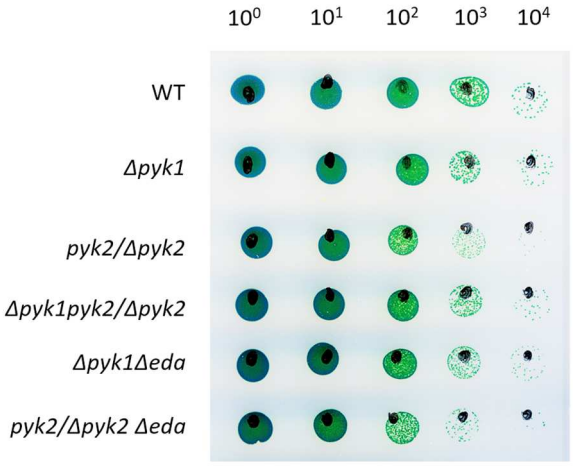

Figure 5:11: Spot assay on solid BG-11 agar of *Synechocystis* WT and pyruvate kinase mutants under photoautotrophic condition. Dilution is indicated in the top row. The spot assay was evaluated after nine days of cultivation.

As previously seen, *pyk2/Δpyk2* and *pyk2/Δpyk2Δeda*, showed reduced growth compared to the WT. *Δeda*, *Δpyk1Δeda* and *Δpyk1pyk2/Δpyk2* also showed a slightly reduced growth behavior than the WT. However, *Δpyk1* showed no deficiency in growth. It is evident that the main part of the pyruvate is formed via the lower glycolysis since *pyk2/Δpyk2* grew worse than *Δeda*. It can also be concluded that the isoenzyme PYK2 plays a more dominant role in the conversion of PEP into pyruvate under autotrophic conditions than PYK1. In Kniese tubes, under photomixotrophic (Figure 5:10 B, E) and heterotrophic (Figure 5:10 C, F) conditions, *pyk2/Δpyk2* had even more problems in growth. The double mutant grew somewhat better in both cases, but since *pyk2/Δpyk2* is not segregated, it cannot be ruled out that there are more WT gene copies of *pyk2/Δpyk2* in the double mutant *Δpyk1pyk2/Δpyk2* than in the single mutant and therefore it looks as if the double mutant had fewer problems growing.

In summary, the ED pathway plays a role to satisfy the pyruvate requirement of the cell. However, the primary source of pyruvate is the lower glycolysis. If the flux through the lower glycolysis is entirely closed, the cell cannot survive. During gluconeogenesis or the regeneration of the CBB cycle, the ED pathway can “step in” to produce pyruvate, but this is more a matter of fine regulation than complete compensation. Whether the ED pathway is compensating a reduced flux of the lower glycolysis, or a complete lack of the lower glycolysis for a short time, could not be differentiated.

5.3. Physiological characterization of the phosphoketolase pathway

Pyruvate serves as the substrate for various metabolic pathways, but the oxidative decarboxylation of pyruvate to acetyl-CoA represents the pivot of energy metabolism in *Synechocystis*. Acetyl-CoA is the important supplier of the TCA cycle with an acetyl group, which is oxidized to CO_2 and water. During this process, the main part of the cells needed intermediates is generated. However, acetyl-CoA can be generated not only from pyruvate but also from acetyl phosphate, which is produced in *Synechocystis* via the phosphoketolase pathway (Figure 5:12).

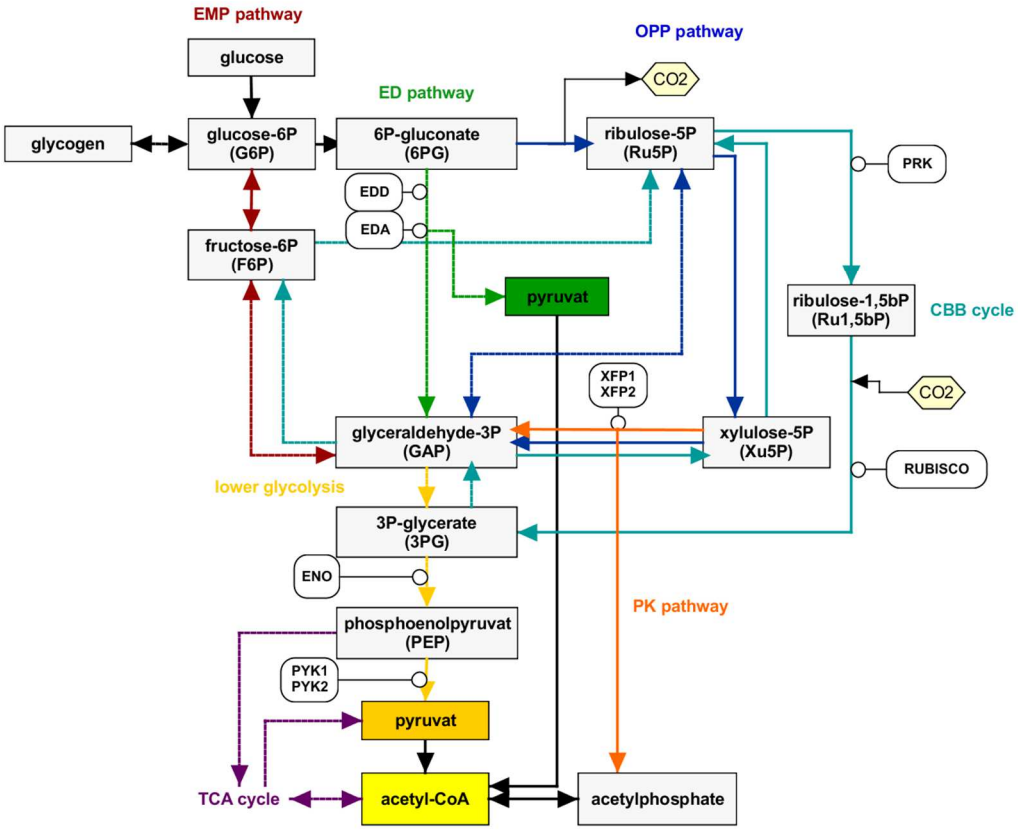

Figure 5:12: Pyruvate of the lower glycolysis and the phosphoketolase (PK) pathway as a potential alternative route to provide acetyl-CoA. Simplified scheme of the central carbon metabolism in *Synechocystis*.

Synechocystis has two putative isoenzymes of the phosphoketolase, XFP1 (slr0453) and putative XFP2 (sll0529). Theoretically, phosphoketolase can catalyze three reactions. (i) The conversion of xylulose-5P to glyceraldehyde-3P (GAP). This reaction runs parallel to the OPP pathway and in the opposite direction to the CBB cycle. (ii) The conversion of fructose-6P to erythrose-4P (not shown), running parallel to the CBB cycle. (iii) The conversion of fructose-6P (not shown) or xylulose-5P to acetyl phosphate. This reaction takes place without opposing reactions and bypasses the entire lower glycolysis. It is not known yet which reactions are catalyzed by putative XFP1 or/and XFP2 in *Synechocystis*. This leads to the third question of this thesis, whether and to what extent the pyruvate produced in the ED pathway is required as an acetyl-CoA source. To clarify this question, deletion mutants for the genes *xfp1* and *xfp2* were constructed (Table 4.11).

5.3.1. Construction of the phosphoketolase (*Δxfp1, Δxfp2*) deletion mutants

Via homologue recombination, the *xfp1*-WT gene was replaced by a spectinomycin resistance cassette. The *xfp2* WT gene was replaced by a kanamycin resistance cassette. *Δxfp1* was generated via Gibson Assembly (4.2.2). For this purpose, 200-300bp long DNA fragments, up and downstream of *xfp1*, were amplified by PCR (4.2.1). The Gibson primers for this are listed in (Table 4.7). Also, the spectinomycin resistance cassette was amplified via PCR. All PCR products were gel-purified (4.2.8). The Bluescript vector (Table 4.10) was opened with EcoRV (Table 4.6) and acted as the recipient vector. The two fragments, the spectinomycin resistance cassette and the opened vector were then cloned together.

Since *Δxfp2* was to be cloned quickly to *Δxfp1*, the flanking regions were synthesized externally in a pUC57-Simple vector (Table 4.10). The vector was also opened through an EcoRV cutting side between the flanking regions. A kanamycin resistance cassette produced by PCR and subsequently gel-purified was then classically ligated into the vector. As described in 4.2.5 and 4.2.6, the vectors were propagated, segregated and checked. After the sequence was found to be correct, *Synechocystis* WT and the deletion mutants *Δeda* and *Δgap1* (4.2.11) were transformed with the *Δxfp1* vector. After the *Δxfp2* construct had also been completed, the newly generated mutants *Δxfp1*, *Δxfp1Δeda*, *Δxfp1Δgap1* and the WT were transformed with it as well. For segregation, the transformed cultures were grown on BG-11 plates containing the corresponding antibiotics. The segregation was checked by Southern Blot (4.2.15). Therefore, the genomic DNA of WT and all mutants were isolated (4.2.13) and digested with HindIII (Table 4.6). As shown in Figure 5:13, the HindIII enzyme cut in the WT of *xfp1* and *xfp2*, at different locations than in the respective antibiotic resistance cassettes of the deletion mutants. It enables a distinction between WT copies and mutated copies.

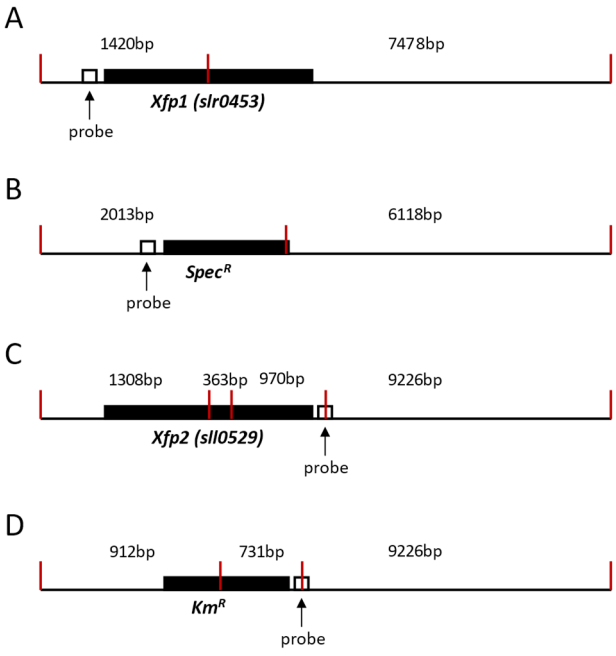

Figure 5:13: Position of HindIII restriction sites (shown in red) and hybridization site of PCR-probe. (A) *xfp1* WT gene, (B) *Δxfp1,* (C) *xfp2* WT gene, (D) *Δxfp2.*

Complete segregation of *Δxfp1* (Figure 5:14 A) and *Δxfp2* (Figure 5:14 B), within the corresponding single mutants *Δxfp1* and the double mutant *Δxfp1Δxfp2* and the triple mutants *Δxfp1Δxfp2Δeda*, *Δxfp1Δxfp2Δgap1, Δxfp1Δxfp2ΔedaΔgap1* could thus be confirmed.

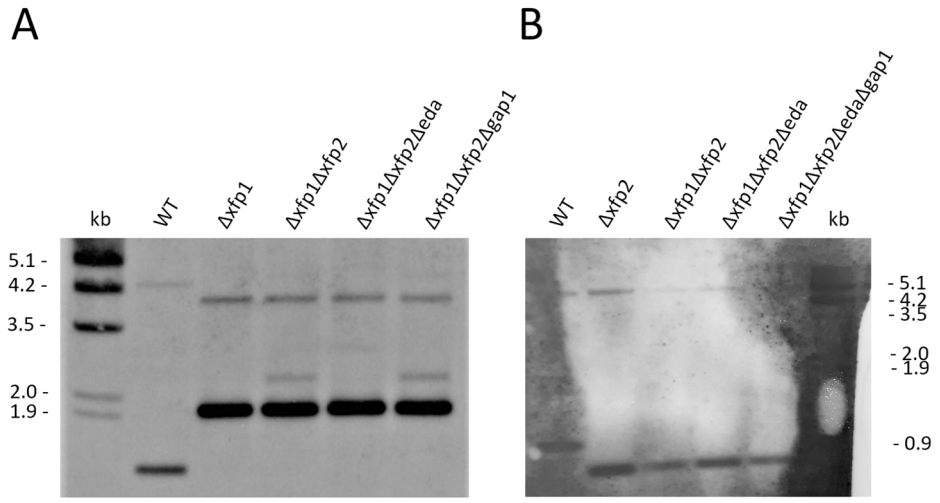

Figure 5:14: Southern blot with genomic DNA of *Synechocystis* WT and different *Δxfp* mutants. It is showing that *Δxfp1, Δxfp1Δxfp2, Δxfp1Δxfp2Δeda* and *Δxfp1Δxfp2Δgap1* are completely segregated. (A) DIG-labelled Λ-HindIII ladder (lane 1). The blot was hybridized with a probe against *xfp1*. Expected size for WT:1420bp and *Δxfp1*: 2013bp. (B) DIG-labelled Λ-HindIII ladder (lane 6). The blot was hybridized with a probe against *xfp2*. Expected size for WT: 970bp and *Δxfp2*: 731bp.

5.3.2. Growth analysis of the phosphoketolase (*Δxfp1, Δxfp2*) deletion mutants

As analyzed in the previous chapter, the main pyruvate and therefore probably also a large part of the acetyl-CoA supply of *Synechocystis* is provided via the lower glycolysis. If the acetyl-CoA source, the phosphoketolase (PK) pathway, is shut down, does the Entner-Doudoroff (ED) pathway compensate for it or is the pyruvate supply sufficient through the lower glycolysis only?

For a physiological characterization, the growth of the *Δxfp* mutants was examined under photoautotrophic, photomixotrophic and heterotrophic conditions (Figure 5:15). For this, the cells were grown as described in 4.4.2. To assess possible phenotypes of the mutants, growth was shown once through the optical density over time (4.4.3) and the growth values of the replicated growth curves (4.4.5). Even before the growth experiments, it was noticeable that *Δxfp1Δxfp2Δeda* grew more slowly on the BG-11 plates in comparison to the other *Δxfp* mutants. In addition, like the *pyk2/Δpyk2* mutants, *Δxfp1Δxfp2Δeda* could not be precultivated in shaking flasks. This turned out to be lethal. Precultivation therefore, did not take place. The growth experiments were started directly with cells from BG-11 plates. Cultivated in Kniese tubes, *Δxfp2, Δxfp1Δxfp2* and *Δxfp1Δxfp2Δeda* showed reduced growth compared to WT and *Δxfp1*. However, *Δxfp1Δxfp2Δeda* did not show the reduced growth that it had shown on plates (Figure 5:15).

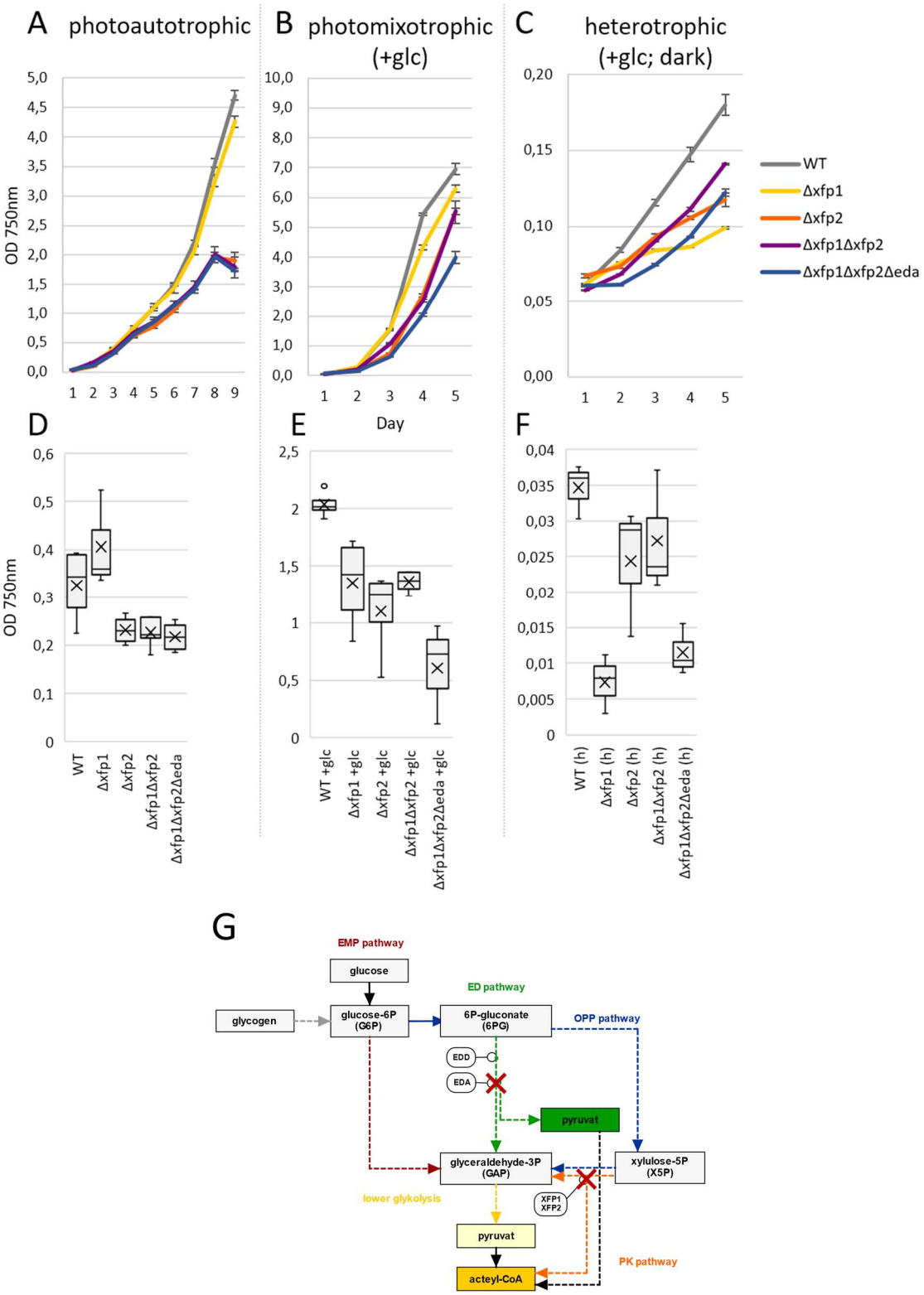

Figure 5:15: Growth of *Synechocystis* WT and different *Δxfp* mutants. Cultures error bars represent the standard deviation from at least three independent cultures, each measured in triplicate. Each growth experiment was repeated at least three times independently to ensure reproducibility. In the graph, the data of one growth experiment is shown. (A) Cultures were grown under photoautotrophic conditions in continuous light. (B) Cultures were grown under photomixotrophic (+10mM glucose) conditions in continuous light. (C) Cultures were grown under heterotrophic (+10mM glucose, dark) conditions in the dark. (D) Cultures growth rate grown under photoautotrophic conditions in continuous light. WT n=12, *Δxfp1* n=9, *Δxfp2* n=12, *Δxfp1Δxfp2* n=15. (E) Cultures growth rate grown under photomixotrophic (+10mM glucose) conditions in continuous light. WT+glc n=15, *Δxfp1*+glc n=12, *Δxfp2*+glc n=12, *Δxfp1Δxfp2*+glc n=15. (F) Cultures growth rate grown under heterotrophic (+10mM glucose, dark) conditions in darkness. WT(h) n=9, *Δxfp1*(h) n=9, *Δxfp2*(h) n=9, *Δxfp1Δxfp2*(h) n=9. (G) Simplified scheme illustrating the lower glycolysis and the phosphoketolase (PK) pathway as possible routes to provide pyruvate and acetyl-CoA.

Therefore, additional spot assays were carried out (Figure 5:16). The spot assays illustrated the result of the growth tests in Kniese tubes that *Δxfp2* and *Δxfp1Δxfp2* are significantly reduced in growth. The fact that *Δxfp1Δxfp2Δeda* shows an even greater deficiency in growth could be made visible by the spot assay.

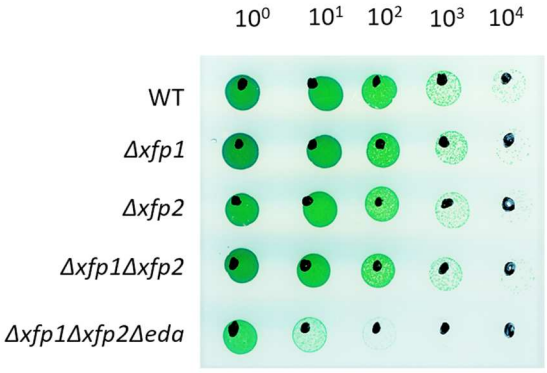

Figure 5:16: Spot assay on solid BG-11 agar of *Synechocystis* WT and phosphoketolase mutants under photoautotrophic condition. Dilution is indicated in the top row. The spot assay was evaluated after 9 days of cultivation.

One interpretation of these results could be that the ED pathway and lower glycolysis might be insufficient as suppliers of acetyl-CoA and that the phosphoketolase pathway might be important to satisfy *Synechocystis*' demand for acetyl-CoA. The photomixotrophic (Figure 5:15 B, E) and heterotrophic (Figure 5:15 C, F) growth experiments in Kniese tubes confirmed this. Under photomixotrophic conditions, all *Δxfp* mutants showed reduced growth, while the triple mutant *Δxfp1Δxfp2Δeda* grew particularly poorly. Under heterotrophic conditions, the mutants behaved similarly. However, *Δxfp1* grew even worse than *Δxfp1Δxfp2Δeda*. It should be noted, however, that all mutants showed very reduced growth in comparison to the WT and that the measured OD_{750} was in the range of fluctuation of the photometer. Nonetheless, it can be summarized that under photoautotrophic, photomixotrophic and probably under heterotrophic conditions, the ED pathway might be a route to provide pyruvate as a precursor for acetyl-CoA. However, the ED pathway is not able to compensate for the loss of the phosphoketolase (PK) pathway fully.

5.4. Experimental analysis of the organization and dynamic of anabolic and catabolic key enzymes

Synechocystis is a non-compartmentalized cell. It is already known that anabolic and catabolic metabolism co-occurs. CO_2 fixation via the Calvin-Bensons-Bassham (CBB) cycle operates in parallel to carbohydrate oxidation via glycolytic routes. Glycolytic routes are roughly a reverse of the CBB cycle. Some enzymes operate in both processes. As an enzyme is not able to simultaneously support a metabolic flux in opposing directions, anabolic and catabolic processes must be regulated. Photoautotrophic eukaryotes such as plants have organelles that create different reaction spaces and separates anabolic and catabolic reactions. This fact leads to the fourth question of this thesis, how the anabolic and catabolic metabolism in *Synechocystis*, as a non-compartmentalized cell, is organized and how dynamically this organization takes place.

It is already known that the key enzymes PRK and GAP2 (also referred to as GAPDH) of the anabolic CBB cycle are regulated depending on light (Michelet et al. 2013). The small protein CP12 mediates this regulation by forming a redox-dependent trinary complex with PRK and GAP2. In light, the conditions are reducing, and CP12 is inactive (Gontero and Maberly 2012). In light, there are oxidized conditions and CP12 releases binding sites for GAP2 and PRK (Reichmann and Jakob 2013). The complex formation inactivates GAP2 and PRK. This will stop the CBB cycle. This complex formation was discovered and described using various proteomic based methods, such as X-ray crystallography and cryo-microscopy (cryoEM; McFarlane et al. 2019). Nevertheless, with these methods, the enzyme complex was “only” detected *in vitro*. The organization and dynamics *in vivo* have not yet been investigated. We hypothesize that the PRK-CP12-GAP2 complex formation can be detected by fluorescence microscopy via formed fluorescence clusters. Conversely, this means that the dissolution of the clusters under light and thus a dispersed fluorescence signal is detectable as well. This approach should serve as a “proof of principle” of fluorescence microscopy as a suitable method to investigate *in vivo*, the organization and dynamics of enzyme complexes as well as a positive control for further experiments investigating the organization and dynamics of catabolic enzymes.

As recently discovered, the CBB cycle does not run entirely autonomously (Makowka et al. 2020). Glycolytic pathways as the Entner-Doudoroff (ED), oxidative pentose phosphate (OPP) and Embden-Meyerhof-Parnas (EMP) pathway do not only exist for breaking down glucose to pyruvate and acetyl-CoA, they also function as so-called glycolytic shunts under photoautotrophic conditions and replenish the CBB cycle. How this process is organized enzymatically is not known yet. Photomixotrophically, the cell has a high supply on bioavailable carbon, bound in the form of CO_2 by the Rubisco of the CBB cycle and by the breakdown of glucose via the glycolytic pathways. Therefore, we hypothesize that the key enzymes of the CBB cycle and the glycolytic enzymes of the ED, OPP, and EMP pathway could also be organized glucose-dependent.

5.4.1. Construction of the fluorescence strains (*GFP-His, YFP-His*)

To examine the organization and dynamics of the PRK-CP12-GAP2 complex via fluorescence microscopy, a PRK YFP-His, PRK GFP-His, GAP2-YFP-His and GAP2 GFP-His mutant was constructed. As key enzymes of the catabolic metabolism, EDA and EDD (ED pathway), GND and ZWF (OPP pathway) and GAP1 (lower glycolysis) were tagged with GFP-His and YFP-His, each, as well.

To produce *Synechocystis* mutants in which the gene of interest is C-terminally tagged with GFP-His or YFP-His, a mutagenesis vector was cloned for each protein of interest. The mutagenesis vectors all had the same structure. They contained the following gene sequences: The last 200bp of the gene of interest (GOI) as the first flanking region, the fluorophore eGFP (hereafter GFP) or YFP, a His-tag, the respective resistance cassette and at the end 200bp downstream of the GOI as the second flanking region (4.2.3; Figure 4:1). *Synechocystis* WT was transformed with each mutagenesis vector, generating the following mutants: PRK GFP-His, PRK YFP-His, GAP2 GFP-His, GAP2 YFP-His, EDA GFP-His, EDA YFP-His, EDD GFP-His, EDD YFP-His, GND GFP-His, GND YFP-His, ZWF GFP-His, ZWF YFP-His, GAP1 GFP-His and GAP1 YFP-His. For segregation, the transformed cultures were grown on BG-11 plates containing the corresponding antibiotic (4.4.2, Table 4.2). The segregation was checked by a PCR and subsequently by gel electrophoresis (4.2.7). No untagged WT gene could be amplified from genomic DNA of PRK GFP-His, PRK YFP-His, GAP2 GFP-His, EDA GFP-His, EDA YFP-His, EDD GFP-His, EDD YFP-His, GND GFP-His, GND YFP-His, ZWF YFP-His, GAP1 GFP-His and GAP1 YFP-His mutants (Figure 5:17) and could thus be confirmed as fully segregated. However, GAP2 YFP-His and ZWF GFP-His could not be fully segregated (Figure 5:17). The transformation was attempted three times.

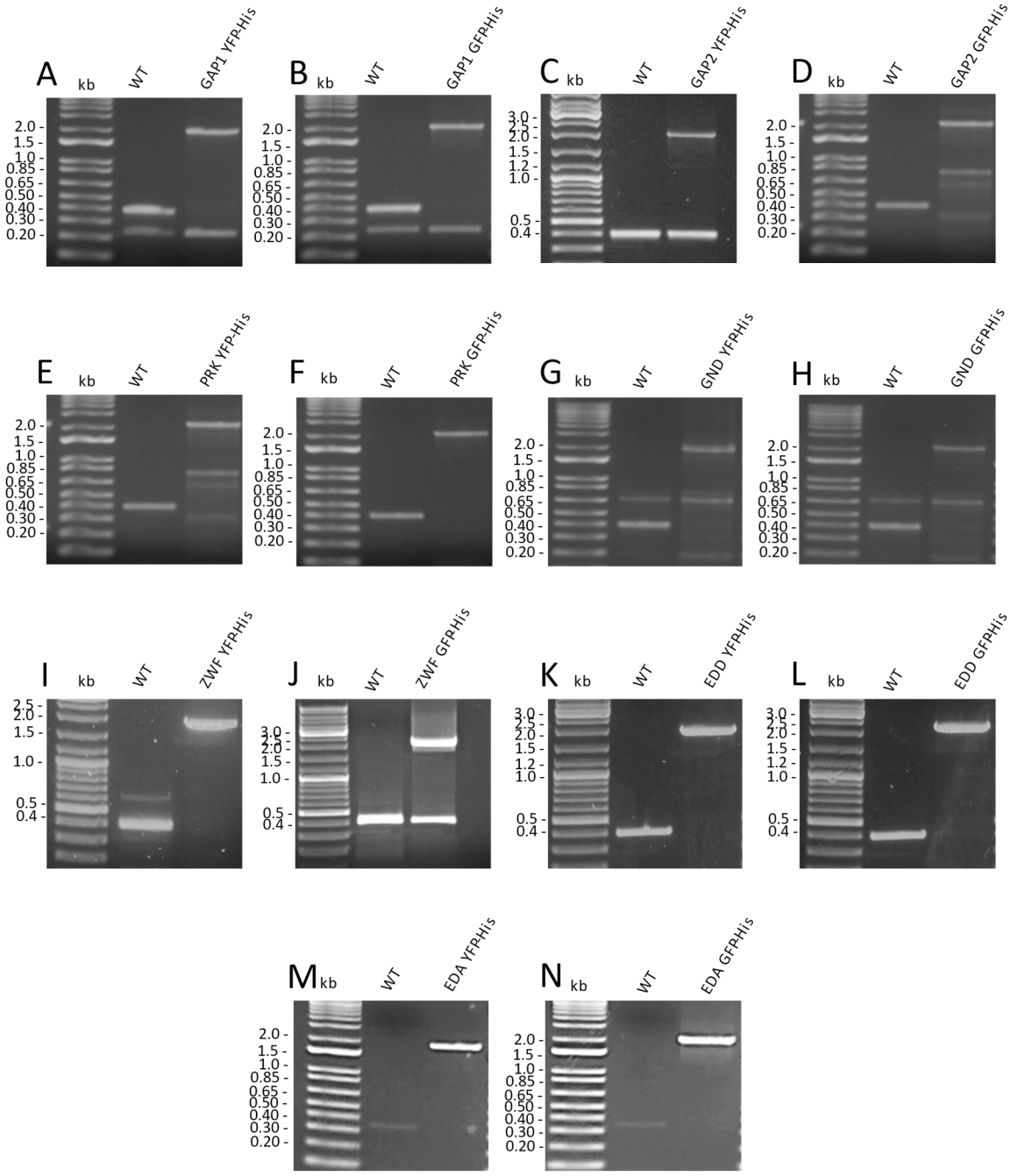

Figure 5:17: PCR with genomic DNA of WT and different fluorescence mutants. It is showing that (A) GAP1 YFP-His, (B) GAP1 GFP-His, (D) GAP2 GFP-His, (E) PRK YFP-His, (F) PRK GFP-His, (G) GND YFP-His, (H) GND GFP-His, (I) ZWF-YFP-His, (K) EDD YFP-His, (L) EDD-GFP-His, (M) EDA YFP-His, (N) EDA GFP-His are completely segregated. (C) GAP2 YFP-His, (J) ZWF GFP-His could not be deleted from all genomic copies. Expected size for WT: 400bp, GFP-His: 2210bp, YFP-His: 1994bp. Used DNA ladder: C, I, J, K, L GeneRuler™ 1kb Plus DNA ladder; A, B, D, E, F, G, H, M, N E-Gel™ 1kb Plus DNA ladder.

5.4.2. Verification of the fluorophore tagged proteins

After the mutants had been constructed, it was checked if the GFP-His or the YFP-His was expressed together with the upstream protein of interest. Simplified, it should be excluded that free GFP-His or YFP-His is detected during microscopy instead of the expression of the protein of interest. Western blots were carried out for this (4.3.1- 4.3.4; Figure 5:18). Whole-cell extracts of the mutants, which were cultured photoautotrophically, photomixotrophically and heterotrophically for four days (4.4.2), were analyzed. Since the gene sequence of YFP differs from GFP only by seven base pairs, the GFP antibody (Table 4.27) was also used for YFP mutants. To have options in the choice of antibodies and for possible pull-down assays in the future, the mutants were constructed with a His-tag attached to the fluorophore at the C-terminal. This His-Tag was additionally detected with an antiHis antibody (Table 4.27). The samples were normalized based on the chlorophyll content. However, based on the Coomassie gels (Figure 5:18), it was clear that the normalization of the probes based on the chlorophyll content was not sufficiently homogeneous. A quantitative interpretation between the different conditions and mutants is therefore difficult. The data were only evaluated qualitatively. It was conspicuous that the antiHis antibody was more sensitive than the antiGFP antibody, and thus, even low expression could be detected. However, just in the case of the YFP-His samples, except for EDA, all proteins could be detected with the antiHis antibody under all cultivation conditions (Figure 5:18 D). It is known that EDA is only slightly expressed natively and could not be detected at all (Figure 5:18 C, D). Based on these results, it was decided to continue with the YFP-His mutants for further microscopy studies.

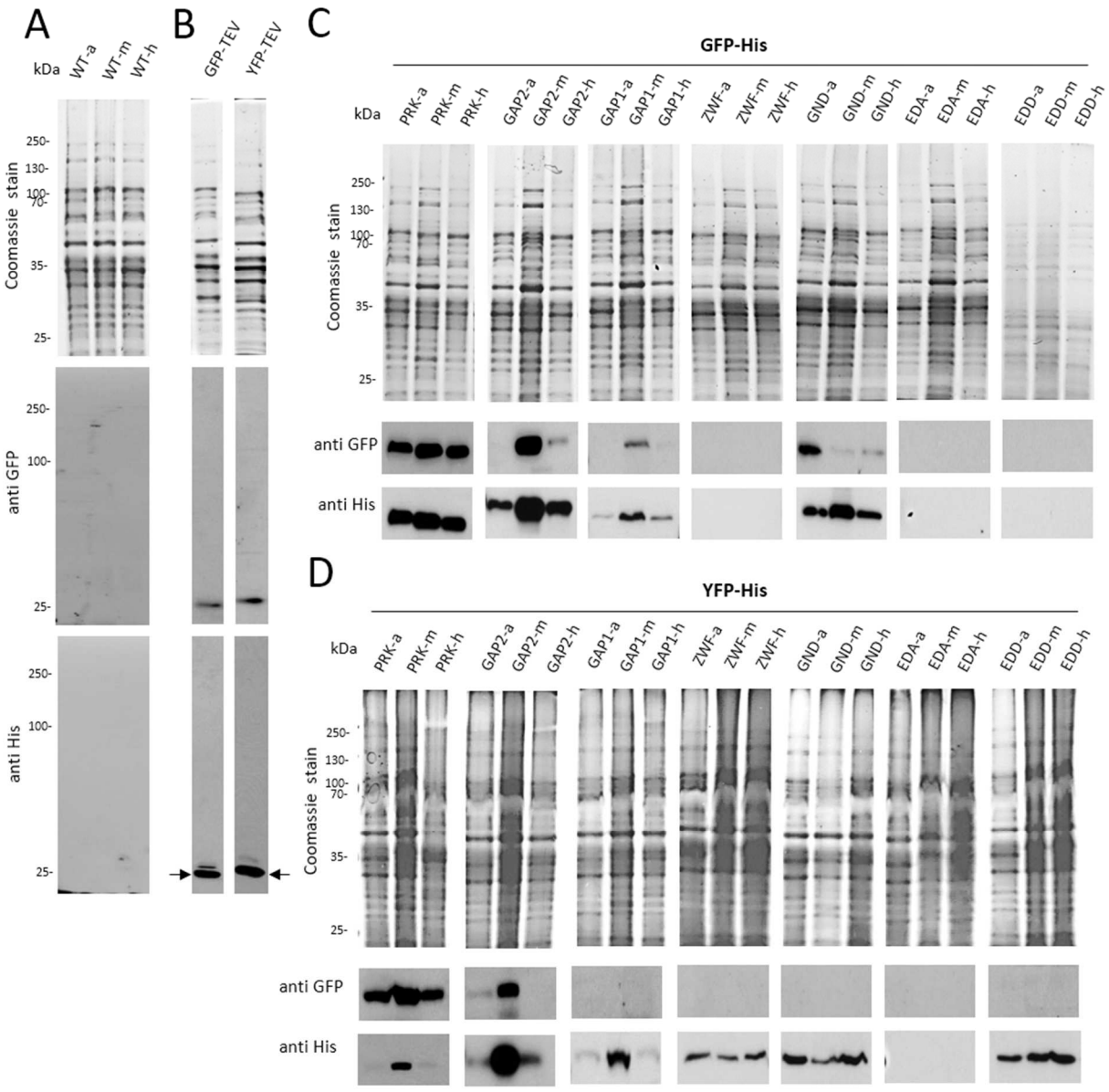

Figure 5:18: Coomassie gel and Western Blot detection of anabolic and catabolic key enzymes under photoautotrophic (-a), photomixotrophic (-m) and heterotrophic (-h) conditions. Whole-cell extract was used to check that the attached GFP-His and YFP-His of the respective tagged proteins are expressed and that the fluorophores are not free but are bound to the protein of interest. According to the results of the chlorophyll determination, in each lane, the same amount of chlorophyll (0.15µg) was loaded. (A) Negative control with the untagged WT: Coomassie stain and Western Bot against GFP and His-Tag. (B) Positive control for free GFP and YFP as well as GFP-His and YFP-His: Exemplary, the GFP-His was cut off the PRK GFP-His mutant, and the YFP-His was cut off the PRK YFP-His mutant with a TEV protease. The TEV protease itself contains a His sequence, which results in the Western blot against antiHis in an extra band (marked with arrows). Expected size for the TEV protease: 27kDa. Expected size for GFP and YFP: ~26.5kDa. Expected size for GFP-His and YFP-His: ~27.5kDa. (C) Coomassie stain and Western blot against GFP and His-Tag of all GFP-His tagged proteins of interest. Expected sizes for the GFP-His tagged proteins: PRK GFP-His ~53kDa, GAP2 GFP-His ~68kDa, GAP1 GFP-His ~69kDa, ZWF GFP-His ~76kDa, GND GFP-His ~84kDa, EDA GFP-His ~53kDa, EDD GFP-His ~54kDa. (D) Coomassie stain and Western blot against YFP and His-Tag of all YFP-His tagged proteins of interest. Expected sizes for the YFP-His tagged proteins: PRK YFP-His ~53kDa, GAP2 YFP-His ~68kDa, GAP1 YFP-His ~69kDa, ZWF YFP-His ~76kDa, GND YFP-His ~84kDa, EDA YFP-His ~53kDa, EDD YFP-His ~54kDa.

5.4.3. Growth experiment of mutants with fluorophore tagged proteins

Before the microscopy experiment was started, it had to be checked that the attachment of a YFP-His to the protein of interest does not interfere with the functionality of the enzyme. For this, growth experiments, as described in 4.4.2 and 4.4.3, were carried out (Figure 5:19).

.

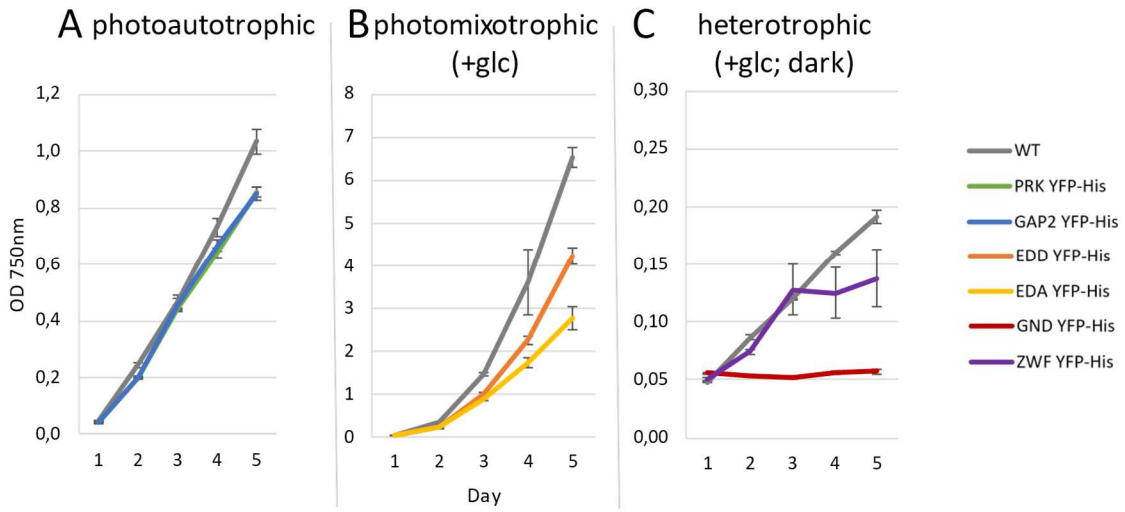

Figure 5:19: Growth of different *Synechocystis* YFP-His. Cultures Error bars represent the standard deviation from at least three independent cultures, each measured in triplicate. Each growth experiment was repeated independently two times. In the graph, the data of one growth experiment is shown. (A) Cultures grown under photoautotrophic conditions in continuous light. (B) Cultures grown under photomixotrophic (+glc) conditions in continuous light. (C) Cultures were grown under heterotrophic (+glc, dark) conditions in darkness.

The mutants were grown under the conditions (photoautotrophic, photomixotrophic, heterotrophic) under which it is known that a deletion of the gene results in a strong growth phenotype. A functionless PRK or GAP2 (Makowka 2019) would be lethal for *Synechocystis* cells under photoautotrophic conditions. A functionless EDA or EDD (Chen et al. 2016) would lead to reduced growth under photomixotrophic conditions. A functionless GND or ZWF (Makowka et al. 2020) would also lead to reduced growth under heterotrophic conditions. For the deletion of GAP1, however, no phenotype has yet been described, which is why this mutant was not tested for its growth behavior in this work. An impairment of the catabolic key enzymes PRK and GAP2 by the C-terminal YFP-His could not be detected (Figure 5:19 A). The mutants PRK YFP-His and GAP2 YFP-His grew photoautotrophically like the WT. EDA YFP-His and EDD YFP-His, on the other hand, showed a “deletion” phenotype under photomixotrophic condition (Figure 5:19 B), which may indicate that the YFP-His Tag disrupts the protein function. The same for GND YFP-His, which showed a reduced growth phenotype. In contrast, ZWF YFP-His showed no deletion phenotype (Figure 5:19 C). Despite these results, experiments were continued with all YFP-His mutants and evaluated microscopically, since it is not known whether the impairment in growth is caused by a "misfolded" protein or by a failure to interact with other proteins.

5.4.4. Investigation of the organization and dynamics of anabolic and catabolic key enzymes

As a reminder, the overall aim was to examine the organization and dynamics of the anabolic enzymes PRK and GAP2 (CBB cycle) as well as of the catabolic enzymes EDA and EDD (ED pathway), GND and ZWF (OPP pathway) and GAP1 (EMP pathway), *in vivo*. To investigate the organization and dynamics of the key proteins in general, we treated all cultures for three days (long term experiment, 5.4.4.1), under the influence of light (photoautotrophic), under the influence of light with glucose (photomixotrophic) and in the dark with the addition of glucose (heterotrophic). The three days were chosen because it is known from previous research (Makowka et al. 2020) that *Synechocystis* cells metabolize the total glucose (10mM) of the cultivation media, within four days. Accordingly, on day three, all cells should have shifted to a "real" photomixotrophic and heterotrophic metabolism. The cell cultures were then prepared as described in 4.4.7.1 for fluorescence microscopy, which in turn was carried out as described in 4.4.7.2. The resulting microscopy images were evaluated as described in 4.4.7.3. The mean YFP fluorescence intensity, YFP standard deviation, the number of clusters per cell and the average cluster intensity, were determined for each cell. Clusters are, in this thesis, defined signal spots, which indicate an accumulation of fluorophore-tagged enzymes.

Since GAP2 YFP-His was not completely segregated, it should be excluded that untagged "WT" cells of the culture are measured. Therefore, GAP2 YFP-His cells were evaluated that had at least twice the mean fluorescence intensity of the WT (4.5.2). The image analyzation was made using the program Fiji, for which a macro was specially written by Marius Theune from our group (4.4.7.3). Fluorescence signals with at least twice the intensity of the mean YFP fluorescence intensity were defined as enzyme clusters. The absolute fluorescence intensity per cell and the signal to noise ratio (SNR) per cell were determined as described in 4.5.2. Each cell was considered as a biological replicate. A minimum sample size of n=1500 cells per investigated condition was set.

Due to the large sample size, we encountered difficulties in determining the mathematical significance as the p-value was always close to zero or even zero using non-parametric tests. This is known by statisticians as the p-value problem (Lin et al. 2011). Therefore, the focus of this work was to assess the data based on their technical significance. First, a better tool has to be developed for future work to determine the mathematical significance of large sample sizes.

5.4.4.1. Long time experiment

The aim of the microscopy study could be itemized into four intentions: First, a “proof of principle” should be made that fluorescence microscopy is a suitable method to investigate *in vivo* enzymatic organizations and dynamics. Second, *in vivo,* to demonstrate the organization and dynamics of the PRK-CP12-GAP2 complex formation. Third, to use these results to establish a positive control for enzyme accumulations so-called "clusters" and to set thresholds for further image evaluation and fourth, to investigate whether an organization and dynamics of the anabolic and catabolic enzymes can also be detected influenced by glucose.

First, the data from PRK YFP-His and GAP2 YFP-His proteins were examined, as this was assumed to be the most strongly expressed within this experiment. PRK YFP-His (Figure 5:20 A) and GAP2 YFP-His (Figure 5:20 B) showed a significantly higher intensity of the absolute fluorescence under photoautotrophic, photomixotrophic and heterotrophic conditions than in comparison to the absolute autofluorescence of the WT under the same conditions. This already confirmed that the resolution of the CLSM fluorescent microscope was applicative to investigate protein expressions *in vivo*.

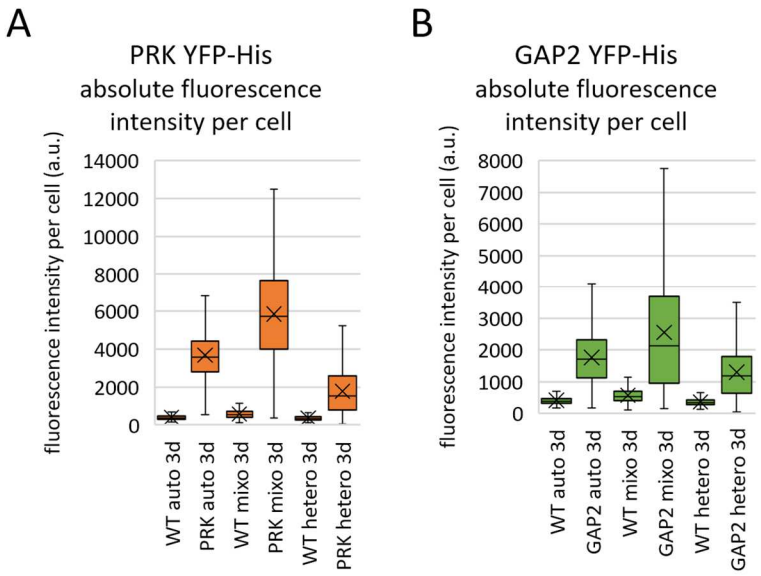

Figure 5:20: Absolute fluorescence intensity per cell under photoautotrophic (auto), photoautotrophic (mixo) and heterotrophic (hetero) conditions. The YFP signal of each *Synechocystis* cells tagged with YFP was measured and multiplicated with the measured area and scaled as arbitrary unit (a.u.). WT represents the absolute autofluorescence of the cells measured in the YFP channel. Since the cells were measured on the same days, the WT in A and B is the same. The graph shows the data of cells measured in three independent cultures. Error bars represent the standard deviation. Cells were incubated for three days (3d) under the indicated conditions. WT auto 3d n=2823, WT mixo 3d n=3081, WT hetero 3d n=2922. (A) PRK auto 3d n=1874, PRK mixo 3d n=3671, PRK hetero 3d n=1909. (B) GAP2 auto 3d n=1856, GAP2 mixo 3d n=2252, GAP2 hetero 3d n=2252.

Next, the distributions of the absolute net fluorescence intensity of PRK YFP-His and GAP2 YFP-His, minus the autofluorescence of the WT, were determined (Figure 5:21). One, for further statistics and second to exclude that the average values are due to deviations between the technical replicas. Although the sample size for each mutant and condition was very large, all data sets were non-normal distributed. However, it was subsequently checked and excluded that the distinct non-normal distribution of PRK hetero 3d (Figure 5:21 A) was caused by one technical replication. All technical replicas showed a similar distribution.

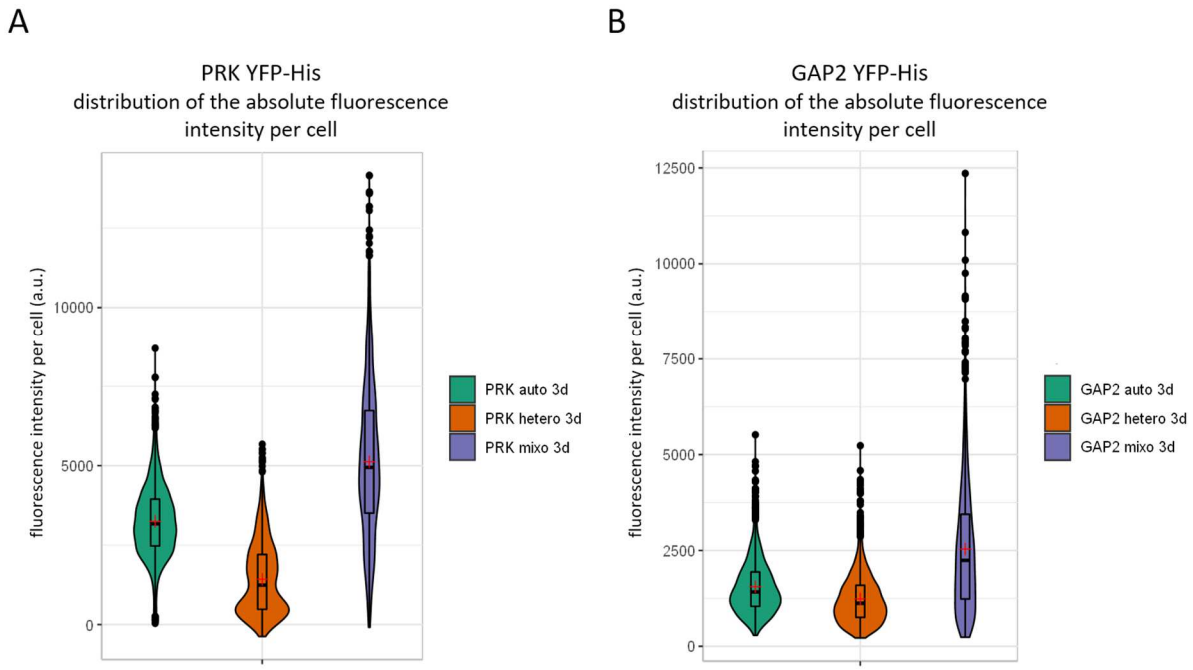

Figure 5:21: Distribution of the absolute net fluorescence intensity per cell under photoautotrophic (auto), photomixotrophic (mixo) and heterotrophic (hetero) conditions. The YFP signal of each *Synechocystis* cells tagged with YFP was measured and multiplicated with the measured area and scaled as arbitrary unit (a.u.). The average absolute fluorescence of the WT was subtracted. The violin plots show the net fluorescence of the expressed YFP signal. The graph shows the data of cells measured in three independent cultures. Cells were incubated for three days (3d) under the indicated conditions. Violin plots show a combination of a box plot and a vertical histogram. The width of the blot reflects the frequency of the measured data. Uniformity of frequency gives information about the distribution of the data. WT auto 3d n=2823, WT mixo 3d n=3081, WT hetero 3d n=2922. (A) PRK auto 3d n=1874, PRK mixo 3d n=3671, PRK hetero 3d n=1909. (B) GAP2 auto 3d n=1856, GAP2 mixo 3d n=2252, GAP2 hetero 3d n=2252.

After that, the dynamics of the PRK-CP12-GAP2 complex were examined. In dark conditions, the PRK-CP12-GAP2 enzyme complex is formed; in light, the proteins are unbound. Accordingly, it was expected that the fluorescence signal from PRK YFP-His and GAP2 YFP-His would be organized more heterogeneously under dark conditions and accordingly, more homogeneously distributed within the cell in light conditions. To check this, the homogeneity of the signal within the cells was examined by calculating the so-called signal to noise ratio (SNR) of the cells (4.5.2). The SNR is the quotient of the average fluorescence intensity and the associated standard deviation. The smaller the SNR, the more heterogeneous the fluorescence signal is distributed in the cell. As expected, intracellular PRK YFP-His and GAP2 YFP-His were more heterogeneous distribution in the dark than in light (Figure 5:22). However, the effect was more noticeable with PRK YFP-His than with GAP2 YFP-His.

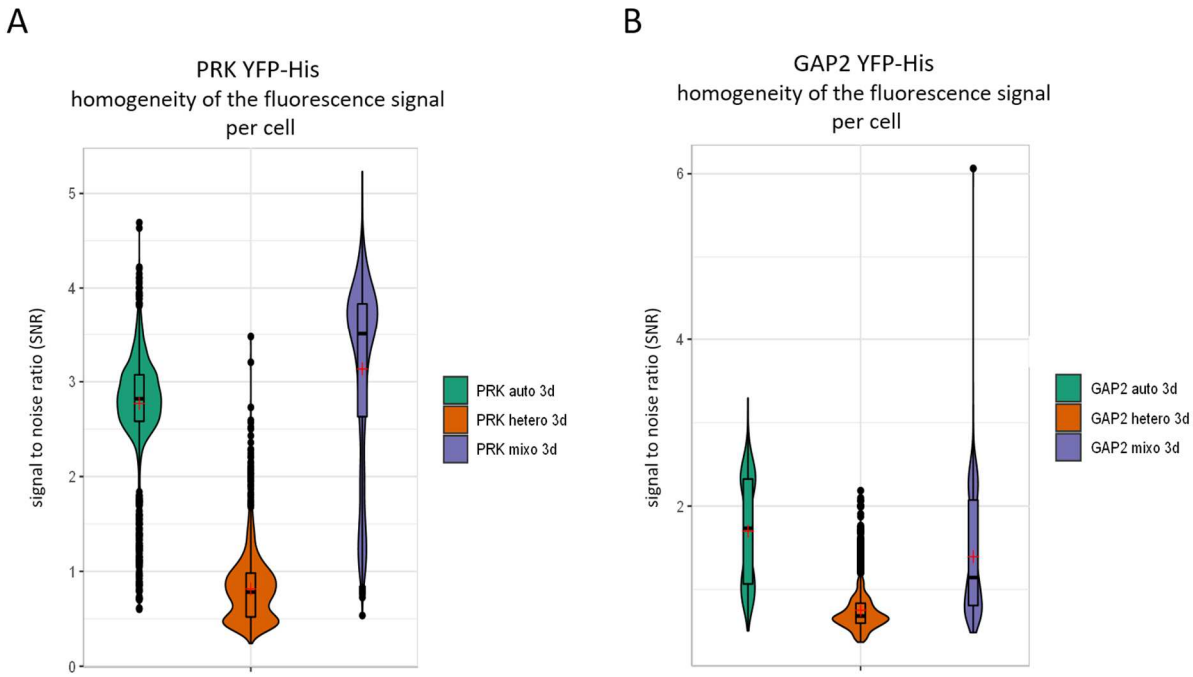

Figure 5:22: Homogeneity (SNR) of the fluorescence intensity per cell under photoautotrophic (auto), photomixotrophic (mixo) and heterotrophic (hetero) conditions. The signal to noise ratio (SNR) is calculated using the quotient of the mean value and the standard deviation and indicates how evenly the fluorescence signal is distributed within the cells. The higher the SNR, the more homogeneous the signal. The graph shows the data of cells measured in three independent cultures. Cells were incubated for three days (3d) under the indicated conditions. Violin plots show a combination of a box plot and a vertical histogram. The width of the blot reflects the frequency of the measured data. Uniformity of frequency gives information about the distribution of the data. WT auto 3d n=2823, WT mixo 3d n=3081, WT hetero 3d n=2922. (A) PRK auto 3d n=1874, PRK mixo 3d n=3671, PRK hetero 3d n=1909. (B) GAP2 auto 3d n=1856, GAP2 mixo 3d n=2252, GAP2 hetero 3d n=2252.

Considering the microscopy images, the heterogeneity for the fluorescence signal of GAP2 YFP-His and PRK YFP-His was even more apparent. Compared to the WT (Figure 5:23), not only was the fluorescence intensity higher, but the heterogeneity of the fluorescence signal in the form of enzyme clusters was also clearly visible (Figure 5:24).

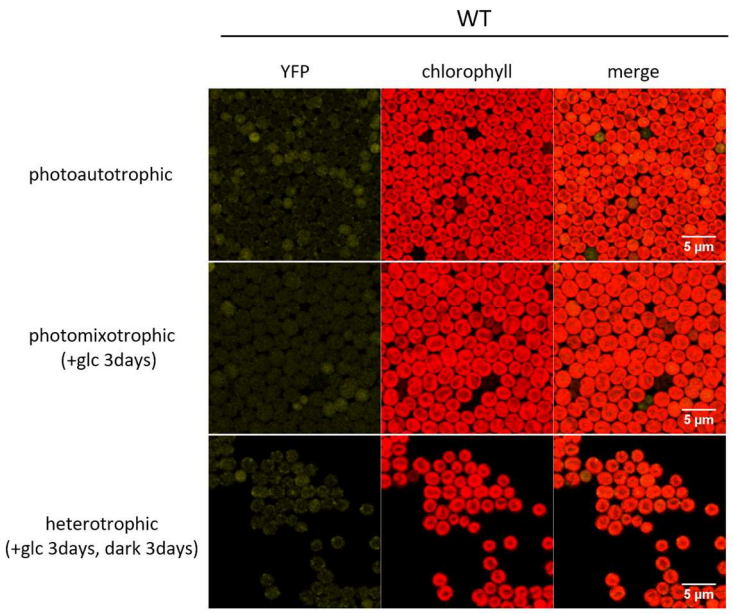

Figure 5:23: Autofluorescence of WT under photoautotrophic, photomixotrophic (+glc) and heterotrophic (+glc, dark) conditions. Images show the autofluorescence of untagged *Synechocystis* WT cells. Cells were fixed before microscopy. Cells that show a signal in the YFP channel but no chlorophyll autofluorescence are dead cells.

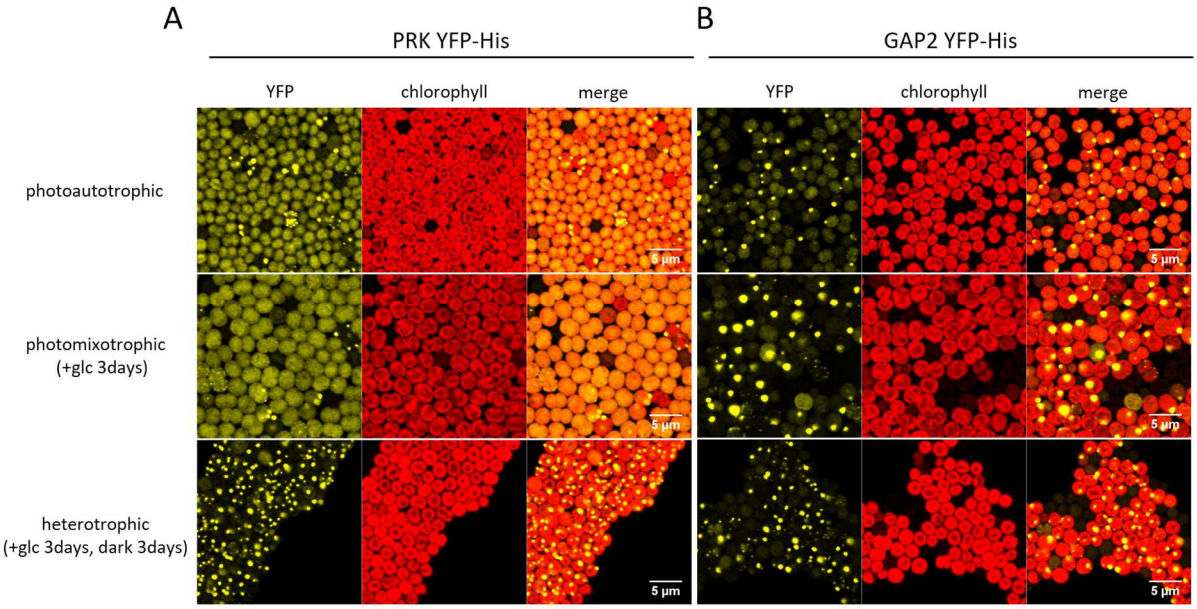

Figure 5:24: Fluorescence microscopy of PRK and GAP2 fused with YFP under photoautotrophic, photomixotrophic (+glc) and heterotrophic (+glc, dark) conditions. Images show examples of the distribution of the YFP signal within the cell. YFP signal spots with at least twice the average fluorescence intensity are defined as clusters. Evenly distributed YFP signal is defined as disperse signal. Cells were fixed before microscopy. Cells that show a signal in the YFP channel but no chlorophyll autofluorescence are dead cells. PRK: phosphoribulokinase. GAP2: glyceraldehyde-3P dehydrogenase.

Fluorescence spots were defined as clusters that had at least twice the mean fluorescence intensity of all cells in the measurement group. This high threshold was set to exclude cells with a high but dispersed fluorescence intensity to be defined as a cluster. The appearance of clusters indicates that several PRK-CP12-GAP2 enzyme complexes formed groups. Grouping enzyme complexes is an effective method to create reaction spaces within non-compartmentalized cells.

PRK YFP-His showed eight times more clusters under heterotrophic conditions than in light (Figure 5:25 A). For GAP2 YFP-His, it was around twice the number of clusters under the same conditions (Figure 5:25 B). A possible influence of glucose on the organization of GAP2 YFP-His was detectable too since the number of clusters in relation to the photoautotrophic cluster is significantly increased. These data are supported by the proportional distribution of the fluorescence signal within clusters. These are proportional to the number of clusters per cell. In short, the more clusters, the more fluorescence is measured within clusters, which in turn means that there is an accumulation of protein.

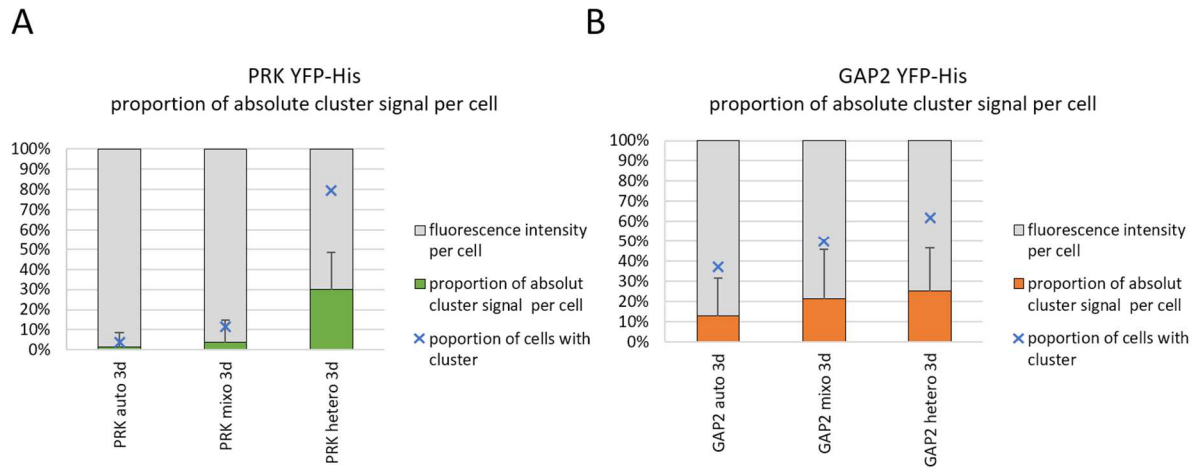

Figure 5:25: Proportion of the absolute cluster signal per cell under photoautotrophic (auto), photomixotrophic (mixo) and heterotrophic (hetero) conditions. Graphic shows how much of the fluorescence signal, cluster signal is. Gray indicates the signal within the entire cell. Organ or green indicates the percental signal within the cluster. The blue X indicates the percental proportion of cells with clusters. The graph shows the data of cells measured in three independent cultures. Error bars represent the standard deviation. Cells were incubated for three days (3d) under the indicated conditions. WT auto 3d n=2823, WT mixo 3d n=3081, WT hetero 3d n=2922. (A) PRK auto 3d n=1874, PRK mixo 3d n=3671, PRK hetero 3d n=1909. (B) GAP2 auto 3d n=1856, GAP2 mixo 3d n=2252, GAP2 hetero 3d n=2252. PRK: phosphoribulokinase. GAP2: glyceraldehyde-3P dehydrogenase. PRK: phosphoribulokinase. GAP2: glyceraldehyde-3P dehydrogenase.

In summary, the following statements can be made. First, fluorescence microscopy is basically a suitable method to study the organization and dynamics of enzymes *in vivo*. Second, the formation of PRK and GAP2 enzyme complexes could be detected *in vivo*. It is assumed that these are PRK-CP12-GAP2 enzyme complexes, and thus, the inactivation of the CBB cycle could be observed under dark conditions. In addition, the light-dependent grouping of PRK and GAP2 enzyme complexes could be made visible. Third, a positive control could be created to identify enzyme clusters based on this data.

After fluorescence microscopy had now been checked as a suitable method and a positive control for enzyme clusters was created, the catabolic enzymes EDA, EDD, GND, ZWF and GAP1 were examined under the same conditions. The question was whether glycolytic pathways, i.e. the catabolic metabolism, are also organized by enzyme complex formation and whether this organization is depending on glucose or light. The microscopy images of the catabolic enzymes were evaluated and analyzed in the same way as described for the anabolic enzymes in this chapter.

It is suspected that the expression level of glycolytic enzymes is much lower than that of the enzymes of the CBB cycle. Therefore, it was not surprising that the absolute fluorescence intensity of the catabolic enzymes was much lower (Figure 5:26) than that of the anabolic enzymes (Figure 5:20). No expression could be detected for GAP1 YFP-His (Figure 5:26 E) under photoautotrophic conditions and for EDA YFP-His (Figure 5:26 A) at all. This matches the result of the Western blots (Figure 5:18 C, D) in which no expression of EDA YFP-His could be detected and also fits the result of the growth experiment (Figure 5:19 B) in which EDA YFP-His grew like a deletion mutant. It is, therefore, possible that EDA is expressed below the resolution limit and/or has lost its function due to the fused YFP-His. For this reason, the mutant EDA YFP-His was not analyzed further in this work.

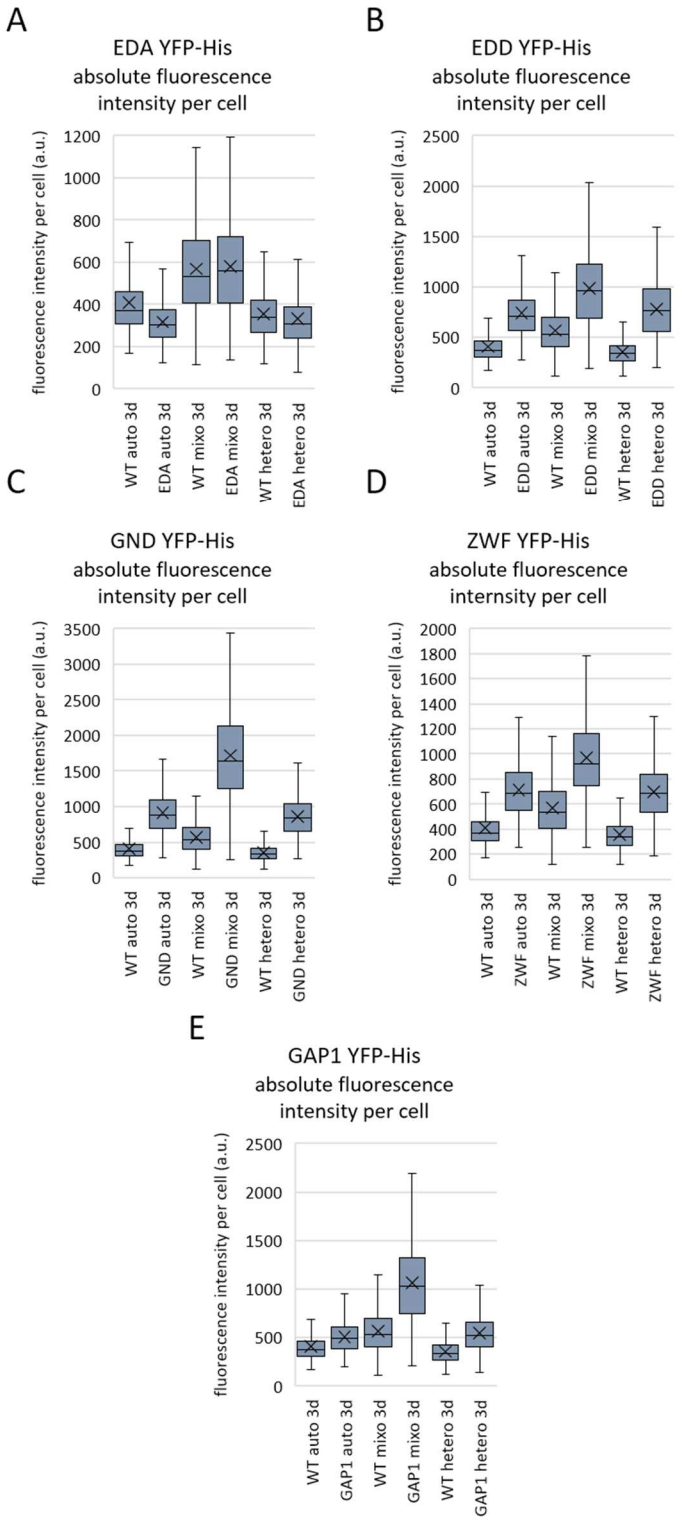

Figure 5:26: Absolute fluorescence intensity of per cell under photoautotrophic (auto), photomixotrophic (mixo) and heterotrophic (hetero) conditions. The YFP signal of each *Synechocystis* cells tagged with YFP was measured and multiplicated with the measured area and scaled as arbitrary unit (a.u.). WT represents the absolute autofluorescence of the cells measured in the YFP channel. Since the cells were measured on the same days, the WT in A, B, C, D and E is the same. The graph shows the data of cells measured in three independent cultures. Error bars represent the standard deviation. Cells were incubated for three days (3d) under the indicated conditions. WT auto 3d n=2823, WT mixo 3d n=3081, WT hetero 3d n=2922. (A) EDA auto 3d n=2394, EDA mixo 3d n=1996, EDA hetero 3d n=2705. (B) EDD auto 3d n=2533, EDD mixo 3d n= 3398, EDD hetero 3d n=2592. (C) GND auto 3d n=2604, GND mixo 3d n=2566, GND hetero 3d n=3551. (D) ZWF auto 3d n=2652, ZWF mixo 3d n=3033, ZWF hetero 3d n=3137. (E) GAP1 auto 3d n=2305, GAP1 mixo 3d n=2754, GAP1hetero 3d n=3842. EDA: KDPG aldolase. EDD: phosphogluconate dehydratase. GND: 6-phosphogluconate dehydrogenase. ZWF: glucose-6-phosphate dehydrogenase. GAP1: Glyceraldehyde 3-phosphate.

As for the anabolic enzymes, the distribution of the absolute net fluorescence intensity of the catabolic enzymes was non-normal distributed (Figure 5:27). The data supported the fact that the net fluorescence level of the catabolic enzymes was very low, especially for GAP1 YFP-His (Figure 5:27 D). Differences were partly within the range of the fluorescence intensity of the WT. Therefore, it was not possible to interpret whether the differences in fluorescence intensity depends on light or glucose. The same applies to the homogeneity data (Figure 5:28). The microscopy images (Figure 5:29) shown as well that the fluorescence intensity of the YFP mutants is just slightly above the fluorescence intensity of the WT (Figure 5:23). However, GND YPF-His (Figure 5:28 B, Figure 5:30) has an increased fluorescence signal under photomixotrophic conditions and a slightly increased cluster formation under heterotrophic conditions. Since the GND culture showed a full deletion phenotype (Figure 5:19 C), it cannot be excluded that this is due to a stress-related increase in autofluorescence.

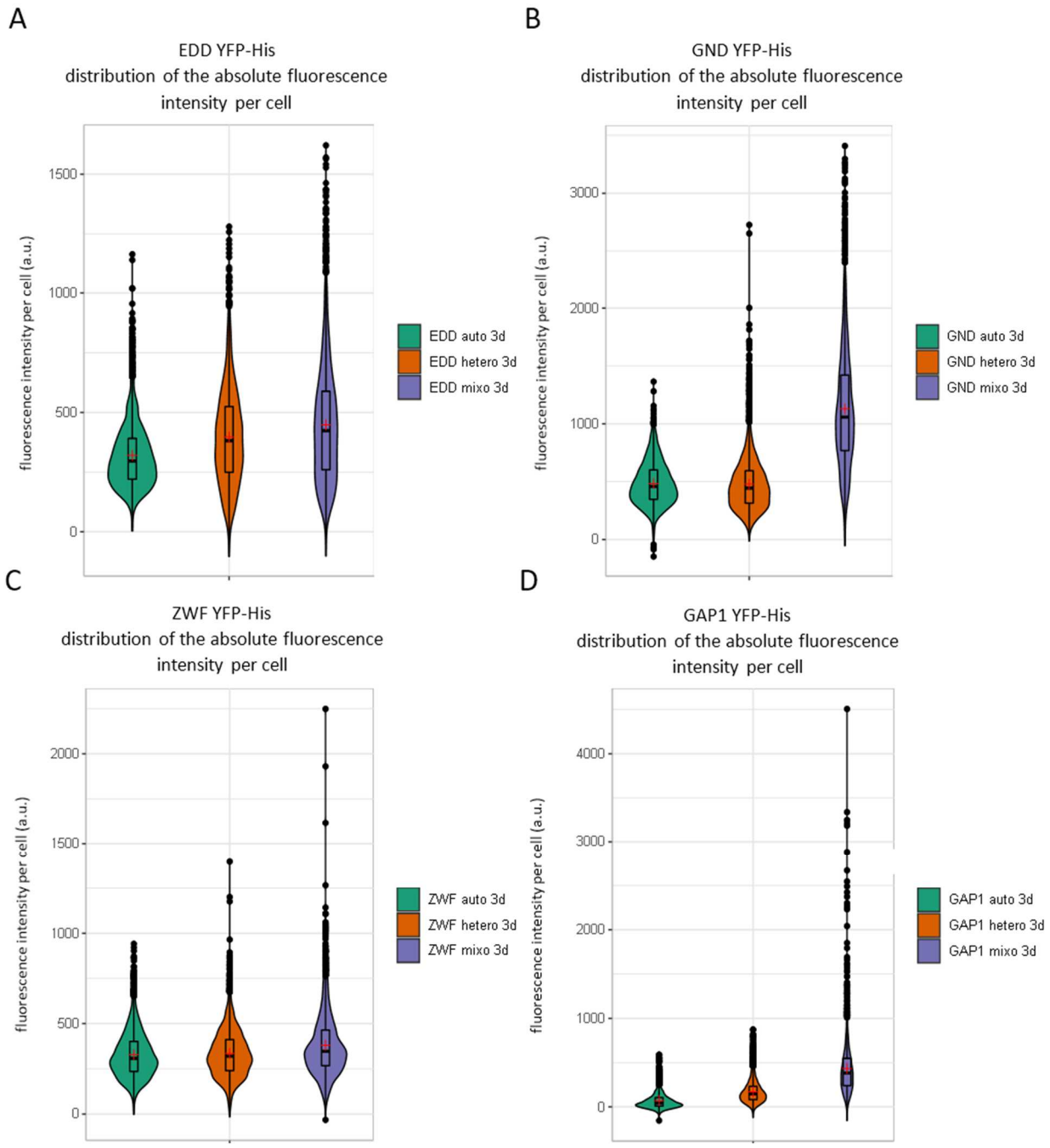

Figure 5:27: Distribution of the absolute net fluorescence intensity per cell under photoautotrophic (auto), photomixotrophic (mixo) and heterotrophic (hetero) conditions. The YFP signal of each *Synechocystis* cells tagged with YFP was measured and multiplicated with the measured area and scaled as an arbitrary unit (a.u.). The average absolute fluorescence of the WT was subtracted. The violin plots show the net fluorescence of the expressed YFP signal. The graph shows the data of cells measured in three independent cultures. Cells were incubated for three days (3d) under the indicated conditions. Violin plots show a combination of a box plot and a vertical histogram. The width of the blot reflects the frequency of the measured data. Uniformity of frequency gives information about the distribution of the data. WT auto 3d n=2823, WT mixo 3d n=3081, WT hetero 3d n=2922. (A) EDD auto 3d n=2533, EDD mixo 3d n=3398, EDD hetero 3d n=2592. (B) GND auto 3d n=2604, GND mixo 3d n=2566, GND hetero 3d n=3551. (C) ZWF auto 3d n=2652, ZWF mixo 3d n=3033, ZWF hetero 3d n=3137. (D) GAP1 auto 3d n=2305, GAP1 mixo 3d n=2754, GAP1hetero 3d n=3842. EDA: KDPG aldolase. EDD: phosphogluconate dehydratase. GND: 6-phosphogluconate dehydrogenase. ZWF: glucose-6-phosphate dehydrogenase. GAP1: glyceraldehyde 3-phosphate.

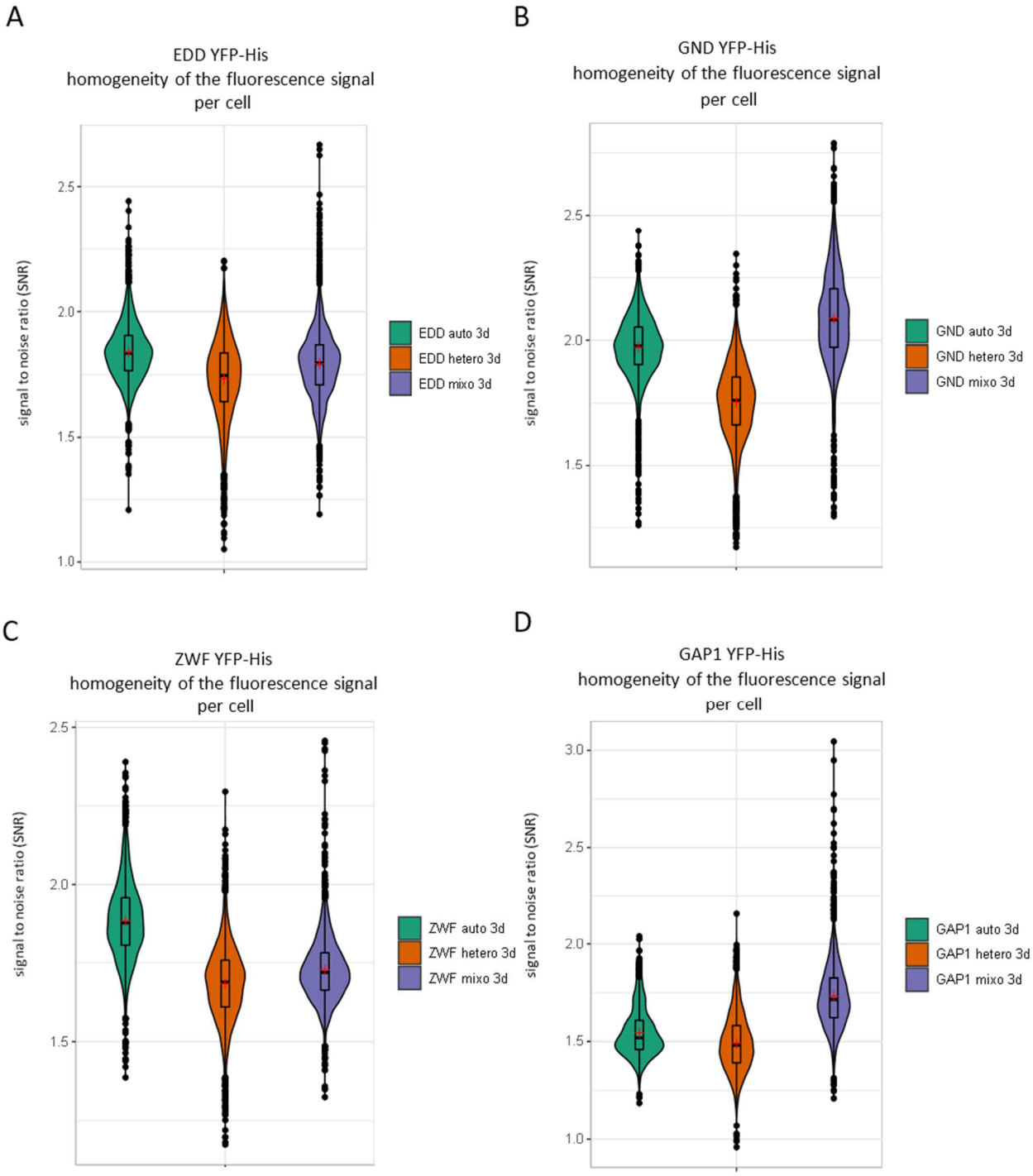

Figure 5:28: Homogeneity (SNR) of the fluorescence intensity per cell under photoautotrophic (auto), photomixotrophic (mixo) and heterotrophic (hetero) conditions. The signal to noise ratio (SNR) is calculated using the quotient of the mean value and the standard deviation and indicates how evenly the fluorescence signal is distributed within the cells. The higher the SNR, the more homogeneous the signal. The graph shows the data of cells measured in three independent cultures. Cells were incubated for three days (3d) under the indicated conditions. Violin plots show a combination of a box plot and a vertical histogram. The width of the blot reflects the frequency of the measured data. Uniformity of frequency gives information about the distribution of the data. WT auto 3d n=2823, WT mixo 3d n=3081, WT hetero 3d n= 2922. (A) EDD auto 3d n=2533, EDD mixo 3d n= 3398, EDD hetero 3d n=2592. (B) GND auto 3d n=2604, GND mixo 3d n= 2566, GND hetero 3d n=3551. (C) ZWF auto 3d n=2652, ZWF mixo 3d n=3033, ZWF hetero 3d n=3137. (D) GAP1 auto 3d n=2305, GAP1 mixo 3d n=2754, GAP1hetero 3d n=3842. EDA: KDPG aldolase. EDD: phosphogluconate dehydratase. GND: 6-phosphogluconate dehydrogenase. ZWF: glucose-6-phosphate dehydrogenase. GAP1: Glyceraldehyde 3-phosphate.

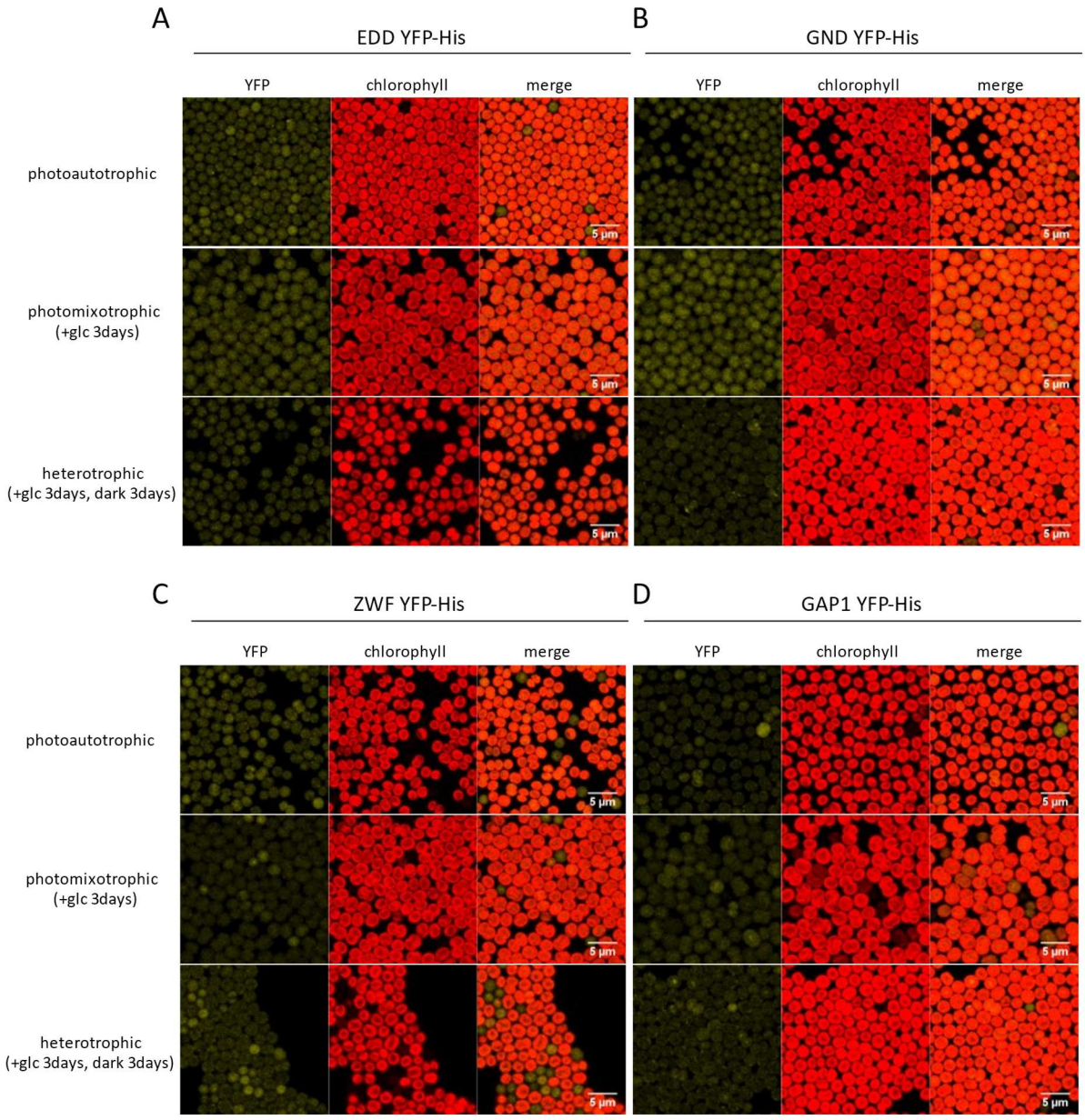

Figure 5:29: Fluorescence microscopy of catabolic proteins fused with YFP under photoautotrophic, photomixotrophic (+glc) and heterotrophic (+glc, dark) conditions. Images show examples of the distribution of the YFP signal within the cell. Cells were fixed before microscopy. Cells that show a signal in the YFP channel but no chlorophyll autofluorescence are dead cells. EDA: KDPG aldolase. EDD: phosphogluconate dehydratase. GND: 6-phosphogluconate dehydrogenase. ZWF: glucose-6-phosphate dehydrogenase. GAP1: Glyceraldehyde 3-phosphate.

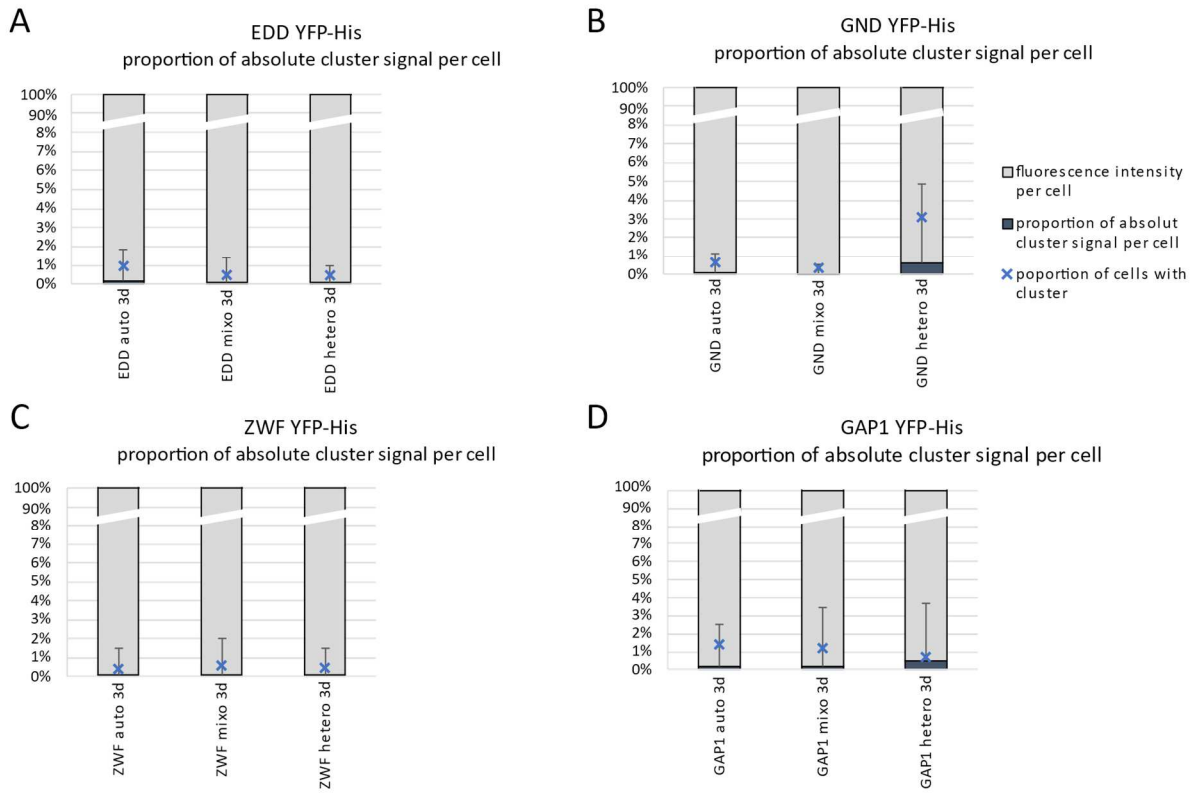

Figure 5:30: Proportion of the absolute cluster signal per cell under photoautotrophic (auto), photomixotrophic (mixo) and heterotrophic (hetero) conditions. Graphic shows how much of the fluorescence signal, cluster signal is. Gray indicates the signal within the entire cell. Dark blue indicates the percental signal within the cluster. The light blue X indicates the percental proportion of cells with clusters. The graph shows the data of cells measured in three independent cultures. Error bars represent the standard deviation. Cells were incubated for three days (3d) under the indicated conditions. WT auto 3d n=2823, WT mixo 3d n=3081, WT hetero 3d n=2922. (A) EDD auto 3d n=2533, EDD mixo 3d n=3398, EDD hetero 3d n=2592. (B) GND auto 3d n=2604, GND mixo 3d n=2566, GND hetero 3d n=3551. (C) ZWF auto 3d n=2652, ZWF mixo 3d n=3033, ZWF hetero 3d n=3137. (D) GAP1 auto 3d n=2305, GAP1 mixo 3d n=2754, GAP1hetero 3d n=3842. EDA: KDPG aldolase. EDD: phosphogluconate dehydratase. GND: 6-phosphogluconate dehydrogenase. ZWF: glucose-6-phosphate dehydrogenase. GAP1: Glyceraldehyde 3-phosphate.

Overviewing, the fluorescence intensities of the anabolic (Figure 5:20), catabolic (Figure 5:26) YFP tagged mutants and especially of the WT, it becomes apparent that the fluorescence intensity fluctuates greatly between photoautotrophic, photomixotrophic and heterotrophic conditions. This may indicate that the amount of YFP tagged enzymes differs between the conditions. However, the interpretability of the data depends on the fact that the total amount of enzymes does not change, since we are interested in comparing the regulatory effect of light, darkness and glucose. In nature, especially as an aquatic photosynthetic prokaryote, *Synechocystis* cannot afford it with, e.g. sudden darkening or sudden lack of nutrients having a slow, regulated metabolism. The regulation of the photosynthesis and thus also the CBB cycle is therefore assumed as a matter of seconds or a few minutes. The same may be the case for glycolytic metabolism. Three days of incubation are, therefore, may be too long in this experimental setup.

5.4.4.2. Short time experiment

The experiment was adapted in that the cells were examined after a brief incubation in the dark and glucose. A time window of one minute of darkness and a maximum of one hour of glucose is short enough that the change in the amount of enzyme is small and therefore negligible, but long enough that the metabolism can regulate itself through the intracellular organization of enzymes. However, the low fluorescence of the catabolic enzymes not only made it necessary to adapt the sample cultivation. But also, the bioinformatic evaluation of the data as to be improved in the future. Programming a new deep learning macro is very complex. For reasons of time, in this work, only the anabolic enzymes PRK YFP-His and GAP2 YFP-His, with a high mean fluorescence, were investigated further.

As part of the short time experiment, the mutants PRK YFP-His and GAP2 YFP-His were incubated as follows: 1min photoautotrophic, 1min dark, 1min photomixotrophic, 1min heterotrophic (1min dark+ 1min photomixotrophic), 1h photomixotrophic and 1h heterotrophic (1min dark+1h photomixotrophic). The additional examination of cells that were “only” cultivated in the dark should enable the possible effect of glucose on GAP2 YFP-His to be confirmed. Because it is unknown how quickly glucose gets metabolized by *Synechocystis*, the cells were cultivated with glucose for 1min and 1h. The sample preparation is described in detail in 4.4.7.1. The fluorescence microscopy (4.4.7.2) and image evaluation (4.4.7.3, 4.5.2) was performed as in the long-time experiment.

As intended, the fluctuation in the absolute fluorescence intensity of PRK YFP-His (Figure 5:31 A) and GAP2 YFP-His (Figure 5:31 B) under the different conditions could be minimized by shortening the incubation times. However, there was still slight noise in the absolute fluorescence intensity between cells that were incubated with and without glucose. Interestingly, the autofluorescence of the WT and the area of the cells treated with glucose were increased as well (data not shown). Since the absolute fluorescence intensities are considered, the fluctuation is primarily due to the increase in area and of the autofluorescence.

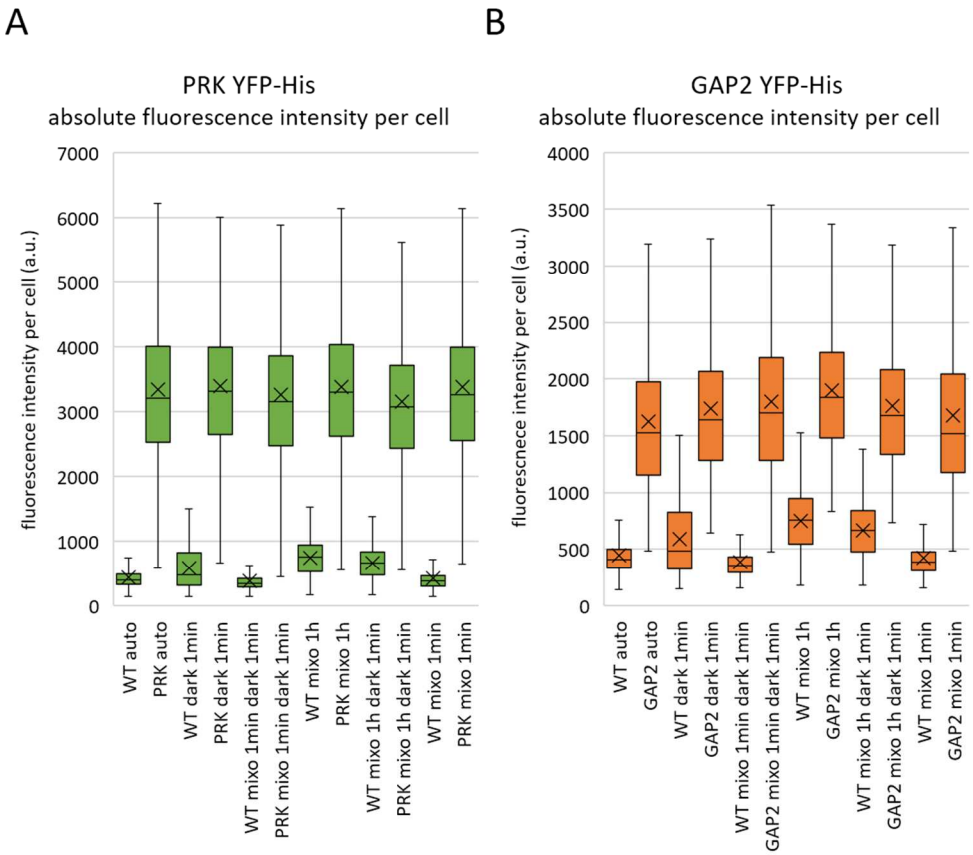

Figure 5:31: Absolute fluorescence intensity per cell under photoautotrophic (auto), photomixotrophic (mixo) and heterotrophic (mixo, dark) conditions. The YFP signal of each *Synechocystis* cells tagged with YFP was measured and multiplicated with the measured area and scaled as an arbitrary unit (a.u.). WT represents the absolute autofluorescence of the cells measured in the YFP channel. Since the cells were measured on the same days, the WT in A and B is the same. The graph shows the data of cells measured in three independent cultures. Error bars represent the standard deviation. Cells were incubated photoautotrophically for three days (3d). Then the cells were incubated in the dark for 1min and/or incubated with 10mM glucose for 1min or 1h. WT auto n=6669, WT dark 1min n=4457, WT mixo 1h n=4516, WT mixo 1h dark 1min n=3905, WT mixo 1min n=4445, WT mixo 1min dark 1min n=5390. (A) PRK auto n=3291, PRK dark 1min n=3581, PRK mixo 1h n=3738, PRK mixo 1h dark 1min n=4316, PRK mixo 1min n=5728, PRK mixo 1min dark 1min n=4112. (B) GAP2 auto n=3518, GAP2 dark 1min n=3341, GAP2 mixo 1h n=1739, GAP2 mixo 1h dark 1min n=2296, GAP2 mixo 1min n=3564, GAP2 mixo 1min dark 1min n=3707. PRK: phosphoribulokinase. GAP2: glyceraldehyde-3P dehydrogenase.

The cells in the short-time experiment were similarly non-normal distributed (Figure 5:32) as in the long-time experiment. The “double” distribution of PRK heterotrophic could not be replicated. This additionally indicated that other metabolic reactions strongly influenced the long-term values over time.

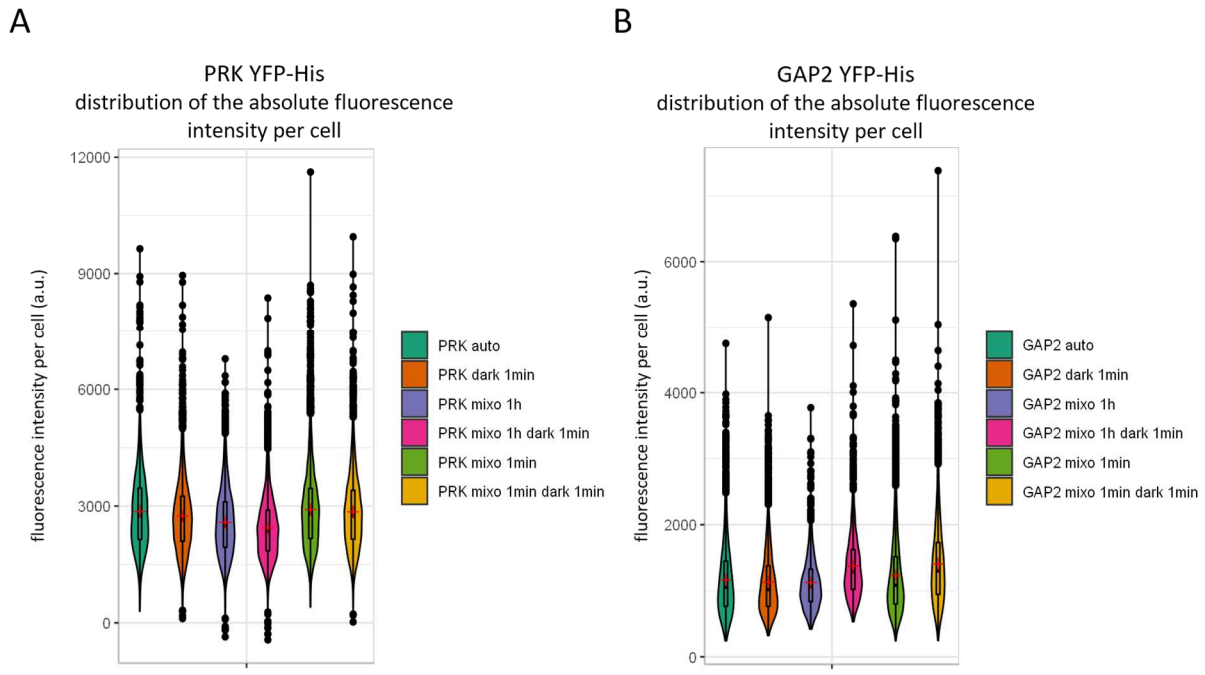

Figure 5:32: Distribution of the absolute net fluorescence intensity per cell under photoautotrophic (auto), photomixotrophic (mixo) and heterotrophic (mixo, dark) conditions. The YFP signal of each *Synechocystis* cells tagged with YFP was measured and multiplicated with the measured area and scaled as an arbitrary unit (a.u.). The average absolute fluorescence of the WT was subtracted. The violin plots show the net fluorescence of the expressed YFP signal. The graph shows the data of cells measured in three independent cultures. Cells were incubated photoautotrophically for three days (3d). Then the cells were incubated in the dark for 1min and/or incubated with 10mM glucose for 1min or 1h. Violin plots show a combination of a box plot and a vertical histogram. The width of the blot reflects the frequency of the measured data. Uniformity of frequency gives information about the distribution of the data. WT auto n=6669, WT dark 1min n=4457, WT mixo 1h n=4516, WT mixo 1h dark 1min n=3905, WT mixo 1min n=4445, WT mixo 1min dark 1min n=5390. (A) PRK auto n=3291, PRK dark 1min n=3581, PRK mixo 1h n=3738, PRK mixo 1h dark 1min n=4316, PRK mixo 1min n=5728, PRK mixo 1min dark 1min n=4112. (B) GAP2 auto n=3518, GAP2 dark 1min n=3341, GAP2 mixo 1h n=1739, GAP2 mixo 1h dark 1min n=2296, GAP2 mixo 1min n=3564, GAP2 mixo 1min dark 1min n=3707. PRK: phosphoribulokinase. GAP2: glyceraldehyde-3P dehydrogenase.

It was possible to replicate that the homogeneity of PRK YFP-His (Figure 5:33 A) were, under these experimental terms, only light-regulated. For GAP2 YFP-His (Figure 5:33 B), however, it could be confirmed that this is not only regulated by light or darkness. The short time values showed that 1h of incubation with glucose had an influence on the distribution of the fluorescence signal and that it was more heterogeneous than the respective photoautotrophic distribution. This effect could not yet be observed after 1min glucose incubation. That means GAP2, and thus, the CBB cycle could be directly regulated by glucose.

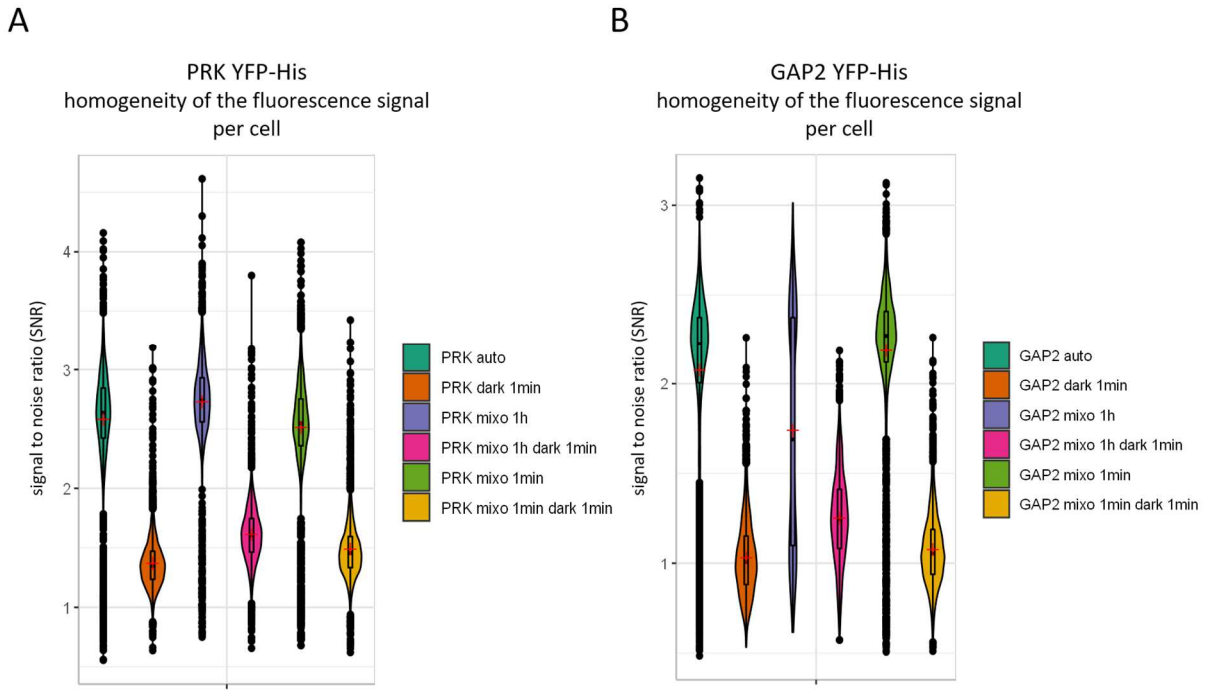

Figure 5:33: Homogeneity (SNR) of the fluorescence intensity per cell under photoautotrophic (auto), photomixotrophic (mixo) and heterotrophic (mixo, dark) conditions. The signal to noise ratio (SNR) is calculated using the quotient of the mean value and the standard deviation and indicates how evenly the fluorescence signal is distributed within the cells. The higher the SNR, the more homogeneous the signal. The graph shows the data of cells measured in three independent cultures. Cells were incubated photoautotrophically for three days (3d). Then the cells were incubated in the dark for 1min and/or incubated with 10mM glucose for 1min or 1h. Violin plots show a combination of a box plot and a vertical histogram. The width of the blot reflects the frequency of the measured data. Uniformity of frequency gives information about the distribution of the data. WT auto n=6669, WT dark 1min n=4457, WT mixo 1h n=4516, WT mixo 1h dark 1min n=3905, WT mixo 1min n=4445, WT mixo 1min dark 1min n=5390. (A) PRK auto n=3291, PRK dark 1min n=3581, PRK mixo 1h n=3738, PRK mixo 1h dark 1min n=4316, PRK mixo 1min n=5728, PRK mixo 1min dark 1min n=4112. (B) GAP2 auto n=3518, GAP2 dark 1min n=3341, GAP2 mixo 1h n=1739, GAP2 mixo 1h dark 1min n=2296, GAP2 mixo 1min n=3564, GAP2 mixo 1min dark 1min n=3707. PRK: phosphoribulokinase. GAP2: glyceraldehyde-3P dehydrogenase.

The microscopy images confirmed this assumption. As in the long term experiment, the YFP signal of PRK YFP-His (Figure 5:35 A) and GAP2 YFP-His (Figure 5:35 B) was visually stronger than that of the WT (Figure 5:34). However, the WT autofluorescence increased slightly after 1h of glucose treatment. PRK YFP-His clustered, glucose independently only in the dark (Figure 5:35 A).

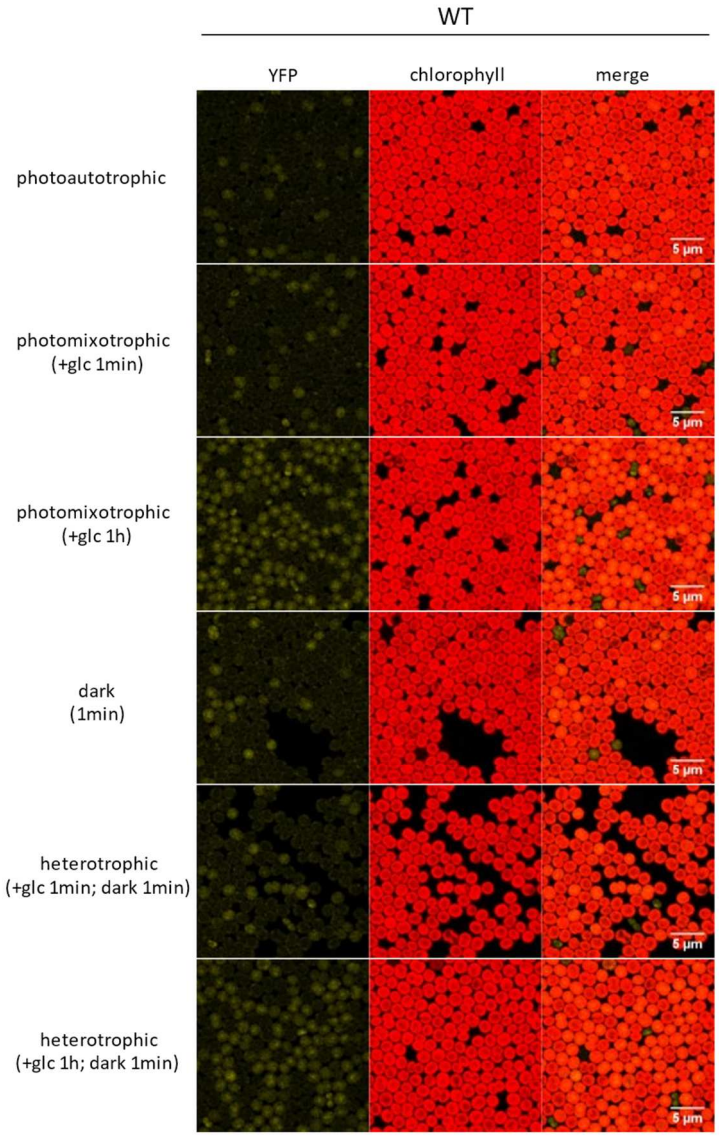

Figure 5:34: Autofluorescence of WT under photoautotrophic, photomixotrophic (+glc) and heterotrophic (+glc, dark) conditions. Images show the autofluorescence of untagged *Synechocystis* WT cells. Cells were fixed before microscopy. Cells that show a signal in the YFP channel but no chlorophyll autofluorescence are dead cells.

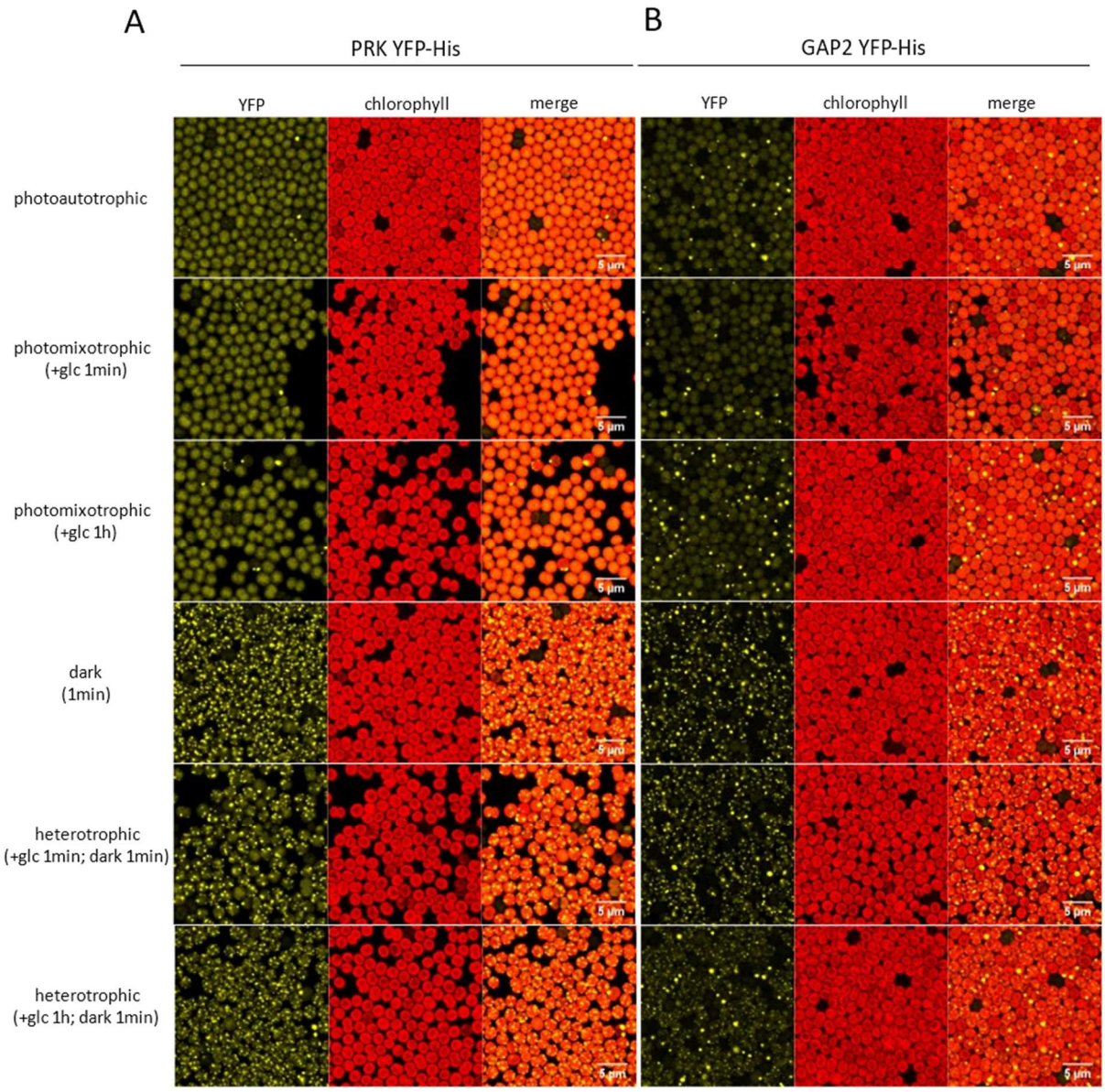

Figure 5:35: Fluorescence microscopy of PRK and GAP2 fused with YFP under photoautotrophic, photomixotrophic (+glc) and heterotrophic (+glc, dark) conditions. Images show examples of the distribution of the YFP signal within the cell. YFP signal spots with at least twice the average fluorescence intensity are defined as clusters. Evenly distributed YFP signal is defined as disperse signal. Cells were fixed before microscopy. Cells that show a signal in the YFP channel but no chlorophyll autofluorescence are dead cells. PRK: phosphoribulokinase. GAP2: glyceraldehyde-3P dehydrogenase.

Interestingly, the number of clusters decreased in darkness after 1h (Figure 5:36 A). 1min of darkness did not show this effect. It was concluded that glucose could have a certain destabilizing effect on PRK within the PRK-CP12-GAP2 complex. An impact of glucose is clearly measurable for GAP2 YFP-His (Figure 5:35 B, Figure 5:36 B). After 1h photo-mixotrophically cultivated, the number of clusters and the proportion of the fluorescence signal in clusters increased significantly and were comparable to the number of clusters of the "dark" samples (Figure 5:36 B). GAP2 seemed to be regulated not only by light but also by glucose.

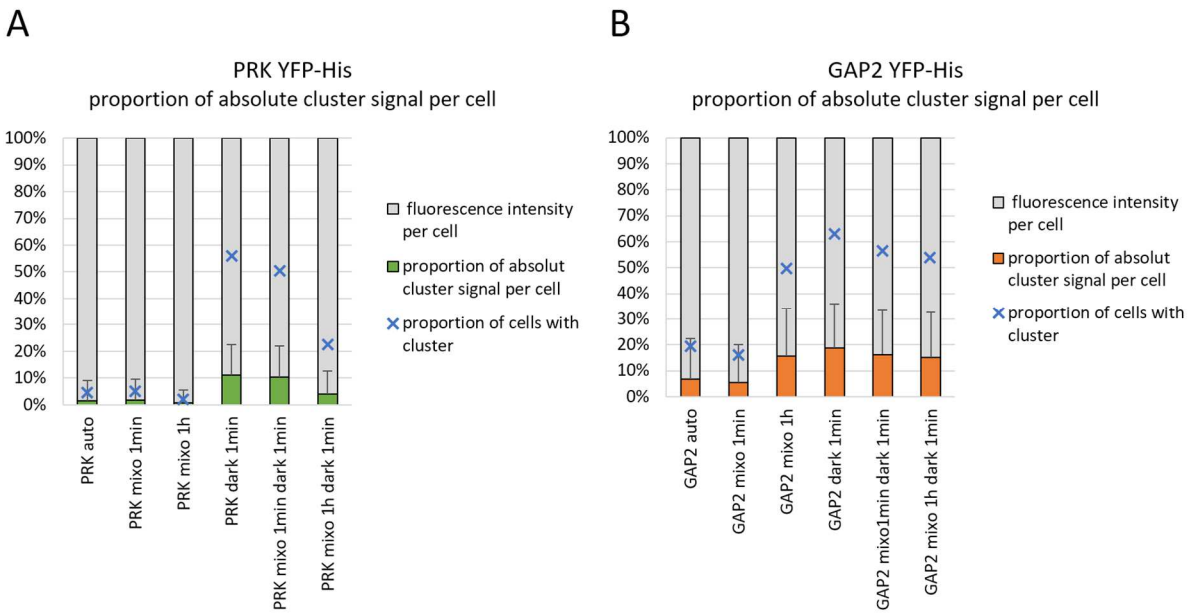

Figure 5:36: Proportion of the absolute cluster signal per cell under photoautotrophic (auto), photomixotrophic (mixo) and heterotrophic (hetero) conditions. Graphic shows how much of the fluorescence signal, cluster signal is. Gray indicates the signal within the entire cell. Orange or green indicates the percental signal within the cluster. The blue X indicates the percental proportion of cells with clusters. The graph shows the data of cells measured in three independent cultures. Error bars represent the standard deviation. Cells were incubated photoautotrophically for three days (3d). Then the cells were incubated in the dark for 1min and/or incubated with 10mM glucose for 1min or 1h. WT auto n=6669, WT dark 1min n=4457, WT mixo 1h n=4516, WT mixo 1h dark 1min n=3905, WT mixo 1min n=4445, WT mixo 1min dark 1min n=5390. (A) PRK auto n=3291, PRK dark 1min n=3581, PRK mixo 1h n=3738, PRK mixo 1h dark 1min n=4316, PRK mixo 1min n=5728, PRK mixo 1min dark 1min n=4112. (B) GAP2 auto n=3518, GAP2 dark 1min n=3341, GAP2 mixo 1h n=1739, GAP2 mixo 1h dark 1min n=2296, GAP2 mixo 1min n=3564, GAP2 mixo 1min dark 1min n=3707.

In summary, the short time experiment provided more reliable data than the long time experiment. Within the short time experiment, the organization and trophy-dependent dynamics of a PRK and GAP2 enzyme complex could be observed and confirmed, *in vivo,* for the first time. Besides, it was found out that the enzyme GAP2 and thus also the CBB cycle is not only light-regulated but also glucose-regulated.

6. Discussion

6.1. Deletion studies

6.1.1. The Entner-Doudoroff pathway exclusively branches off the oxidative pentose phosphate pathway

Initial physiology studies indicated that the Entner-Doudoroff (ED) pathways' entry of *Synechocystis* is catalysed by a glucose dehydrogenase (GDH) and gluconate kinase (GK; Chen et al. 2016; Figure 2:1). Newest enzyme studies, however, could not detect any enzyme activity for putative GDH1 (sll1709) or GDH2 (slr1608) and hypothesized that the entrance of the ED pathway is catalysed by hexokinase (HK) parallel to the oxidative pentose phosphate (OPP) pathway (Makowka 2019). To finally clarify the question of how the entry of the ED pathway is organized, hexokinase deletion mutants (*Δhk)* were generated (4.2.11) and physiologically examined together with potential glucose dehydrogenase deletion mutants (*Δgdh1Δgdh2*; 5.1). If a functional pathway via GDH exists in *Synechocystis*, the deletion of the hexokinase would have to be compensated.

In this work, it was proven that *Synechocystis* metabolizes added glucose only via the hexokinase (HK; sll0593; 5.1.2). *Δhk* deletion mutants grew under photomixotrophic conditions like under photoautotrophic conditions. Unable to metabolize glucose, they could not grow heterotrophically at all (Figure 5:3). Measurements of the glucose concentration in the medium of *Δhk* cell cultures confirmed that *Δhk* mutants were not able to metabolize glucose (Figure 5:4). This assumption was supported by dark-interval relaxation kinetics (DIRK) analysis performed by members of the working group (Theune et al. 2020, unpublished). If glucose is metabolized, the additional reduction equivalents are supposed to feed the plastoquinone (PQ) pool, which can be measured in an increased electron flow on photosystem I (PS I). This additional electron flow could not be detected in *Δhk* (Theune et al. 2020, unpublished).

The metabolization of glucose via a GDH/GK pathway has been described for various organisms like archaea (Ahmed et al. 2005), yeasts (Iwasa et al. 2018) heterotrophic bacteria (Hommes et al. 1984) and higher eukaryotes (Sygmund et al. 2011). Although a glucose dehydrogenase has been described for the cyanobacteria *Nostoc* (Pulich et al. 1976; Han et al. 2017), little is still known about the relevance of a pathway via GDH in cyanobacteria or photoautotrophic organisms. *Nostoc* employs an NADPH depending GDH, which is discussed to regulate the NADPH pool and to compensate for imbalances in cofactors (Park and Choi 2017). Recently performed Blast Analysis in our group demonstrated a connection between the occurrence of the ED pathway and the OPP pathway in the presence of the GDH/GK pathway in cyanobacteria and higher plants. It was postulated that a majority of the cyanobacteria examined, coded for GDH (glucose dehydrogenase) and GK (gluconate kinase; Mai 2020; unpublished).

Synechocystis, however, seems to be one of the exceptions, since no sufficient sequence homology could be found for a GDH1, GDH2 or GK, in *Synechocystis* (Mai 2020; unpublished). In addition, performed enzyme tests could not demonstrate any enzyme activity for either of the two glucose dehydrogenases (Makowka 2019).

6.1.2. The putative GDH1 (sll1709) and GDH2 (slr1608) are of importance for the central carbon metabolism of *Synechocystis*

Nevertheless, growth experiments (5.1.2; Figure 5:3) showed that the deletion of the putative *Δgdh1* led to slightly reduced growth, photomixotrophically. Under heterotrophic conditions, the deletion of both putative *Δgdh1* and *Δgdh2* seemed to have a strong influence on carbon metabolism, as growth was significantly reduced. However, glucose measurements (Figure 5:4) in the medium showed that the putative *Δgdh1Δgdh2* mutant was able to metabolize glucose comparable to the WT. It can, therefore, be assumed that the decrease in growth does not happen because the glucose cannot be transported into the cell or metabolized. Previous growth studies revealed (Chen et al. 2016) that due to a potential PGI shunt, a triple mutant in which Δ*pfkΔzwfΔgnd* were deleted, grew under photomixotrophic conditions like the WT (Makowka et al. 2020). However, the mutant *ΔpfkΔzwfgdh1/Δgdh1* was not able to grow photomixotrophically at all (Chen et al. 2016). These results support the assumption that the putative *gdh* sequences code for enzymes with yet unknown function, that seem to be of importance for the catabolic carbon metabolism of *Synechocystis*.

6.1.3. The Entner-Doudoroff pathway is essential when the lower glycolysis is discontinued

The Calvin-Benson-Bassam (CBB) cycle (Appendix Figure 1) provides the intermediate 3P-glycerate, which can be metabolized in three different ways. (i) Via the lower glycolysis, to yield pyruvate. (ii) It can be converted to glyceraldehyde-3P (GAP) and be utilized for the regeneration of the CBB cycle and (iii) it is used for gluconeogenesis to generate glycogen. That implies, if 3P-glycerate feeds the gluconeogenesis or is involved in the regeneration of the CBB cycle, no pyruvate could be generated via the lower glycolysis. Therefore, we assume that the Entner-Doudoroff (ED) pathway might represent an alternative route to provide pyruvate, especially when lower glycolysis is either disrupted or without flux. To test our hypothesis, we attempted to generate *Synechocystis* mutants without functional lower glycolysis by producing an enolase (*eno/Δeno*) deletion mutant (5.2.1; Figure 5:7). However, *eno/Δeno* could not be entirely segregated. The enolase mediates the oxidation of 2P-glycerate to phosphoenolpyruvate (PEP) which plays a central metabolic and regulatory role in carbon metabolism. PEP is mainly produced in the lower glycolysis and acts as a substrate to generate oxaloacetate, catalysed by a phosphoenolpyruvate carboxylase (PEPC). Studies measured a high flux through the PEPC shortcut since around a quarter of the CO_2 is fixed by PEPC (Takeya et al. 2017; Veaudor et al. 2020).

Besides, the PEP serves as a substrate for chorismate and shikimate synthesis, via the amino acids phenylalanine and tyrosine are generated. It was estimated “that the production of these two amino acids corresponds to 56% of the total fixed carbon” in *Synechocystis* (Brey et al. 2020). We speculate that the impairment of enolase could result in a deficiency of PEP and pyruvate, which might be lethal when fully segregated.

Since the importance of the Entner-Doudoroff (ED) pathway as potential pyruvate source was to be investigated in this work, a pyruvate kinase (PYK) deletion mutant was created (5.2.2), which might lead to a deficiency in pyruvate but not PEP. Pyruvate kinase mediates the conversion of PEP to pyruvate, gaining ATP. Two putative isoenzymes for pyruvate kinase are annotated in *Synechocystis*, PYK1 (sll0587) and PYK2 (sll1275; Kaneko et al. 1996). Pyruvate kinase has been postulated, being a crucial control point in regulating the carbon metabolism (Bricker et al. 2004; Xiong et al. 2017). However, it is not yet known, whether PYK1 or PYK2 are functional pyruvate kinases, and if so, what their exact function of in *Synechocystis* is (Jablonsky et al. 2013). The question generally arises whether isoenzymes in unicellular cells also fulfil different functions or whether they are not isoenzymes at all. Therefore, growth studies were carried out to characterize PYK1 and PYK2 (5.2.3).

Two aspects of the growth study indicated that the putative PYK1 might not be as essential as PYK2. (i) *pyk2/Δpyk2* would probably have been fully segregated (Figure 5:9) since PYK1 could have compensated for the loss of PYK2 (ii) the *Δpyk1* mutant, neither photoautotrophic, photomixotrophic or heterotrophic, was significantly impaired in growth (Figure 5:10). Even unsegregated, *pyk2/Δpyk2* showed slightly reduced growth under photoautotrophic conditions on BG11 plates (Figure 5:11) and severely restricted growth under photomixotrophic and heterotrophic conditions, cultivated in Kniese tubes. A homologous pyruvate kinase to PYK2 (sll1275) was characterized in *Synechococcus* PCC6301 (Knowles et al. 2001). Interestingly, *Synechococcus* does not appear to have a PYK1. Coleman and Colman postulated 1981 that the pyruvate kinase is regulated depending on the cellular ATP/AMP concentration. High AMP concentration during darkness, caused by lacking CO_2 fixation and photosynthetic electron transport, led to an increased PYK activity. Vice versa, during light and high ATP concentration, PYK was downregulated. Since ATP is generated during the oxidation of PEP to pyruvate, it can be speculated that PYK can function as an alternative ATP source in the dark. This would explain the reduced growth of *pyk2/Δpyk2* under heterotopic conditions. However, the reduced growth of *pyk2/Δpyk2* under photoautotrophic and photomixotrophic conditions indicate that PYK2 has a crucial regulatory role in *Synechocystis*.

Gluconeogenesis, which takes place under photoautotrophic and photomixotrophic conditions, is hypothesized to be initiated by phosphoenolpyruvate synthase (PPS) and malic enzyme (ME; Yang et al. 2002). PPS and PYK convey opposing reactions. It was postulated that the reduced or inhibited pyruvate production via PYK could be compensated by the malic enzyme (ME) since photoautotrophic growth of

Δme deletion mutants (3WEZ) was impaired under continuous light (Zhang et al. 2004; Bricker et al. 2004). What speaks against this hypothesis is that no phenotype could be observed under diurnal light. Since day/night rhythm in the natural habitat of cyanobacteria never leads to permanent light situations, it is therefore quite unlikely that the malic enzyme supplies the cell with larger amounts of pyruvate. Another counterargument is that *Δme* was not able to grow heterotrophically at all (Bricker et al. 2004), although PYK has been proven to be the most active in darkness.

The only alternative route to provide pyruvate known so far, in *Synechocystis* is the ED pathway (Chen et al. 2016). We speculate that the ED pathway not only compensates for possible pyruvate bottlenecks but also supplies the cell with pyruvate in general since *pyk2/Δpyk2Δeda* double mutants grew reduced photoautotrophically on BG11 plates (Figure 5:11). Furthermore, cultivation or even a pre-cultivation in liquid culture of *pyk2/Δpyk2Δeda* was not possible at all.

In addition, a *Δpyk1pyk2/Δpyk2Δeda* triple mutant could not be generated at all. Inactivation of the lower glycolysis, as well as the ED pathway, turned out to be lethal for *Synechocystis*. This indicates that the putative PYK1 has a crucial regulatory role in *Synechocystis*, even if it should not be a pyruvate kinase. Attempts to purify and further characterize putative PYK1 and PYK2 are currently being carried out in the working group.

6.1.4. The Entner-Doudoroff pathway is important when the phosphoketolase pathway is discontinued

We go one step further and hypothesize that the Entner-Doudoroff (ED) pathway might also play an important role in supplying the cell with acetyl-CoA when the phosphoketolase pathway is discontinued. Acetyl-CoA can be generated not only from oxidizing pyruvate but also from reducing acetyl phosphate, which might be produced in *Synechocystis* via the phosphoketolase (PK) pathway (Appendix Figure 1). Two putative phosphoketolase XFP1 (slr0453) and XFP2 (sll0752) are annotated in *Synechocystis*; however, the exact function of the phosphoketolase has not yet been clarified.

Acetyl-CoA mainly supplies the TCA cycle with an acetyl group, which is oxidized to CO_2 and water. During this process, a prominent part of the cells needed intermediates and reducing intermediates are generated. Especially the energetic flexibility that acetyl-CoA enables is interesting. While the carbon used in the TCA cycle, makes NADPH available for CO_2 fixation, acetyl-CoA as a substrate of the PHB synthesis, however, can be used as an electron sink when, e.g. there is an excess of NADH in intense light that needs to be compensated (Batista et al. 2018). For *Aspergillus nidulans,* it has been postulated that the PK pathway is an effective alternative to produce acetyl-CoA while flux through the lower glycolysis is discontinued (Panagiotou et al. 2008), a condition that has been shown in a *Synechocystis Δxfp1* (slr0453) mutant under heterotrophic condition (Xiong et al. 2015). *Δxfp1* did not produce any acetate under heterotrophic conditions and lead to the assumption that acetate production via the

PDH/PFOR pathway is inhibited (Xiong et al. 2015). Within this thesis, it could be shown that *Δxfp1Δxfp2* mutants were able to grow under heterotrophic conditions (5.3.2; Figure 5:15), an indication that the ED pathway might compensate for the cell's need for acetyl-CoA. However, heterotrophic growth also indicates the PDH/PFOR pathway not being completely inhibited, since the pyruvate of the ED pathway is probably metabolized to acetyl-CoA via the PDH/PFOR pathway, too. In addition, the ED pathway could not completely compensate for the acetyl-CoA requirement, since the double mutant photoautotrophic, photomixotrophic and heterotrophic grew worse than the WT, which on the other hand indicates that the phosphoketolase pathway plays, indeed, an important role in central carbon metabolism.

To further investigate whether the ED pathway could act as a route to yield acetyl-CoA, a *Synechocystis Δxfp1Δxfp2Δeda* triple mutant was generated additionally (5.3.1). The additional deletion of the ED pathway worsened the growth of *Synechocystis*, heterotrophically, photomixotrophically and photoautotrophically (5.3.2; Figure 5:15; Figure 5:16), which indicates that the ED pathway, might play an important role in supplying the cell with acetyl-CoA. However, the fact that full segregation of an *Δxfp1Δxfp2Δeda* mutant was possible (Figure 5:14) contradicts the assumption that the ED pathway is the only route to provide pyruvate or acetyl under heterotrophic conditions. Noor et al. 2010 postulated that the effectiveness of the central carbon metabolism could be based on the pathways between metabolites being enzymatically as short as possible. Comparing, the PK pathway and the ED pathway with each other, both form two intermediates breaking down 6P-gluconate respectively xylulose-5P to acetyl-CoA. However, via the lower glycolysis, five intermediates have to be generated to oxidize glyceraldehyde-3P to acetyl-CoA fully. Very time and energy-consuming, since more proteins are needed. Therefore, if the cell is in an energy deficit, it would be thermodynamically advantageous to compensate for acetyl-CoA requirement additionally through the ED pathway (Bar-Even et al. 2012). Another beneficial aspect may be that the ED pathway could indirectly meet the need for xylulose-5P. Xylulose-5P is an intermediate of the CBB cycle. The synthesis of acetyl phosphate and the generation of the CBB cycle are therefore in competition with each other. Although it has been postulated the ED pathway itself functioning as a shunt to regenerate the CBB cycle (Makowka et al. 2020) it could be speculated that it might also be used for the synthesis of acetyl-CoA.

6.2. Fluorescence microscopy studies

6.2.1. Fluorescence microscopy is a suitable method to investigate the organization and dynamics of enzyme complexes *in vivo*

In *Synechocystis*, metabolons, substrate channels and enzyme clusters might be crucial features to regulate the metabolic flux and to compensate for lacking cellular compartmentalization. The prime example of how efficiently the metabolism can be regulated is the ternary PRK-CP12-GAPDH enzyme complex, which regulates the CO_2 fixation in a light-dependent manner. Numerous *in vitro* studies (Pohlmeyer et al. 1996; Avilan et al. 1997; Wedel et al. 1997; Howard et al. 2008; Agarwal et al. 2009; Moparthi et al. 2015; McFarlane et al. 2019) have shown that the CBB cycle is regulated in redox-dependent manner by forming a PRK-CP12-GAPDH enzyme complex. In darkness, CP12 forms a complex with PRK and GAPDH (referred to as GAP2 in *Synechocystis*), which inactivates the Calvin-Benson-Bassham (CBB) cycle. In light, the enzyme complex dissolves, which leads to an immediate reactivation of the CBB cycle.

However, *in vitro* methods provided “only” indirect proof of a PRK-CP12-GAPDH enzyme complex formation (Spivey and Ovádi 1999; Wheeldon et al. 2016; Fleming et al. 2018; Sweetlove and Fernie 2018; Tanner 2019; Obata 2020). In *Synechocystis,* redox-dependent enzyme organization could already be shown *in vivo* via fluorescence microscopy (Burroughs et al. 2014). GFP-tagged HoxF diaphorase subunits of hydrogenase were proven to be localized on the thylakoids. Two populations of hydrogenases were found, one that was evenly dispersed associated to thylakoids and another population that was localized as puncta in the distal thylakoids. Under anoxygenic conditions or prolonged darkness, the signal ratio shifted, and more puncta were detected (Burroughs et al. 2014). It has been suggested, puncta being related to hydrogenase production. In addition, via time-lapse fluorescence microscopy and isotope labelling, it was demonstrated recently, that several metabolic enzymes were condensed (puncta) or soluble (disperse), regulated by the circadian clock. It has been speculated that protein condensation might regulate a metabolic "night's rest" in *Synechococcus elongatus* (Pattanayak et al. 2020).

We hypothesized that the assembly of PCR-CP12-GAPDH could also be detected in the form of single puncta or in the form of lager enzyme clusters since it is highly discussed; metabolons or enzyme complexes being assembled on membranes or proteins (Zajchowski and Robbins 2002; Jørgensen et al. 2005; Bobik 2006; Barchewitz et al. 2019).

Within the scope of this work, seven *Synechocystis* strains were generated (5.4.1) in which the enzymes PRK and GAP2 (CBB cycle), EDD and EDA (Entner-Doudoroff pathway), GND and ZWF (oxidative pentose phosphate pathway) and GAP1 (Emden-Meyerhof-Parnas pathway) were fused to a fluorescent protein (YFP). As expected, we were able to visualize bright fluorescence signals for PRK and GAP2

(5.4.4.1; Figure 5:20). However, it became clear that the chosen cultivation time of 3 days (long-time experiment) was too long since the autofluorescence intensity fluctuated greatly between the photoautotrophic, photomixotrophic and heterotrophic cultivated WT (Figure 5:23). Additionally, caused by lower expression level, the fluorescence intensity of all investigated catabolic enzymes (Figure 5:26) appeared to be in the range of fluctuations of the autofluorescence, which led to the fact that no statement could be made whether glucose, light or darkness has a significant influence on the fluorescence intensity or signal distribution (Figure 5:27) of the catabolic enzymes. Electron flow analyses showed that it takes a maximum of 10min for the CBB cycle to stop completely in darkness (Makowka et al. 2020). Studies on *Pea* leaves illustrated the enzyme complex dissociating or associating within 1min (Howard et al. 2008; López-Calcagno et al. 2014). We suspect that the glycolytic enzymes could be regulated in a similar time frame since the catabolic metabolism has to be quickly adapted to environmental changes too.

To investigate the organization and dynamics of PRK, GAP2 and the catabolic enzymes further, we established a short-time cultivation protocol (4.4.7.1) that minimized the fluorescence noise of the negative control (WT; Figure 5:34). The fact that many enzymes of the central metabolism show an expression below the detectable resolution limit is a known problem, which unfortunately mostly leads to these enzymes not being investigated further, *in vivo* (Wallace et al. 2015; Pattanayak et al. 2020). Therefore, a bioinformatic evaluation needs to be established to improve the images analysis of low expressed proteins. Only recently a deep-learning-based framework was developed, that enables the resolution of confocal fluorescence images to be increased to the high-resolution quality of stimulated emission depletion (STED) microscopy images (Wang et al. 2019), which possess a resolution rate beyond the diffraction limit of light (Stockhammer and Bottanelli 2020). This tool could help to minimize the problem of low fluorescence intensity and to increase the resolution.

However, the development of a deep learning macro is very time-consuming and complex. The glycolytic enzymes were, therefore, not investigated further in this work.

6.2.2. Visualization of the light-dependent dynamic of the PRK-CP12-GAP2 enzyme complex *in vivo*

By establishing the short-time cultivation protocol (5.4.4.2), it was possible to minimize the fluorescence noise of the negative control (WT) significantly (Figure 5:31). As a reminder based on *in vitro* studies, it was postulated that in darkness, CP12 forms a complex with PRK and GAPDH, which inactivates the CBB cycle. Conversely, it was assumed that in light, the enzyme complex dissolves, which leads to an immediate reactivation of the CBB cycle. For the first time, we successfully, visualized the light-depended assembly and disassembly, of PRK and GAP2, by fluorescence microscopy, *in vivo* (Figure 5:36). As suspected, PRK and GAP2 organized themselves in the form of enzyme clusters in the dark and dispersed distributed in light (Figure 5:35). To visualize the complete formation of the PRK-CP12-GAP2 complex, the CP12 dependence of the dynamic has to be shown in future.

6.2.3. The organization of a PRK-CP12-GAP2 enzyme complex could be regulated glucose-dependent

Surprisingly, our results indicate that the CBB cycle could be regulated not only light- but also glucose-dependently since GAP2 formed enzyme clusters under photomixotrophic conditions (Figure 5:35). In *Synechococcus sp.* PCC 7942, it was investigated that the activation of the CP12 protein and thus the formation of the PRK-CP12-GAPDH complex is dependent on “the decrease in the NADP(H)/NAD(H) ratio” (Tamoi et al. 2005). Takahashi et al. (2008) postulated that CP12 could also have an inhibiting effect on the CBB cycle under photomixotrophic conditions since the NADP(H)/NAD(H) ratio decreased significantly when glucose was added. It could also be shown that the amount of CBB-generated intermediates decreased under photomixotrophic conditions (Takahashi et al. 2008). However, we could not find any increased clustering of PRK under photomixotrophic conditions (Figure 5:36) that could indicate downregulation of the CBB cycle. However, in an engineered strain of *Synechococcus elongates* PCC 7942, the deletion of CP12 in a *gnd/zwf* overexpression strain led to an accumulation of ribulose-5P under photomixotrophic conditions (Kanno et al. 2017). It was assumed that the increased conversion of ribulose-5P to ribulose-15bP led to an increased PRK activity, caused by the lack of CP12.

7. Conclusion

In summary, we can draw the following conclusions:

Via growth experiments and glucose concentration measurements, it could finally be determined that the Enter-Doudoroff (ED) pathway exclusively branches off the oxidative pentose phosphate (OPP) pathway and does not additionally result from a flux via the glucose dehydrogenase/gluconate kinase (GDH/GK) pathway in *Synechocystis*. We consider it to be proven that putative GDH1 (sll1709) and GDH2 (slr1608) are not glucose dehydrogenase; however, they might code for enzymes with yet unknown function that play a role in the carbon metabolism of *Synechocystis*.

Via growth experiments, it could be shown that, in *Synechocystis,* the ED pathway gets essential when the lower glycolysis is discontinued. It has been hypothesized that if 3P-glycerate feeds the gluconeogenesis or is involved in the regeneration of the Calvin-Benson-Bassham (CBB) cycle, no pyruvate can be generated via the lower glycolysis. We assume that the ED pathway might represent an alternative route to provide pyruvate during these metabolic conditions.

In addition, growth experiments showed that the ED pathway is important when the phosphoketolase (PK) pathway is discontinued. Impaired or folded pyruvate production through lower glycolysis during gluconeogenesis or regeneration of the CBB cycle, could also cause a deficiency in acetyl-CoA.
We hypothesize that the ED pathway might represent an alternative route to provide pyruvate as a precursor for acetyl-CoA in the absence of the PK pathway.

The conclusion of the microscopy study can be itemized into five statements: (i) We could show that fluorescence microscopy is a suitable method to investigate *in vivo* enzymatic organizations and dynamics of the central carbon metabolism. (ii) For the first time, *in vivo,* the light-depended organization and dynamics of the PRK-CP12-GAP2 complex formation were demonstrated, though the dependence of CP12 still has to be proven. (iii) The results indicate that the PRK-CP12-GAP2 formation might also be glucose-dependent. (iv) A positive-control for enzyme accumulations so-called "clusters" has been established and (v) no statement could be made so far about the dynamics and organization of the catabolic enzymes EDA, EDD, GND, ZWF, GAP1 since the expression level was too low and the evaluation parameters were not sensitive enough. Work is ongoing to improve the protocol further.

8. Outlook

Within this work, it could be shown that the putative pyruvate kinases PYK1 (sll0587) and PYK2 (sll1275), as well as the putative phosphoketolases XFP1 (sll0453) and XFP2 (sll0529), play a physiologically essential or important role in the central carbon metabolism of *Synechocystis*. However, in *Synechocystis,* these enzymes have not yet been characterized biochemically. Attempts are currently being made to purify the enzymes for future enzyme tests. For phosphoketolase, it would be interesting to determine the substrate specificity in particular, as very little is known about the function of the phosphoketolase pathway and its place in the carbon metabolism of *Synechocystis*.

For the first time, we successfully, visualized the light-depended PRK-CP12-GAP2 complex assembly and disassembly by fluorescence microscopy, *in vivo,* by visualizing the light-dependent assembly of PRK and GAP2. However, the dependence of CP12 still has to be proven, for this purpose a PRK-YFP-*Δcp12* and GAP2-YFP-*Δcp12* deletion mutant in which the PRK and GAP2 should no longer be able to assemble in darkness, will be constructed in the working group soon.
Within this work, it could already be observed that the assembly of the PRK-CP12-GAP2 complex takes place in a time frame of a few minutes. However, how quickly the enzyme complex disassembles and whether the assembly and disassembly react consistent to changes in light, is still unexplored and could be investigated by time-lapse imaging of a fluorophore tagged PRK-CP12-GAP2 triple mutant. In addition, it would be interesting to establish microfluidic experiments to observe the influence of glucose and light on the enzyme dynamics “live”. Caused by low expression levels, the organization and dynamics of catabolic enzymes could not be investigated in this work. Only recently a deep-learning-based framework was developed, that enables the resolution of confocal fluorescence images to be increased to the high-resolution quality of stimulated emission depletion (STED) microscopy images (Wang et al. 2019), which possess a resolution rate beyond the diffraction limit of light (Stockhammer and Bottanelli 2020). This tool could help to minimize the problem of low fluorescence intensity and to increase the resolution. Deep learning or machine learning approaches could also improve the detection of enzyme clusters by adapting the determination of thresholds. The determination of the threshold to identify an enzyme cluster was chosen in a way, that only extreme differences in the heterogeneity and intensity of the fluorescence signal were assumed as a cluster. Performing deep or machine learning approaches would enable a better segmentation of cells and clustered signals. While being more time consuming, they would allow the detection of small changes in a broader range of features when comparing different enzymes or conditions. Therefore, these analyses could be an elegant way of increasing the sensitivity for detecting enzyme clusters and, therefore, giving more profound insights into the dynamic protein organization of the central carbon metabolism in *Synechocystis*.

9. References

Agapakis CM, Boyle PM, Silver PA (2012) Natural strategies for the spatial optimization of metabolism in synthetic biology. *Nature Chemical Biology* 8:527–535, https://doi.org/10.1038/nchembio.975

Agarwal R, Ortleb S, Sainis JK, Melzer M (2009) Immunoelectron microscopy for locating Calvin cycle enzymes in the thylakoids of synechocystis 6803. *Molecular Plant* 2:32–42, https://doi.org/10.1093/mp/ssn075

Ahmed H, Ettema TJG, Tjaden B, Geerling ACM, Van Der Oost J, Siebers B (2005) The semi-phosphorylative Entner-Doudoroff pathway in hyperthermophilic archaea: A re-evaluation. *Biochemical Journal* 390:529–540, https://doi.org/10.1042/BJ20041711

Alagesan S, Gaudana SB, Sinha A, Wangikar PP (2013) Metabolic flux analysis of Cyanothece sp. ATCC 51142 under mixotrophic conditions. *Photosynthesis Research* 118:191–198, https://doi.org/10.1007/s11120-013-9911-5

Alberts B, Johnson A, Lewis J, Raff M, Roberts K, Walter P (2002) The Self-Assembly and Dynamic Structure of Cytoskeletal Filaments. *Molecular Biology of the Cell* 4:367–397, https://www.ncbi.nlm.nih.gov/books/NBK26862/

Alonso C, Pernthaler J (2006) Roseobacter and SAR11 dominate microbial glucose uptake in coastal North Sea waters. *Environmental Microbiology* 8:2022–2030, https://doi.org/10.1111/j.1462-2920.2006.01082.x

Ambasht PK, Kayastha AM (2002) Plant pyruvate kinase. *Biologia Plantarum* 45:1–10, https://doi.org/10.1023/A:1015173724712

Anderson SL, McIntosh L (1991) Light-activated heterotrophic growth of the cyanobacterium Synechocystis sp. strain PCC 6803: A blue-light-requiring process. *Journal of Bacteriology* 173:2761–2767, https://doi.org/10.1128/jb.173.9.2761-2767.1991

Anfelt J, Kaczmarzyk D, Shabestary K, Renberg B, Rockberg J, Nielsen J, Uhlén M, Hudson EP (2015) Genetic and nutrient modulation of acetyl-CoA levels in Synechocystis for n-butanol production. *Microbial Cell Factories* 14:167, https://doi.org/10.1186/s12934-015-0355-9

Angermayr SA, Van Der Woude AD, Correddu D, Vreugdenhil A, Verrone V, Hellingwerf KJ (2014) Exploring metabolic engineering design principles for the photosynthetic production of lactic acid by Synechocystis sp. PCC6803. *Biotechnology for Biofuels* 7:99, https://doi.org/10.1186/1754-6834-7-99

Arnon DI (1971) The light reactions of photosynthesis. *Proceedings of the National Academy of Sciences of the United States of America* 68:2883–2892, https://doi.org/10.1073/pnas.68.11.2883

Ausmees N, Kuhn JR, Jacobs-Wagner C (2003) The bacterial cytoskeleton: An intermediate filament-like function in cell shape. *Cell* 115:705–713, https://doi.org/10.1016/S0092-8674(03)00935-8

Avilan L, Gontero B, Lebreton S, Ricard J (1997) Memory and Imprinting Effects in Multienzyme Complexes. I. Isolation, Dissociation, and Reassociation of a Phosphoribulokinase-Glyceraldehyde-3-Phosphate Dehydrogenase Complex from Chlamydomonas Reinhardtii Chloroplasts. *European Journal of Biochemistry* 246:78–84, https://doi.org/10.1111/j.1432-1033.1997.00078.x

Bada JL, Lazcano A (2002) Some like it hot, but not the first biomolecules. *Science* 296:1982–1983, https://doi.org/10.1126/science.1069487

Baqué M, Böttger U, Leya T, de Vera J-PP (2017) Experiment on the ISS: Algae survive heat, cold and cosmic radiation. *Fraunhofer Research News* February 01:1–4, https://doi.org/https://www.fraunhofer.de/content/dam/zv/en/press-media/2017/February/ResearchNews/rn02_2017_IZI_Algae survive heat, cold and cosmic radiation.pdf

Bar-Even A, Flamholz A, Noor E, Milo R (2012) Rethinking glycolysis: on the biochemical logic of metabolic pathways. *Nature Chemical Biology* 8:509–517, https://doi.org/10.1038/nchembio.971

Barbrook AC, Howe CJ, Kurniawan DP, Tarr SJ (2010) Organization and expression of organellar genomes. *Philosophical Transactions of the Royal Society B: Biological Sciences* 365:785–797, https://doi.org/10.1098/rstb.2009.0250

Barchewitz T, Guljamow A, Meissner S, Timm S, Henneberg M, Baumann O, Hagemann M, Dittmann E (2019) Non-canonical localization of RubisCO under high-light conditions in the toxic cyanobacterium Microcystis aeruginosa PCC7806. *Environmental Microbiology* 21:1462-2920.14837, https://doi.org/10.1111/1462-2920.14837

Barten R, Lill H (1995) DNA-uptake in the naturally competent cyanobacterium, *Synechocystis sp.* PCC 6803. *FEMS Microbiology Letters* 129:83–87, https://doi.org/10.1111/j.1574-6968.1995.tb07561.x

Batista MB, Teixeira CS, Sfeir MZTT, Alves LPSS, Valdameri G, Pedrosa F de O, Sassaki GL, Steffens MBRR, de Souza EM, Dixon R, Müller-Santos M (2018) PHB biosynthesis counteracts redox stress in Herbaspirillum seropedicae. *Frontiers in microbiology* 9:472, https://doi.org/10.3389/fmicb.2018.00472

Belnap J (2003) The world at your feet: desert biological soil crusts. *Frontiers in Ecology and the Environment* 1:181–189, https://doi.org/10.1890/1540-9295(2003)001[0181:twayfd]2.0.co;2

Bi E, Lutkenhaus J (1991) FtsZ ring structure associated with division in Escherichia coli. *Nature* 354:161–164, https://doi.org/10.1038/354161a0

Blankenship RE (2017) How Cyanobacteria went green. *Science* 355:1372–1373, https://doi.org/10.1126/science.aam9365

Bobik TA (2006) Polyhedral organelles compartmenting bacterial metabolic processes. *Applied Microbiology and Biotechnology* 70:517–525, https://doi.org/10.1007/s00253-005-0295-0

Bogorad IW, Lin T-SS, Liao JC (2013) Synthetic non-oxidative glycolysis enables complete carbon conservation. *Nature* 502:693–697, https://doi.org/10.1038/nature12575

Bommarito S, Peyret N, SantaLucia J (2000) Thermodynamic parameters for DNA sequences with dangling ends. *Nucleic Acids Research* 28:1929–1934, https://doi.org/10.1093/nar/28.9.1929

Brandina I, Graham J, Lemaitre-Guillier C, Entelis N, Krasheninnikov I, Sweetlove L, Tarassov I, Martin RP (2006) Enolase takes part in a macromolecular complex associated to mitochondria in yeast. *Biochimica et Biophysica Acta - Bioenergetics* 1757:1217–1228, https://doi.org/10.1016/j.bbabio.2006.07.001

Brearley J, Venis MA, Blatt MR (1997) The effect of elevated CO2 concentrations on K+ and anion channels of Vicia faba L. guard cells. *Planta* 203:145–154, https://doi.org/10.1007/s004250050176

Brey LF, Włodarczyk AJ, Bang Thøfner JF, Burow M, Crocoll C, Nielsen I, Zygadlo Nielsen AJ, Jensen PE (2020) Metabolic engineering of Synechocystis sp. PCC 6803 for the production of aromatic amino acids and derived phenylpropanoids. *Metabolic Engineering* 57:129–139, https://doi.org/10.1016/j.ymben.2019.11.002

Bricker TM, Zhang S, Laborde SM, Mayer PR, Frankel LK, Moroney J V. (2004) The malic enzyme is required for optimal photoautotrophic growth of Synechocystis sp. strain PCC 6803 under continuous light but not under a diurnal light regimen. *Journal of Bacteriology* 186:8144–8148, https://doi.org/10.1128/JB.186.23.8144-8148.2004

Buchanan BB (1980) Role of Light in the Regulation of Chloroplast Enzymes. *Annual Review of Plant Physiology* 31:341–374, https://doi.org/10.1146/annurev.pp.31.060180.002013

Buchanan BB (1991) Regulation of CO2 assimilation in oxygenic photosynthesis: The ferredoxin/thioredoxin system. Perspective on its discovery, present status, and future development. *Archives of Biochemistry and Biophysics* 288:1–9, https://doi.org/10.1016/0003-9861(91)90157-E

Buchanan BB, Balmer Y (2005) Redox regulation: A broadening horizon. *Annual Review of Plant Biology* 56:187–220, https://doi.org/10.1146/annurev.arplant.56.032604.144246

Buick R (2008) When did oxygenic photosynthesis evolve? *Philosophical Transactions of the Royal Society B: Biological Sciences* 363:2731–2743, https://doi.org/10.1098/rstb.2008.0041

Burnap RL, Hagemann M, Kaplan A (2015) Regulation of CO2 concentrating mechanism in cyanobacteria. *Life* 5:348–371, https://doi.org/10.3390/life5010348

Burroughs NJ, Boehm M, Eckert C, Mastroianni G, Spence EM, Yu J, Nixon PJ, Appel J, Mullineaux CW, Bryan SJ (2014) Solar powered biohydrogen production requires specific localization of the hydrogenase. *Energy and Environmental Science* 7:3791–3800, https://doi.org/10.1039/c4ee02502d

Calvin M (1962) The Path of Carbon in Photosynthesis. *Angewandte Chemie International Edition in English* 1:65–75, https://doi.org/10.1002/anie.196200651

Cannon GC, Heinhorst S, Kerfeld CA (2010) Carboxysomal carbonic anhydrases: Structure and role in microbial CO2 fixation. *Biochimica et Biophysica Acta - Proteins and Proteomics* 1804:382–392, https://doi.org/10.1016/j.bbapap.2009.09.026

Carreras J, Mezquita J, Bosch J, Bartrons R, Pons G (1982) Phylogeny and ontogeny of the phosphoglycerate mutases—IV. Distribution of glycerate-2,3-P2 dependent and independent phosphoglycerate mutases in algae, fungi, plants and animals. *Comparative Biochemistry and Physiology Part B: Comparative Biochemistry* 71:591–597, https://doi.org/10.1016/0305-0491(82)90467-9

Celler K, Koning RI, Koster AJ, van Wezel GP (2013) Multidimensional view of the bacterial cytoskeleton. *Journal of Bacteriology* 195:1627–1636, https://doi.org/10.1128/JB.02194-12

Chen X, Schreiber K, Appel J, Makowka A, Fähnrich B, Roettger M, Hajirezaei MR, Sönnichsen FD, Schönheit P, Martin WF, Gutekunst K (2016) The Entner–Doudoroff pathway is an overlooked glycolytic route in cyanobacteria and plants. *Proceedings of the National Academy of Sciences* 113:5441–5446, https://doi.org/10.1073/pnas.1521916113

Christensen CD, Hofmeyr JHS, Rohwer JM (2015) Tracing regulatory routes in metabolism using generalised supply-demand analysis. *BMC Systems Biology* 9:1–18, https://doi.org/10.1186/s12918-015-0236-1

Chuong SDX, Good AG, Taylor GJ, Freeman MC, Moorhead GBG, Muench DG (2004) Large-scale identification of tubulin-binding proteins provides insight on subcellular trafficking, metabolic channeling, and signaling in plant cells. *Molecular and Cellular Proteomics* 3:970–983, https://doi.org/10.1074/mcp.M400053-MCP200

Coleman JR, Colman B (1981) Inorganic Carbon Accumulation and Photosynthesis in a Blue-green Alga as a Function of External pH. *Plant Physiology* 67:917–921, https://doi.org/10.1104/pp.67.5.917

Collin V, Issakidis-Bourguet E, Marchand C, Hirasawa M, Lancelin JM, Knaff DB, Miginiac-Maslow M (2003) The Arabidopsis plastidial thioredoxins. New functions and new insights into specificity. *Journal of Biological Chemistry* 278:23747–23752, https://doi.org/10.1074/jbc.M302077200

Conway T (1992) The Entner-Doudoroff pathway: history, physiology and molecular biology. *FEMS Microbiology Letters* 103:1–28, https://doi.org/10.1111/j.1574-6968.1992.tb05822.x

Cornell B (2016) Photosynthesis vs. Respiration. https://ib.bioninja.com.au/higher-level/topic-8-metabolism-cell/untitled-2/photosynthesis-vs-respirati.html. Accessed 9 Nov 2020

Court SJ, Waclaw B, Allen RJ (2015) Lower glycolysis carries a higher flux than any biochemically possible alternative. *Nature Communications* 6:8427, https://doi.org/10.1038/ncomms9427

D'Souza SF, Srere PA (1983) Binding of citrate synthase to mitochondrial inner membranes. *Journal of Biological Chemistry* 258:4706–4709, https://doi.org/10.1016/S0021-9258(18)32479-7

Dagan T, Roettger M, Stucken K, Landan G, Koch R, Major P, Gould SB, Goremykin V V., Rippka R, De Marsac NT, Gugger M, Lockhart PJ, Allen JF, Brune I, Maus I, Pühler A, Martin WF (2013) Genomes of stigonematalean cyanobacteria (subsection V) and the evolution of oxygenic photosynthesis from prokaryotes to plastids. *Genome Biology and Evolution* 5:31–44, https://doi.org/10.1093/gbe/evs117

Dai S, Johansson K, Miginiac-Maslow M, Schürmann P, Eklund H (2004) Structural basis of redox signaling in photosynthesis: Structure and function of ferredoxin:thioredoxin reductase and target enzymes. *Photosynthesis Research* 79:233–248, https://doi.org/10.1023/B:PRES.0000017194.34167.6d

Deusch O, Landan G, Roettger M, Gruenheit N, Kowallik K V., Allen JF, Martin W, Dagan T (2008) Genes of cyanobacterial origin in plant nuclear genomes point to a heterocyst-forming plastid ancestor. *Molecular Biology and Evolution* 25:748–761, https://doi.org/10.1093/molbev/msn022

Du H, Huang Y, Tang Y (2010) Genetic and metabolic engineering of isoflavonoid biosynthesis. *Applied Microbiology and Biotechnology* 86:1293–1312, https://doi.org/10.1007/s00253-010-2512-8

Edwards A, Bowling DJF (1985) Evidence for a CO2 inhibited proton extrusion pump in the stomatal cells of Tradescantia virginiana. *Journal of Experimental Botany* 36:91–98, https://doi.org/10.1093/jxb/36.1.91

Eisenhut M, Von Wobeser EA, Jonas L, Schubert H, Ibelings BW, Bauwe H, Matthijs HCP, Hagemann M (2007) Long-term response toward inorganic carbon limitation in wild type and glycolate turnover mutants of the cyanobacterium Synechocystis sp. strain PCC 6803. *Plant Physiology* 144:1946–1959, https://doi.org/10.1104/pp.107.103341

Engineer CB, Hashimoto-Sugimoto M, Negi J, Israelsson-Nordström M, Azoulay-Shemer T, Rappel WJ, Iba K, Schroeder JI (2016) CO2 Sensing and CO2 Regulation of Stomatal Conductance: Advances and Open Questions. *Trends in Plant Science* 21:16–30, https://doi.org/10.1016/j.tplants.2015.08.014

Fandi KG, Ghazali HM, Yazid AM, Raha AR (2001) Purification and N-terminal amino acid sequence of fructose-6-phosphate phosphoketolase from Bifidobacterium longum BB536. *Letters in Applied Microbiology* 32:235–239, https://doi.org/10.1046/j.1472-765X.2001.00895.x

Farrokh P, Sheikhpour M, Kasaeian A, Asadi H, Bavandi R (2019) Cyanobacteria as an eco-friendly resource for biofuel production: A critical review. *Biotechnology Progress* 35:e2835, https://doi.org/10.1002/btpr.2835

Fernie AR, Zhang Y, Sweetlove LJ (2018) Passing the Baton: Substrate Channelling in Respiratory Metabolism. *Research* 2018:1–16, https://doi.org/10.1155/2018/1539325

Fischer WW, Hemp J, Johnson JE (2016) Evolution of Oxygenic Photosynthesis. *Annual Review of Earth and Planetary Sciences* 44:647–683, https://doi.org/10.1146/annurev-earth-060313-054810

Flamholz A, Noor E, Bar-Even A, Liebermeister W, Milo R, Designed RM, Performed WL (2013) Glycolytic strategy as a tradeoff between energy yield and protein cost. *Proceedings of the National Academy of Sciences of the United States of America* 110:10039–10044, https://doi.org/10.1073/pnas.1215283110

Fleming JR, Schupfner M, Busch F, Baslé A, Ehrmann A, Sterner R, Mayans O (2018) Evolutionary Morphing of Tryptophan Synthase: Functional Mechanisms for the Enzymatic Channeling of Indole. *Journal of Molecular Biology* 430:5066–5079, https://doi.org/10.1016/j.jmb.2018.10.013

Fuhrer T, Fischer E, Sauer U (2005) Experimental Identification and Quantification of Glucose Metabolism in Seven Bacterial Species. *Journal of bacteriology* 187:1581–1590, https://doi.org/10.1128/JB.187.5.1581-1590.2005

Fujisawa T, Narikawa R, Maeda SI, Watanabe S, Kanesaki Y, Kobayashi K, Nomata J, Hanaoka M, Watanabe M, Ehira S, Suzuki E, Awai K, Nakamura Y (2017) CyanoBase: A large-scale update on its 20th anniversary. *Nucleic Acids Research* 45:551–554, https://doi.org/10.1093/nar/gkw1131

Fukayama H, Fukuda T, Masumoto C, Taniguchi Y, Sakai H, Cheng W, Hasegawa T, Miyao M (2009) Rice plant response to long term CO2 enrichment: Gene expression profiling. *Plant Science* 177:203–210, https://doi.org/https://doi.org/10.1016/j.plantsci.2009.05.014

Fushinobu S (2010) Unique sugar metabolic pathways of bifidobacteria. *Bioscience, Biotechnology and Biochemistry* 74:2374–2384, https://doi.org/10.1271/bbb.100494

Gademann K, Portmann C (2008) Secondary Metabolites from Cyanobacteria: Complex Structures and Powerful Bioactivities. *Current Organic Chemistry* 12:326–341, https://doi.org/10.2174/138527208783743750

Galperin MY (2005) A census of membrane-bound and intracellular signal transduction proteins in bacteria: Bacterial IQ, extroverts and introverts. *BMC Microbiology* 5:35, https://doi.org/10.1186/1471-2180-5-35

Gantt E, Conti SF (1969) Ultrastructure of blue-green algae. *Journal of bacteriology* 97:1486–1493, https://doi.org/10.1128/JB.97.3.1486-1493.1969

Geiger DR, Servaites JC (1994) Diurnal regulation of photosynthetic carbon metabolism in C3 plants. *Annual Review of Plant Physiology and Plant Molecular Biology* 45:235–256, https://doi.org/10.1146/annurev.pp.45.060194.001315

Gibson DG, Young L, Chuang RY, Venter JC, Hutchison CA, Smith HO (2009) Enzymatic assembly of DNA molecules up to several hundred kilobases. *Nature Methods* 6:343–345, https://doi.org/10.1038/nmeth.1318

Giegé P, Heazlewood JL, Roessner-Tunali U, Harvey Millar A, Fernie AR, Leaver CJ, Sweetlove LJ (2003) Enzymes of glycolysis are functionally associated with the mitochondrion in arabidopsis cells. *Plant Cell* 15:2140–2151, https://doi.org/10.1105/tpc.012500

Gontero B, Maberly SC (2012) An intrinsically disordered protein, CP12: Jack of all trades and master of the Calvin cycle. *Biochemical Society Transactions* 40:995–999, https://doi.org/10.1042/BST20120097

Graham JWA, Williams TCR, Morgan M, Fernie AR, Ratcliffe RG, Sweetlove LJ (2007) Glycolytic enzymes associate dynamically with mitochondria in response to respiratory demand and support substrate channeling. *Plant Cell* 19:3723–3738, https://doi.org/10.1105/tpc.107.053371

Green R, Rogers EJ (2013) Transformation of chemically competent E. coli. *Methods in Enzymology* 529:329–336, https://doi.org/10.1016/B978-0-12-418687-3.00028-8

Grigorieva G, Shestakov S (1982) Transformation in the cyanobacterium Synechocystis sp. 6803. *FEMS Microbiology Letters* 13:367–370, https://doi.org/10.1111/j.1574-6968.1982.tb08289.x

Grill JP, Crociani J, Ballongue J (1995) Characterization of fructose 6 phosphate phosphoketolases purified from Bifidobacterium species. *Current Microbiology* 31:49–54, https://doi.org/10.1007/BF00294634

Gründel M, Scheunemann R, Lockau W, Zilliges Y (2012) Impaired glycogen synthesis causes metabolic overflow reactions and affects stress responses in the cyanobacterium Synechocystis sp. PCC 6803. *Microbiology (United Kingdom)* 158:3032–3043, https://doi.org/10.1099/mic.0.062950-0

Gutekunst K (2018) Hypothesis on the Synchronistic Evolution of Autotrophy and Heterotrophy. *Trends in Biochemical Sciences* 43:402–411, https://doi.org/10.1016/j.tibs.2018.03.008

Habeeb AFSA, Hiramoto R (1968) Reaction of proteins with glutaraldehyde. *Archives of Biochemistry and Biophysics* 126:16–26, https://doi.org/10.1016/0003-9861(68)90554-7

Hamouda RAEF, Sorour NM, Yeheia DS (2016) Biodegradation of crude oil by Anabaena oryzae, Chlorella kessleri and its consortium under mixotrophic conditions. *International Biodeterioration and Biodegradation* 112:128–134, https://doi.org/10.1016/j.ibiod.2016.05.001

Han PP, Yao SY, Guo RJ, Yan RR, Wu YK, Shen SG, Jia SR (2017) Influence of culture conditions on extracellular polysaccharide production and the activities of enzymes involved in the polysaccharide synthesis of: Nostoc flagelliforme. *RSC Advances* 7:45075–45084, https://doi.org/10.1039/c7ra07982f

Heath EC, Hurwitz J, Horecker BL, Ginsburg A (1958) Pentose fermentation by Lactobacillus plantarum. I. The cleavage of xylulose 5-phosphate by phosphoketolase. *The Journal of biological chemistry* 231:1009–1029, https://doi.org/10.1016/S0021-9258(18)70463-8

Hoch G, Owens O v. H, Kok B (1963) Photosynthesis and respiration. *Archives of Biochemistry and Biophysics* 101:171–180, https://doi.org/10.1016/0003-9861(63)90547-2

Hofmeyr JHS, Cornish-Bowden A (2000) Regulating the cellular economy of supply and demand. *FEBS Letters* 476:47–51, https://doi.org/10.1016/S0014-5793(00)01668-9

Hohmann-Marriott MF, Blankenship RE (2011) Evolution of Photosynthesis. *Annual Review of Plant Biology* 62:515–548, https://doi.org/10.1146/annurev-arplant-042110-103811

Hommes RWJ, Postma PW, Neijssel OM, Tempest DW, Dokter P, Duine JA (1984) Evidence of a quinoprotein glucose dehydrogenase apoenzyme in several strains of *Escherichia coli*. *FEMS Microbiology Letters* 24:329–333, https://doi.org/10.1111/j.1574-6968.1984.tb01329.x

Howard TP, Metodiev M, Lloyd JC, Raines CA (2008) Thioredoxin-mediated reversible dissociation of a stromal multiprotein complex in response to changes in light availability. *Proceedings of the National Academy of Sciences of the United States of America* 105:4056–4061, https://doi.org/10.1073/pnas.0710518105

Howe C., Barbrook A., Nisbet RE., Lockhart P., Larkum AW. (2008) The origin of plastids. *Philosophical Transactions of the Royal Society B: Biological Sciences* 363:2675–2685, https://doi.org/10.1098/rstb.2008.0050

Hu H, Boisson-Dernier A, Israelsson-Nordström M, Böhmer M, Xue S, Ries A, Godoski J, Kuhn JM, Schroeder JI (2010) Carbonic anhydrases are upstream regulators of CO2-controlled stomatal movements in guard cells. *Nature Cell Biology* 12:87–93, https://doi.org/10.1038/ncb2009

Ikeuchi M, Tabata S (2001) Synechocystis sp. PCC 6803 - A useful tool in the study of the genetics of cyanobacteria. *Photosynthesis Research* 70:73–83, https://doi.org/10.1023/A:1013887908680

Ito S, Koyama N, Osanai T (2019) Citrate synthase from Synechocystis is a distinct class of bacterial citrate synthase. *Scientific Reports* 9:1–9, https://doi.org/10.1038/s41598-019-42659-z

Iwasa H, Ozawa K, Sasaki N, Kinoshita N, Yokoyama K, Hiratsuka A (2018) Fungal FAD-dependent glucose dehydrogenases concerning high activity, affinity, and thermostability for maltose-insensitive blood glucose sensor. *Biochemical Engineering Journal* 140:115–122, https://doi.org/https://doi.org/10.1016/j.bej.2018.09.014

Jablonsky J, Hagemann M, Schwarz D, Wolkenhauer O (2013) Phosphoglycerate Mutases Function as Reverse Regulated Isoenzymes in Synechococcus elongatus PCC 7942. *PLoS ONE* 8:e58281, https://doi.org/10.1371/journal.pone.0058281

Jansén T, Kurian D, Raksajit W, York S, Summers ML, Mäenpää P (2010) Characterization of trophic changes and a functional oxidative pentose phosphate pathway in Synechocystis sp. PCC 6803. *Acta Physiologiae Plantarum* 32:511–518, https://doi.org/10.1007/s11738-009-0428-7

Jones LJF, Carballido-López R, Errington J (2001) Control of cell shape in bacteria: Helical, actin-like filaments in Bacillus subtilis. *Cell* 104:913–922, https://doi.org/10.1016/S0092-8674(01)00287-2

Jørgensen K, Rasmussen AV, Morant M, Nielsen AH, Bjarnholt N, Zagrobelny M, Bak S, Møller BL (2005) Metabolon formation and metabolic channeling in the biosynthesis of plant natural products. *Current Opinion in Plant Biology* 8:280–291, https://doi.org/10.1016/j.pbi.2005.03.014

Kamo M, Tsugita A, Wiessner C, Wedel N, Bartling D, Herrmann RG, Aguilar F, Gardet-Salvi L, Schürmann P (1989) Primary structure of spinach-chloroplast thioredoxin f: Protein sequencing and analysis of complete cDNA clones for spinach-chloroplast thioredoxin f. *European Journal of Biochemistry* 182:315–322, https://doi.org/10.1111/j.1432-1033.1989.tb14832.x

Kaneko T, Sato S, Kotani H, Tanaka A, Asamizu E, Nakamura Y, Miyajima N, Hirosawa M, Sugiura M, Sasamoto S, Kimura T, Hosouchi T, Matsuno A, Muraki A, Nakazaki N, Naruo K, Okumura S, Shimpo S, Takeuchi C, Wada T, Watanabe A, Yamada M, Yasuda M, Tabata S (1996) Sequence analysis of the genome of the unicellular cyanobacterium Synechocystis sp. strain PCC6803. II. Sequence determination of the entire genome and assignment of potential protein-coding regions. *DNA research : an international journal for rapid publication of reports on genes and genomes* 3:109–136, https://doi.org/10.1093/dnares/3.3.109

Kanno M, Carroll AL, Atsumi S (2017) Global metabolic rewiring for improved CO2 fixation and chemical production in cyanobacteria. *Nature Communications* 8:1–11, https://doi.org/10.1038/ncomms14724

Kerfeld CA, Heinhorst S, Cannon GC (2010) Bacterial microcompartments. *Annual review of microbiology* 64:391–408, https://doi.org/10.1146/annurev.micro.112408.134211

Kesaano M, Sims RC (2014) Algal biofilm based technology for wastewater treatment. *Algal Research* 5:231–240, https://doi.org/10.1016/j.algal.2014.02.003

Kim BH, Gadd GM (2008) Anaerobic fermentation. *Bacterial Physiology and Metabolism* 265:267, https://doi.org/10.1017/CBO9780511790461

Kispal G, Sumegi B, Alkonyi I (1986) Isolation and characterization of 3-hydroxyacyl coenzyme A dehydrogenase-binding protein from pig heart inner mitochondrial membrane. *Journal of Biological Chemistry* 261:14209–14213, https://doi.org/10.1016/S0021-9258(18)67005-X

Klingner A, Bartsch A, Dogs M, Wagner-Döbler I, Jahn D, Simon M, Brinkhoff T, Becker J, Wittmann C (2015) Large-Scale 13 C Flux Profiling Reveals Conservation of the Entner-Doudoroff Pathway as a Glycolytic Strategy among Marine Bacteria That Use Glucose. *Applied and Environmental Microbiology* 81:2408–2422, https://doi.org/10.1128/aem.03157-14

Knoop H, Gründel M, Zilliges Y, Lehmann R, Hoffmann S, Lockau W, Steuer R (2013) Flux Balance Analysis of Cyanobacterial Metabolism: The Metabolic Network of Synechocystis sp. PCC 6803. *PLoS Computational Biology* 9:e1003081, https://doi.org/10.1371/journal.pcbi.1003081

Knowles VL, Smith CSCR, Smith CSCR, Plaxton WC (2001) Structural and Regulatory Properties of Pyruvate Kinase from the Cyanobacterium Synechococcus PCC 6301. *Journal of Biological Chemistry* 276:20966–20972, https://doi.org/10.1074/jbc.M008878200

Kocharin K, Siewers V, Nielsen J (2013) Improved polyhydroxybutyrate production by Saccharomyces cerevisiae through the use of the phosphoketolase pathway. *Biotechnology and Bioengineering* 110:2216–2224, https://doi.org/10.1002/bit.24888

Koksharova O, Schubert M, Shestakov S, Cerff R (1998) Genetic and biochemical evidence for distinct key functions of two highly divergent GAPDH genes in catabolic and anabolic carbon flow of the cyanobacterium Synechocystis sp. PCC 6803. *Plant Molecular Biology* 36:183–194, https://doi.org/10.1023/A:1005925732743

Koonin E V., Aravind L (2002) Origin and evolution of eukaryotic apoptosis: The bacterial connection. *Cell Death and Differentiation* 9:394–404, https://doi.org/10.1038/sj.cdd.4400991

Kopp D, Bergquist PL, Sunna A (2020) Enzymology of alternative carbohydrate catabolic pathways. *Catalysts* 10:1–25, https://doi.org/10.3390/catal10111231

Kresge N, Simoni RD, Hill RL (2005) Otto Fritz Meyerhof and the elucidation of the glycolytic pathway. *The Journal of biological chemistry* 280:e3, https://doi.org/10.1016/S0021-9258(20)76366-0

Krüsemann JL, Lindner SN, Dempfle M, Widmer J, Arrivault S, Debacker M, He H, Kubis A, Chayot R, Anissimova M, Marlière P, Cotton CAR, Bar-Even A (2018) Artificial pathway emergence in central metabolism from three recursive phosphoketolase reactions. *FEBS Journal* 285:4367–4377, https://doi.org/10.1111/febs.14682

Kühn J, Briegel A, Mörschel E, Kahnt J, Leser K, Wick S, Jensen GJ, Thanbichler M (2010) Bactofilins, a ubiquitous class of cytoskeletal proteins mediating polar localization of a cell wall synthase in Caulobacter crescentus. *EMBO Journal* 29:327–339, https://doi.org/10.1038/emboj.2009.358

Kumar D, Pandey LK, Gaur JP (2016) Metal sorption by algal biomass: From batch to continuous system. *Algal Research* 18:95–109, https://doi.org/10.1016/j.algal.2016.05.026

Laemmli UK (1970) Cleavage of structural proteins during the assembly of the head of bacteriophage T4. *Nature* 227:680–685, https://doi.org/10.1038/227680a0

Lane N, Martin WF (2012) The origin of membrane bioenergetics. *Cell* 151:1406–1416, https://doi.org/10.1016/j.cell.2012.11.050

Leliaert F, Smith DR, Moreau H, Herron MD, Verbruggen H, Delwiche CF, De Clerck O (2012) Phylogeny and Molecular Evolution of the Green Algae. *Critical Reviews in Plant Sciences* 31:1–46, https://doi.org/10.1080/07352689.2011.615705

Li H, Ban Z, Qin H, Ma L, King AJ, Wang G (2015) A heteromeric membrane-bound prenyltransferase complex from hop catalyzes three sequential aromatic prenylations in the bitter acid pathway. *Plant Physiology* 167:650–659, https://doi.org/10.1104/pp.114.253682

Ligrone R, Ligrone R (2019) The Chloroplast and Photosynthetic Eukaryotes. *Biological Innovations that Built the World* 1:269–310, https://doi.org/10.1007/978-3-030-16057-9_9

Lin M, Lucas HC, Shmueli G (2011) Too Big to Fail: Larger Samples and False Discoveries. *Robert H Smith School Research Paper* No. RHS:6–68, https://doi.org/10.2139/ssrn.1336700

Lin PP, Jaeger AJ, Wu TY, Xu SC, Lee AS, Gao F, Chen PW, Liao JC (2018) Construction and evolution of an Escherichia coli strain relying on nonoxidative glycolysis for sugar catabolism. *Proceedings of the National Academy of Sciences of the United States of America* 115:3538–3546, https://doi.org/10.1073/pnas.1802191115

Liu L, Zhang L, Tang W, Gu Y, Hua Q, Yang S, Jiang W, Yang C (2012) Phosphoketolase pathway for Xylose Catabolism in Clostridium acetobutylicum revealed by 13C metabolic flux analysis. *Journal of Bacteriology* 194:5413–5422, https://doi.org/10.1128/JB.00713-12

López-Calcagno PE, Howard TP, Raines CA (2014) The CP12 protein family: A thioredoxin-mediated metabolic switch? *Frontiers in Plant Science* 5:9, https://doi.org/10.3389/fpls.2014.00009

Luinenburg I, Coleman JR (1990) A requirement for phosphoenolpyruvate carboxylase in the cyanobacterium Synechococcus PCC 7942. *Archives of Microbiology* 154:471–474, https://doi.org/10.1007/BF00245230

Maeda K, Tsugita A, Dalzoppo D, Vilboise F, Schürmann P (1986) Further characterization and amino acid sequence of m-type thioredoxins from spinach chloroplasts. *European Journal of Biochemistry* 154:197–203, https://doi.org/10.1111/j.1432-1033.1986.tb09379.x

Mai J (2020) Beginnt der ED-Weg in Cyanobakterien & Pflanzen über zwei alternative Routen? *Christian-Albrechts-Univeristät zu Kiel*. Bachelor Thesis (unpublished)

Makowka A (2019) Glycolytic shunts are anaplerotic reactions for the Calvin-Benson-Bassham cycle. *Christian-Albrechts-Univerisity of Kiel*, Dissertation. https://doi.org/https://macau.uni-kiel.de/servlets/MCRFileNodeServlet/macau_derivate_00000975/Kurzfassung.pdf

Makowka A, Nichelmann L, Schulze D, Spengler K, Wittmann C, Forchhammer K, Gutekunst K (2020) Glycolytic Shunts Replenish the Calvin–Benson–Bassham Cycle as Anaplerotic Reactions in Cyanobacteria. *Molecular Plant* 13:471–482, https://doi.org/10.1016/j.molp.2020.02.002

Marsan DW, Conrad SM, Stutts WL, Parker CH, Deeds JR (2018) Evaluation of microcystin contamination in blue-green algal dietary supplements using a protein phosphatase inhibition-based test kit. *Heliyon* 4:e00573, https://doi.org/10.1016/j.heliyon.2018.e00573

Martin W, Russell MJ, Horner D, Blankenship R, Cavalier-Smith T, Nisbet E (2003) On the origins of cells: A hypothesis for the evolutionary transitions from abiotic geochemistry to chemoautotrophic prokaryotes, and from prokaryotes to nucleated cells. *Philosophical Transactions of the Royal Society B: Biological Sciences* 358:59–85, https://doi.org/10.1098/rstb.2002.1183

Matuszyńska A, Saadat NP, Ebenhöh O (2019) Balancing energy supply during photosynthesis – a theoretical perspective. *Physiologia Plantarum* 166:392–402, https://doi.org/10.1111/ppl.12962

Mayer AMS, Rodríguez AD, Berlinck RGS, Hamann MT (2007) Marine pharmacology in 2003–4: Marine compounds with anthelmintic antibacterial, anticoagulant, antifungal, anti-inflammatory, antimalarial, antiplatelet, antiprotozoal, antituberculosis, and antiviral activities; affecting the cardiovascular, immune and. *Comparative Biochemistry and Physiology Part C: Toxicology & Pharmacology* 145:553–581, https://doi.org/10.1016/j.cbpc.2007.01.015

McFarlane CR, Shah NR, Kabasakal B V., Echeverria B, Cotton CARR, Bubeck D, Murray JW (2019) Structural basis of light-induced redox regulation in the Calvin–Benson cycle in cyanobacteria. *Proceedings of the National Academy of Sciences of the United States of America* 116:20984–20990, https://doi.org/10.1073/pnas.1906722116

Meile L, Rohr LM, Geissmann TA, Herensperger M, Teuber M (2001) Characterization of the D-xylulose 5-phosphate/D-fructose 6-phosphate phosphoketolase gene (xfp) from Bifidobacterium lactis. *Journal of bacteriology* 183:2929–2936, https://doi.org/10.1128/JB.183.9.2929-2936.2001

Meléndez-Hevia E, Waddell TG, Heinrich R, Montero F, Meléndez-Hevia E, Waddell TG, Heinrich R, Montero F (1997) Theoretical approaches to the evolutionary optimization of glycolysis: chemical analysis. *European journal of biochemistry* 244:527–543, https://doi.org/10.1111/j.1432-1033.1997.t01-1-00527.x

Meyer FM, Gerwig J, Hammer E, Herzberg C, Commichau FM, Völker U, Stülke J (2011) Physical interactions between tricarboxylic acid cycle enzymes in Bacillus subtilis: Evidence for a metabolon. *Metabolic Engineering* 13:18–27, https://doi.org/10.1016/j.ymben.2010.10.001

Miao R, Xie H, Liu X, Lindberg P, Lindblad P (2020) Current processes and future challenges of photoautotrophic production of acetyl-CoA-derived solar fuels and chemicals in cyanobacteria. *Current Opinion in Chemical Biology* 59:69–76, https://doi.org/10.1016/j.cbpa.2020.04.013

Michelet L, Zaffagnini M, Morisse S, Sparla F, Pérez-Pérez ME, Francia F, Danon A, Marchand CH, Fermani S, Trost P, Lemaire SD (2013) Redox regulation of the Calvin-Benson cycle: Something old, something new. *Frontiers in Plant Science* 4:470, https://doi.org/10.3389/fpls.2013.00470

Mishra U, Pabbi S (2004) Cyanobacteria: A potential biofertilizer for rice. *Resonance* 9:6–10, https://doi.org/10.1007/bf02839213

Moore GE, Gadol SM, Robinson JB, Srere PA (1984) Binding of citrate synthase and malate dehydrogenase to mitochondrial inner membranes: Tissue distribution and metabolite effects. *Biochemical and Biophysical Research Communications* 121:612–618, https://doi.org/10.1016/0006-291X(84)90226-2

Moparthi SB, Thieulin-Pardo G, de Torres J, Ghenuche P, Gontero B, Wenger J (2015) FRET analysis of CP12 structural interplay by GAPDH and PRK. *Biochemical and Biophysical Research Communications* 458:488–493, https://doi.org/https://doi.org/10.1016/j.bbrc.2015.01.135

Moriyama T, Tajima N, Sekine K, Sato N (2015) Characterization of three putative xylulose 5-phosphate/fructose 6-phosphate phosphoketolases in the cyanobacterium Anabaena sp. PCC 7120. *Bioscience, Biotechnology and Biochemistry* 79:767–774, https://doi.org/10.1080/09168451.2014.993357

Muchowska KB, Varma SJ, Chevallot-Beroux E, Lethuillier-Karl L, Li G, Moran J (2017) Metals promote sequences of the reverse Krebs cycle. *Nature Ecology and Evolution* 1:1716–1721, https://doi.org/10.1038/s41559-017-0311-7

Nabout JC, da Silva Rocha B, Carneiro FM, Sant'Anna CL (2013) How many species of Cyanobacteria are there? Using a discovery curve to predict the species number. *Biodiversity and Conservation* 22:2907–2918, https://doi.org/10.1007/s10531-013-0561-x

Nakajima T, Kajihata S, Yoshikawa K, Matsuda F, Furusawa C, Hirasawa T, Shimizu H (2014) Integrated metabolic flux and omics analysis of Synechocystis sp. PCC 6803 under mixotrophic and photoheterotrophic conditions. *Plant and Cell Physiology* 55:1606–1612, https://doi.org/10.1093/pcp/pcu091

Noffke N, Christian D, Wacey D, Hazen RM (2013) Microbially induced sedimentary structures recording an ancient ecosystem in the ca. 3.48 Billion-year-old dresser formation, pilbara, Western Australia. *Astrobiology* 13:1103–1124, https://doi.org/10.1089/ast.2013.1030

Noor E, Eden E, Milo R, Alon U (2010) Central Carbon Metabolism as a Minimal Biochemical Walk between Precursors for Biomass and Energy. *Molecular Cell* 39:809–820, https://doi.org/10.1016/j.molcel.2010.08.031

Obata T (2019) Metabolons in plant primary and secondary metabolism. *Phytochemistry Reviews* 18:1483–1507, https://doi.org/10.1007/s11101-019-09619-x

Obata T (2020) Toward an evaluation of metabolite channeling in vivo. *Current Opinion in Biotechnology* 64:55–61, https://doi.org/10.1016/j.copbio.2019.09.013

Orgel LE (2008) The implausibility of metabolic cycles on the prebiotic earth. *PLoS Biology* 6:5–13, https://doi.org/10.1371/journal.pbio.0060018

Orthwein T, Scholl J, Spät P, Lucius S, Koch M, Macek B, Hagemann M, Forchhammer K (2020) The Novel PII-Interacting Regulator PirC (Sll0944) Identifies 3-Phosphoglycerate Mutase (PGAM) as Central Control Point of Carbon Storage Metabolism in Cyanobacteria. *bioRxiv* 53:1689–1699, https://doi.org/10.1101/2020.09.11.292599

Paerl HW, Paul VJ (2012) Climate change: Links to global expansion of harmful cyanobacteria. *Water Research* 46:1349–1363, https://doi.org/10.1016/j.watres.2011.08.002

Panagiotou G, Anderson MR, Grotkjær T, Regueira TB, Hofmann G, Nielsen J, Olsson L (2008) Systems analysis unfolds the relationship between the phosphoketolase pathway and growth in Aspergillus nidulans. *PLoS ONE* 3:e3847, https://doi.org/10.1371/journal.pone.0003847

Park J, Choi Y (2017) Cofactor engineering in cyanobacteria to overcome imbalance between NADPH and NADH: A mini review. *Frontiers of Chemical Science and Engineering* 11:66–71, https://doi.org/10.1007/s11705-016-1591-1

Pattanayak GK, Liao Y, Wallace EWJ, Budnik B, Drummond DA, Rust MJ (2020) Daily Cycles of Reversible Protein Condensation in Cyanobacteria. *Cell Reports* 32:108032, https://doi.org/10.1016/j.celrep.2020.108032

Peekhaus N, Conway T (1998) What's for dinner?: Entner-Doudoroff metabolism in Escherichia coli. *Journal of Bacteriology* 180:3495–3502, https://doi.org/10.1128/jb.180.14.3495-3502.1998

Pelroy RA, Rippka R, Stanier RY (1972) Metabolism of glucose by unicellular blue-green algae. *Archiv für Mikrobiologie* 87:303–322, https://doi.org/10.1007/BF00409131

Peña KL, Castel SE, De Araujo C, Espie GS, Kimber MS (2010) Structural basis of the oxidative activation of the carboxysomal γ-carbonic anhydrase, CcmM. *Proceedings of the National Academy of Sciences of the United States of America* 107:2455–2460, https://doi.org/10.1073/pnas.0910866107

Petrareanu G, Balasu MC, Vacaru AM, Munteanu CVA, Ionescu AE, Matei I, Szedlacsek SE (2014) Phosphoketolases from Lactococcus lactis, Leuconostoc mesenteroides and Pseudomonas aeruginosa: Dissimilar sequences, similar substrates but distinct enzymatic characteristics. *Applied Microbiology and Biotechnology* 98:7855–7867, https://doi.org/10.1007/s00253-014-5723-6

Philip S, Keshavarz T, Roy I (2007) Polyhydroxyalkanoates: Biodegradable polymers with a range of applications. *Journal of Chemical Technology and Biotechnology* 82:233–247, https://doi.org/10.1002/jctb.1667

Planavsky NJ, Asael D, Hofmann A, Reinhard CT, Lalonde S V., Knudsen A, Wang X, Ossa Ossa F, Pecoits E, Smith AJB, Beukes NJ, Bekker A, Johnson TM, Konhauser KO, Lyons TW, Rouxel OJ (2014) Evidence for oxygenic photosynthesis half a billion years before the Great Oxidation Event. *Nature Geoscience* 7:283–286, https://doi.org/10.1038/ngeo2122

Pohlmeyer K, Paap BK, Soll J, Wedel N (1996) CP12: A small nuclear-encoded chloroplast protein provides novel insights into higher-plant GAPDH evolution. *Plant Molecular Biology* 32:969–978, https://doi.org/10.1007/BF00020493

Posthuma CC, Bader R, Engelmann R, Postma PW, Hengstenberg W, Pouwels PH (2002) Expression of the xylulose 5-phosphate phosphoketolase gene, xpkA, from lactobacillus pentosus MD363 is induced by sugars that are fermented via the phosphoketolase pathway and is repressed by glucose mediated by CcpA and the mannose phosphoenolpyruvate phosphotransferase system. *Applied and Environmental Microbiology* 68:831–837, https://doi.org/10.1128/AEM.68.2.831-837.2002

Pulich WM, Baalen C, Gibson JL, Tabita FR (1976) Purification and Characterization of Glucose Dehydrogenase from a Heterotrophically Grown Blue-Green Alga. *Plant Physiology* 58:393–397, https://doi.org/10.1104/pp.58.3.393

Purves WK, Sadava D, Orians GH, Heller HC, Markl J (2007) Die Erforschung des Lebens. *Purves Biologie - Springer Berlin Heidelberg* 7:2–17

R Core Team (2020) R: a language and envirmonemtal for Statistical Computing, https://www.r-project.org/

Reichmann D, Jakob U (2013) The roles of conditional disorder in redox proteins. *Current Opinion in Structural Biology* 23:436–442, https://doi.org/10.1016/j.sbi.2013.02.006

Rohwer JM, Hofmeyr J-HS (2008) Identifying and characterising regulatory metabolites with generalised supply–demand analysis. *Journal of Theoretical Biology* 252:546–554, https://doi.org/https://doi.org/10.1016/j.jtbi.2007.10.032

Romano AH, Conway T (1996) Evolution of carbohydrate metabolic pathways. *Research in Microbiology* 147:448–455, https://doi.org/10.1016/0923-2508(96)83998-2

Rueden CT, Schindelin J, Hiner MC, DeZonia BE, Walter AE, Arena ET, Eliceiri KW (2017) ImageJ2: ImageJ for the next generation of scientific image data. *BMC Bioinformatics* 18:529, https://doi.org/10.1186/s12859-017-1934-z

Ruelland E, Miginiac-Maslow M (1999) Regulation of chloroplast enzyme activities by thioredoxins: Activation or relief from inhibition? *Trends in Plant Science* 4:136–141, https://doi.org/10.1016/S1360-1385(99)01391-6

Saadatnia H, Riahi H (2009) Cyanobacteria from paddy fields in Iran as a biofertilizer in rice plants. *Plant Soil Environ* 55:207–212, https://doi.org/10.17221/384-pse

Saha R, Liu D, Hoynes-O'Connor A, Liberton M, Yu J, Bhattacharyya-Pakrasi M, Balassy A, Zhang F, Moon TS, Maranas CD, Pakrasia HB (2016) Diurnal regulation of cellular processes in the cyanobacterium Synechocystis sp. strain PCC 6803: Insights from transcriptomic, fluxomic, and physiological analyses. *mBio* 7:e00464, https://doi.org/10.1128/mBio.00464-16

Sánchez B, Zúñiga M, González-Candelas F, de los Reyes-Gavilán CG, Margolles A (2010) Bacterial and Eukaryotic Phosphoketolases: Phylogeny, Distribution and Evolution. *Journal of Molecular Microbiology and Biotechnology* 18:37–51, https://doi.org/10.1159/000274310

Sanger F, Nicklen S, Coulson AR (1977) DNA sequencing with chain-terminating inhibitors. *Proceedings of the National Academy of Sciences of the United States of America* 74:5463–5467, https://doi.org/10.1073/pnas.74.12.5463

Scheibe R (1991) Redox-modulation of chloroplast enzymes: A common principle for individual control. *Plant Physiology* 96:1–3, https://doi.org/10.1104/pp.96.1.1

Scheidig AJ, Horvath D, Szedlacsek SE (2019) Crystal structure of a xylulose 5-phosphate phosphoketolase. Insights into the substrate specificity for xylulose 5-phosphate. *Journal of Structural Biology* 207:85–102, https://doi.org/10.1016/j.jsb.2019.04.017

Schindelin J, Arganda-Carreras I, Frise E, Kaynig V, Longhair M, Pietzsch T, Preibisch S, Rueden C, Saalfeld S, Schmid B, Tinevez J-Y, White DJ, Hartenstein V, Eliceiri K, Tomancak P, Cardona A (2012) Fiji: an open-source platform for biological-image analysis. *Nature Methods* 9:676–682, https://doi.org/https://doi.org/10.1038/nmeth.2019

Schönheit P, Buckel W, Martin WF (2016) On the Origin of Heterotrophy. *Trends in Microbiology* 24:12–25, https://doi.org/10.1016/j.tim.2015.10.003

Schramm M, Klybas V, Racker E (1958) Phosphorolytic cleavage of fructose-6-phosphate by fructose-6-phosphate phosphoketolase from Acetobacter xylinum. *The Journal of biological chemistry* 233:1283–1288, https://doi.org/10.1016/S0021-9258(18)49327-1

Schreiber K (2016) Aufklärung verschiedener Glukoseabbauwege und deren Einfluss auf den Wasserstoffmetabolismus im Cyanobakterium Synechocystis spec. PCC 6803. *Christian-Albrechts-Universität zu Kiel.* Dissertation. https://doi.org/https://macau.uni-kiel.de/receive/diss_mods_00018989?lang=de

Schürmann P, Buchanan BB (2008) The ferredoxin/thioredoxin system of oxygenic photosynthesis. *Antioxidants and Redox Signaling* 10:1235–1273, https://doi.org/10.1089/ars.2007.1931

Schürmann P, Jacquot JP (2000) Plant thioredoxin systems revisited. *Annual Review of Plant Biology* 51:371–400, https://doi.org/10.1146/annurev.arplant.51.1.371

Selig M, Xavier KB, Santos H, Schönheit P (1997) Comparative analysis of Embden-Meyerhof and Entner-Doudoroff glycolytic pathways in hyperthermophilic archaea and the bacterium Thermotoga. *Archives of Microbiology* 167:217–232, https://doi.org/10.1007/BF03356097

Shatalin K, Lebreton S, Rault-Leonardon M, Vélot C, Srere PA (1999) Electrostatic channeling of oxaloacetate in a fusion protein of porcine citrate synthase and porcine mitochondrial malate dehydrogenase. *Biochemistry* 38:881–889, https://doi.org/10.1021/bi982195h

Sheu KFR, Blass JP (1999) The α-ketoglutarate dehydrogenase complex. *Annals of the New York Academy of Sciences* 893:61–78, https://doi.org/10.1111/j.1749-6632.1999.tb07818.x

Shih PM, Matzke NJ (2013) Primary endosymbiosis events date to the later Proterozoic with cross-calibrated phylogenetic dating of duplicated ATPase proteins. *Proceedings of the National Academy of Sciences of the United States of America* 110:12355–12360, https://doi.org/10.1073/pnas.1305813110

Shimakawa G, Hasunuma T, Kondo A, Matsuda M, Makino A, Miyake C (2014) Respiration accumulates Calvin cycle intermediates for the rapid start of photosynthesis in Synechocystis sp. PCC 6803. *Bioscience, Biotechnology and Biochemistry* 78:1997–2007, https://doi.org/10.1080/09168451.2014.943648

Shively JM, Decker GL, Greenawalt JW (1970) Comparative ultrastructure of the thiobacilli. *Journal of Bacteriology* 101:618–627, https://doi.org/10.1128/jb.101.2.618-627.1970

Soo RM, Hemp J, Parks DH, Fischer WW, Hugenholtz P (2017) On the origins of oxygenic photosynthesis and aerobic respiration in Cyanobacteria. *Science* 355:1436–1440, https://doi.org/10.1126/science.aal3794

Spengler K (2019) Wechselwirkungen von Kohlenstoff-und Stickstoff-Metabolismus in Synechocystis sp. PCC 6803. *Christian-Albrechts-Univerisität zu Kiel*, Master Thesis (unpublished)

Spivey HO, Merz JM (1989) Metabolic Compartmentation. *BioEssays* 10:127–129, https://doi.org/10.1002/bies.950100409

Spivey HO, Ovádi J (1999) Substrate Channeling. *Methods* 19:306–321, https://doi.org/https://doi.org/10.1006/meth.1999.0858

Srere PA (1985) The metabolon. *Trends in Biochemical Sciences* 10:109–110, https://doi.org/10.1016/0968-0004(85)90266-X

Srere PA (2000) Macromolecular interactions: Tracing the roots. *Trends in Biochemical Sciences* 25:150–153, https://doi.org/10.1016/S0968-0004(00)01550-4

Stal LJ (2012) Cyanobacterial mats and stromatolites. *Ecology of Cyanobacteria II: Their Diversity in Space and Time - Springer Netherlands* 1:65–125, https://doi.org/10.1007/978-94-007-3855-3_4

Stanier RY, Kunisawa R, Mandel M, Cohen-Bazire G (1971) Purification and properties of unicellular blue-green algae (order Chroococcales). *Bacteriological reviews* 35:171–205, https://doi.org/10.1128/mmbr.35.2.171-205.1971

Stockhammer A, Bottanelli F (2020) Appreciating the small things in life: STED microscopy in living cells. *Journal of Physics D: Applied Physics* 54:033001, https://doi.org/10.1088/1361-6463/abac81

Strunecký O, Kopejtka K, Goecke F, Tomasch J, Lukavský J, Neori A, Kahl S, Pieper DH, Pilarski P, Kaftan D, Koblížek M (2019) High diversity of thermophilic cyanobacteria in Rupite hot spring identified by microscopy, cultivation, single-cell PCR and amplicon sequencing. *Extremophiles* 23:35–48, https://doi.org/10.1007/s00792-018-1058-z

Sukenik A, Hadas O, Kaplan A, Quesada A (2012) Invasion of Nostocales (cyanobacteria) to subtropical and temperate freshwater lakes - physiological, regional, and global driving forces. *Frontiers in Microbiology* 3:86, https://doi.org/10.3389/fmicb.2012.00086

Sumegi B, Sherry AD, Malloy CR, Srere PA (1993) Evidence for Orientation-Conserved Transfer in the TCA Cycle in Saccharomyces cerevisiae: 13C NMR Studies. *Biochemistry* 32:12725–12729, https://doi.org/10.1021/bi00210a022

Sumegi B, Srere PA (1984) Complex I binds several mitochondrial NAD-coupled dehydrogenases. *Journal of Biological Chemistry* 259:15040–15045, https://doi.org/10.1016/S0021-9258(17)42511-7

Summer H, Grämer R, Dröge P (2009) Denaturing urea polyacrylamide gel electrophoresis (Urea PAGE). *Journal of Visualized Experiments* 32:e1485, https://doi.org/10.3791/1485

Sutherland JD (2017) Opinion: Studies on the origin of life-The end of the beginning. *Nature Reviews Chemistry* 1:1–7, https://doi.org/10.1038/s41570-016-0012

Sutter JM, Tästensen JB, Johnsen U, Soppa J, Schönheit P (2016) Key enzymes of the semiphosphorylative entner-doudoroff pathway in the haloarchaeon Haloferax volcanii: Characterization of glucose dehydrogenase, gluconate dehydratase, and 2-Keto-3-Deoxy-6-phosphogluconate aldolase. *Journal of Bacteriology* 198:2251–2262, https://doi.org/10.1128/JB.00286-16

Sweetlove LJ, Fernie AR (2018) The role of dynamic enzyme assemblies and substrate channelling in metabolic regulation. *Nature Communications* 9:2136, https://doi.org/10.1038/s41467-018-04543-8

Sygmund C, Klausberger M, Felice AK, Ludwig R (2011) Reduction of quinones and phenoxy radicals by extracellular glucose dehydrogenase from Glomerella cingulata suggests a role in plant pathogenicity. *Microbiology* 157:3203–3212, https://doi.org/10.1099/mic.0.051904-0

Takahashi H, Uchimiya H, Hihara Y (2008) Difference in metabolite levels between photoautotrophic and photomixotrophic cultures of Synechocystis sp. PCC 6803 examined by capillary electrophoresis electrospray ionization mass spectrometry. *Journal of Experimental Botany* 59:3009–3018, https://doi.org/10.1093/jxb/ern157

Takeya M, Hirai MY, Osanai T (2017) Allosteric inhibition of phosphoenolpyruvate carboxylases is determined by a single amino acid residue in cyanobacteria. *Scientific Reports* 7:1–9, https://doi.org/10.1038/srep41080

Tamoi M, Miyazaki T, Fukamizo T, Shigeoka S (2005) The Calvin cycle in cyanobacteria is regulated by CP12 via the NAD(H)/NADP(H) ratio under light/dark conditions. *Plant J* 42:504–513, https://doi.org/10.1111/j.1365-313X.2005.02391.x

Tanner JJ (2019) Structural biology of proline catabolic enzymes. *Antioxidants and Redox Signaling* 30:650–673, https://doi.org/10.1089/ars.2017.7374

Taylor SW, Fahy E, Zhang B, Glenn GM, Warnock DE, Wiley S, Murphy AN, Gaucher SP, Capaldi RA, Gibson BW, Ghosh SS (2003) Characterization of the human heart mitochondrial proteome. *Nature Biotechnology* 21:281–286, https://doi.org/10.1038/nbt793

Teeling H, Fuchs BM, Becher D, Klockow C, Gardebrecht A, Bennke CM, Kassabgy M, Huang S, Mann AJ, Waldmann J, Weber M, Klindworth A, Otto A, Lange J, Bernhardt J, Reinsch C, Hecker M, Peplies J, Bockelmann FD, Callies U, Gerdts G, Wichels A, Wiltshire KH, Glöckner FO, Schweder T, Amann R (2012) Substrate-controlled succession of marine bacterioplankton populations induced by a phytoplankton bloom. *Science* 336:608–611, https://doi.org/10.1126/science.1218344

Theune ML, Hildebrandt S, Steffen-Heins A, Bilger W, Gutekunst K, Appel J (2020) In-vivo quantification of electron flow through photosystem I – cyclic electron transport makes up about 35% in a cyanobacterium. *Biochimica et Biophysica Acta - Bioenergetics* (accepted)

Thiel K, Vuorio E, Aro EM, Kallio PT (2017) The effect of enhanced acetate influx on Synechocystis sp. PCC 6803 metabolism. *Microbial Cell Factories* 16:1–12, https://doi.org/10.1186/s12934-017-0640-x

Thieulin-Pardo G, Remy T, Lignon S, Lebrun R, Gontero B (2015) Phosphoribulokinase from Chlamydomonas reinhardtii: A Benson-Calvin cycle enzyme enslaved to its cysteine residues. *Molecular BioSystems* 11:1134–1145, https://doi.org/10.1039/c5mb00035a

Veaudor T, Blanc-Garin V, Chenebault C, Diaz-Santos E, Sassi JF, Cassier-Chauvat C, Chauvat F (2020) Recent advances in the photoautotrophic metabolism of cyanobacteria: Biotechnological implications. *Life* 10:71, https://doi.org/10.3390/life10050071

Vélot C, Mixon MB, Teige M, Srere PA (1997) Model of a quinary structure between krebs TCA cycle enzymes: A model for the metabolon. *Biochemistry* 36:14271–14276, https://doi.org/10.1021/bi972011j

Wallace EWJ, Kear-Scott JL, Pilipenko E V., Schwartz MH, Laskowski PR, Rojek AE, Katanski CD, Riback JA, Dion MF, Franks AM, Airoldi EM, Pan T, Budnik BA, Drummond DA (2015) Reversible, Specific, Active Aggregates of Endogenous Proteins Assemble upon Heat Stress. *Cell* 162:1286–1298, https://doi.org/10.1016/j.cell.2015.08.041

Wang H, Rivenson Y, Jin Y, Wei Z, Gao R, Günaydın H, Bentolila LA, Kural C, Ozcan A (2019) Deep learning enables cross-modality super-resolution in fluorescence microscopy. *Nature Methods* 16:103–110, https://doi.org/10.1038/s41592-018-0239-0

Wang HL, Postier BL, Burnap RL (2004) Alterations in Global Patterns of Gene Expression in Synechocystis sp. PCC 6803 in Response to Inorganic Carbon Limitation and the Inactivation of ndhR, a LysR Family Regulator. *Journal of Biological Chemistry* 279:5739–5751, https://doi.org/10.1074/jbc.M311336200

Wase N V, Wright PC (2008) Systems biology of cyanobacterial secondary metabolite production and its role in drug discovery. *Expert Opinion on Drug Discovery* 3:903–929, https://doi.org/10.1517/17460441.3.8.903

Webb AAR, McAinsh MR, Mansfield TA, Hetherington AM (1996) Carbon dioxide induces increases in guard cell cytosolic free calcium. *Plant Journal* 9:297–304, https://doi.org/10.1046/j.1365-313X.1996.09030297.x

Wedel N, Soll J (1998) Evolutionary conserved light regulation of Calvin cycle activity by NADPH-mediated reversible phosphoribulokinase/CP12/ glyceraldehyde-3-phosphate dehydrogenase complex dissociation. *Proceedings of the National Academy of Sciences of the United States of America* 95:9699–9704, https://doi.org/10.1073/pnas.95.16.9699

Wedel N, Soll J, Paap BK (1997) CP12 provides a new mode of light regulation of Calvin cycle activity in higher plants. *Proceedings of the National Academy of Sciences of the United States of America* 94:10479–10484, https://doi.org/10.1073/pnas.94.19.10479

Weiss MC, Sousa FL, Mrnjavac N, Neukirchen S, Roettger M, Nelson-Sathi S, Martin WF (2016) The physiology and habitat of the last universal common ancestor. *Nature Microbiology* 1:1–8, https://doi.org/10.1038/nmicrobiol.2016.116

Weyers JDB, Fitzsimons PJ, Mansey GM, Martin ES (1983) Guard cell protoplasts - Aspects of work with an important new research tool. *Physiologia Plantarum* 58:331–339, https://doi.org/10.1111/j.1399-3054.1983.tb04189.x

Wheeldon I, Minteer SD, Banta S, Barton SC, Atanassov P, Sigman M (2016) Substrate channelling as an approach to cascade reactions. *Nature Chemistry* 8:299–309, https://doi.org/10.1038/nchem.2459

Whitton BA, Potts M (2012) Introduction to the cyanobacteria. *Ecology of Cyanobacteria II: Their Diversity in Space and Time - Springer Netherlands* 1:1–13, https://doi.org/10.1007/978-94-007-3855-3_1

Wolfe AJ (2005) The Acetate Switch. *Microbiology and Molecular Biology Reviews* 69:12–50, https://doi.org/10.1128/mmbr.69.1.12-50.2005

Xiong W, Cano M, Wang B, Douchi D, Yu J (2017) The plasticity of cyanobacterial carbon metabolism. *Current Opinion in Chemical Biology* 41:12–19, https://doi.org/10.1016/j.cbpa.2017.09.004

Xiong W, Lee TC, Rommelfanger S, Gjersing E, Cano M, Maness PC, Ghirardi M, Yu J (2015) Phosphoketolase pathway contributes to carbon metabolism in cyanobacteria. *Nature Plants* 1:15187, https://doi.org/10.1038/nplants.2015.187

Yang C, Hua Q, Shimizu K (2002) Metabolic flux analysis in Synechocystis using isotope distribution from 13C-labeled glucose. *Metabolic Engineering* 4:202–216, https://doi.org/10.1006/mben.2002.0226

Yeates TO, Kerfeld CA, Heinhorst S, Cannon GC, Shively JM (2008) Protein-based organelles in bacteria: carboxysomes and related microcompartments. *Nature Reviews Microbiology* 6:681–691, https://doi.org/10.1038/nrmicro1913

Yevenes A, Frey PA (2008) Cloning, expression, purification, cofactor requirements, and steady state kinetics of phosphoketolase-2 from Lactobacillus plantarum. *Bioorganic Chemistry* 36:121–127, https://doi.org/10.1016/j.bioorg.2008.03.002

Young JD, Shastri AA, Stephanopoulos G, Morgan JA (2011) Mapping photoautotrophic metabolism with isotopically nonstationary 13C flux analysis. *Metabolic Engineering* 13:656–665, https://doi.org/10.1016/J.YMBEN.2011.08.002

Zajchowski LD, Robbins SM (2002) Lipid rafts and little caves: Compartmentalized signalling in membrane microdomains. *European Journal of Biochemistry* 269:737–752, https://doi.org/10.1046/j.0014-2956.2001.02715.x

Zavřel T, Očenášová P, Červený J (2017) Phenotypic characterization of Synechocystis sp. PCC 6803 substrains reveals differences in sensitivity to abiotic stress. *PLoS ONE* 12:e0189130, https://doi.org/10.1371/journal.pone.0189130

Zhang S, Laborde SM, Frankel LK, Bricker TM (2004) Four Novel Genes Required for Optimal Photoautotrophic Growth of the Cyanobacterium Synechocystis sp. Strain PCC 6803 Identified by In Vitro Transposon Mutagenesis. *Journal of Bacteriology* 186:875–879, https://doi.org/10.1128/JB.186.3.875-879.2004

Zhang Y, Beard KFM, Swart C, Bergmann S, Krahnert I, Nikoloski Z, Graf A, George Ratcliffe R, Sweetlove LJ, Fernie AR, Obata T (2017) Protein-protein interactions and metabolite channelling in the plant tricarboxylic acid cycle. *Nature Communications* 8:1–11, https://doi.org/10.1038/ncomms15212

Acknowledgement

Zuallererst möchte ich Prof. Dr. Rüdiger Schulz danken, dass er mir drei Jahre lang die Möglichkeit gegeben hat zu forschen und zu dissertieren. Danke dafür, dass ich Ihre Labore nutzen konnte, um mir einen Lebenstraum zu erfüllen, mich vollkommen auf meine Promotion konzentrieren konnte und stets unterstützt und verstanden worden zu sein. Ich danke Ihnen für einen respektvollen Umgang auf Augenhöhe und kulinarisch hervorragende Weihnachtsfeiern.

Mein nächster Dank geht an Dr. Kirstin Gutekunst für die Vergabe des Themas. Danke für das Vertrauen in mich und meine Arbeit und für jegliche Unterstützung. Danke dafür, dass du als Ratgeberin über den Tellerrand schaust und uns Doktoranden einfach mal hast machen lassen. Danke für die stehst offene Tür und eine unerschöpfliche Begeisterung für das was die Wissenschaft ausmacht. Konsens, Kreativität und den Mut mal Neues auszuprobieren.

Außerdem möchte ich Prof. Dr. Conrad Mullineaux und Prof. Dr. Marc Bramkamp danken. Danke, dass Sie mich in Ihre Labore gelassen haben und mir wertvolle Tipps zur erfolgreichen Fluoreszenz-Mikroskopie gegeben haben.

Ein weiterer Dank geht an Dr. Amke Caliebe vom Institut für Medizinische Informatik und Statistik, die uns in statistischen Fragen beratend zur Seite stand.

Marko, vielen Dank für all die Ratschläge und Hilfe, die du mir gegeben hast. Danke für die Idee einen Mutagenese-Vektor zur Konstruktion der GFP- und YFP-Mutanten zu verwenden. Ohne diesen würde ich wahrscheinlich immer noch klonieren. Vielen Dank für deine ansteckende Begeisterung für Western Blots, deine Hilfe und Unterstützung dabei diese zu realisieren. Dank dir habe ich gelernt, dass die Molekularbiologie wie Kochen ist. Manchmal hilft Viel eben doch viel. Dank dir gehe ich auf Masse, bis jetzt ein echtes Erfolgsrezept.

Marius, danke für all die tollen wissenschaftlichen Gespräche mit dir. Ich danke dir vor allem für die Hilfe und die Ideen zur Auswertung der Fluoreszenzbilder. Danke dafür, dass du all das machst, was du machst einfach, weil du Spaß an der Sache hast. In frustrierenden Momenten erinnerst du einen daran, warum man eigentlich Biologe geworden ist. Danke für all die „man sind wir super nerdig und wir stehen drauf“ Momente.

Vanessa, danke dafür, dass ich hunderte großartige Labortage hatte. Die frühen Stunden am Morgen eines langen Labortages haben so viel Spaß mit dir gemacht. Besonders während Corona, eine tolle Zeit, in der viele gute Gespräche entstanden sind und man sich weder einsam noch verloren gefühlt hat. Danke dafür, dass du immer eine Antwort auf die Fragen „Wie war das noch mal nach dem Waschschritt?“ hattest. Ich werde die gemeinsamen Mittagsessen und die „sich über den Autoklaviermüll aufregen“ - Momente sehr vermissen.

Johanna, ich bin so froh eine so tolle Back-to-back Sitznachbarin gehabt zu haben. Du bist eine Person, die man einfach gernhaben muss. Immer gut gelaunt immer hilfsbereit. Ich kann mich nicht erinnern dich jemals schlechtgelaunt gesehen zu haben. Du bist ein echtes Vorbild mentaler Stärke, Geselligkeit und Hilfsbereitschaft. Danke dafür, dass es einfach toll ist dich zu kennen und dafür, dass man dich immer über alles ausfragen konnte.

Katharina, danke für alles. Ohne dich wäre das ganze Labor nur auf Notbetrieb gelaufen. Ich konnte dich immer um Platten und Medium bitten. Du hast als TA den Laden geschmissen und nicht nur ohne zu murren, sondern auch noch gutgelaunt unseren Müll gespült. Vielen Dank dafür, dass du der entspannteste Mensch bist, den ich kenne. Du bist der Beweis dafür, dass Leben auch ohne Aufregung und Stress funktioniert.

Berit, vielen Dank für alles. Für tolle Gespräche, Verständnis, dein offenes Ohr. Danke dafür, dass du immer ehrlich mit mir warst, ehrlicher als manch anderer sich getraut hätte. Mir hat es imponiert. Du bist ein echtes Powerhouse mit einem wunderbar zwielichtigen Humor.

Alex, danke dafür, dass ich dich „beerben durfte“. Danke für die Steilvorlage, die deine Arbeit meiner gibt und dafür, dass du mir erklärt hast wie Enzymtests funktionieren. Danke dafür, dass du ein echtes Vorbild bist, dass das Leben einfach schön und entspannt ist.

Mein Dank geht auch an Vanessa Dombrowski, die die Eno-Mutante untersucht und traumhafte PCRs gemacht hat.

Jens, Lars, Cedric. Vielen Dank für alles. Ich konnte euch immer alles fragen und um Gefallen bitten und habe immer Antwort und Equipment bekommen. Das ist nicht selbstverständlich und ich weiß das sehr zu schätzen. Danke für eine tolle Zeit im Labor und ein geistreiches Miteinander.

Ein weiterer großer Dank geht an Lena Uebele. Danke, dass deine Grammatikkünste besser als meine sind und du dir Zeit genommen hast meine Arbeit zu korrigieren. Ich vermisse unsere Lernsessions sehr und denke gerne an die „guten alten KIT Zeiten" zurück.

Natürlich spielt die Familie ein ebenso große, wenn nicht sogar die größte Rolle, dass das Projekt 23 Jahre Schulausbildung durch eine Promotion so gut geschmückt und abgeschlossen werden. Mama, Papa danke für alles. Ohne euch gäbe es mich nicht, ohne euch wäre ich nicht so wie ich bin und ohne euch würde ich nicht dastehen, wo ich im Leben stehe: Geerdet, glücklich, geliebt (und schuldenfrei). Ihr habt alles richtig gemacht. Philipp und ich sind wirklich gut gelungen. Für diese Selbsterkenntnis und das Bewusstsein meines Selbst danke ich euch.

Philipp, mein Bruder und größtes Vorbild. Immer noch und das wird auch immer so bleiben.

Nun der größte und innigste Dank. Den Dank an meinen Ehemann. Danke dafür, dass dein Name Programm ist. Ich kenne niemand friedliebenderen Menschen als dich. Du heißt nicht nur Friedemann, du bist ein Friedemann. Das können wenige Menschen von sich behaupten. Du unterstützt mich in allem, egal wie irre und größenwahnsinnig meine Lebensträume und Pläne auch sind. Du respektierst alle meine Facetten auch die super nerdigen und die super nervigen. ILD.

Der Deutschen Forschungsgemeinschaft (DFG) danke ich für die finanzielle Unterstützung.

Declaration of authorship

I herewith declare that the presented thesis is entirely my own work except where otherwise stated.

This thesis has not been submitted either partially or wholly as part of a doctoral degree to another examination body.

I herewith declare that no academic degree has ever been withdrawn.

Besides this, I declare that the thesis has been prepared subject to the Rule of Good Scientific Practice of the German Research Foundation.

Sarah Hildebrandt

Appendix

List of figures

List of tables

Additional Figure

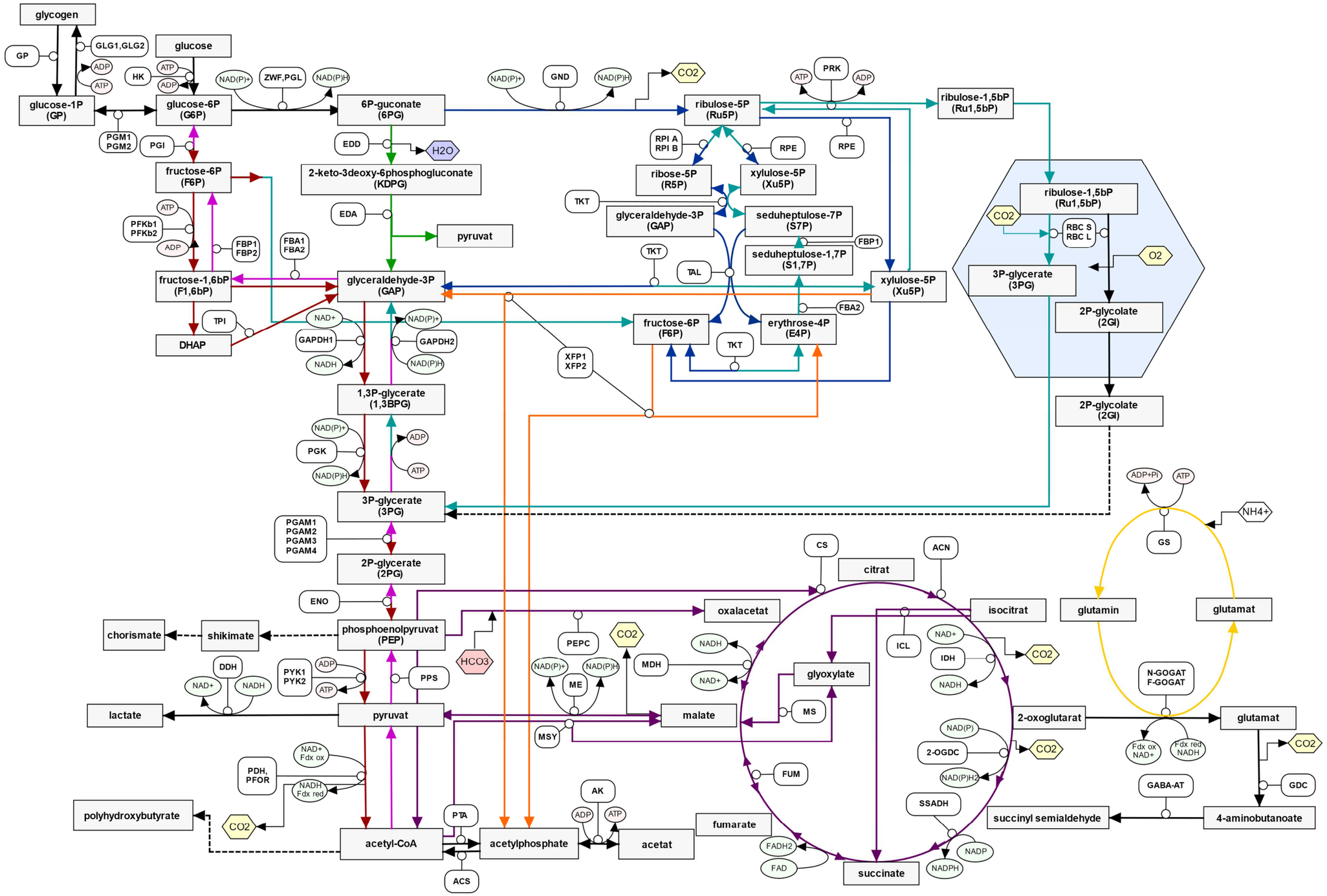

Appendix Figure 1: Overview of the carbon metabolism in cyanobacteria. Green: Entner-Doudoroff (ED) pathway. Red: Emden-Meyerhof-Parnas (EMP) pathway. Pink: gluconeogenesis. Blue: oxidative pentose phosphate (OPP) pathway. Cyan: Calvin-Benson-Bassam (CBB) cycle. Orange: Phosphoketolase (PK) pathway. Purple: TCA cycle. Yellow: GOGAT/GS cycle. Blue hexagon represents a carboxysome GP: glycogen phosphorylase; GLG: glycogen synthase; HK: hexokinase; PGM: phosphoglucomutase; PGI:phosphoglucose isomerase;GDH: glucose dehydrogenase; ZWF: glucose-6-phosphate dehydrogenase; PGL: 6-phosphogluconolactonase; PFK:6-phosphofructokinase; FBP: fructose 1,6-bisphosphate; TPI: triosephosphateisomerase; GK: gluconate kinase; EDD: phosphogluconate dehydratase; EDA: KDPG-aldolase; GAPDH: glyceraldehyde phosphate dehydrogenase; PGK: phosphoglycerate kinase; PYK: pyruvate kinase; ENO: enolase; PGAM: phosphoglycerate mutase; PPS: phosphoenolpyruvate synthetase; PDH: pyruvate dehydrogenase; PFOR: pyruvate ferredoxin oxidoreductase; ACS: acteyl CoA synthetase; PTA: phosphate acetyltransferase; AK: acteate kinase; ME: malic enzyne ; PEPC: phosphoenolpyruvate carboxylase; MDH: malat dehydrogenase; FUM: fumarase; MS: malat synthase; CS: citrate synthase; ACN: aconitase; ICL: isocitrate lyase; IDH: isocitrate dehydrogenase; 2-OGDC: 2-oxoglutarat decarboxylase; SSDAH: succinic semialdehyde dehydrogenase; GND: 6-phophogluconate dehydrogenase; PRK: phosphoribulokinase; XFP: xylulose-5- phosphate/fructose-6-phosphate phosphoketolase; RPI:ribulose-5-phosphate isomerase;RPE: ribulose-5-phosphate epimerase; TKT: transketolase; TAL: transaldolase;DDH: lactate dehydrogenase; GS: glutamine synthase; GOGAT: glutamin oxoglutarat aminotransferase; GABA-AT: ϒ-aminobutyrat aminotransferase; GDC: glutamate decarboxylase; RBC: rubisco.